



University of **HUDDERSFIELD**

University of Huddersfield Repository

Al-Arbi, Salem

Condition Monitoring of Gear Systems using Vibration Analysis

Original Citation

Al-Arbi, Salem (2012) Condition Monitoring of Gear Systems using Vibration Analysis. Doctoral thesis, University of Huddersfield.

This version is available at <http://eprints.hud.ac.uk/id/eprint/17821/>

The University Repository is a digital collection of the research output of the University, available on Open Access. Copyright and Moral Rights for the items on this site are retained by the individual author and/or other copyright owners. Users may access full items free of charge; copies of full text items generally can be reproduced, displayed or performed and given to third parties in any format or medium for personal research or study, educational or not-for-profit purposes without prior permission or charge, provided:

- The authors, title and full bibliographic details is credited in any copy;
- A hyperlink and/or URL is included for the original metadata page; and
- The content is not changed in any way.

For more information, including our policy and submission procedure, please contact the Repository Team at: E.mailbox@hud.ac.uk.

<http://eprints.hud.ac.uk/>

CONDITION MONITORING OF GEAR SYSTEMS USING VIBRATION ANALYSIS

Salem K. Al-Arbi

A thesis submitted to the University of Huddersfield in
partial fulfilment of the requirements for the degree of
Doctor of Philosophy.

University of Huddersfield

August 2012

DECLARATION

DECLARATION

No portion of the work referred to in this thesis has been submitted in support of an application for another degree or qualification of this or any other university or other institute of learning.

DEDICATION

DEDICATION

To my mother and my father in law, I wish you were still with us. Thank you for your love and support and helping me to believe. I dedicate this to you.

ABSTRACT

It is often impractical to measure vibrations directly at /or close to their sources when condition monitoring gearbox systems. It is common to measure the vibration distant from the source due to limited access to the component which is to be monitored. In addition, operating the gearbox under different loads and speeds also produces vibration signals within different components. Vibration measured in this way may be significantly distorted by the effect of signal transmission paths and interference from other sources. Therefore, suppression of distortions is a key issue for remote measurement based condition monitoring. In this research work, the influences of transducer locations and operating conditions on the vibration signal have been investigated on a typical gearbox transmission system for the detection of faults induced within the gearbox. Vibration signals corresponding to a healthy (baseline) and faulty conditions on two-stage helical gearbox at various load and speed levels were recorded. The baseline vibration data were examined using conventional methods in the time, frequency and the joint time-frequency domains, and are referenced for comparison with more advanced methods. Several parameters have been proposed for monitoring gear condition locally (gearbox casing) including time, frequency, and joint time-frequency domain representation. The results show that traditional signal processing techniques were insufficient for revealing fault detection information due to the low signal to noise ratio (SNR). This research also presents a mathematical model for the simulation of vibration signals in order to further understand the source of the vibration. The model represents a two stage gear system using a suitable stiffness function to represent the forces acting between each pair of gears. Rotational stiffness and damping are also used to simulate the angular motion of the gears and shafts. Results show that the frequency spectrum of acceleration outputs from the model take the expected form with peaks at the meshing frequency and associated harmonics.

Furthermore, if the stiffness function between the first pair of gears is simulated with a broken tooth, and various degrees of damage, outputs from the simulation have similar sideband effects to the signals produced in the experimental investigation.

ABSTRACT

In addition, the model also demonstrates that variation of load and speed produces a corresponding effect to that seen in the experiments. Consequently, although relatively simple, the mathematical model can be used to explain vibration mechanisms in real gearbox systems used in condition monitoring.

Time synchronous averaging (TSA) has been applied to the vibration signals from the gearbox to remove random noise combined with the raw signal. The angular domain signal, the order spectrum and the order-frequency presentation were used to characterise gearbox vibration in these new domains in more detail. Results obtained following TSA were compared with those obtained through conventional analysis from waveform characteristics, spectrum patterns and corresponding feature parameters under different operating loads and fault conditions. In addition, continuous wavelet transform (CWT) of TSA was also compared with the conventional CWT results of raw signals to further characterise vibrations.

As part of this research study, the vibration transmission path has been estimated using the frequency response function (FRF) technique. A response based estimation method has been developed to revise the base path and adapted to operating conditions for more accurate fault estimation. Both theoretical analysis and test results showed that improved diagnosis when the path information was included in vibration signal processing and feature selection.

Finally, the vibration data recorded from the two accelerometers located on the gearbox casing and motor flange were analyzed using different signal processing methods to investigate the effect of path transmission (transducer location) on the detection and diagnosis of the seeded gear tooth faults. Results from the angular domain, the order spectrum and the order-frequency analysis are presented to demonstrate use of these techniques for fault detection in gearboxes and that the effect of path transmissions can be observed on the vibration signals.

Results showed that CWT of the TSA signal could be used to detect and indicate the severity of the gear damage effectively even if vibration signals originated from a remote motor flange.

LIST OF CONTENTS

LIST OF CONTENTS

DECLARATION	2
DEDICATION	3
ABSTRACT	4
LIST OF CONTENTS	6
LIST OF FIGURES.....	11
LIST OF TABLES.....	17
LIST OF NOMENECLATURE	18
ACKNOWLEDGMENTS.....	26
LIST OF PUBLICATIONS	27
CHAPTER 1 INTRODUCTION.....	28
1.1 RESEARCH MOTIVATION	29
1.2 BACKGROUND	29
1.2.1 MAINTENANCE STRATEGIES AND CONDITION MONITORING	30
1.2.1.1 THE IMPORTANCE OF MAINTENANCE	30
1.2.1.2 REACTIVE MAINENANCE OR RUN TO FAILURE	30
1.2.1.3 PREVENTIVE OR TIME-BASED MAINENANCE	31
1.2.1.4 PREDICTIVE OR CONDITION-BASED MAINTENANCE.....	31
1.3 GEARBOX CONDITION MONITORING THROUGH VIBRATION ANALYSIS	31
1.4 GEAR TYPES AND THEIR OPERATION	35
1.5 GEAR FAILURES	40
1.6 GEAR VIBRATION AND MODULATION.....	42
1.7 CHARACTERISTICS OF GEARBOX VIBRATION	44
1.7.1 GEAR MESHING VIBRATION.....	45
1.7.1.1 DEVIATION FROM THE IDEAL TOOTH PROFILE	45

LIST OF CONTENTS

1.7.2 MODULATION EFFECTS	47
1.7.2.1 TOOTH LOADING EFFECT ON AMPLITUDE MODULATION	47
1.7.2.2 SPEED FLUCTUATION EFFECT ON FREQUENCY MODULATION	47
1.7.3 ADDITIVE IMPULSES	48
1.7.4 TRANSMISSION PATHS	48
1.8 AIM AND OBJECTIVES	48
1.9 THESIS OUTLINE	49
 CHAPTER 2 REVIEW OF VIBRATION-BASED GEAR FAULT DETECTION	
TECHNIQUES	53
2.1 TIME-DOMAIN ANALYSIS	54
2.1.1 PEAK VALUE	55
2.1.2 THE ROOT MEAN SQUARE (RMS)	55
2.1.3 THE CREST FACTOR (CF)	56
2.1.4 KURTOSIS	57
2.2 FREQUENCY (SPECTRUM) DOMAIN ANALYSIS	57
2.2.1 MESHING FREQUENCY CHARACTERISTICS	59
2.2.2 SIDEBANDS CHARACTERISTICS	59
2.2.3 SPEED VARIATION EFFECT	60
2.3 JOINT TIME-FREQUENCY APPROACHES	60
2.3.1 SHORT-TIME FOURIER TRANSFORM (STFT)	62
2.3.2 WIGNER-VILLE DISTRIBUTION (WVD)	64
2.3.3 WAVELET TRANSFORMS (WTs)	67
2.3.4 CONTINUOUS (MORLET) WAVELET TRANSFORMATION	69
2.4 TIME SYNCHRONOUS AVERAGING (TSA)	72
2.5 ORDER ANALYSIS	73
2.6 SUMMARY	74
 CHAPTER 3 TEST RIG FACILITIES, TEST PROCEDURE AND BASELINE VIBRATION	75
3.1 TEST RIG CONSTRUCTION	76
3.1.1 MECHANICAL COMPONENTS	76
3.1.2 ELECTRICAL CONTROL OF TEST RIG	81

LIST OF CONTENTS

3.2 INSTRUMENTATION	83
3.2.1 VIBRATION MEASUREMENTS	83
3.2.2 SPEED MEASUREMENTS.....	85
3.2.3 DATA ACQUISITION SYSTEM	86
3.3 TEST PROCEDURE (VARIABLE SPEED TESTS, VARIABLE LOAD TESTS).....	89
3.4 GEAR FAULT SIMULATION	90
3.5 CALCULATION OF GEARS CHARACTERISTIC FREQUENCIES	93
3.6 BASELINE DATA OF GEARBOX VIBRATION.....	94
3.6.1 SIGNATURE IN THE TIME DOMAIN	94
3.6.2 SIGNATURE IN THE FREQUENCY DOMAIN	96
3.6.3 SIGNATURE IN THE TIME-FREQUENCY DOMAIN (CWT REPRESENTATION)	101
3.7 SUMARRY	104
CHAPTER 4 CONVENTIONAL GEAR SYSTEM CONDITION MONITORING	106
4.1 INTRODUCTION.....	107
4.2 TIME DOMAIN ANALYSIS.....	107
4.2.1 TIME DOMAIN SIGNALS (WAVEFORM)	107
4.2.2 SIGNAL STRENGTH BASED DIAGNOSIS (PEAK VALUE AND RMS)	109
4.2.3 SIGNAL STRUCTURE BASED DIAGNOSIS (CREST FACTOR AND KURTOSIS)	111
4.3 FREQUENCY DOMAIN ANALYSIS	115
4.3.1 CHARACTERISTICS OF GEARBOX SPECTRUM	115
4.3.2 MESHING FREQUENCY BASED DIAGNOSIS	117
4.3.3 SIDEBAND BASED DIAGNOSIS	119
4.4 CONTINUOUS WAVELET TRANSFORM (CWT) ANALYSIS	121
4.5 SUMMARY	124
CHAPTER 5 MATHEMATICAL MODEL	125
5.1 INTRODUCTION.....	126
5.2 MODELLING OVERVIEW	127
5.3 MESH STIFFNESS FOR HELICAL GEAR MATING.....	128
5.4 DYNAMIC MODILLING OF A HELICAL GEARBOX.....	132

LIST OF CONTENTS

5.5 NUMERICAL IMPLEMENTATION OF THE MODEL	140
5.6 MODEL PARAMETER TUNING AND CALIBRATION	142
5.7 SIMULATION STUDY OF FAULTY GEARS	144
5.8 SUMMARY	151
CHAPTER 6 EFFECTIVENESS OF TIME SYNCHRONOUS AVERAGING	152
6.1 INTRODUCTION.....	153
6.2 IMPLEMENTATION OF TSA	154
6.3 TSA SIGNAL IN THE ANGULAR DOMAIN	155
6.3.1 WAVEFORM CHARACTERISTICS	155
6.3.2 SIGNAL STRENGTH BASED DIAGNOSIS (PEAK VALUE AND RMS).....	159
6.3.3 SIGNAL STRUCTURE BASED DIAGNOSIS (CREST FACTOR AND KURTOSIS)	162
6.4 ORDER SPECTRUM OF TSA SIGNAL	164
6.4.1 CHARACTERISTICS OF ORDER SPECTRUM	164
6.4.2 PERFORMANCE OF MESH ORDER BASED DIAGNOSIS	169
6.4.3 PERFORMANCE OF SIDEBAND ORDER BASED DIAGNOSIS	170
6.5 CONTINUOUS WAVELET TRANSFORM (CWT) ANALYSIS OF TSA SIGNALS	172
6.6 SUMMARY	176
CHAPTER 7 FREQUENCY RESPONSE FUNCTION (FRF)	178
7.1 INTRODUCTION.....	179
7.2 FREQUENCY RESPONSE FUNCTION (FRF) OVERVIEW	180
7.3 FREQUENCY RESPONSE FUNCTION (FRF) MEASUREMENT	181
7.3.1 SHAKER TEST SETUP	181
7.4 RESULT AND DISCUSSION	183
7.4.1 CHARACTERISTICS OF THE FRF_s	183
7.4.2 PERFORMANCE OF GEAR FAULT DETECTION	186
7.5 SUMMARY	189
CHAPTER 8 PERFORMANCE EVALUATION OF REMOTELY MEASURED VIBRATION ..	190
8.1 INTRODUCTION.....	191
8.2 TSA SIGNAL IN THE ANGULAR DOMAIN	191

LIST OF CONTENTS

8.2.1 WAVEFORM CHARACTERISTICS	191
8.2.2 SIGNAL STRENGTH BASED DIAGNOSIS USING PEAK AND RMS VALUES OF TSA SIGNALS	193
8.2.3 SIGNAL STRUCTURE BASED DIAGNOSIS USING KURTOSIS AND CREST FACTOR OF TSA SIGNALS	195
8.3 ORDER SPECTRUM OF TSA SIGNAL	198
8.3.1 CHARACTERISTICS OF ORDER SPECTRUM	198
8.3.2 PERFORMANCE OF MESHING (34TH) ORDER BASED DIAGNOSIS	201
8.3.3 PERFORMANCE OF SIDEBAND ORDER BASED DIAGNOSIS	203
8.4 CONTINUOUS WAVELET TRANSFORM (CWT) ANALYSIS OF TSA SIGNAL.....	208
8.5 SUMMARY	211
CHAPTER 9 CONCLUSIONS AND FUTURE WORK.....	214
9.1 REVIEW OF THE OBJECTIVES AND ACHIEVEMENTS	215
9.2 CONCLUSIONS ON GEAR TRANSMISSION SYSTEM CM USING VIBRATION ANALYSIS	223
9.2.1 EXPERIMENTAL STUDY	223
9.2.2 CONCLUSIONS ON GEAR TRANSMISSION SYSTEM MODEL	227
9.3 NOVEL FEATURE SUMMARY AND CONTRIBUTIONS TO KNOWLEDGE	228
9.4 THE CONTRIBUTIONS TO KNOWLEDGE	228
9.5 RECOMENDATIONS FOR FUTURE WORK.....	229
REFERENCES	231
APPENDIX A.....	243
APPENDIX B.....	245
APPENDIX C	247
APPENDIX D	248

LIST OF FIGURES

<i>Figure 1.1-Spur gears</i>	<i>36</i>
<i>Figure 1.2-Helical gears</i>	<i>36</i>
<i>Figure 1.3-Bevel gears.....</i>	<i>37</i>
<i>Figure 1.4-Worm gears.....</i>	<i>38</i>
<i>Figure 1.5-Tooth breakages.....</i>	<i>40</i>
<i>Figure 1.6-Tooth pitting.....</i>	<i>41</i>
<i>Figure 1.7-Tooth scoring</i>	<i>41</i>
<i>Figure 1.8-Tooth wear</i>	<i>42</i>
<i>Figure 2.1-Waveform of the vibration signal for a gearbox with healthy and faulty gears.....</i>	<i>54</i>
<i>Figure 2.2-Definition of the Crest factor, peak and RMS levels</i>	<i>56</i>
<i>Figure 2.3-Spectrum of gearbox vibration signal for healthy and faulty gears</i>	<i>58</i>
<i>Figure 2.4-STFT of test signal</i>	<i>62</i>
<i>Figure 2.5-Different types of wavelets</i>	<i>69</i>
<i>Figure 2.6-Scaling and shafting operation in CWT.....</i>	<i>71</i>
<i>Figure 3.1-Photograph of experimental test rig</i>	<i>76</i>
<i>Figure 3.2- Schematic diagram of the test rig showing the position of accelerometers.</i>	<i>77</i>
<i>Figure 3.3-Photograph of AC Motor/Gearbox combination</i>	<i>78</i>
<i>Figure 3.4-Schematic of fundamental structure and working principles of two-stage helical gearbox.....</i>	<i>79</i>
<i>Figure 3.5-Cut-away view showing DC motor field/armature circuit; Re-drawn by ML.....</i>	<i>81</i>
<i>Figure 3.6-Test rig control panel front.....</i>	<i>81</i>
<i>Figure 3.7-Block diagram of the experimental test rig.....</i>	<i>83</i>
<i>Figure 3.8-PCB Model 338C04</i>	<i>84</i>
<i>Figure 3.9-Mounting of motor encoder</i>	<i>86</i>
<i>Figure 3.10-Main data inspection panel</i>	<i>89</i>
<i>Figure 3.11-Simulated broken tooth</i>	<i>92</i>

LIST OF FIGURES

<i>Figure 3.12-Gearbox vibration baseline data (in time domain) at low operating conditions</i>	<i>95</i>
<i>Figure 3.13-Gearbox vibration baseline data (in time domain) at high operating conditions</i>	<i>95</i>
<i>Figure 3.14-Variation in RMS for various gear operating conditions</i>	<i>96</i>
<i>Figure 3.15-Gearbox vibration baseline data (in frequency domain) at low operating conditions</i>	<i>99</i>
<i>Figure 3.16-Gearbox vibration baseline data (in frequency domain) at high operating conditions</i>	<i>100</i>
<i>Figure 3.17-Variation in 1st meshing frequency amplitude for various gear operating conditions</i>	<i>101</i>
<i>Figure 3.18-Variation in 2nd meshing frequency amplitude for various gear operating conditions</i>	<i>101</i>
<i>Figure 3.19-Gearbox vibration baseline data (in time-frequency domain) at low operating conditions</i>	<i>103</i>
<i>Figure 3.20-Gearbox vibration baseline data (in time-frequency domain) at high operating conditions</i>	<i>103</i>
<i>Figure 4.1-Local vibration signal for a healthy and faulty gear cases at low operating condition and at high operating.....</i>	<i>108</i>
<i>Figure 4.2-Average Peak value of the vibration signal for healthy and faulty gears... ..</i>	<i>110</i>
<i>Figure 4.3-Average value of RMS of the vibration signal for healthy and faulty gears</i>	<i>111</i>
<i>Figure 4.4-Average values of Kurtosis of the vibration signal for healthy and faulty gears</i>	<i>112</i>
<i>Figure 4.5-Average values of Crest factor of the vibration signal for healthy and faulty gears.....</i>	<i>113</i>
<i>Figure 4.6-Spectrum of local vibration signals for healthy and faulty cases at low operating conditions</i>	<i>116</i>
<i>Figure 4.7-Spectrum of local vibration signals for healthy and faulty cases at high operating conditions</i>	<i>117</i>

LIST OF FIGURES

<i>Figure 4.8-First stage mesh frequency (f_{m11}) amplitude on gearbox casing for healthy and faulty cases and different operating.....</i>	<i>118</i>
<i>Figure 4.9-Second stage mesh frequency (f_{m21}) amplitude on gearbox casing for healthy and faulty cases and different operating conditions</i>	<i>119</i>
<i>Figure 4.10-Average amplitudes of two sidebands around f_{m11} on gearbox casing for healthy and faulty cases and different operating conditions</i>	<i>120</i>
<i>Figure 4.11 CWT of vibration measurements for healthy and faulty cases under low operating conditions</i>	<i>122</i>
<i>Figure 4.12-CWT of vibration measurements for healthy and faulty cases under high operating conditions</i>	<i>123</i>
<i>Figure 5.1-Stiffness of single pair of teeth.....</i>	<i>129</i>
<i>Figure 5.2-Meshing stiffness function for the pinion and the gear of the first pair ..</i>	<i>131</i>
<i>Figure 5.3-Two-stage gearbox models with torsional and vertical vibration of the first gear pair.....</i>	<i>134</i>
<i>Figure 5.4-Analysis procedure of gearbox dynamic performance</i>	<i>140</i>
<i>Figure 5.5-Angular speed for the input shaft.....</i>	<i>141</i>
<i>Figure 5.6-Predicted vibration waveform (a) and spectrum (b)</i>	<i>142</i>
<i>Figure 5.7-Measured vibration waveform (a) and spectrum (b).....</i>	<i>143</i>
<i>Figure 5.8-Predicted spectrum of the vertical acceleration of position one and two of healthy gear.....</i>	<i>144</i>
<i>Figure 5.9-Predicted spectrum of the vertical acceleration of position one and two of faulty gear</i>	<i>145</i>
<i>Figure 5.9(a)-Sidebands around the 1st meshing frequency (f_{m11}).....</i>	<i>145</i>
<i>Figure 5.10-Measured spectrums of gearbox casing and motor casing for Healthy gear.....</i>	<i>145</i>
<i>Figure 5.11-Measured spectrums of gearbox casing and motor casing for faulty gear.</i>	<i>146</i>
<i>Figure 5.11(a)-Sidebands around the 1st meshing frequency (f_{m11}).....</i>	<i>146</i>
<i>Figure 5.12-Predicted (Left) and measured (Right) amplitude values of the 1st stage meshing frequency on Position 1 and gearbox casing at different gear operating conditions</i>	<i>148</i>

LIST OF FIGURES

<i>Figure 5.13-Predicted (Left) and measured (Right) amplitude values of the 1st stage meshing frequency on position 2 and motor casing at different gear operating conditions</i>	<i>149</i>
<i>Figure 5.14-Predicted (Left) and measured (Right) spectral feature on position 1 and gearbox casing at different gear operating conditions</i>	<i>150</i>
<i>Figure 5.15-Predicted (Left) and measured (Right) spectral feature on position 2 and motor casing at different gear operating conditions</i>	<i>151</i>
<i>Figure 6.1-Time domain (Left) and angular (Right) waveforms for a healthy and faulty gear cases at low operating conditions</i>	<i>156</i>
<i>Figure 6.2-Time domain (Left) and angular (Right) waveforms for a healthy and faulty gear cases at high operating conditions.....</i>	<i>157</i>
<i>Figure 6.3- Average peak values with and without TSA for healthy and faulty gears under different operating conditions</i>	<i>160</i>
<i>Figure 6.4-Average RMS without (left) and with (right) TSA for healthy and faulty gears under different operating conditions</i>	<i>161</i>
<i>Figure 6.5-Average values of Kurtosis without (left) and with (right) TSA for healthy and faulty g under different operating conditions</i>	<i>162</i>
<i>Figure 6.6- Average values of Crest factor before (left) and after (right) TSA for healthy and faulty gears under different operating conditions.</i>	<i>163</i>
<i>Figure 6.7-Conventional spectra for healthy and faulty gears under low operating condition</i>	<i>165</i>
<i>Figure 6.8- Order spectra of healthy and faulty gears under low operating condition</i>	<i>166</i>
<i>Figure 6.9-Conventional spectra for healthy and faulty gears under high operating condition</i>	<i>167</i>
<i>Figure 6.10- Order spectra of healthy and faulty gears under high operating condition</i>	<i>168</i>
<i>Figure 6.11-TSA mesh frequency (f_{m11}) amplitude of the gearbox casing for healthy gears and different operating conditions</i>	<i>170</i>
<i>Figure 6.12- TSA spectral features of the gearbox casing for healthy faulty gears at different operating conditions</i>	<i>171</i>

LIST OF FIGURES

<i>Figure 6.13- CWT (left) and CWT of TSA (right) of vibration measurements for healthy and faulty gear cases at low operating conditions.</i>	173
<i>Figure 6.14- CWT (left) and CWT of TSA (right) of vibration measurements for healthy and faulty gear cases at high operating conditions</i>	164
<i>Figure 7.1-Single input multiple output system analysis</i>	181
<i>Figure 7.2-Test rig and shaker position</i>	181
<i>Figure 7.3-Schematic diagram of the shaker test setup.....</i>	182
<i>Figure 7.4-FRF Amplitudes at 802.5Hz</i>	184
<i>Figure 7.5-FRF Amplitudes at 325Hz</i>	184
<i>Figure 7.6-Typical distributions of FRF amplitudes in low frequency range</i>	185
<i>Figure 7.7-Typical distributions of FRF amplitudes in high frequency range.....</i>	186
<i>Figure 7.8-Comparison of FRF measured from gearbox casing and motor flange ..</i>	186
<i>Figure 7.9-Frequency spectra at 50% speed obtained (a) from the signal obtained from the gearbox casing and (b) obtained from the motor flange.....</i>	187
<i>Figure 7.10-Frequency spectra at 100% speed obtained (a) from the signal obtained from the gearbox casing and (b) obtained from the motor flange.....</i>	188
<i>Figure 7.11-Comparison of vibration amplitudes around meshing frequency.....</i>	188
<i>Figure 8.1-Angular vibration waveform for healthy and faulty gear systems under low high and operating conditions</i>	192
<i>Figure 8.2-Average of peak values of the vibration signal for healthy and faulty gears</i>	194
<i>Figure 8.3-Average values of RMS of TSA vibration signal for healthy and faulty gears.....</i>	195
<i>Figure 8.4-Average values of Kurtosis of TSA vibration signal for healthy and faulty gears.....</i>	197
<i>Figure 8.5-Average values of Crest factor of TSA vibration signal for healthy and faulty gears</i>	198
<i>Figure 8.6-TSA spectrum of signals for healthy and faulty cases at low operation conditions</i>	199
<i>Figure 8.7-TSA spectrum of signals for healthy and faulty cases at high operation conditions</i>	200

LIST OF FIGURES

<i>Figure 8.8- Order 34 amplitudes on the gearbox casing (left) and the motor flange (right) for healthy and faulty gear conditions at different operating conditions</i>	<i>203</i>
<i>Figure 8.9- Feature one amplitudes on the gearbox casing (left) and motor casing (right) for healthy and faulty cases under different operating conditions</i>	<i>205</i>
<i>Figure 8.10- Feature two amplitudes on the gearbox casing (left) and motor casing (right) for healthy and faulty gear cases under different operating conditions</i>	<i>207</i>
<i>Figure 8.11-CWT of TSA vibration signal from gearbox casing and motor flange for healthy and faulty gears under low operating condition</i>	<i>209</i>
<i>Figure 8.12-CWT of TSA vibration signal from gearbox casing and motor flange for healthy and faulty gears under high operating condition (80% load and 100% speed)</i>	<i>210</i>

LIST OF TABLES

<i>Table 1.1 Common parameters used as indicators of machine condition</i>	<i>33</i>
<i>Table 1.2 Types and function of spur and helical gears</i>	<i>39</i>
<i>Table 2.1 Comparison of different time-frequency techniques</i>	<i>68</i>
<i>Table 3.1 Gearbox design data</i>	<i>78</i>
<i>Table 3.2 Control panel functions</i>	<i>82</i>
<i>Table 3.3 Healthy tooth meshing frequencies and their harmonics</i>	<i>93</i>
<i>Table 5.1 Main parameters of the gear transmission system</i>	<i>139</i>

LIST OF NOMENECLATURE

Acronyms

CM	Condition monitoring
RM	Reactive maintenance
PM	Preventive maintenance
CBM	Condition based maintenance
PV	Peak value
RMS	Root mean square
CF	Crest factor
FT	Fourier transforms
FFT	Fast Fourier transforms
STFT	Short-time Fourier transforms
WVD	Wigner-Ville distribution
WTs	Wavelets transform
CWT	Continuous Wavelet transforms
TSA	Time synchronous averaging
DC	Direct current
AC	Alternating current
<i>A</i>	Ampere
Hz	Hertz
kW	kilo-Watt
kHz	kilo-Hertz

LIST OF NOMENECLATURE

F	Force
m	Mass
a	Acceleration
ICP	Integrated circuit piezoelectric
IAS	Instantaneous Angular Speed
DAQ	Data acquisition card
DAS	Data acquisition system
PC	Personal computer
ADC	Analog digital convertor
V	Volt
μ V	micro-Volt
Nm	Newton-meter
RPM	Revaluation per min
S/N	Signal to noise ratio
L	Load
S	Speed
DOF	Degree of freedom
SDOF	Single degree of freedom
MDOF	Multiple degree of freedom
GDM	Gear dynamic models
IC	Integrated circuit
FRF	Frequency response function
OT	Order tracking

LIST OF NOMENECLATURE

Symbols

R_s	Speed reduction ratio
Z_1	Number of teeth on the pinion gear at the 1 st stage
Z_2	Number of teeth on the driven gear at the 1 st stage
Z_3	Number of teeth on the pinion gear at 2 nd stage
Z_4	Number of teeth of the driven gear at 2 nd stage
f_m	Tooth meshing frequency
$x_{vib}(t)$	Gear mesh vibration
k	Number of mesh frequency harmonics
A_k	Amplitude of harmonics
φ_k	Phase of Harmonics
$w(t)$	Noise signal
$a_k(\theta)$	Amplitude modulating function
$b_k(\theta)$	Phase Modulating Function
$y(t)$	Average vibration signal
f_r	Shaft rotation frequency
N_T	Number of teeth on the gear
m	Meshing harmonic number
k	Integer number
N	Number of samples taken in the signal
\bar{x}	Mean Value of the N amplitudes

LIST OF NOMENECLATURE

$x(n)$	Amplitude of the signal for the n^{th} sample
x_i	Amplitude of the signal for the i^{th} sample
f_{m11}	Mesh frequency of the 1 st gear pair
f_{m12}	2 nd harmonic of mesh frequency of the 1 st gear pair
f_{m21}	Mesh frequency of the 2 nd Gear Pair.
f_{m22}	2 nd harmonic of mesh frequency of the 2 nd gear pair.
$g(t)$	Sliding window function
$W(t, f)$	Wigner-Ville Distribution function
$W_{12}(t, f)$	Cross-Wigner distribution
A_1, A_2	Amplitudes of the signals f_1 and f_2
τ	Time to perform a “time-localized” Fourier transform
$*$	Complex conjugate
w^*	Complex conjugate of the analyzing wavelet $w(t)$
s	scale or dilation factor
u	Shift or translation parameter
$w(f)$	Fourier transform of the wavelet $w(t)$
ω_0	Frequency parameter
f_0	Frequency at which the window is cantered in the frequency domain for a given scale s
ε_c	Contact ratio

LIST OF NOMENECLATURE

ε_a	Overlap ratio
f_{sup}	Supply frequency,
p	Number of pole pairs
s_l	Slip
$^{\circ}\text{C}$	Degree centigrade
Δ_t	Time interval between two samples
f_s	Sampling frequency
f_{max}	Nyquist frequency
T	Period of rotation of the pinion shaft
$k(t)$	Mesh stiffness
f_{r1}	1 st shaft rotational frequency
f_{SD}	Sidebands Frequency
f_{r2}	2 nd Shaft Rotational Frequency
f_{r3}	3 rd Shaft Rotational Frequency
I_m	Moment of inertia for electric motor
I_l	Moments of inertia for the load system
I_{p1}	Moments of inertia of gear one (pinion1) in the first stage
I_{g1}	Moment of inertia of gear 2 in the first stage
I_{p2}	Moment of inertia of gear one (pinion2) in the second stage
I_{g2}	Moment of inertia of gear 2 in the second stage
F_1	First stage gearing stiffness force

LIST OF NOMENECLATURE

F_2	Second stage gearing stiffness force
F_{1t}	First stage gearing damping force;
F_{2t}	Second stage gearing damping force
M_m	Input motor torque
M_1	Internal moments in first shaft
M_{1t}	Coupling damping in first shaft
M_2	Internal moment in second shaft
M_{2t}	Coupling damping in second shaft
M_3	Internal moments and coupling damping in third shaft
M_{3t}	Coupling damping in third shaft
ϕ_1	Angular displacement of load system
ϕ_2	Angular displacement of gear one (pinion) in 1 st stage
ϕ_3	Angular displacement of gear two in 1 st stage
ϕ_4	Angular displacement of gear one (pinion) in 2 nd stage
ϕ_5	Angular displacement of gear two in 2 nd stage
ϕ_6	Angular displacement of load system
r_{p1}	Base circle radius of gear one in the 1 st stage
r_{g1}	Base circle radius of gear two in the 1 st stage
r_{p2}	Base circle radius of gear one in the 2 nd stage
r_{g2}	Base circle radius of gear two in the 2 nd stage
y_p	Vertical displacement of the pinion in the 1 st stage
y_g	Vertical displacement of the gear in the 1 st stage

LIST OF NOMENECLATURE

y_{c1}	Vertical displacement of upper casings
y_{c2}	Vertical displacement of lower casings
m_{p1}	Mass of the pinion in the 1 st stage
m_{g1}	Mass of the gear in the 1 st stage
m_{p2}	Mass of the pinion in the 2 nd stage
m_{g2}	Mass the of the gear in the 2 nd stage
m_{c1}	Mass of the upper casing
m_{c2}	Mass of the lower casing
$c_{p\setminus}$	First stage pinion shaft damping
$c_{g\setminus}$	First stage gear shaft damping
$c_{1\setminus}$	Shaft one damping
$c_{2\setminus}$	Shaft two damping
$c_{3\setminus}$	Shaft three damping
$c_{z1\setminus}$	First stage gearing damping
c_{z2}	Second stage gearing damping;
$c_{c1\setminus}$	Upper casing support damping
$c_{c2\setminus}$	Lower casing support damping
$k_{p\setminus}$	First stage pinion shaft stiffness
$k_{g\setminus}$	First stage gear shaft stiffness
$k_{1\setminus}$	Shaft 1 stiffness (rotational stiffness)
$k_{2\setminus}$	Shaft 2 stiffness
k_3	Shaft 3 stiffness

LIST OF NOMENECLATURE

k_{z1}	First stage gearing stiffness (meshing stiffness)
k_{z2}	Second stage gearing stiffness;
k_{c1}	Upper casing support stiffness
k_{c2}	Lower gearing support stiffness
ζ	Damping ratio
s	Second
$F(\omega)$	Fourier transform of the input force
$X(\omega)$	Fourier transform of the output force
H_{ij}	Frequency response function between DOF j and i
X_j	Input spectrum
Y_i	Output spectrum

ACKNOWLEDGEMENTS

ACKNOWLEDGEMENTS

First and foremost, all thanks and praises are due to ALLAH (God) the Almighty for his blessing that made this work possible and to be completed on time.

Secondly, I would like to express my sincere thanks (with an honorary bow) to **Prof Andrew Ball** and **Dr Fengshou Gu**, my academic supervisors, for their guidance and support. Their very active part in initiating this work, and their valuable suggestions during all its phases were indispensable. Special thanks for their help in reviewing and his constructive comments and continuous support during the preparation of this thesis. They are also a source of inspiration throughout my study in the University of Huddersfield in my academic life. The completion of this work owes much to his valuable and endless assistance. To all their present and future students - you are very fortunate.

Many thank to my families for their emotional support and encouragement especially my mother for her support and substantial encouragements from the time I was in my primary school till now. By no means least, my special thanks to my wife: **Nawal** and my children: **Abdulrahman**, **Alfarok**, **Omnia**, **Emtenan** and **Menat Allah**, for their support, encouragement and patience over the last years. I promise you to make amends for the past years with much fun in the coming years.

I would like to acknowledge my fellow research students for their many and interesting conversations, in particular: **Mr Barno Ragarjo**, **Mr Shokri Alghawal**, **Mr Mahmoud Belgasem** and **Mr Monsef Haram**.

The time I spent in the United Kingdom; the 5 years at University of Huddersfield (PhD 2007-2012) will always be in my memory.

LIST OF PUBLICATIONS

- ❖ Al-Arbi, S., Talbot, C., Wang, T., Fengshou, G. and Ball, A. (2010) 'Characterization of vibration transmission paths for gearbox condition monitoring'. In: Inter noise 2010 39th International congress on Noise Control Engineering, 13-16 June 2010, Lisbon, Portugal
- ❖ Al-Arbi, S., Fengshou, G., Guan, L., Fan, Y. et al., "Gearbox Fault Diagnosis Based on Continuous Wavelet Transformation of Vibration Signals Measured Remotely," SAE Technical Paper 2010-01-0899, 2010, doi: 10.4271/2010-01-0899.
- ❖ Al-Arbi, S., Gu, F., Guan, L., Ball, A. and Naid, A. (2009) 'Gearbox Fault Diagnosis based on Vibration Signals Measured Remotely' Key Engineering Materials, 413-41, pp. 175-180. ISSN 1013-9826
- ❖ Al-Arbi, S., Gu, F., Guan, L. and Ball, A. (2009) 'Remotely gear condition monitoring using traditional signal processing techniques'. In: Proceedings of Computing and Engineering Annual Researchers' Conference 2009: CEARC'09. Huddersfield: University of Huddersfield. pp. 111-117. ISBN 9781862180857.

CHAPTER 1

INTRODUCTION

This chapter starts by presenting the motivation for choosing this particular topic for research. It provides a brief description of conventional condition monitoring techniques followed by a review of condition monitoring of a gearbox and explains why vibration methods have been chosen as a suitable technique for research into the detection and diagnosis of gear faults. Finally, the aim and research objectives are given in detail and the chapter ends by describing the thesis content and layout.

1.1 Research Motivation

A large amount of research has been carried out into the condition monitoring (CM) of gearboxes, but it is a fact that remote gearbox monitoring under different operational conditions (different load and speed) has not been studied in depth. Most of the published research either investigates CM at constant load and speed with a sensor usually located on the gearbox casing, while others do not include details of the measurement positions and/or conditions [1,2,3,4]. This research will attempt to use the vibration signals collected from different locations under different load conditions and shaft speeds to investigate the condition of the gearbox. The effect of transmission path on the vibration signal will be investigated by recording and comparing vibration signals at different locations (e.g. gearbox casing and motor casing). The effect of operational conditions on the vibration signals will be examined by recording vibration signals at different shaft speeds, from 20% to 100% full speed and at different loads ranging from 0% load to 80% of the full load.

1.2 Background

Machine CM helps ensure the reliability and low-cost operation of industrial facilities [5]. CM can provide early detection of machine faults so that appropriate action can be taken before that fault causes breakdown and, possibly, a catastrophic failure. Continuous CM allows a machine repair and maintenance to be planned, which should improve economical operation and reduce possible harmful emissions. Many technologies have been used to enhance the applicability, accuracy and reliability of CM systems [6].

Run-to-failure is a maintenance strategy which is now widely discredited for many process and manufacturing operations as it is relatively uneconomical. Alternative CM systems, based on the collection and analysis of real-time machine data, have become more widely used and acceptable because of their ability to provide early detection of machinery problems [7]. Selecting the most appropriate CM system is important to maximise machine availability, performance and life span, and minimise spare parts inventories and break down maintenance [8].

1.2.1 Maintenance Strategies and Condition Monitoring

1.2.1.1 The Importance of Maintenance

It has been estimated that US industry has spent more than \$300 billion a year on plant maintenance and repair, and the vast majority of this huge sum has been used to correct chronic and catastrophic failures of machines and systems [5]. Although chronic failures may be small and invisible, because they occur more frequently, they are more costly than catastrophic failures which, while dramatic and even fatal, are much rarer occurrences [5]. Both types of failure can cause severe disruption to work schedules, lower product quality, increase costs, and increase risk to machine operators. Downtime, because it can halt production, often exceeds maintenance costs by many magnitudes. Regular maintenance can reduce downtime by minimizing failures, and so increase productivity and improve operational safety.

The most common methods of managing maintenance operation and maintenance practice are reactive maintenance, preventive maintenance and predictive maintenance. Historically, industrial plant was maintained and repaired either when it developed a fault (reactive) or according to rigid and inflexible timetables. However, advances in computer technology have allowed many industries to implement responsive periodic time-based preventive maintenance strategies. By the 1990s, advances in technology enabled the development of cost-effective instrumentation and technologies for predictive maintenance, allowing the identification of machine problems by measuring the condition of the machine and predicting maintenance requirements.

1.2.1.2 Reactive Maintenance (RM) or Run to Failure

Reactive maintenance is adopted when no action has been taken until the machine has failed. This method can be appropriate depending on the size of the operation and the number of available maintenance staff. RM is a method that can be used if machine downtime is not important. Reactive maintenance can cause costly and unexpected downtime and maintenance costs, and possible secondary damage. It is the most expensive maintenance method because it has the highest rate of lost production and

expensive maintenance method because it has the highest rate of lost production and requires a large spare parts inventory to minimise downtime [9].

1.2.1.3 Preventive or Time-Based Maintenance (PM)

Preventive maintenance is where a machine or parts of a machine are serviced on a regular basis regardless of their condition [5]. This procedure requires replacement of parts after a certain fixed period of operation. Time based maintenance requires replacement of good parts along with worn parts, this has a double cost: the cost of the parts themselves and the down time required to replace those parts. Preventive maintenance is widely used and is the first level of maintenance beyond reactive maintenance. The main aim of preventive maintenance is to avoid unexpected catastrophic failures. One study has shown that a successful preventive maintenance program can provide a 30% reduction in maintenance costs relative to reactive maintenance [5].

1.2.1.4 Predictive or Condition-Based Maintenance (CBM)

Condition based maintenance is evolving rapidly and can be considered as a system that integrates all existing on-line monitoring schemes. The aim of condition-based maintenance is to eliminate machinery breakdown (especially catastrophic failure) by assessing the condition of the machine, identifying any problem, and enabling corrective action to be taken at a suitable time prior to any failure. This is possible because incipient machine problems invariably give some early warning of failure and condition-based maintenance can be performed while the system is in operation. Such a maintenance system will not only minimise machine downtime, but also facilitate efficient manpower scheduling, enable other repairs to be included into any downtime and allow ordering of replacement parts in advance. All of these factors are significant factors in reducing production costs.

1.3 Gearbox Condition Monitoring through Vibration Analysis

Due to the industrial importance of gears in power transmission systems, the effective CM of gearboxes is essential. There is constant pressure to improve measuring techniques and tools for the early detection and diagnosis of gearbox faults. The gears themselves are the most important elements in the gearbox, and the degree of wear

CHAPTER 1

INTRODUCTION

and fatigue to which they are subjected even under normal operating conditions means that they are often subject to premature failure. *Ma and Li* claim that up to two-thirds of gearbox failures are due to faults which develop in the gears, and almost all of these are due to localised defects such as fatigue induced fractures [10].

Increased demand for lower production and maintenance costs means that the CM of gear transmissions has become an important area of research. The severe conditions under which gears operate relative to other machine components, means that they deteriorate quite rapidly, especially their teeth [11]. *Fakhfakh et al* have defined three general types of gear defects that cause transmission error and gearbox failure: manufacturing defects (e.g. error in the tooth profile), installation defects (e.g. the alignment of the gears) and defects which occur during the work process (e.g. cracking of teeth) [11]. Sudden loading of the gear teeth during operation is the main factor causing fatigue cracks that appear at the root of the tooth and weaken the structural integrity of the gear.

Lin and Zuo have described tooth breakage as the most serious problem for gears because it can lead to complete failure of the gearbox [3]. Initially a fatigue crack at the base of a tooth will not be considered a serious problem, but as the crack propagates, damage will accelerate and may result in catastrophic tooth failure. If the crack can be detected and its development tracked, the gear can be replaced before the tooth breaks.

Much effort has gone into developing reliable methods for fault detection in gearboxes. Proven techniques include oil analysis [7], temperature distribution within the gearbox, the noise produced by the gearbox when in operation, motor current analysis [9] and, most popular today, vibration analysis [6]. Unfortunately, no single technique has been found that is able to detect all machine faults. Vibration measurement, which is the most widely used CM technique in industry, because of its proven ability to detect the early presence of faults, can identify only 60% to 70% of machine faults [12,13].

Vibration analysis is now usually performed online via a computer-based machine CM system and does not require shutdown of the machinery. Table 1.1 compares

CHAPTER 1

INTRODUCTION

vibration analysis against two simple monitoring parameters (temperature and oil analysis) which whilst not as powerful and versatile as vibration measurement, can be used to provide warning of an impending machine breakdown [14].

As the gear teeth mesh and rotate there will be periodic variations in torque and force, so that the primary vibration generated will be at the tooth meshing frequency [15].

However, because of frictional forces due to the rubbing together of surfaces there will also be a significant random component in the vibration signal. *Martin and Ismail* have shown that the amplitude of the vibration signal will be dependent on both the size of the forces and the physical properties and geometries of the gears themselves – thus depending on factors such as tooth stiffness, shaft misalignment, errors in profile and pitch, gear eccentricity and load on each tooth as a function of angle of rotation [15]

Table 1.1-Common parameters used as indicators of machine condition [14]

Machine Fault	Vibration	Temperature	Oil Analysis
Out of Balance	√		
Misalignment/Bent Shaft	√		
Damaged Rolling Element Bearing	√		√
Damaged Journal Bearing	√	√	√
Damaged or Worn Gears	√		√
Mechanical Looseness	√		

As the teeth mesh, the vibration will travel via the gear to the mounting shaft, to the bearings and to the gear casing where it is detected, usually by an accelerometer. As the vibration travels from the point of generation to the accelerometer on the gear casing it will be attenuated and contaminated by vibrations from a multitude of other sources. Thus the detected signal will usually need processing and, possibly, filtering.

Analysis of vibration signals is very appropriate for monitoring gearboxes because any change in the vibration signature of the gearbox is most likely a result due a change in gearbox condition. This is because as defects on a gear will alter both the amplitude and phase modulations of the gear's vibrations. Thus, any changes in vibration signal can be analyzed to provide an indication of possible faults [16, 17].

CHAPTER 1

INTRODUCTION

Most natural phenomena are non-linear and the majority of these signals have varying frequency content. The vibrations of multi-stage gearboxes contain non-stationary transients, e.g. the short periodic impulsive components produced by impacts between components. Typically, vibration signals generated in gearboxes will contain three main components, (1) periodic components such as those resulting from interactions between the gears during meshing, (2) transient components caused by short duration events, such as repeated impacts due to a tooth having broken off, and (3) broad-band background noise. In the early stages of damage and fault initiation, the resulting low amplitude vibration signal will be masked by other sources present in the gearbox and cannot therefore be used directly for damage detection. However, it is precisely at this stage that detection of these faults is important. As a result, more effective signal processing methods are required to better analyse vibration measurements and more reliable gearbox condition monitoring and health diagnosis.

Analysis of the time-domain signal uses statistical parameters such as peak value, root mean square (RMS), kurtosis and Crest factor (CF) and their use is well established in assessing the condition of gears [16]. *Stevens et al* have claimed that these measures are suitable for detection and diagnosis when mechanical faults take the form of impulses which impose periodic pulses of short time duration (wide frequency bandwidth) onto the base vibration signal [18].

However, the most common method used for detection and diagnosis of gear failure is spectral analysis of the vibration signal in the frequency-domain. This is because the most important CM elements in the vibration spectra of gears are: the tooth meshing frequency, harmonics and sidebands (due to modulation phenomena) located on either side of the gear tooth meshing frequency. The sidebands are separated by integer multiples of the gear rotation frequency. The behaviour of these sidebands can be strongly indicative of the presence of a fault, e.g., through an increase in the number of sidebands and their relative amplitudes. *Randall* found that the first three gear meshing harmonics and their sidebands provided sufficient information for gear fault identification [19].

Thus tracking and monitoring changes in the amplitude of particular sidebands in the spectrum can provide a good predictor of gear failure. In practice, it is often difficult

to extract meaningful information from vibration spectra based on a simple Fourier Transform (FT) of time-domain to frequency-domain. In the early stages of fault development, important defining frequencies have low amplitude and can be masked by other vibration sources or buried in background noise [20]. This is particularly relevant because the individual vibration impulses generated by gear defects typically tend to be of short duration causing the corresponding frequency pulse to spread over a wide frequency band with low amplitude [19]. It can also be very difficult to identify a particular frequency indicative of a defect when a large number of spectral components are present.

Today, combined time and frequency analysis is increasingly used in gear fault diagnosis and is gradually replacing conventional time-domain analysis and frequency-domain analysis. Representing the signal in the time and frequency-domains simultaneously is a powerful tool for examining non-stationary vibration signals and the results can be easily interpreted. *Wang and McFadden* claim that it is relatively easy to characterise the local features of the signal, and all distinctive components in the frequency range of interest, their sequences causality and changes with time can be displayed on a single chart [21].

During the past twenty years, a number of time-frequency signal processing techniques have proved to be suitable for analysis of vibration signals and have gained acceptance in the field of CM [22]; such approaches as the Short-Time Fourier Transform (STFT) [21], Wigner-Ville Distribution (WVD) [23] and Wavelet Transforms (WTs) [24,25, 26] are widely used. *Peng and Chu* have claimed that the WT technique has proved eminently suitable for analysis of vibration signals because most signals contain instantaneous impulse trains and other elements which are transient and non-stationary in nature [26]. The WT decomposes a signal into different frequencies with different resolutions i.e. it provides time-scale (frequency) representation of a signal [25].

1.4 Gear Types and their Operation

Helical, spur, bevel and worm gears are the most common types of gears used in industry [27]. All have a driven wheel and a driving wheel, but differ in the arrangement and shape of the wheels. Spur gears, Figure 1.1, have teeth that are

CHAPTER 1

INTRODUCTION

normal to the face of the gear (parallel to the shaft) and cannot be used where a change of direction between two shafts is required [28].



Figure 1.1-Spur gear [29]

A helical gear, Figure 1.2, has similarities with the spur gear but the teeth are at an angle to the shaft and the teeth form part of a helix. The teeth on a helical gear are therefore longer than the teeth on a spur gear of equivalent width. Helical gears run more smoothly but are more expensive than spur gears so they tend to be used less frequently. They are also slightly less efficient than a spur gear of the same size [28]. At any instant, the load on a helical gear is distributed over a larger tooth area than for spur gears which means less wear, and because of the more gradual engagement of the teeth during meshing there is less noise and less vibration than spur gears.



Figure 1.2-Helical gear [30]

Because the teeth on a helical gear are not parallel to the shaft, during operation there is a thrust along the gear shaft which requires thrust bearings to absorb the thrust load and maintain gear alignment [31]. Helical gears can transfer power between shafts

CHAPTER 1

INTRODUCTION

that are at an angle other than 90° to each other [32].

Helical gear boxes can provide reduction ratios of between 3 and 500, though the higher ratios require the use of multiple stages [33].

The bevel gear, Figure 1.3, is often used to transfer power from one shaft to another when shafts are at 90° . The teeth of these gears are formed on a conical surface and normally the two shafts would be at right angles to each other and “intersect” at the apex of the cone. Bevel gears have teeth that are cut straight, and are all parallel to the line pointing to the apex of the cone on which the teeth are based. However, they cannot be used for parallel shafts and can be noisy at high speeds [28].

Worm gears, Figure 1.4, can be used to drive spur or helical gears and allow two non-intersecting and perpendicular shafts to mesh. An important aspect of worm gear meshes is their irreversibility.



Figure 1.3-Bevel gear [34]

When a worm gear turns, the meshing spur also turns, but turning the spur will not turn the worm gear. The result is a ‘self-locking’ mechanism useful for ratcheting [28]. Worm gears can tolerate large loads and can be used to convert rotational motion to translational motion. In addition, worm gears can have a very large pitch diameter [28].

Gears tend to operate with the teeth of one engaging the teeth of another to transmit power without slippage. When the teeth are meshed, driving one gear (e.g. with an electric motor) will force the other to turn, transmitting power but allowing the rotational speed and direction of rotation to be changed.



Figure 1.4-Worm gear [29]

The gear with the fewer teeth is called the pinion. The speed of rotation is increased when the gear drives the pinion, and reduced when the pinion drive the gear. The speed reduction ratio R_s is given by:

$$R_s = \frac{z_1}{z_2} \quad (1.1)$$

where: z_1 is the number of pinion teeth and z_2 is the number of gear teeth.

CHAPTER 1
INTRODUCTION

Table 1.2 lists properties of the most common types of gears: spur and helical.

Table 1.2-Types and Function of Spur and Helical Gears

Gear type	Sub-type	Comments
Spur gears	Normal Spur Gears	<ul style="list-style-type: none"> ➤ The most common; relatively easy to design and make. ➤ Parallel shafts. ➤ High efficiency; up to 99% per train. ➤ No side thrust. ➤ Can back drive. ➤ Single ratio up to 1:10. ➤ Produce low vibration and noise with accurate design. ➤ Steel pinions require lubrication, plastic do not.
	Internal Spur Gears	<ul style="list-style-type: none"> ➤ Similar performance to normal spur gears. ➤ Results in compact drive geometry. ➤ Commonly used in manufacture of epicyclic/planetary gears.
Helical gears	Single Helical Gears	<ul style="list-style-type: none"> ➤ Have similar properties to spur gear, but drive results in axial thrust. ➤ Gears are smoother and quieter for the same size/specification. ➤ The gears can run at high speeds up to large diameters. ➤ Higher torque/ life capabilities for same size as spur gears
	Double Helical	<ul style="list-style-type: none"> ➤ Similar benefits to single helical but with no generated side thrust. ➤ Gives higher performance than single helical.
	Crossed-Helical	<ul style="list-style-type: none"> ➤ Shaft at 90°. ➤ Difficult to make accurately ➤ Smooth drive

1.5 Gear Failures

Gear failures tend to occur when a gear is working under high stress conditions [35, 36, 37]. Local faults are the more dangerous because they tend to develop rapidly once initiated, and usually have significant effects on power transmission. If not detected early there can be dramatic consequences with tooth breakage, pitting and scoring are the most important local faults.

Tooth breakage: is the most dangerous type of gear failure and leads to disablement of the drive and often damage of other gearbox components such as the shaft, bearing, etc, by pieces of the broken tooth. As shown in Figure 1.5 tooth breakage can be due to overload and/or impact and damage. However, the most common cause bending fatigue due to repetitive loads on the gear teeth. These usually begin with a small crack which spreads until part or the entire tooth breaks off. The remnants of the remaining tooth will have greater impact loading and be prone to further breakage [28]. This research will emphasise the progression of a fault in a single tooth.

Pitting is a surface fatigue failure of the gear tooth. It occurs when contact stress is greater than the fatigue tolerance limit and typical tooth pitting damage is shown in Figure 1.6. After a certain period of operation with repeated variation of the load, small areas of metal on the tooth surface fatigue and drop off. Once pitting has occurred it tends to spread at an accelerating rate because the un-pitted areas which remain must support the extra load previously carried by the damaged area.

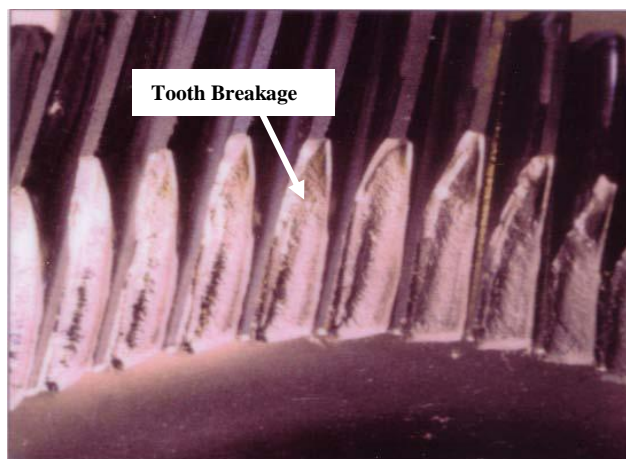


Figure 1.5-Tooth Breakage [38]

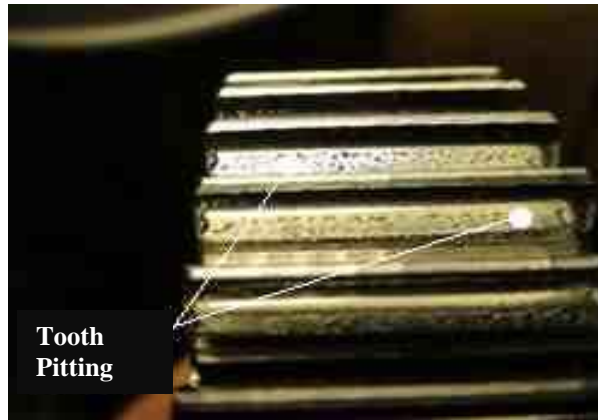


Figure 1.6-Tooth Pitting [38]



Figure 1.7-Tooth Scoring [38]

Scoring: inadequate or unsuitable lubrication, overloading and misalignment can all cause the lubricant film to break down and allow direct metal-to-metal contact as shown in Figure 1.7. The result can be very high temperatures and local welding of mating surfaces. These welded spots break away as the gear rotates causing other problems elsewhere.

With distributed faults there is a significant, possibly substantial, delay between failure initiation and complete loss of service. These faults tend to progress slowly and the gear can still transmit power as the fault develops.

A typical distributed gear fault is tooth wear as shown in Figure 1.8. Wear occurs when layers of metal are removed more or less uniformly from the surface and can take two forms:

Adhesive Wear: characterized by transfer of metal particles from one tooth to its mating tooth by welding action.

Abrasive Wear: caused by to abrasive particles in the meshing area.



Figure 1.8-Tooth Wear [38]

Other distributed gear defects include surface inaccuracy and misalignment.

Both localized and distributed gear faults generate transmission errors and increase vibration levels of the machinery. Localized defects are more important from the CM point of view, especially tooth breakage which can occur with little warning and cause catastrophic failure in machines such as helicopters [1, 39]

1.6 Gear Vibration and Modulation

Nowadays, vibration measurement is the most common technique for monitoring the condition of gear transmission systems. Signals from accelerometers mounted on gearboxes have a distinct frequency spectrum dependent on internal meshing dynamics. Since the gear transmission system is periodic, its spectrum contains components at shaft frequencies and associated harmonics, as well as the fundamental gear mesh frequencies and harmonics. These are considered the regular components of the system.

Ideally, in the absence of defects, gear systems are dominated by the regular component and the Gaussian noise floor resulting in smooth and uniform power transmission and angular motion. Any deviation from the ideal causes variation in the transmitted power which results in a fluctuating force between the meshing teeth [40].

CHAPTER 1

INTRODUCTION

Even when the gear speed and load are constant there can be a varying force on the gear. If the teeth on a pair of meshing gears are not perfectly rigid, the contact stiffness will vary periodically both with the number of teeth in contact and the position of contact on the tooth surface. The varying force will excite a vibration at the tooth meshing frequency [41].

The resulting vibration signal [42] may be approximated in terms of tooth meshing frequency f_m and its harmonics using.

$$x_{vib}(t) = \sum_{k=0}^K A_k \cos(2\pi k f_m t + \varphi_k + w(t)) \quad (1.2)$$

where: $x_{vib}(t)$ is the gear mesh vibration,

f_m is the tooth mesh frequency ($f_m = \text{no. of teeth} * \text{shaft rotational frequency}$).

k is the number of mesh frequency (f_m) harmonics considered.

$w(t)$ is the noise which is assumed to have a normal distribution.

A_k and φ_k are the amplitude and phase of the k^{th} harmonics,

Manufacturing errors in tooth spacing, tooth profile, alignment, as well as gear faults (such as local defects) all reduce the meshing stiffness and generate variations in both amplitude and phase of the tooth mesh vibrations [41].

The variation can be approximated by modulating amplitude and phase functions $a_k(t)$ and $b_k(t)$, and these modulating functions are also periodic with the shaft frequency and can be written as:

$$a_k(t) = \sum_{k=0}^{\infty} A_k \cos(2\pi f_s k t + \alpha_k)$$

$$b_k(t) = \sum_{k=0}^{\infty} B_k \cos(2\pi f_s k t + \beta_k)$$

where: B_k is the amplitudes of k^{th} harmonic.

α_k and β_k are the phase.

CHAPTER 1

INTRODUCTION

The shaft frequency is given f_s . For amplitude modulation, the sidebands represent a scaled version of the frequency spectrum of the modulating function

Introducing these modulations into Equation 1.2 we have:

$$y(t) = \sum_{k=0}^K A_k [1 + a_k(t)] \cos(2\pi k f_m t + \varphi_k + b_k(t) + w(t)) \quad (1.3)$$

Equation (1.2) demonstrates that detecting errors in the gear system is possible by analyzing the sideband activity of the signal. For example, an eccentric shaft gives a slight change in centre distance between gears every cycle. This is apparent as a once-per-revolution fluctuation in mesh force produces an amplitude modulation signal that results in sidebands spaced at the shaft frequency. Other contributors to amplitude modulation are tooth profile errors, and broken teeth. In addition, the relative relationship between the gears and sensors also creates sidebands. The modulation can often be seen as a lobe pattern in the data associated with the gear system.

1.7 Characteristics of Gearbox Vibration

To use vibration effectively and efficiently to monitor the condition of gear transmission systems it is necessary to understand the more important characteristics of the vibration generation, especially if remote model-based CM is to be used.

Welbourn has suggested that the main sources of gearbox vibrations are geometric errors: the difference between the actual orientation and position of a gear and the orientation and position it would have if the gear drive was positioned perfectly [43]. Imperfections (errors) in the gears during manufacture will also be a source of vibration as will the elastic deformation of the gear teeth as they mesh. The fundamental frequency of the transmitted vibration is the gear mesh frequency. There will also, of course, be multiple harmonics. Importantly for CM of gears there will be sidebands to these frequencies which are separate from the gearbox shaft frequency. *Randall* [19]. in his classical work on gear vibration, classified the vibrations generated by gear meshing as being caused by

- 1) deviations from the ideal tooth profile producing a vibration signal at f_m , the tooth-meshing frequency,

- 2) variations in tooth loading which generate amplitude modulation,
- 3) fluctuations in the rotational speed, and/or non-uniform tooth spacing which produce frequency modulation effects, and
- 4) local tooth faults which generate additional impulses

1.7.1 Gear Meshing Vibration

During real gear meshing the load and its direction on the tooth vary with time, causing tooth deflection to also vary [44]. This produces the dominant vibration at the gear meshing frequency, f_m , and its harmonics.

$$f_m = N_T \cdot f_r \quad (1.4)$$

Where; N_T is the number of teeth on the gear and f_r is the shaft rotation frequency. This basic signal will be modulated in amplitude and phase due to imperfection in the gears and teeth such as eccentricity. This modulation appears as sidebands either side of the gear meshing frequency (and the harmonics) in the vibration spectrum, and is separated from them by multiples of the modulating frequency [45] In fact there will be a number of modulation frequencies and determination of these is often very useful in diagnosis of faults. Even the vibration signal generated by healthy gears will contain harmonics and sidebands of the gear meshing frequency.

Thus the sideband frequencies will be:

$$f_{SD,mk} = m \cdot f_m \pm k \cdot f_r \quad (1.5)$$

Where: m is the number of the meshing harmonic, and k is an integer [19].

1.7.1.1 Deviation from the Ideal Tooth Profile

Real gear teeth will invariably deviate from the ideal tooth profile. This will be due to, amongst other things: wear, geometric errors in manufacture and elastic deformation on loading.

- Tooth Wear (Due to Sliding Action)

CHAPTER 1

INTRODUCTION

As gear teeth mesh there is a sliding of the face of one tooth over the face of the other which produces non-uniform wear over the profile of the tooth, which eventually distorts both profiles.

If the wear is uniform over all the teeth on the gear, there will be a regular deformation at the tooth meshing frequency, producing vibration at that frequency and its harmonics. The greater the wear the greater the amplitudes of the gear meshing harmonics, especially at the higher harmonics [19, 46].

- Manufacturing Errors

During gear manufacturing, small profile errors on the gear teeth can be created, and these errors can be considered as a mean error component which will be identical for all gear teeth. Small errors in the profile of the gear tooth can be generated during manufacture and these errors will produce vibration at the tooth meshing frequency and its harmonics. These small errors will vary slightly - possibly randomly - from tooth to tooth and contribute a slightly different vibration from tooth to tooth. Although the vibrations will vary from one tooth to another, for each tooth they will have a period equal to that of the gear rotation. Since gears are subject to stringent quality checks this source will, at least initially, produce low amplitude vibrations but with a large number of harmonics of the frequency of rotation of the gear shaft.

- Tooth Deflection under Load

As with any elastic metal component, a gear tooth will be subject to deflection under the action of a force or load. The tooth flanks (sides of the tooth between the centre line and the base of the tooth) are subject to dynamic loads, the pattern of which give rise to a deflection in the tooth with a step-like form [47].

The resulting vibration signal will have the appearance in the time domain of a series of pulses, occurring at intervals equal to the period of the tooth meshing frequency. It is well known that the corresponding frequency-domain representation of such a signal is a strong fundamental at the tooth meshing frequency with a series of harmonics on either side. The amplitudes of the harmonics will be determined by the

nature of the shape of the repeated pulse. The amplitude of the fundamental will be a function of the load [48].

Modification to the tooth profile might be considered a possible solution to reducing these vibration issues and this approach is sometimes used but will only be effective at the design load. For loads below and above this value higher vibration amplitudes can be produced. As a consequence, in CM it is important that vibration measurements are always be based on the same load and this load should be enough to ensure that the tooth is always in contact with the meshing gear and to ensure that there is no backlash [46, 49].

1.7.2 Modulation Effects

1.7.2.1 Tooth Loading Effect on Amplitude Modulation

If the load fluctuates during gear meshing then the amplitude of the vibration should vary accordingly. Faults which give rise to amplitude modulation are generally categorized by the time-domain pattern of the fault vibration signal, for example:

Localized faults such as pitting of the tooth would produce a short pulse whose duration is similar to that of the tooth-mesh period, and with periodicity equal to that of the gear.

Distributed faults such as eccentricity of a gear would produce a continuous modulation at a frequency corresponding to the rotational speed of the gear.

1.7.2.2 Speed Fluctuation Effects on Frequency Modulation

Fluctuations in tooth contact load will not only cause amplitude modulation of the vibration signal, it will also feed back to the drive (even back to the electric motor driving the system) and cause variations in the rotation speed of the gears themselves. This will cause modulation of the meshing frequency. This can be interpreted as an additional inertia on the frequency modulation of the rotating elements and affects the amplitude modulation [44]. It has been found that the higher the inertial effect, the more frequency modulation effects will be reduced.

1.7.3 Additive Impulses

Because local defects have a short duration, their corresponding frequency spectrum is very wide.

Thus, over and above any amplitude and frequency modulation effects, the repeated impacts from a local defect can excite resonances anywhere along the transmission path from source (defect) to the sensor [50, 51]. The resulting spectrum will contain peaks at frequencies corresponding to these resonances [51]. Modulation effects on the other hand are (in the time domain) symmetrical about a zero line.

1.7.4 Transmission Paths

Fault detection and diagnosis of gearboxes, like most rotating machinery, is based upon vibration signal monitoring. Under normal operating conditions, mechanical components in the gearbox generate signals at specific frequencies related to the component's rotational frequency. In the case of a faulty component, the signals generated by this component will be different from the signals normally generated by an undamaged component. This will be reflected at the component's rotational frequency and in its harmonics. Consequently, an indication of the fault within the component can be found by monitoring the changes in vibration signals. In practice, however, changes in the measured vibration signal as a result of component faults are not always distinct due to the attenuation of the vibration signals by the housing and other components through which the vibration travels, the noise contaminating the signal [46].

In this research, the gear vibrations were measured on the outside of the gearbox casing for convenience. As a point of note, it is possible that signal interference can occur between the transducer and the gearbox structure, contributing to the vibration measurements.

1.8 Aim and Objectives

The main aim of this research is to develop a system for the effective remote monitoring of gear condition. This work will include selection and development of signal processing techniques for remote machine CM and fault detection.

CHAPTER 1

INTRODUCTION

The work plan and prioritised objectives for this research programme are:

- ✚ To develop experimental procedures for remote CM of a two stage helical gear transmission system, primarily focusing on a faulty gear (pinion) in the first stage gear transmission system.
- ✚ To review the literature and assess the performance of commonly used diagnostic techniques in terms of early gearbox fault detection.
- ✚ To evaluate the baseline of vibration data under different operating condition using conventional signal processing methods, which will be referenced for comparison with more advanced methods.
- ✚ To develop mathematical models to help understand vibration signal characteristics under healthy and faulty gear conditions.
- ✚ To correlate experimental and simulated results obtained from the mathematical models developed.
- ✚ To investigate the sensitivity and robustness of well-accepted Time Synchronous Averaging (TSA) techniques in the analysis of vibration signals.
- ✚ To perform Frequency Response Function (FRF) analysis using a vibration shaker in order to study the dynamic characteristics of the experimental test rig.
- ✚ To perform a comparison of locally and remotely-measured vibration characteristics, and hence to understand the relative capabilities of remote gear condition monitoring and any constraints that should be considered in its usage.
- ✚ To provide guidelines for future research in this field.

1.9 Thesis Outline

This thesis is organised in nine chapters describing the work that was done to achieve the aims and objectives of this project. This thesis is laid out as follows:

Chapter 2

This chapter surveys the literature on signal processing techniques used to monitor

CHAPTER 1

INTRODUCTION

the condition of geared transmission systems on the basis of vibration signals. Relevant techniques are briefly discussed here to assist the understanding of results presented in the following chapters.

Chapter 3

Chapter three describes the test rig facility and fault simulation. It starts by describing the test rig components and control systems and summarising the main specification of the gear in testing. Then it explains the instrumentation of the vibration measurement by describing each component involved.

In this chapter the baseline data of vibration were also evaluated under different operating condition using time domain, frequency domain and joint time-frequency domain analysis (using Morlet continuous wavelet transform) domain respectively, which will be referenced for comparison with more advanced methods.

Chapter 4

In this chapter, the vibration signals for different gear conditions (healthy and faulty) and different operation conditions were recorded from a sensor mounted on the gearbox casing.

These signals were analyzed using conventional methods made in the time domain, frequency domain and joint time-frequency domain (using Morlet continuous wavelet transform) to obtain a set of effective feature for detecting and diagnosing the seeded gear tooth faults. The time domain analysis leads to popular statistical feature parameters such as peak value, RMS, kurtosis and crest factor. The frequency domain (standard Fourier spectrum) analysis produces spectral features including amplitudes at meshing frequencies, their harmonics and their associated sidebands. The performance of these feature are evaluated in separating the faults at different conditions. In the same way the time-frequency representations of the vibration data are also obtained. However, feature parameters are not developed because they are visualised to have little consistency with the fault levels induced. The exploration of these methods will demonstrate that they are not able to show the presence and progression of breakage tooth faults in gears and demands further analysis methods are need to be investigated to overcome the drawbacks in diagnosis the gear faults.

CHAPTER 1

INTRODUCTION

Chapter 5

This chapter presents a mathematical model that simulates vibration signals. The model represents a two stage gear system using a suitable stiffness function to represent the forces acting between each pair of gears. Rotational stiffness and damping are also used to simulate the angular motion of the gears and shafts.

Chapter 6

In order to investigate the influence of Time Synchronous Averaging (TSA) on vibration signals, the results of applying traditional signal processing techniques as described in chapter four are compared to the results obtained by applying TSA.

The angular domain signal, the order spectrum and the order-frequency presentation are obtained to further characterise the gearbox vibration in these new domains.

Chapter 7

In this chapter, the Frequency Response Function (FRF) is used to study the dynamic characteristics of the experimental test rig. The FRFs of the system were determined using specialised frequency analysis equipment with an electromagnetic shaker. FRFs are used to study the transmission path effect on the vibration signal generated in the gear transmission system. This is then related to the identification of the dynamic properties of the gearbox components.

Chapter 8

In this chapter, the vibration data recorded from the two accelerometers located on gearbox casing and motor flange are analyzed using different signal processing methods in order to investigate the effect of path transmission (transducer location) on the detection and diagnosis of the seeded gear tooth faults. Results from the angular domain, the order spectrum and the order-frequency analysis are presented to show that these techniques can be used to remotely detect faults in gearboxes and that the effect of the path transmissions can be observed from the vibration signals.

Chapter 9

In this chapter, a review of the objectives and achievements is displayed. It starts by describing the achievements one by one by comparing them to the objectives described in chapter one. Furthermore, a summary of the novel features and

CHAPTER 1

INTRODUCTION

contribution to knowledge is provided in details, and it starts by displaying the novel features and then it describes the contributions to knowledge regarding this research. Finally, the author addresses the recommendations for future work.

CHAPTER 2

REVIEW OF VIBRATION-BASED GEAR FAULT DETECTION TECHNIQUES

This chapter presents a literature review of signal processing techniques which are used to monitor the condition of geared transmission systems based on vibration signals. Relevant techniques are briefly discussed here to assist the understanding of the results presented in the following chapters of this thesis.

2.1 Time-domain Analysis

Time domain analysis of vibration signals is one of the simplest and cheapest fault detection approaches. Conventional time-domain analysis attempts to use the amplitude and temporal information contained in the gear vibration time signal to detect gear faults. The amplitude of the signal can be used to signal that a fault is present and the periodicity of the vibration can then indicate a likely source for the fault [18]. Time domain approaches are appropriate when periodic vibration is observed and faults produce wideband frequencies due to periodic impulses [18]. Use of the waveform enables changes in the vibration signature caused by faults to be detected, but it is difficult to diagnose the source of faults. Figure 2.1 (from section 4.2.1) shows the gearbox vibration waveform for healthy and faulty gear systems.

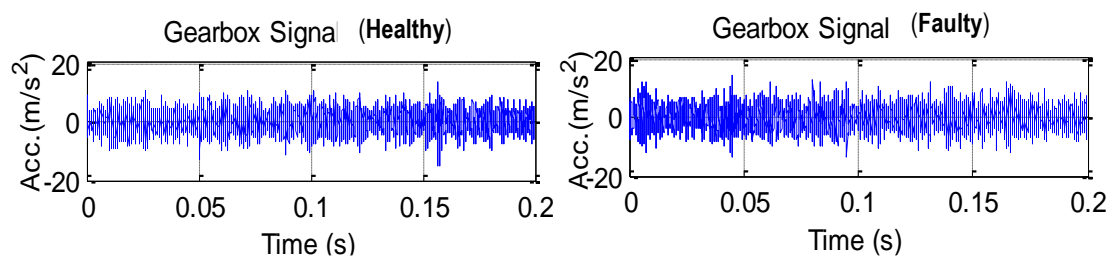


Figure 2.1-Waveform of the vibration signal for a gearbox with healthy and faulty gears

Some mechanical systems generate high vibration levels throughout their operation. When these systems develop a progressive fault, the resulting vibration level is likely to increase consistently with time but the increase in vibration may be very small and difficult to identify. If the rate of development of the fault vibration is small, it may not be possible to clearly determine a fault symptom from variations in the waveform of the signal [52].

Mechanical systems are termed deterministic if their properties such as displacement, acceleration, etc. can be predicted over time. Mechanical systems such as a gearbox with a localised fault reveal characteristics which cannot be estimated over time. The characteristics of such systems, termed random or non-deterministic, cannot be accurately predicted, but they can be estimated by statistical parameters and these parameters can be used to predict fault progression [53].

Statistical indicators, which are commonly used for mechanical fault detection and based on the time-domain waveform include: the Peak Value (PV), Root Mean Square (RMS), Kurtosis and Crest Factor (CF) [46, 54]. These indicators are also referred to as “condition indices”, [55]. The vibration signal from a gearbox is processed and a single value returned to indicate whether its condition is within normal operating parameters or not.

The condition index should increase as the fault increases; indicating the deteriorating condition of the gearbox. Sometimes this analysis can be performed by simple visual observation of the vibration time-domain waveform, but it is more likely that the time-domain signal will be processed to provide a statistical parameter (feature) which bears a known relation to the severity of the vibration.

2.1.1 Peak Value (PV)

Peak value is defined as the maximum vibration amplitude [46]:

$$PV = y_{\max}(t) \quad (2.1)$$

where y_{\max} is maximum amplitude of the signal.

2.1.2 The Root Mean Square (RMS)

RMS is related to the energy of the signal and the presence of defects can be directly detected by the increase in the vibration signal [56].

The RMS is the normalized second central moment of the signal; it is used for overall vibration level measurements [46]. It can be effective in tracking system noise, but it does not give meaningful information to identify which component is failing.

RMS can be defined as [57]:

$$RMS = \sqrt{\frac{1}{N} \sum_{n=1}^N (x(n) - \bar{x})^2} \quad (2.2)$$
$$\bar{x} = \frac{1}{N} \sum_{n=1}^N x(n)$$

where ; N is the number of samples taken in the signal

$x(n)$ is the amplitude of the signal for the n^{th} sample

\bar{x} is the mean value of the N samples.

CHAPTER 2

REVIEW OF VIBRATION-BASED GEAR FAULT DETECTION TECHNIQUES

From this definition it is clear that RMS is not sensitive to sudden short duration, isolated peaks in the signal and, thus is often not sensitive enough to detect incipient tooth failure. RMS becomes more useful as tooth failure progresses and is a measure of the overall vibration level of the system. It is therefore considered a very good descriptor of the overall condition of gearboxes and is sensitive to changes in operational conditions such as load and speed [58].

2.1.3 The Crest Factor (CF)

The overall vibration level does not produce any essential information about the waveform of the vibration signal. With several types of gear fault, the shape of the signal is a better indicator of damage rather than the overall vibration level. CF is the ratio of the peak value of the input signal to the RMS value as demonstrated in Figure 2.2. It is useful in detecting the change in the signal pattern due to impulsive vibration sources such as tooth breakage in the gear and is typically used on the raw vibration signal. A discrete fault on a gear will theoretically generate an impulsive (short duration) signal during meshing.

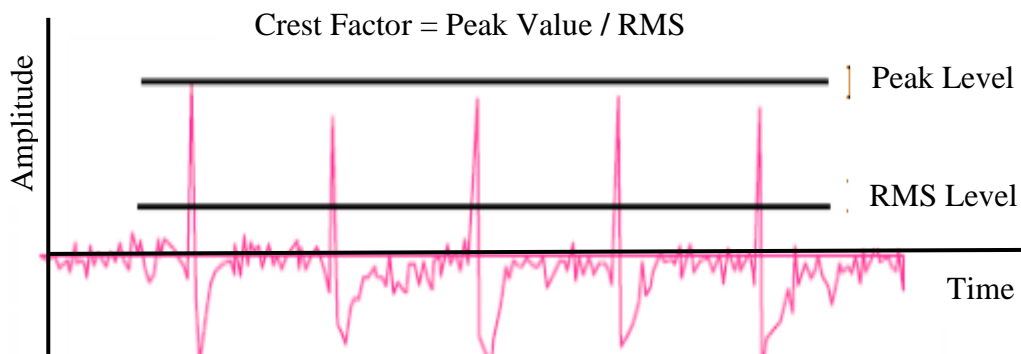


Figure 2.2- Definition of the Crest Factor, Peak and RMS levels [59]

The peak value of the impulsive signal will increase as the damage grows while the RMS level of the overall acceleration (vibration) will change only slightly because the time over which the impulse acts does not significantly increase [60].

CF is useful for detecting discrete impulses above the background signal which do not occur frequently enough or have sufficient duration to significantly increase the RMS level.

$$CF = \frac{PV}{RMS} \quad (2.3)$$

where: PV is the peak value and RMS is the root mean square

2.1.4 Kurtosis

Kurtosis is a non-dimensional quantity used to detect the presence of significant peaks in the time-domain of the vibration signal. Kurtosis is the 4th order statistical moment of the vibration signal, and because it raises the signal to the fourth power it effectively amplifies the isolated peaks in the signal [61]. The normalized kurtosis for a distribution $x(t)$ given by its sample values x_1, \dots, x_N measured at times t_1, \dots, t_N can be defined as:

$$kurtosis = \frac{\frac{1}{N} \sum_{i=1}^N (x_i - \bar{x})^4}{\left[\frac{1}{N} \sum_{i=1}^N (x_i - \bar{x})^2 \right]^2} \quad (2.4)$$

The higher the kurtosis value the sharper the peak(s), and the longer the tails of the signal. The lower the kurtosis, the more rounded the peak(s).

When the vibration signal is random noise, then it follows Gaussian (Normal) distribution and has a kurtosis value equal to 3.0 and -1.5 for a pure sine wave. A vibration signal collected from a healthy gear usually shows a uniform pattern and the value of kurtosis is approximately 3.0 or lower. As the gear fault progresses, kurtosis increases indicating that the distribution of the vibration is no longer a Gaussian distribution. This is primarily due to impulses (isolated peaks with high amplitude) generated by the affected gears [62]. Consequently, kurtosis is commonly used as a parameter for the detection of gear faults [63].

2.2 Frequency (Spectral) Domain Analysis

Frequency-domain analysis is a powerful conventional technique for vibration analysis and has been demonstrated as a useful tool for detection and diagnosis of faults in simple rotating machinery [46,64]. Using this technique, the time-domain of the vibration signal is transformed into its frequency equivalent. It has been found that

CHAPTER 2

REVIEW OF VIBRATION-BASED GEAR FAULT DETECTION TECHNIQUES

the spectral content of the measured signal is often much more useful than the time-domain for determining gear condition because the complex time-domain signal can be broken down into several frequency components. It is therefore easy for analysts to focus on these frequencies which are valuable in fault diagnosis [46], whereas the overall vibration is a measure of the vibration produced over a broadband of frequencies; the spectrum is a measure of the vibrations over a large number of discrete contiguous narrow frequency bands. Thus the common approach to vibration CM is use the Fast Fourier Transform (FFT) to transform the vibration signal to the frequency domain. This approach is perfectly acceptable if the measured signal does not vary in spectral content over time (i.e. no variations in the rotational speed of the machine). The mathematical basis for frequency analysis is provided in Appendix A. For machines operating with known constant speed, the vibration frequencies of the vibrations produced by each component in the machine can be estimated (see section 1.7) therefore, any change in vibration level within a particular frequency band can be related to a particular component. Analysis of relative vibration levels at different frequency bands can provide some diagnostic information.

As seen in Figure 2.3 (from section 7.4.2), local defects such as gear tooth breakage are often found in the vibration spectrum through changes in amplitude of particular frequencies (sidebands around the gear meshing frequencies f_{m11} , f_{m21} and their harmonics f_{m12} , f_{m13} and f_{m22} , f_{m23}) [65].

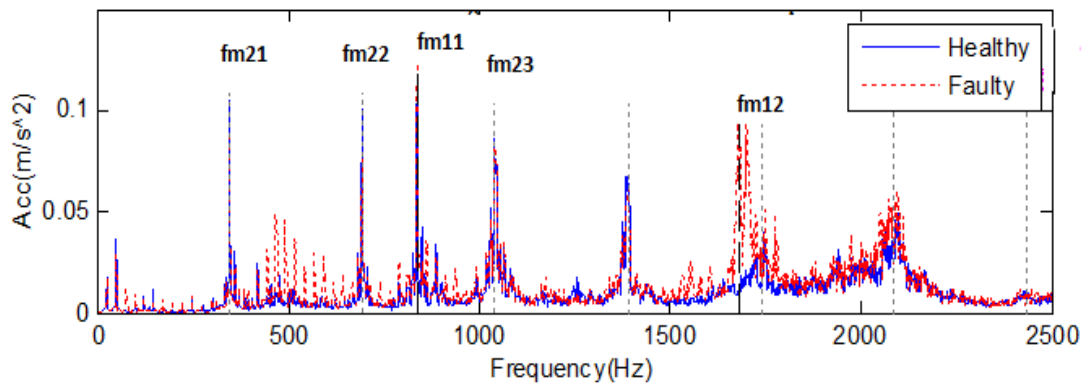


Figure 2.3-Spectrum of Gearbox Vibration Signal for Healthy (blue) and Faulty (red) gears

CHAPTER 2

REVIEW OF VIBRATION-BASED GEAR FAULT DETECTION TECHNIQUES

Sidebands generated by either amplitude modulation or frequency modulation of the vibration signal often provide useful information. Amplitude modulation is attributed to tooth fracture or eccentricity of the gear or shaft with a damaged tooth generating pulses at a rate equal to the gear speed (see section 1.6). Frequency modulation, on the other hand, is caused by errors generated during gear manufacture (e.g. non-uniform tooth spacing). As previously stated, *Randall* has claimed that the first three gear meshing harmonics and their sidebands provide sufficient information for the successful identification of gear faults [64].

Therefore, changes in the amplitude of a particular frequency peak or sidebands of a signal can provide a good indicator of potential gear failure. In practice, the spacing of the sidebands depends on periodic properties of the loading and on the transmission path, it can be difficult therefore to extract useful features directly from vibration spectra based solely on a FFT. When the signal to noise (S/N) is low and the vibration spectrum has a large number of frequency components due to the complexity of the system, it becomes almost impossible to distinguish the peaks due to faults from peaks from other sources. This is the most difficult problem associated with the FFT based fault detection approach.

2.2.1 Meshing Frequency Characteristics

Every gear set generates a unique profile of frequency components which is highly dependent upon the speed of rotation of the participating gears [66]. The gear-mesh frequencies can appear as transients in the spectrum when the transmission is subjected to angular acceleration and as harmonics when the transmission is operating at a steady speed.

The fundamental gear-mesh frequency is the product of the number of gear teeth and the speed of rotation of the gear (see section 1.6.1). The amplitudes of the gear-mesh frequency components are a strong function of the torque transmitted by participating gears, and any modulating effects on them.

2.2.2 Sideband Characteristics

Vibration spectra of machines have their energy distributed in multiple frequencies. In geared transmission systems, mesh-force modulation is a phenomenon which is

CHAPTER 2

REVIEW OF VIBRATION-BASED GEAR FAULT DETECTION TECHNIQUES

commonly observed [67]. The modulation processes transfer energy from the actual frequency to the sidebands around both sides of the gear mesh fundamental frequencies and their harmonics. In rotating systems, multiple sidebands are observed about each harmonic which are symmetrically spaced about the harmonics and decay exponentially as they separate further away from the gear-mesh frequency. The sidebands need not be symmetric [68]. When analysed in detail, this spectral information provides significant information about gear tooth condition as well as fluctuations in the drive system and condition of the gearbox bearings [69].

As mentioned in section 1.6.1 sidebands can be caused by amplitude modulation or frequency modulation, or a combination of both. The modulating components often manifest as sidebands surrounding the gear-mesh harmonics. Sideband structures are often observed in the measured vibration signatures of rotating machinery such as gearboxes. Such spectral information is usually used for gear fault diagnostics [67].

2.2.3 Speed Variation Effect

The ability to resolve frequencies of machine components is highly reliant on the stability of the vibration signal over the analysis period. Use of an FFT analyser with a constant bandwidth time limitation will cause imposed resolution for all frequencies. Therefore, the vibration frequencies related to rotating components in gear transmission systems will vary according to changes in the rotational speed of the system, and impose a resolution limitation which is a constant percentage of the frequency. Even in machines with a constant rotational speed, a drift in operating speed can occur over time, which in some cases produces frequency variations greater than those due to the bandwidth time limitations. The effect of this variation may be eliminated by using synchronous sampling in which the sampling rate of the analyser is linked to the speed of the machine. However, a speed sensor must be attached to the machine in order to convert the speed signal into a clock pulse signal suitable for driving the signal analyser. More details are provided in section 2.4.

2.3 Joint Time-Frequency Approaches

Analysis of the vibration signals in the time-domain and the frequency-domain produces signal characteristics for their respective domains only. The time-domain

CHAPTER 2

REVIEW OF VIBRATION-BASED GEAR FAULT DETECTION TECHNIQUES

contains no spectral information and when a time-domain signal is transformed to the frequency-domain, the detailed information about the time-domain is lost.

Consequently, both methods have their limitations. Additionally, it must be remembered that there are limits on the results of the Fourier Transform (FT) which are strictly only valid for stationary signals.

FT can be used for analysis of non-stationary signals, to identify which spectral components exist within the signal. However, the time or interval at which these occur cannot be determined. If time information is required, then FT is not a suitable method of analysis.

It is often difficult to detect clear symptoms of any defect in the gear if Time Synchronous Averaging (TSA) is used in isolation [70]. The technique may also fail to detect and differentiate between faults, particularly if multiple faults are present simultaneously in multiple gears within the gearbox. A wide variety of different techniques have been explored over the years to further process the TSA method to make it more sensitive to early fault detection [71].

Recently, much work has been carried out on the analysis of vibration signals in the time-frequency domain, with a view to combining this with frequency domain analysis to give a full representation of a vibration signal [26].

Time-frequency analysis provides information on the evolution of spectral content of the signal with time, allowing investigation of transient features such as impacts [72,73]. In recent years, joint time-frequency representations such as the Short-Time Fourier Transform (STFT) [21], Wigner-Ville Distribution (WVD) [71,32,17], and Wavelet Transform (WT) [24,25,26], have become popular in an attempt to address the lack of either time domain or frequency domain analysis. An overview of the joint time frequency application for the machine diagnostics can be found in *Atles et al.*, [74]

The major differences between these transforms are their respective time and frequency resolutions. WT analysis has been shown as an ideal tool for condition monitoring of gears. In contrast to the STFT, the WT method uses narrow time windows at high frequencies and wide time windows at low frequencies [75,76]. It is

therefore a very effective method for the analysis of transient and non-stationary signals. Abnormal transients generated by early stage gear faults can be detected using discrete [16] and continuous [70] wavelet transformation. It has been found that even though the discrete WT offers a very efficient signal representation with no redundancies, the resulting time-scale map is limited, and not very informative. *Lin et al.* introduced a linear wavelet transform concept, whereby the wavelet map was normalized according to the signal amplitude instead of energy [3]. *Boulaahbal et al* [77] applied both the WT amplitude and phase simultaneously to study cracked and chipped tooth faults and proposed polar representation as a useful tool for pinpointing the location of the gear damage in WT maps. Description of these techniques can be found in the following sections.

2.3.1 Short-Time Fourier Transform (STFT)

The STFT is, essentially, a windowing technique applied to the Fourier Transform. It was developed to overcome the limitations of the FT in analysing non-stationary signals. STFT employs a sliding window function $g(t)$ centred at time τ to perform a “time-localized” Fourier Transform of the signal $x(t)$.

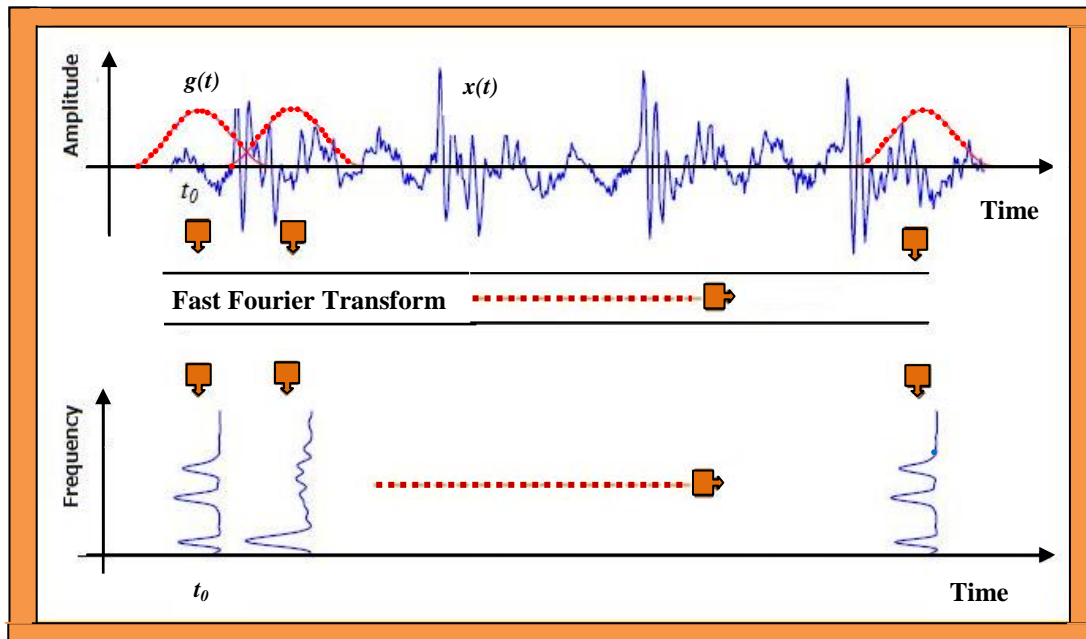


Figure 2.4 STFT of Test Signal $x(t)$, $g(t)$ in the Moving Window Function [76]

CHAPTER 2

REVIEW OF VIBRATION-BASED GEAR FAULT DETECTION TECHNIQUES

Time-localization can be obtained by applying two steps; (1) windowing of the signal to cut off only a small (well-localized) section of the signal at a time $x(t)$, (2) performing a Fourier Transform on this portion of the signal as shown in Figure 2.4.

To achieve this, at each fixed time of interest, t , the time domain vibration signal is multiplied by the sliding window, $g(t-\tau)$. This emphasizes the signal centred at time t , and the FT of the resultant windowed signal is calculated producing the continuous STFT [21]:

$$STFT(\tau, f) = \int_{-\infty}^{\infty} g(t - \tau)x(t)e^{-j2\pi ft} dt \quad (2.5)$$

where the sliding time window function used was a Gaussian window of the form

$$g(t) = e^{-(t/a)^2} \quad (2.6)$$

where a is a constant that defines the width of the window used.

Equation 2.5 can therefore be rewritten as:

$$STFT(\tau, f) = \int_{-x}^x x(t)e^{-\left\{\frac{t-\tau}{a}\right\}^2} e^{-j2\pi ft} dt \quad (2.7)$$

This formula will produce the Fourier Transform of the function $F(t)$ windowed by $g(t)$ centred at time τ . By continuously performing the same analysis at multiple translated locations τ 's, it is possible to obtain a description of how the frequency content of the signal varies with time.

The early application of time-frequency methods to gear faults began with the work of *Forrester, B.D.*, applied the STFT method to the detection of gear failures [78,79].

The disadvantage of the STFT application is that the window width remains constant during the whole analysis. This is a limitation when higher resolution is required to identify sudden changes over time. Once the width of the widow is selected it cannot be changed during the transform.

Although addition of this windowing function introduces time locality into the time-frequency analysis, it affects the resolution of the results in the frequency domain. This phenomenon is known as the uncertainly principle. The uncertainty principle means that good resolution in both time and frequency domains cannot be achieved simultaneously i.e., the choice of window represents a trade-off between the time resolution and the frequency resolution [23,80]. If the signal to be analyzed has a high frequency content and is of short duration, a narrow window should be selected for better time resolution. However, the narrower the window the wider the frequency bands, which results in poor frequency resolution. Similarly, if the signal to be analysed has low frequency components and is of long duration, then a wider window must be selected to obtain better frequency resolution.

Some gear faults can be detected via inspection of the energy distribution of a signal $x(t)$ over a time-frequency space. *Wang et al* have demonstrated the application of combined STFT and the Gaussian window function for vibration signal analysis [70].

2.3.2 Wigner-Ville Distribution (WVD)

An alternative and popular time-frequency analysis technique is the Wigner-Ville transform for representation of the energy of a signal in the time-frequency plane [23]. The WVD is a joint time-frequency signal representation based on a trade-off between the time and frequency resolution [81]. The WVD has a bilinear convolution integral, where both time and frequency domains are linked together in one function, giving better time localization. The basis of the WVD is that it possess a joint function for time and frequency distribution enabling the energy density or intensity of a signal to be described simultaneously in time and frequency [82]. The WVD method can be used to detect the presence of gear faults at very early stages of development [83].

The application of time-frequency methods to gear faults began with the work of *Forrester B.D.* He applied the WVD method to detect gear failures [84]. This work showed that different faults, such as a tooth crack and pitting, could be detected by the WVD. *McFadden and Wang*, applied normal and weighted WVD techniques to detect gear faults [85]. Later, *Baydar and Ball*, demonstrated the use of a smoothed version of WVD to detect various gear failures [86,87].

CHAPTER 2

REVIEW OF VIBRATION-BASED GEAR FAULT DETECTION TECHNIQUES

Fault detection is based on visual observation of the WVD contour plots or through monitoring of changes in the statistical features of the distribution [88]. The WVD can be defined in both time and frequency-domains, but due to better computational efficiency and good time resolution, the time-domain definition is more frequently reported in the literature [88].

The Wigner-Ville Distribution, $W(t, f)$, can be defined in terms of time as [24]:

$$W(t, f) = \int s\left(t + \frac{\tau}{2}\right) s^*\left(t - \frac{\tau}{2}\right) e^{-j2\pi f\tau} d\tau \quad (2.8)$$

where: $W(t, f)$ denotes the WVD of the signal.

s^* is the complex conjugate.

$W(t, f)$, can be also expressed in terms of the frequency spectrum [88]:

$$W(t, f) = \int s\left(f + \frac{\nu}{2}\right) s^*\left(f - \frac{\nu}{2}\right) e^{j2\pi\nu t} d\nu \quad (2.9)$$

By integrating $W(t, f)$, with respect to frequency at a particular time, the energy density at that time can be derived [88]:

$$\int_{-\infty}^{\infty} W(t, f) df = \int_{-\infty}^{\infty} \int_{-\infty}^{\infty} s\left(t + \frac{\tau}{2}\right) s^*\left(t - \frac{\tau}{2}\right) e^{-j2\pi f\tau} d\tau df \quad (2.10)$$

$$= |s(t)|^2 \quad (2.11)$$

Similarly, the integral of $W(t, f)$, with respect to time at a particular frequency will give the spectral energy density at that frequency:

$$\int (t, f) dt = |s(f)|^2 \quad (2.12)$$

Equations 2.11 and 2.12 represent the marginal conditions and are often given as a requirement for a time-frequency energy distribution [89].

One of the major advantages of the WVD method is its ability to overcome limitations of the STFT method by improving the resolution in both time and frequency [90].

CHAPTER 2
REVIEW OF VIBRATION-BASED GEAR FAULT DETECTION TECHNIQUES

The major problem with the WVD is its non-linear behaviour which causes significant interference (the cross-terms) between different signal components. For example, if a signal $x(t)$ has two components represented by:

$$x(t) = x_1(t) + x_2(t) \quad (2.13)$$

and the WVD of this signal is given by:

$$W(t, f) = W_{11}(t, f) + W_{22}(t, f) + W_{12}(t, f) + W_{21}(t, f) \quad (2.14)$$

where;

$$W_{12}(t, f) = \int_{-\infty}^{\infty} x_1\left(t + \frac{\tau}{2}\right) x_2^*\left(t - \frac{\tau}{2}\right) e^{-j2\pi f\tau} d\tau$$

is the cross-Wigner distribution and

$W_{12}(t, f) + W_{21}(t, f)$ is the interference term. This term is a real function that creates non-zero values at an unexpected location of the time-frequency plan.

For instance, the WVD of a $x(t)$ signal with two sinusoids $A_1 e^{j2\pi f_1 t}$ and $A_2 e^{j2\pi f_2 t}$ can be represented as [82]:

$$W(t, f) = A_1^2 \delta(f - f_1) + A_2^2 \delta(f - f_2) + 2A_1 A_2 \delta\left(f - \frac{f_1 + f_2}{2}\right) \cos[2\pi(f_2 - f_1)t] \quad (2.15)$$

where: A_1 and A_2 are the amplitudes and f_1 and f_2 are the frequencies of the two signals respectively.

The third term of Equation 2.15 is an oscillatory interference term which gives non-zero values at the mean of f_1 and f_2 .

For instance, the WVD of a signal with two frequencies at 300 Hz and 900 Hz will have a spurious frequency reading at 600 Hz due to a cross term. Cross-term interference significantly complicates the interpretation of the energy distribution [91] and recovery of the signal can be problematic due to aliasing components. However, aliasing can be reduced by resampling of the signals [90].

For computational purposes, it is often necessary to weight the signals using a window function, before evaluating the WVD [90]. Pseudo-Wigner distribution is used as a smoothed version of the original WVD, with respect to the frequency variable. This modified method is computed efficiently with algorithms using the FFT and other more efficient algorithms [92].

2.3.3 Wavelet Transform (WTs)

The Wavelet Transform method can be used as an alternative technique to the STFT. Where STFT is used to measure the local frequency content of the signal, the WT method compares several components of the vibration signal at different resolutions. The basis of the STFT approach is multiplication of the sine and cosine signals by a fixed sliding resolution. In the case of the WT method, the window is already oscillating and is called a mother window. The mother wavelet, rather than being multiplied by sine and cosine, is expanded and contracted depending on the value of the dilation parameter. Other wavelets are then generated by the mother wavelet, and it is this which forms the basis of wavelet analysis. The Wavelet Transform can be seen as decomposition of a signal into a set of basis functions called wavelets, obtained from a signal prototype wavelet by dilations, scaling and shifts [93].

In recent years, several WT analyses have been accepted as suitable signal processing techniques for machine CM and failure diagnosis. By decomposing a time series into time-frequency space, it is possible to determine not only the existing frequencies in the signal but also the duration of each individual frequency in time [25,26]. This is highly advantageous in examining vibration signals from faulty rotating machinery, where either large or small scale changes in the vibration may occur whether the fault is distributed or local [16]. When monitoring gearbox condition, WTs are used primarily to identify all possible transients in vibration signals which are generated by faults. WTs possess multiple resolutions for localization of short time components, enabling all possible types of gear fault to be displayed by a single time-scale distribution resulting from the transform [22].

Table 2.1 provides a brief comparison of various joint time-frequency techniques. By simply dilating the wavelet size within the transform, the different scales of the local

CHAPTER 2
REVIEW OF VIBRATION-BASED GEAR FAULT DETECTION TECHNIQUES

features can be described by a distribution in the time-scale plane.

Table 2.1- Comparison of different time-frequency techniques [72]

Techniques	Resolution	Interference terms	Speed
CWT	Good frequency resolution and low time resolution for low frequency components. Low frequency resolution and good time resolution for high frequency components.	No	Fast
STFT	Dependent on window function, good time and frequency resolution	No	Slower than CWT
WVD	Good time and frequency resolution	Severe interference terms	Slower than STFT

The most important characteristic of the WT method is the ability to narrow or widen the time window depending on whether the signal frequency is high or low.

Thus, there is a strong correlation between wavelet scale and frequency as revealed by wavelet analysis [75,94,95]. This can be advantageous for resolving very short-lived transient signals in the time dimension, making it is convenient for the analysis of non-stationary vibration signals. Thus the WT method is a technique which is potentially well suited to the detection of early failures in gearboxes.

While the selection of the base wavelet has remained largely an *ad-hoc* process, matching it to the signal which is to be analyzed is critical for WT applications.

Considering Figure 2.5, the top left quadrant of the diagram shows a series of impulsive components forming a non-stationary signal. The effects of using three base wavelets to analyse the signal are also shown in the figure. The three base wavelets are the Daubechies [96], the Morlet [97] and the Mexican hat [98] all of which are in widespread use for machine CM. It can be seen that only the Morlet

CHAPTER 2

REVIEW OF VIBRATION-BASED GEAR FAULT DETECTION TECHNIQUES

wavelet (shown in the bottom left of the figure) effectively extracted the impulsive components [98].

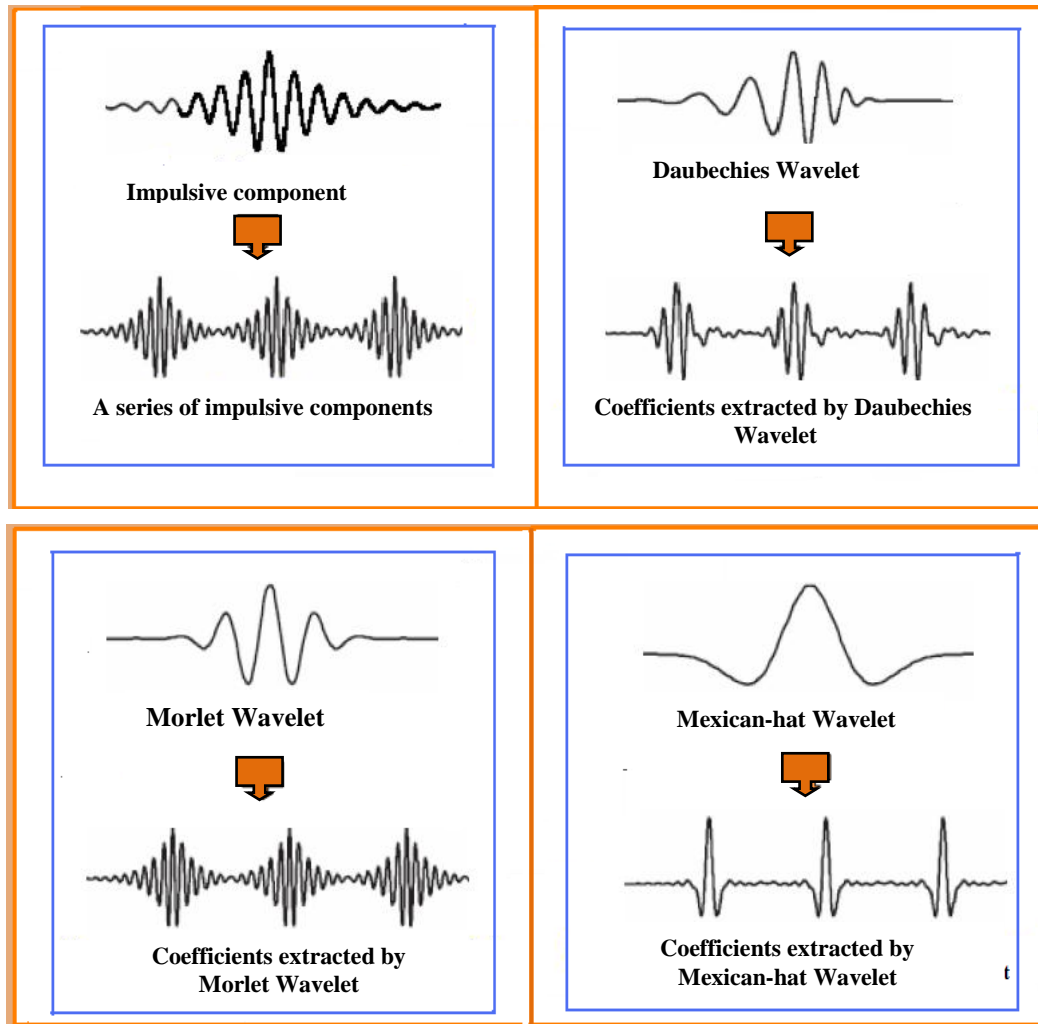


Figure 2.5 Different types of wavelets [97]

This imposes the necessity for the systematic investigation of WT to guarantee effective extraction of vibration signal features.

2.3.4 Continuous and Morlet Wavelet Transformations

In this research, continuous and Morlet wavelet transformation has been used. This technique has been extensively referenced in literature for joint time-frequency analysis of signals. In a comparative study of various wavelet functions, *Yang and Ren* [99] have shown that the Morlet wavelet is superior to other wavelet functions for analysis of signals having periodic impulsive features - most notably existing in

CHAPTER 2
REVIEW OF VIBRATION-BASED GEAR FAULT DETECTION TECHNIQUES

signals from gearboxes because of defective teeth.

In this situation, the vibration signal is broken up into shafted and scaled versions of the original (or mother) wavelets [98].

The Continuous Wavelet Transform (CWT) of a function $y(t)$ is defined in the time and frequency-domain as:

$$CWT(s, u) = \int_{-\infty}^{\infty} y(t) \frac{1}{\sqrt{s}} w^* \left(\frac{t-u}{s} \right) dt \quad (2.16)$$

where: $w((t - \mu)/s)$ is the mother wavelet at scale s (scale or dilation factor) which determines frequency content, and location u (shift or translation parameter) which gives the time location of the wavelet. w^* is the complex conjugate of the analyzing wavelet $w(t)$. A small s produces a high frequency (contracted) wavelet when high time resolution is required, while a large s produces a low frequency (dilated) wavelet when high frequency resolution is required. The analysing wavelet should satisfy the condition of admissibility to ensure existence of the inverse wavelet transform such as:

$$C_w = \int_{-\infty}^{\infty} \frac{|w(f)|^2}{f} df < \infty \quad (2.17)$$

where: $w(f)$ is the Fourier transform of $w(t)$. The signal $y(t)$ may be recovered or reconstructed by the an inverse wavelet transform of $CWT(s, u)$ as defined by

$$y(t) = \frac{1}{C_w} \int_{-\infty}^{\infty} \int_{-\infty}^{\infty} CWT(s, u) w \left(\frac{t-u}{s} \right) \frac{1}{s^2} ds du \quad (2.18)$$

The most striking aspect of the wavelet transform is that the basis function $\{w\}$ is not unique, but rather it is defined according to a set of rules and conditions. This is a great departure from the conventional $\{\text{sine}\}$ and $\{\text{cosine}\}$ basis function in Fourier Transform analysis.

CHAPTER 2

REVIEW OF VIBRATION-BASED GEAR FAULT DETECTION TECHNIQUES

As mentioned earlier, the scale parameter (s) does not remain constant, but varies allowing for the expansion and contraction of the window depending on the value of s . This function allows detailed examination of the vibration signal both for rapidly changing phenomena requiring high resolution, together with simultaneous analysis of slow varying components. Figure 2.6 shows how scaling and shafting affects the CWT.

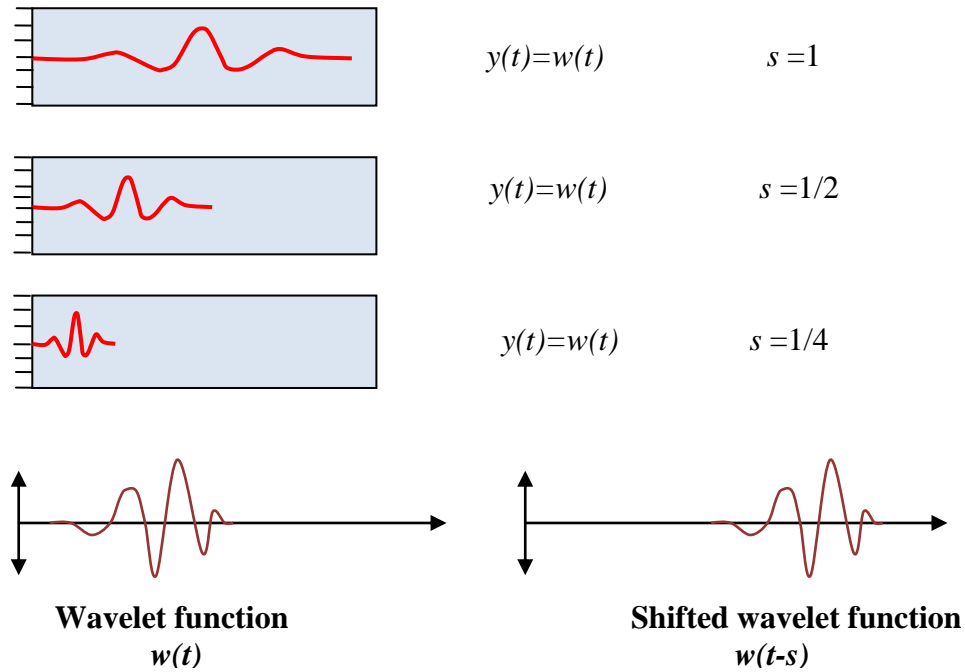


Figure 2.6- Scaling and shafting operation in CWT [98].

Several families of wavelets are available in a wavelet application, but the Morlet wavelet is the most commonly used in processing vibration signals from rotating machines. This is due to the fact that the Morlet wavelet is able to pick up impulses generated by the rotating components. It can be calculated according to:

$$w(t) = g(t)e^{i\omega_0 t} \quad (2.19)$$

where, ω_0 is the frequency parameter; $i = \sqrt{-1}$ and $g(t) = \pi^{-1/4} e^{-t^2/2}$ is a Gaussian window for the modulating waveform fluctuating at frequency ω_0 . The scale s and the frequency ω of the Morlet wavelet function are related as:

$$s = \frac{\omega_0}{\omega} \quad (2.20)$$

The parameter ω_0 is adjusted to balance the time-frequency resolution of the Morlet wavelet. A higher value of ω_0 will increase the frequency resolution, but decrease the time resolution. From Equation 2.19 we can obtain

$$f_0 = \frac{\omega_0}{2\pi} \quad (2.21)$$

Where f_0 is the frequency at which the window is centered in the frequency domain for a given scale s .

2.4 Time Synchronous Averaging (TSA)

Time Synchronous Averaging, or synchronous averaging, is a procedure that allows the removal of non-stationary component noise from a vibration signal [100, 101]. The TSA method is well suited for gearbox analysis, where it allows the vibration signature of the gear under analysis to be separated from other gears and noise sources that are not synchronous with that gear.

The basis of TSA is that all vibration related to gears on the shaft will repeat periodically with shaft rotation. By dividing the vibration signal into adjacent segments, each the same length as the shaft period and ensemble averaging a sufficiently large number of segments, the vibration which is periodic with shaft rotation will be enhanced and other components will cancel out. This then results in a signal which represents the average vibration for one revolution of the shaft [102]. This technique is used to represent the time-domain of the vibration signal produced by the meshing of the gear teeth over one complete revolution.

CHAPTER 2

REVIEW OF VIBRATION-BASED GEAR FAULT DETECTION TECHNIQUES

The TSA of the vibration can help eliminate all frequencies except the fundamental and harmonics of the tooth meshing frequency from the gear vibration signal. In this way, the variation in the vibration signal generated by a single gear tooth can often be identified by visual inspection [101,102].

Successful application of the synchronous averaging method requires a constant frequency deterministic component. In practice, a vibration signal from rotating machinery contains small frequency variations, even when operating at nominally constant speed. The use of interpolation and resampling techniques is essential to reduce the effect of shaft speed variations [101,102,103].

2.5 Order Analysis

Rotating machines such as multistage gearboxes are complex mechanical systems and the condition monitoring of such machines can be determined by measurement of their vibration signals [6]. The waveform of vibration signals generated by these machines depends on rotational speed given by the number of revolutions per minute (RPM). Most rotating machinery operates under continuously changing rotational speeds. This significantly complicates the classical spectrum analysis of vibration signals with constant sampling frequency. This is due to the fact that the signal frequency components, which are proportional to the rotational speed, change position in the spectrum and cause spectrum smearing.

For gearbox condition monitoring, spectral analysis may be unsuitable for detection of gear failures at an early stage, especially in the case of local faults, which primarily affect sidebands in the spectrum. Several gear pairs and other mechanical components usually contribute to the overall vibration. Hence, it may be very difficult to evaluate the spacing and evolution of sideband families in a spectrum. For this reason order analysis is commonly used [104,105].

In Order Analysis the vibration signal is re-sampled from equal time to equal phase increments. This results in a signal containing constant angular frequency components which can be used with TSA. The equal phase spacing used to resample the signal is determined from a synchronously recorded reference signal.

CHAPTER 2

REVIEW OF VIBRATION-BASED GEAR FAULT DETECTION TECHNIQUES

Order analysis is normally accomplished using a reference signal from a tachometer directly coupled to the rotating shaft of interest [106].

Order Analysis allows the sampling rate during data acquisition to be synchronized with the rotation speed of the shaft so as to lock the sampling locations to constant shaft angles. Thus, even if the speed changes, the sampling will still occur at the same shaft angle and the frequency content of the signal will be a function of order. This can be achieved by attaching an encoder to the shaft during data acquisition to record the shaft position. Fourier Transform analysis is then applied to the data to transform it into order domain - the result of which being the amplitude of the sine waves at fixed multiples of the basic rotation frequency, i.e. the amplitude of the order.

2.6 Summary

This chapter explains the theoretical basis of conventional diagnostic methods based on gear vibration signals to assist the understanding of results presented in the following chapters. We first briefly discuss the state-of-the-art data processing techniques that are commonly used in the area of gear fault detection and diagnosis including time domain (section 2.1), frequency domain (section 2.2), joint time-frequency analysis (section 2.3), and time synchronous averaging (section 2.4) and order domain (section 2.5). A brief theoretical background and the advantages and disadvantages of each method are discussed. Along with the above, an overview of applications of each method is also discussed citing various researchers who have successfully implemented these techniques for their applications of interest. The use of time-frequency analysis such as Morlet wavelet transformation was established when analysing vibration data from complex machines such as two-stage gearbox as this domain provides better results for non-stationary signals as vibrations generated by gear impacts.

CHAPTER 3

TEST FACILITIES, TEST PROCEDURE AND BASELINE VIBRATION

This chapter details the test rig facility and fault simulation for the experimental study of gearbox vibrations. It starts by describing the test rig components and control systems and summarising the main specifications of the gear under test conditions. It then explains the instrumentation of the vibration measurement by describing each component involved.

Finally, the baseline data of the vibration are evaluated under different operating conditions using conventional methods in the time, frequency and joint time-frequency domains, which are referenced for comparison with more advanced methods.

3.1 Test rig construction

In order to evaluate gearbox condition monitoring (CM) techniques, experimental work was carried out on a gearbox test rig developed at the University of Huddersfield. The gearbox test rig consists of a 3-phase induction motor, a two stage helical gearbox, shaft couplings and a load device, as shown in Figure 3.1.

The gearbox consists of two-stage helical gear transmissions. It was chosen for this research not only because it is widely used in industry, but also because it allows faults to be easily simulated and various CM techniques to be extensively evaluated.

3.1.1 Mechanical components

Figure 3.1 is an illustrative photograph of the test rig and gearbox used in this study. The motor and gearbox were mounted on I-beams which were anchored to the concrete floor. Figure 3.2 is the schematic diagram showing the key structural features of the rig. Specifications of the test rig components is provided in Appendix B

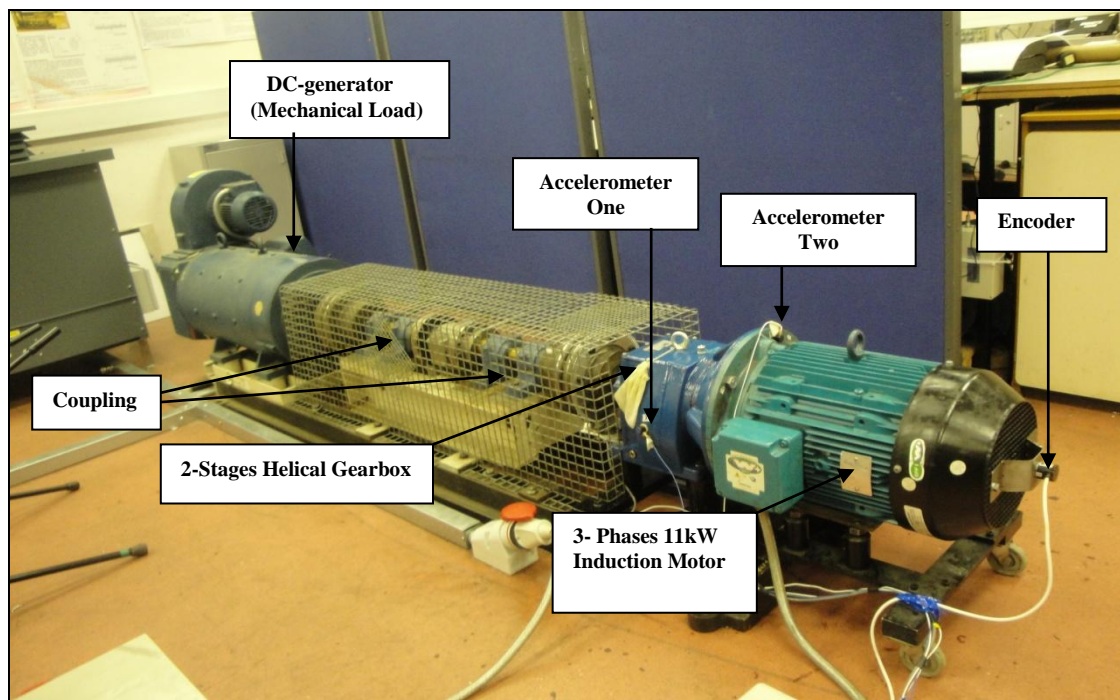


Figure 3.1- Photograph of the experimental test rig

Mechanically, the output of the AC motor is directly connected to the input shaft of the gearbox in order to transmit the mechanical power to the gearbox and its

CHAPTER 3
TEST FACILITIES, TEST PROCEDURE AND BASELINE VIBRATION

downstream equipment. The motor and gearbox are bolted together through two flanges integral to the motor housing and gearbox casing. This compact construction means that the whole system can be installed in a number of situations in which space is restricted or limited, for example in marine transmission. Moreover, in this study, different gear sets can be easily exchanged by unbolting the two flanges access to the inside of the gearbox.

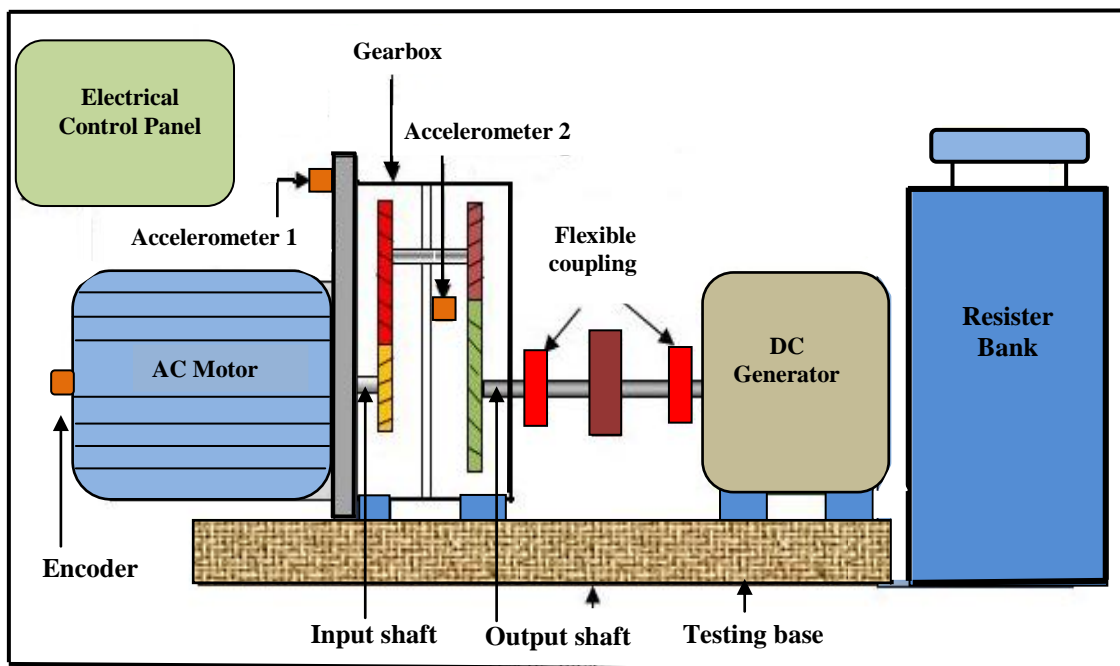


Figure 3.2- Schematic diagram of the test rig showing the position of the accelerometers

A middle shaft supported by two bearing supports couples the mechanical power to the DC motor. The DC motor produces electricity which is consumed by the resistor bank.

In this arrangement, the AC motor absorbs electric power from the supply system via a control cabinet which generates mechanical power and a DC motor which converts the mechanical power into electricity again. By varying the resistance values different loads can be applied to the system.

❖ **AC Motor**

Figure 3.3 is a photograph of the AC Motor/Gearbox combination. The manufacturer's specifications of the AC Motor are shown in Table 3.1 [30]. The basic

CHAPTER 3
TEST FACILITIES, TEST PROCEDURE AND BASELINE VIBRATION

operating principle behind the AC asynchronous motor is a stator winding which induces voltage and current into the rotor leading to a tangential force acting on the rotor. The resultant magnetic field induces the rotor to turn only if the force is sufficient to overcome the mechanical losses in the motor.

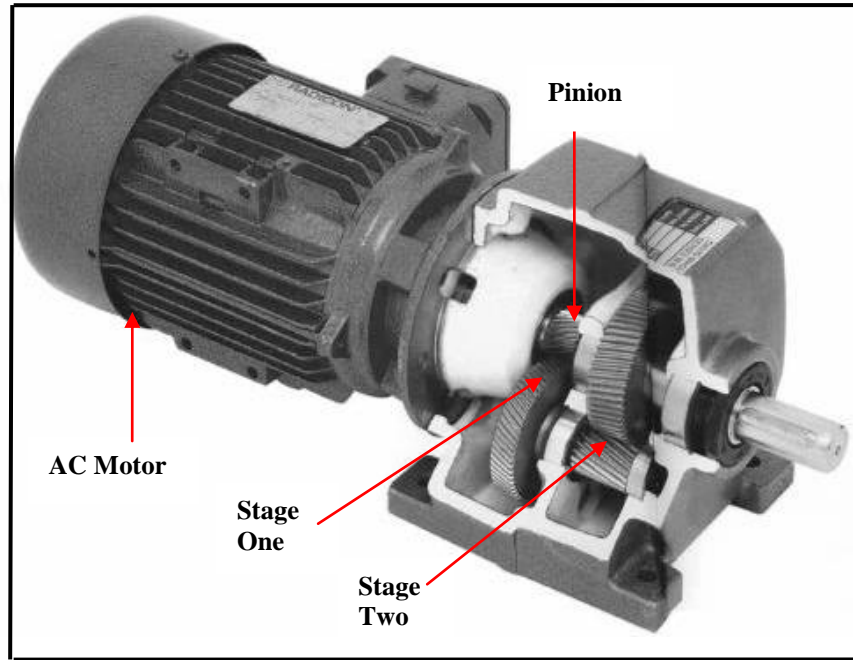


Figure 3.3- Photograph of an AC motor/gearbox combination

Table 3.1-Gearbox Design Data

Description	First Stage (Input Shaft)		Second Stage (Output Shaft)	
Number of teeth, Z	Pinion (Z_1)	Gear (Z_2)	Pinion (Z_3)	Gear (Z_4)
	34	70	29	52
Shaft rotation frequency, f_r (Hz)	24.43 (input) at full load		661 (output) at full load	
Meshing frequency, f_m (Hz)	827.73		342.73	
Contact ratio, \mathcal{E}_c	1.359		1.479	
Overlap ratio	2.89		1.478	
Overall reduction ratio	$(Z_2/Z_1) \times (Z_4/Z_3) = 3.691$			

CHAPTER 3
TEST FACILITIES, TEST PROCEDURE AND BASELINE VIBRATION

In the case of one pole isolated in a motor, the rotor rotates at a specific speed defined as the rotor speed. The number of poles and the frequency applied determines this speed. The equations below (3.1-3.2) allow the calculation of the motor synchronous speed derived from the supply frequency, slip and the number of poles of the motor.

$$N_R = N_s (1 - s_l) \quad (3.1)$$

$$N_s = \frac{120 \cdot f_{sup}}{p} - s_l \quad (3.2)$$

where: f_{sup} = supply frequency,

p = number of poles

s_l = slip

The number of poles and motor slip are fixed once the motor is manufactured, meaning that the only way to control the motor speed is to vary the supply frequency (f_{sup}) and it is this principle which is used to adjust the speed of the test rig.

❖ **Gearbox**

A two stage helical gearbox (manufactured by David Brown Radian Limited) has been combined in a cantilever type arrangement with the AC motor and is shown in Figure 3.3 [30]. The helical gearbox design data is given in Table 3.1, and Figure 3.4 shows the schematic diagram of the two-stage helical gearbox.

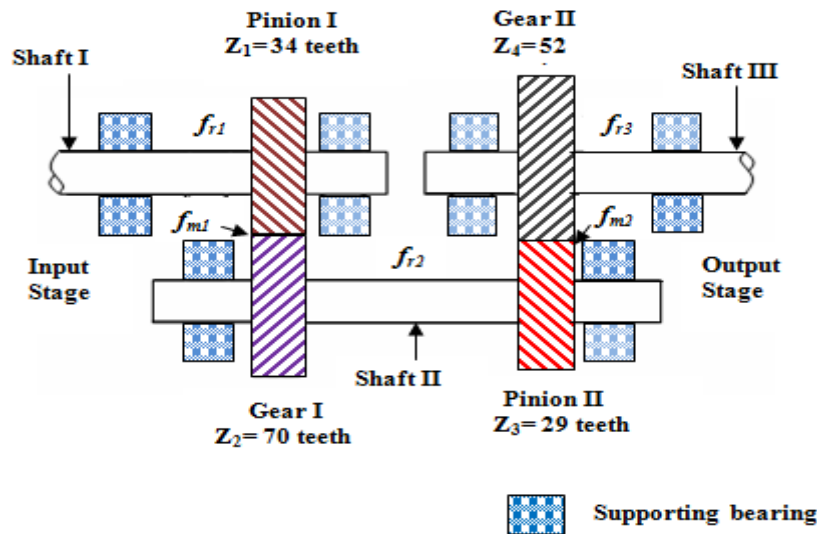


Figure 3.4-Schematic of the fundamental structure and working principles of a two-stage helical gearbox

CHAPTER 3

TEST FACILITIES, TEST PROCEDURE AND BASELINE VIBRATION

Most motors now come with a motor-gearbox combination as an option to avoid having to couple the motor to a separately supplied gearbox. The motor is usually flange-mounted and mates directly to the gearbox front flange plate.

This combination has been popularised by machinery designers and end users requiring convenient, compact designs that come as a complete package without the need for additional mechanical components between the motor and gearbox.

The requirement to drive low-speed loads that require a high-torque has also been a factor, because at any given power, torque in an AC motor is inversely proportional to speed.

High-torque, low-speed motors exist, but these are usually confined to DC machines as their AC equivalents run at a much lower power factor and generate much more heat than the high-speed motors. It is now considered more efficient to use step-down gearboxes for driving lower-speed loads at higher torque values. Most motors now come with a motor-gearbox combination as an option that saves having to couple the motor up to a gearbox supplied separately. The motor is usually flange-mounted and mates directly to the gearbox front flange plate. One of the industry leaders in motor-gearbox combinations is SEW Eurodrive [107]

❖ DC Generator

In this application the DC motor operates as a generator [108]. DC motors are amongst the earliest types of motor consisting of stator and rotor parts. The stator windings (field) generate the magnetising current for the motor. These field windings generate lines of magnetic flux that flow around the stator.

There is a small air gap between the armature and the stator and the magnetic field remains strong through the field core - the lines of magnetic flux cut through the armature windings. The field circuit is low-current with many coil turns generating the magnetic field. The field current only increases slightly with a large increase in the DC motor power.

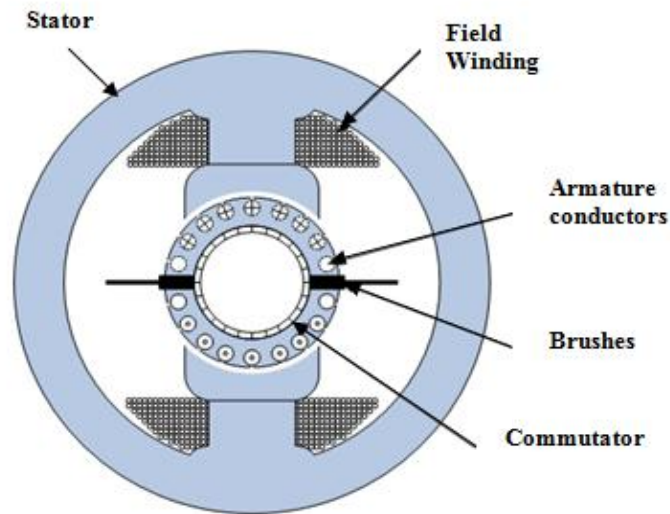


*Figure 3.5- Cut-away view showing the DC motor field/armature circuit;
Re-drawn by ML [109]*

3.1.2 Electrical Control of the Test Rig

A control system was used to allow a repeatable, deterministic series of tests to be undertaken to keep the motor speed and load profile identical throughout each test run for accurate comparative studies [107].

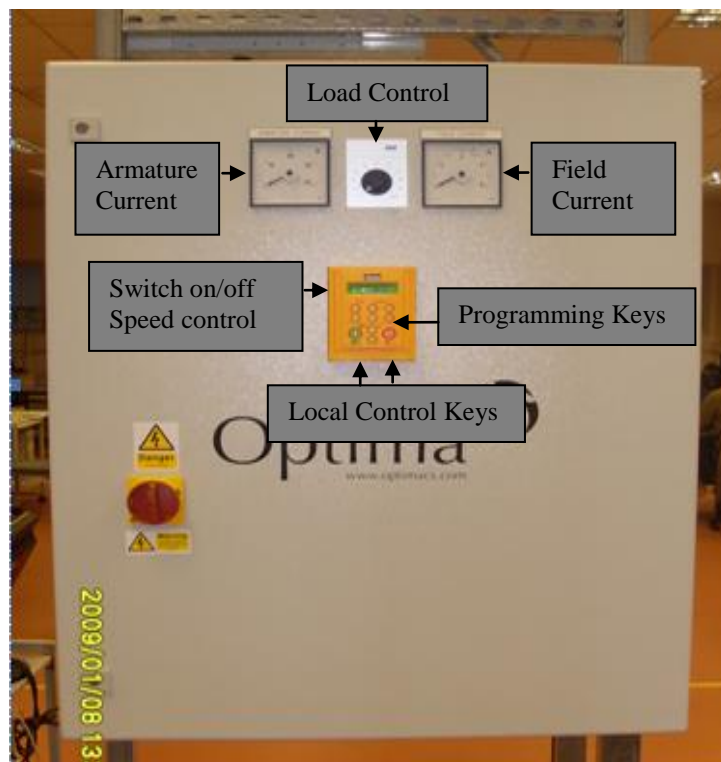


Figure 3.6- The test rig control panel

CHAPTER 3

TEST FACILITIES, TEST PROCEDURE AND BASELINE VIBRATION

Each test run allows faults to be introduced into the gearbox whilst keeping the operating conditions (speed and load) exactly the same.

The AC and DC motor settings were:

- AC motor speed setting (0% to 100%)
- DC motor load setting (0% to 100%)

Table 3.2 Control panel functions [107]

Armature current	Indicates DC motor armature Amperes; Range: 0 to 200A max. This signal is taken from the DC motor current transformer output.
Load control	Used to control the DC motor field current from 0% to 100%. This potentiometer is fed directly into the DC Field Controller
Field Current	Indicates the DC motor field current; Range: 0 to 5.0A max. This output is fed from the buffered output of the DC field controller
Switch On/Off Speed Control (Local Control Keys)	Push buttons controlling the AC Drive Start/Stop Red (Stop); Green (Start) This keypad is connected to the inverter drive by the use of a serial communications lead. The keypad normally resides on the drive front, but an optional remote panel-mount kit was chosen to mount the keypad on the front of the test rig panel.
Programming keys	These are used to access the AC inverter drive parameters. Under normal operating conditions, the keypad is used to increase or decrease the motor speed. If desired, an engineer mode can be selected to modify parameters such as speed loop tuning, ramp times, etc.

The front of the test rig panel is shown in Figure 3.6, with the control elements.

A brief description of the control panel functions is given in Table 3.2 above.

❖ **Speed control**

The major features of this system are given in Figure 3.7. The three-phase (415 VAC) supply is connected to the inverter in order to achieve speed variation. The inverter changes the supply frequency according to the speed set point and generates new supply voltages for the AC motor. This voltage then drives the AC motor and operates the system at a desired speed.

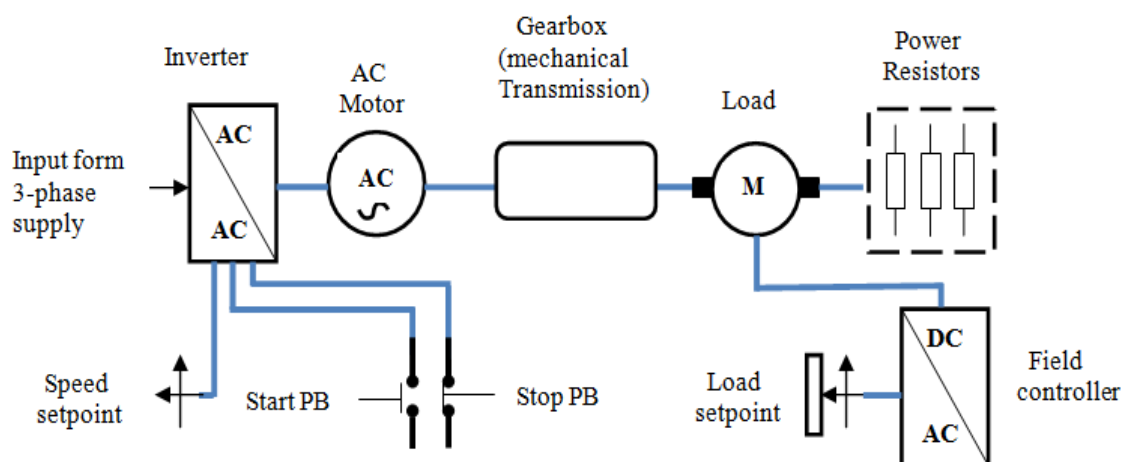


Figure 3.7- Block diagram of the experimental test rig

❖ **Load Control**

The DC motor that provides the load to the AC motor is not controlled by a DC drive. Instead, the motor converts the energy generated by the loading to heat in a resistor bank. The field current of the DC motor is controlled by a simple DC drive connected to two supply phases which are configured to supply a current pre-set by a potentiometer. This allows the test rig to operate from 0 to 100% load on the AC motor.

3.2 Instrumentation

3.2.1 Vibration measurements

The most commonly used transducer for vibration measurement is the piezo-electric accelerometer. This sensor gives stronger signals in a wide frequency range to capture vibrations from different sources such as shaft rotations with a frequency as low as several Hz and gear mesh processes with frequencies as high as several thousand Hz.

CHAPTER 3

TEST FACILITIES, TEST PROCEDURE AND BASELINE VIBRATION

The piezo-electric accelerometer also has high sensitivity for measuring low amplitude signals such as incipient faults. In addition, it is relatively small in size, highly durable, with good measurement stability and linearity [110].

The piezo-electric accelerometer consists of three main parts: the base, piezo-electric crystal and a series of seismic masses [110]. The piezo-electric crystal works as spring when placed between the seismic mass and the accelerometer base. The seismic masses vibrate with the same magnitude and phase as the accelerometer base. When the accelerometer is subjected to vibration, the seismic mass mounted on the crystal exerts a force on the piezo-electric elements equal to the product of their mass and acceleration ($F=ma$). This force causes the piezo-electric crystal to generate a charge proportional to the acceleration level to which it is exposed. The charge can be applied by either an external or an internal charge amplifier for signal recording. The internal charge amplifier accelerometer, also known as an ICP accelerometer, allows for longer distance transfer when compared with a transducer using external amplifiers.

The ICP transducers used in this work (PCB model 338C04) are low output impedance transducers containing built-in integrated circuits to convert the charge signal to a voltage signal. These are used on most vibrating surfaces because their mass does not significantly affect the movement of the surface, and possess a wide enough frequency range appropriate for measuring gearbox vibration (0.5Hz to over 10kHz). They are environmentally robust enough to withstand the conditions existing on gearboxes and are of an adequate sensitivity. However, they do have an upper temperature limit of about 90°C due to their inbuilt microelectronics.

Figure 3.8 shows a picture of the accelerometer. A detailed specification of the accelerometer used in this work is summarized in Appendix C.



Figure 3.8-PCB Model 338C04

To avoid unwanted distortion of the signal the accelerometers were rigidly attached to their respective surfaces via a screw-threaded brass stud glued to the casing with ceramic cement.

Two identical accelerometers were used to measure gearbox vibration for fault detection. One of the main considerations regarding the transducers is that of the accessibility of installing them. As illustrated in Figure 3.1, one accelerometer is mounted on the gearbox casing where the mounting surface is flat and where the sensor can be mounted easily by bolting or gluing. This is common for many condition monitoring applications which place sensors in close proximity to vibration sources in order to acquire good vibration response characteristics.

There are many other applications, however, including oil field machines, marine power transmission systems and crane equipment where it is difficult to install sensors directly to the monitored devices, and they must instead be attached to a nearby device. To investigate the monitoring performance of sensors mounted far away from the device, the second sensor is mounted on the motor side of the flange joining the motor and gearbox. The vibration content of the gearbox will be less when compared with the vibration from the gearbox case.

3.2.2 Speed Measurements

In order to measure the Instantaneous Angular Speed (IAS) and shaft positions for calibration vibration frequencies, an optical encoder (Manufacturer: Hengstle; Type: Type: RS32-O/100ER) is fitted to the end of the induction motor shaft via a bracket mounted to the fan cowl (see Figure 3.9). The device produces a square pulse output for every angular degree (thus termed a 360 line encoder) as well as and for every complete revolution.

The output of the encoder is directly connected to the computer via the data acquisition system (DAQ) to provide a one-pulse-per-revolution synchronising pulse which is used to trigger the start of data capture. This ensures that the signal average produced is synchronised with a known shaft position, and that the location of the broken tooth can be determined [45].



Figure 3.9-Mounting of the motor encoder

3.2.3 Data Acquisition System (DAQ)

A data acquisition system is an electronic device designed to acquire data from sensor and transducers and monitor parameters such as vibration, sound, temperature, etc by conversion of physical analog quantities into digital data and rescaling them into physical quantities according to transducer sensitivities. A DAQ has two parts: hardware and software. The hardware consists of the data acquisition card and a host PC computer with control software and data storage space. The software controls the data collection process and has basic data analysis tools such as spectrum calculation for online data inspection.

The data acquisition card used in this study is a National Instrument data acquisition card of PCI 6221. It has 16-bit data resolution and a sampling frequency of up to 250 kHz for 16 single ended channels. The full specification of the data acquisition card is summarized in Appendix D.

Important parameters of the data acquisition system such as low pass (anti-aliasing) filters, quantization and sampling frequency involved in the ADC process are outlined below:

- **Low Pass Filter**

During data acquisition the accelerometer (analog) vibration signal is passed through a low-pass filter before the signal is sampled and recorded. The anti-aliasing filter built into the data acquisition system automatically adjusts the cut-off frequency of this low pass filter according to the pre-selected sampling rate. This is to guarantee that the aliased frequencies are not digitized. During data acquisition the low pass filter was adjusted at a cut-off frequency equal to 50 kHz.

- **Quantization**

Quantization is a process in which the analog-to-digital-converter (ADC) converts the accelerometer output voltage (analog) signals to discrete (digital) signals. This process is completed by dividing the amplitude range of the system (-5V to 5V in this study) into a number of discrete levels. For example, an n -bit ADC has the ability to produce 2^n quantized levels. Therefore, a 16-bit device will produce (2^{16}) or 65536 levels. A system with a selected input range of -5V to 5V, and divided into 2^{16} levels results in a resolution of $(10/65536) \approx 150\mu\text{V}$. The system also has an adjustable gain from 1 to 1000, therefore at a gain of 100, the system will have a maximum resolution of $1.5\mu\text{V}$.

- **Sampling**

Sampling is an essential process in which the continuous analog signal is converted to a discrete signal.

$y(t)$ the continuous signal to be sampled and this sampling is performed by measuring the value of the continuous signal at equal sampling intervals - Δt seconds. The sampling signal $y[n]$ is given by:

$$y[n] = y[n\Delta t], \quad n = 0, 1, 2, 3, \quad (3.3)$$

And the sampling frequency, f_s is defined as:

$$f_s = \frac{1}{\Delta t} \text{ (Hz)} \quad (3.4)$$

where: Δt is the time interval between samples

The output of any transducer is a continuously varying voltage. The ADC samples the analog signal as discrete values and stores it in the computer.

CHAPTER 3

TEST FACILITIES, TEST PROCEDURE AND BASELINE VIBRATION

A suitable sampling frequency (f_s) plays a major role in the acquisition of data as it determines whether the signal characteristics will be correctly recorded. The sampling frequency should be set high enough to capture the maximum frequency components of interest in the signal. According to the Shannon theorem, the sampling rate must be equal to or greater than the highest frequency (f_{max}) - called the Nyquist frequency - in order to properly reproduce the analytic signal.

Note:

If $f_s < 2f_{max}$ the frequency components are greater than half the sampling frequency and will therefore not be recorded correctly due to an aliasing problem.

Most data acquisition systems cannot sample fast enough to completely avoid the aliasing problem so a hardware-based anti-aliasing low pass filter is normally used to overcome this problem.

- **Amplifier**

The accelerometers are connected to the signal conditioning unit (kemo type VBF/4) providing power to the accelerometers and amplifying the charge signals. The amplified output signals of this device are sent to the data acquisition system for recording and analysis.

The software comprises of the data acquisition logic and the analysis software, as well as other programmes which are used to configure the logic or to move data from the data acquisition memory to the computer. A data acquisition control programme developed on Lab-windows was used in this research, and consisted of a main data inspection panel, as seen in Figures. 3.10.

The software is based on a Windows operating system and has the ability to perform on-line data sampling. It required modifications such as inclusion of the channel number, sampling frequency, data length and filenames, all of which could be selected, recorded and stored on separate set-up page of the software package.

Figure 3.10 shows the data acquisition process in progress. The screen can be divided into three channels, each displaying a different type of data from a different location.

The first channel is the encoder signal; the second, the vibration signal from the gearbox casing and the third, the vibration signal from the motor flange.

CHAPTER 3

TEST FACILITIES, TEST PROCEDURE AND BASELINE VIBRATION

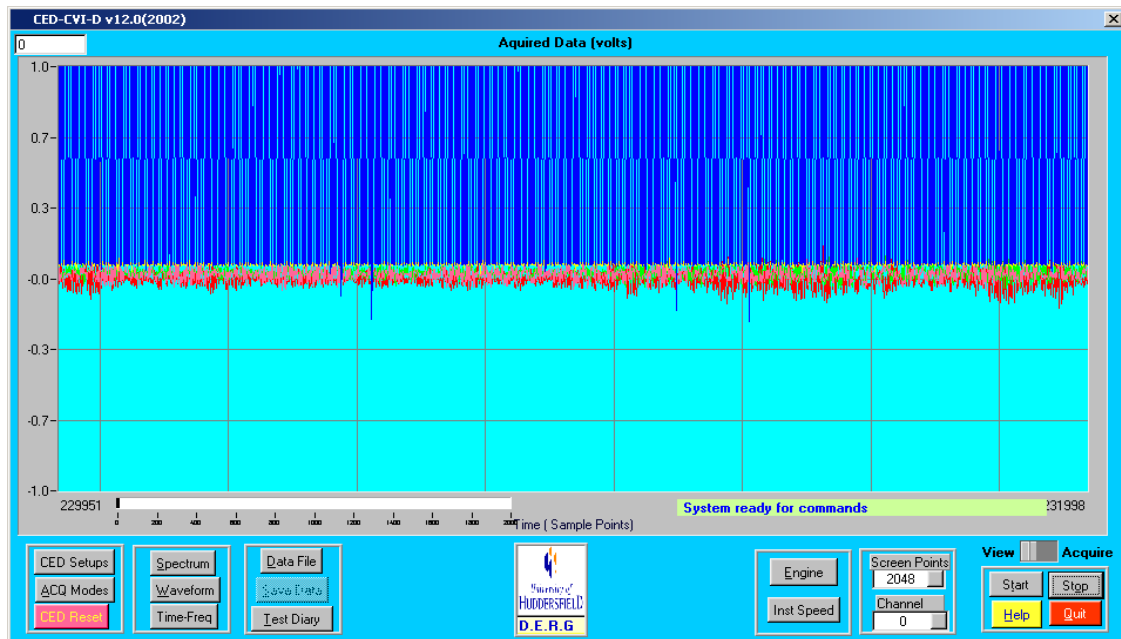


Figure 3.10-The main data inspection panel

The accelerometer output is an analog voltage signal which is converted to a digital signal using the ADC. The ADC is used for further processing and analysis of the data through the programming of different algorithms using the Matlab software.

3.3 Test Procedures (Variable speed and load tests)

Gearboxes are regularly operated under fluctuating or varying load conditions and the assumption that variations in the measured vibration signal (response) occur as a result of a faulty gearbox may be invalid [111]. The change in induced load and rotating frequency is known to modulate the amplitude of the measured response (see section 1.7.2). This may lead to situations where the value of a measured response of a normal (healthy) condition corresponding to a unique combination of induced load and rotating frequency of the shaft may belong to an abnormal (faulty) condition with higher levels of induced load and rotating frequency. Thus, extracting features in such situation may turn out to be tricky and future develops into a challenging task for accurate recognition of the gearbox condition [111].

Commonly, researchers who have investigated the condition of gearboxes when operated at constant loads and rotating speed do not mention the details of these conditions, the fact that a gearbox may operate at different levels of loads and rotating speeds (frequencies) has not been adequately investigated. In this work I will

CHAPTER 3

TEST FACILITIES, TEST PROCEDURE AND BASELINE VIBRATION

investigate the vibration signals originating from the gearbox at different loading conditions and shaft speeds (rotating frequencies).

This research studies the effect of different rotating frequencies of the shaft on the vibration signals. This is carried out by recording vibration signals at different shaft speeds ranging from 20% to 100% with increments of 20%. To investigate the different loading conditions, vibration signals are collected at different load levels:

- ❖ 0% full load (no load)
- ❖ 20% full load
- ❖ 40% full load
- ❖ 60% full load
- ❖ 80% full load

The vibration signals were collected using two accelerometers (PCB Model 338C04) mounted on the gearbox casing and motor flange, see Figure 3.1. The signals were collected and measured simultaneously and were sampled at 50 kHz. For each measurement, 10^6 data points were collected and recorded in 20 seconds to obtain a frequency resolution of 0.05Hz to differentiate rich frequency components in the gearbox vibration signals.

The collected signals consisted of four sets of data: one for a healthy gear and three for faulty gears, which were all collected under the same gear operating conditions.

3.4 Gear Fault Simulation

In this research, three different severities of a local type fault were simulated. Section 1.6 has already described how faults may inhibit gearbox operation. Fault simulation was carried out individually (one fault at a time) and the faults were artificially introduced to the pinion gear of the first stage in the gearbox shown in Figure 3.3.

In an ideal situation, the faults should be introduced onto the same healthy pinion gear, with one tooth.

However, due to time and machining limitations, the faults were introduced onto three identical pinion gears, by removal of a percentage of the tooth face width. The first pinion gear had 25% of one tooth removed; the second, 50% of one tooth; and in the

CHAPTER 3

TEST FACILITIES, TEST PROCEDURE AND BASELINE VIBRATION

third, a complete tooth was removed. Figure 3.11 illustrates the faults in detail. Because of a high overlap ratio the gearbox can still operate without noticeable signs of deterioration even when a full tooth has been removed.

In order to easily describe faults during this fault diagnosis study, the pinion gear faults are labelled throughout this thesis as follows: the 25% broken tooth is referred to as Fault 1, 50% referred to as Fault 2 and the completely broken tooth is Fault 3.

These simulated faults are shown in Figure 3.11 respectively.

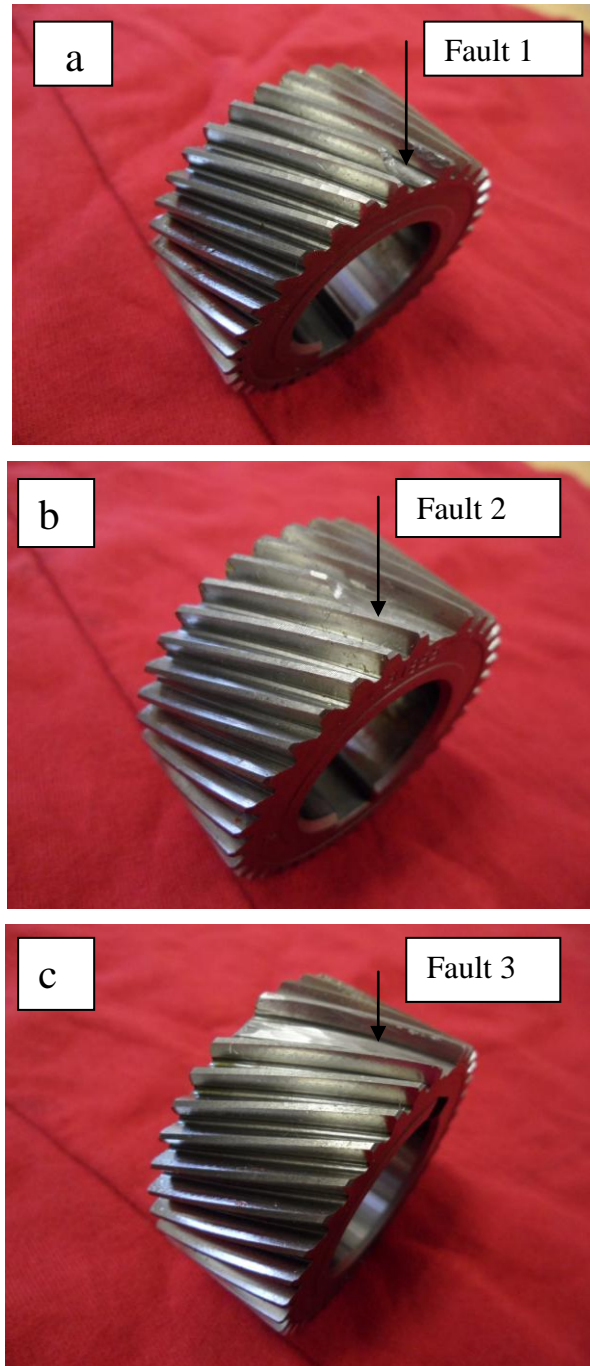


Figure 3.11-Simulated broken tooth (a=25%, b=50%, c= complete tooth removal)

3.5 Calculation of Gear Characteristic Frequencies

The fundamental excitation frequencies of the gearbox (Figure 3.4) can be calculated from Equations 3.8-3.10 [41]. Examination of the amplitude of the frequency spectrum of the vibration signal will often point to a specific gear in the gearbox as the source of a fault. In fact, a change in amplitude at any of these excitation frequencies should be taken as an indication of a fault in the gears.

The most important gearbox vibration is a result of tooth mesh rate, which can be calculated using Equation 3.7. [112].

$$f_m = N \cdot f_r \quad (3.7)$$

where; f_m = mesh frequency, N = no of teeth and f_r = rotation shaft frequency

Any significant increase in the amplitude of the peak in the spectrum corresponding to f_m with no corresponding change in speed or load strongly suggests a fault is developing. If the increase in amplitude extends to both the tooth meshing frequency and its harmonics then it is likely to be a distributed fault such as gear wears [113]. If, however, the increase in amplitude shows as an increase in the tooth meshing frequency and the sidebands are closely grouped around it then the fault is more likely to be misalignment or eccentricity [19]. Table 3.3 lists fundamental frequencies and harmonics of the two-stage gearbox under investigation.

Table 3.3-Healthy tooth meshing frequencies and their harmonics

Fundamental Frequency & Harmonics					
Input Stage	80% Load Full speed	40% load 50% speed	Output Stage	80% Load Full speed	40% load 50% speed
f_{m1}	838.44	428	f_{m2}	347.6	177
$2 f_{m1}$	1679	856	$2 f_{m2}$	695	355
$3 f_{m1}$	2517	1284	$3 f_{m2}$	1042.8	531

CHAPTER 3
TEST FACILITIES, TEST PROCEDURE AND BASELINE VIBRATION

The values of the first, second and third shaft rotational frequencies: f_{r1} , f_{r2} , f_{r3} at high operating condition (80% load and full Speed) can be determined as:

$$f_{r1} = \frac{RPM}{60 \text{ sec}} = \frac{1479.6}{60 \text{ sec}} = 24.66 \text{ Hz} \quad (3.8)$$

$$f_{r2} = f_{r1} \cdot \left(\frac{z_1}{z_2}\right) = 24.66 \left(\frac{34}{70}\right) = 11.977 \text{ Hz} \quad (3.9)$$

$$f_{r3} = f_{r2} \cdot \left(\frac{z_3}{z_4}\right) = 11.977 \left(\frac{29}{52}\right) = 6.68 \text{ Hz} \quad (3.10)$$

The meshing frequencies for the first and second stage are defined as:

$$f_{m11} = f_{r1} \cdot z_1 = 24.66(34) = 838.44 \text{ Hz} \quad (3.11)$$

$$f_{m21} = f_{r2} \cdot z_3 = 11.977(29) = 347.33 \text{ Hz} \quad (3.12)$$

where: Z_1 = number of teeth on the pinion gear at the first stage.

Z_2 = number of teeth on the driven gear at the first stage.

Z_3 = number of teeth on the pinion gear at the second stage.

Z_4 = number of teeth on the driven gear at the second stage.

f_{m11} = meshing frequency of the first gear pair.

f_{m21} = meshing frequency of the second gear pair.

3.6 Baseline Data of Gearbox Vibration

3.6.1 Signature in the time domain

It is well known that each rotating machine will produce its own spectrum of frequencies. If the baseline vibration of a healthy machine is compared to the signal of a similar machine running at the same speed and under similar conditions, any increase over the baseline at any forcing frequency can indicate the presence of abnormalities in the machine. The baseline vibration signals (waveform) were recorded by the transducer for 0.2 seconds. The transducer was mounted on the gearbox casing and baseline data corresponding to low and high operating conditions are shown in Figures 3.12 and 3.13 respectively.

CHAPTER 3

TEST FACILITIES, TEST PROCEDURE AND BASELINE VIBRATION

A change in the operating condition of the gearbox causes a change in the originating vibration signal.

Comparison of the vibration signals in Figures. 3.12 and 3.13, confirms that there is an enormous amount of unknown information associated with the waveform of the signals.

The vibration signals obtained for both operating conditions are characterized by an excessive noise level and are non-stationary and nonlinear in nature.

As seen in Figures 3.12 and 3.13 there are clear differences between the waveforms for different gear conditions at the high operating conditions. The amplitude of the signal is smallest in the case of low operating conditions and largest in the case of high operating conditions.

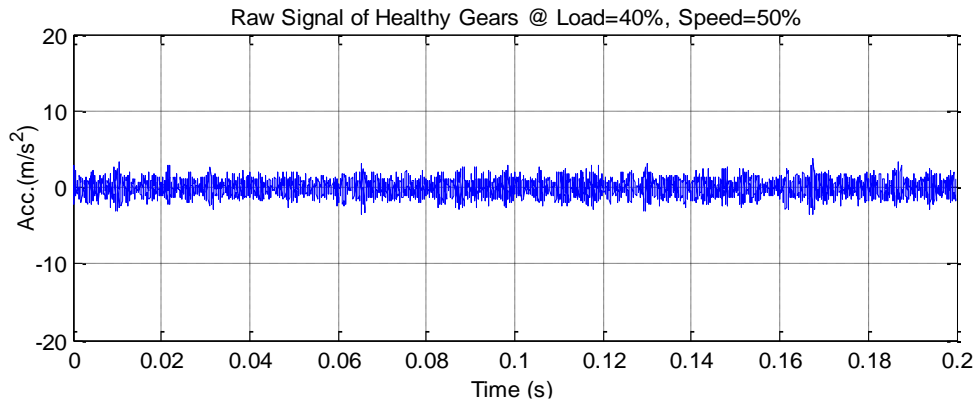


Figure 3.12-Gearbox vibration baseline data (in time domain) at low (L=40%, S=50%) operating conditions

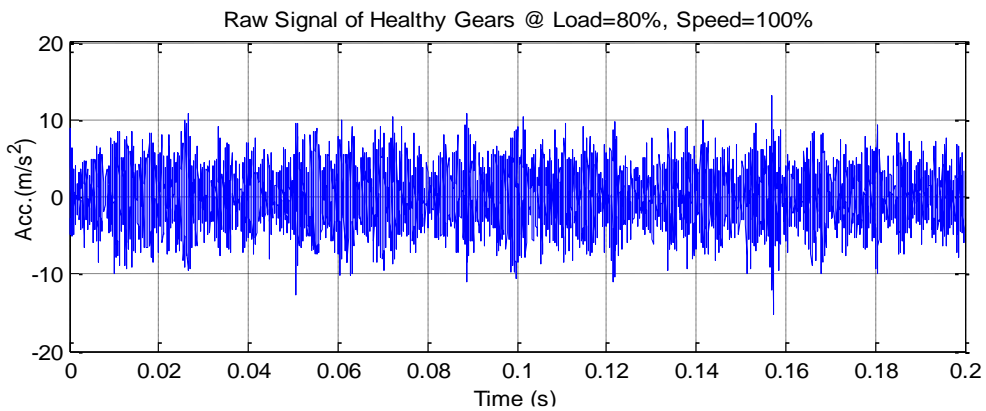


Figure 3.13-Gearbox vibration baseline data (in time domain) at high (L=80%, S=100%) operating conditions

As mentioned in section 2.1.2, the Root Mean Square (RMS) value is one of a series of simple descriptive quantities of the overall vibration level and takes the time history of the vibration signal into account in order to calculate its RMS value. This is expressed in Equation 2.2.

Figure 3.14 shows the RMS values measured by an accelerometer mounted on the gearbox casing. The RMS values increase in a nearly linear fashion with loads and speeds - lower operating conditions produce lower vibration and viscera. This confirms that higher operative conditions cause higher dynamic loads on the gears and bearings etc to produce higher vibration levels.

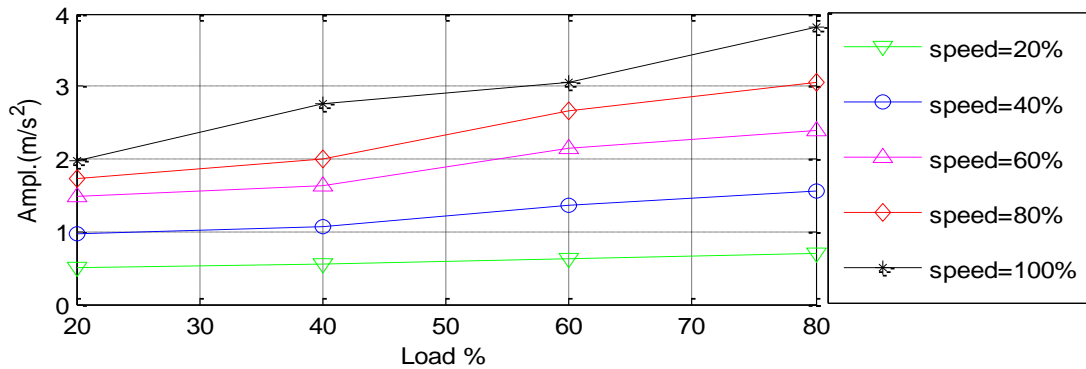


Figure 3.14-Variation in RMS for various gear operating conditions

These changes in vibration are consistent with the effects of the faults and it is only through careful study of the measured signals whether or not a change can be attributed to the operating condition of the system or a fault of the gear.

3.6.2 Signature in the frequency domain

A vibration spectrum taken from a machine in healthy operating conditions is commonly used as a reference for monitoring and analysis.

The most important components in gear vibration spectra are both the gear meshing frequency and its harmonics (due to gear transmission errors and time-varying meshing stiffness), together with the sidebands due to modulation phenomena. Low-level-running-speed sidebands around the gear meshing frequency are also common spectrum features and are usually caused by small amounts of eccentricity or backlash.

CHAPTER 3

TEST FACILITIES, TEST PROCEDURE AND BASELINE VIBRATION

Figures 3.15 and 3.16 show a typical baseline vibration spectrum for a two-stage helical gearbox used in this study and operated at low and high conditions respectively.

Both spectra are rich with components due to the pinion/gear mesh of the first and the second stages. Also included are components due to additional system components. To gain a full understanding of the vibration spectrum, an examination of the spectrum is carried out according to the following spectral contents: 1) the meshing frequency and its sidebands in the first stage, 2) the meshing frequency and its sidebands at the second stage and 3) the shaft frequency components.

1) Spectrum features at the meshing frequency of the first stage

Figures 3.15a and 3.16a show the spectra of the vibration signal obtained from the 2-stage helical gearbox under the two operating conditions. The meshing frequency and its harmonics are illustrated clearly in both figures.

For the two input shaft frequencies of 12.588Hz (corresponding to low operating condition) and 24.67Hz (corresponding to high operating condition) f_{m11} are roughly 428Hz and 838Hz respectively. The first stage meshing frequency and its harmonics for both operating conditions are illustrated clearly in the baseline spectrum shown in Figures 3.15 (b) and 3.16 (b). Each diagram depicts the two meshing frequencies with high amplitudes.

Figure 3.15 (b) is the spectrum around the first stage meshing frequency with a frequency range of 380Hz to 480Hz (the meshing frequency is approximately 428Hz, $755.3.\text{rpm}/60 \times 34 = 428\text{Hz}$) and Figure 3.16 (b) is the spectrum around the first stage meshing frequency with a frequency range from 780Hz to 920Hz (the meshing frequency is approximately 838.44Hz, $1479.6.\text{rpm}/60 \times 34 = 838.44\text{ Hz}$).

It can be seen from Figures 3.15 and 3.16 that the amplitude of the gear meshing frequency can change significantly as a result of the operating conditions (i.e. rpm, load), so gear meshing frequency amplitude alone is not a good indicator of condition. Figures 3.15b and 3.16b show that a pinion rotation modulation sideband occurs around the mesh frequency component. This sideband, however, is not dominant. These sideband frequencies can be modulated by backlash loading of the gear train.

2) Spectrum features at the meshing frequency of the second stage

CHAPTER 3

TEST FACILITIES, TEST PROCEDURE AND BASELINE VIBRATION

The input shaft frequencies f_{m21} are roughly 177Hz and 347Hz respectively and the second stage meshing frequency and its harmonics for both operating conditions are clearly illustrated in the baseline spectra shown in Figures 3.15 (c) and 3.16 (c).

In figure 3.16 (c) the spectrum around the meshing frequency f_{m21} has a frequency band between 140Hz to 220Hz (the meshing frequency is approximately 177.3Hz, $f_{m21} (12.588 * \frac{34}{70}) * 29 = 177.3\text{Hz}$) and in Figure 3.16 (c) the spectrum around the meshing frequency f_{m21} has a frequency band between 250Hz to 450Hz (the meshing frequency is approximately 347.35 Hz, $f_{m21} (24.66 * \frac{34}{70}) * 29 = 347.35\text{ Hz}$). Since the load was applied on the output side, the amplitude of f_{m21} is also clearly pronounced.

3) The shaft frequency components

A section of the baseline spectrum is shown in Figures 3.15 (d) and 3.16 (d). One can see the rotational frequencies of the input shaft (at 12. 588Hz for low speed, and 24.66Hz for high speed) and its first three higher order harmonics. The amplitudes of even number harmonics have higher amplitudes than those of the odd number harmonics, indicating that there is a misalignment in the input shaft. However, compared with the amplitude of the meshing frequencies, the amplitude of the rotational frequency is much smaller, indicating that the vibrations of the signal arise mainly from the gear meshing process.

CHAPTER 3

TEST FACILITIES, TEST PROCEDURE AND BASELINE VIBRATION

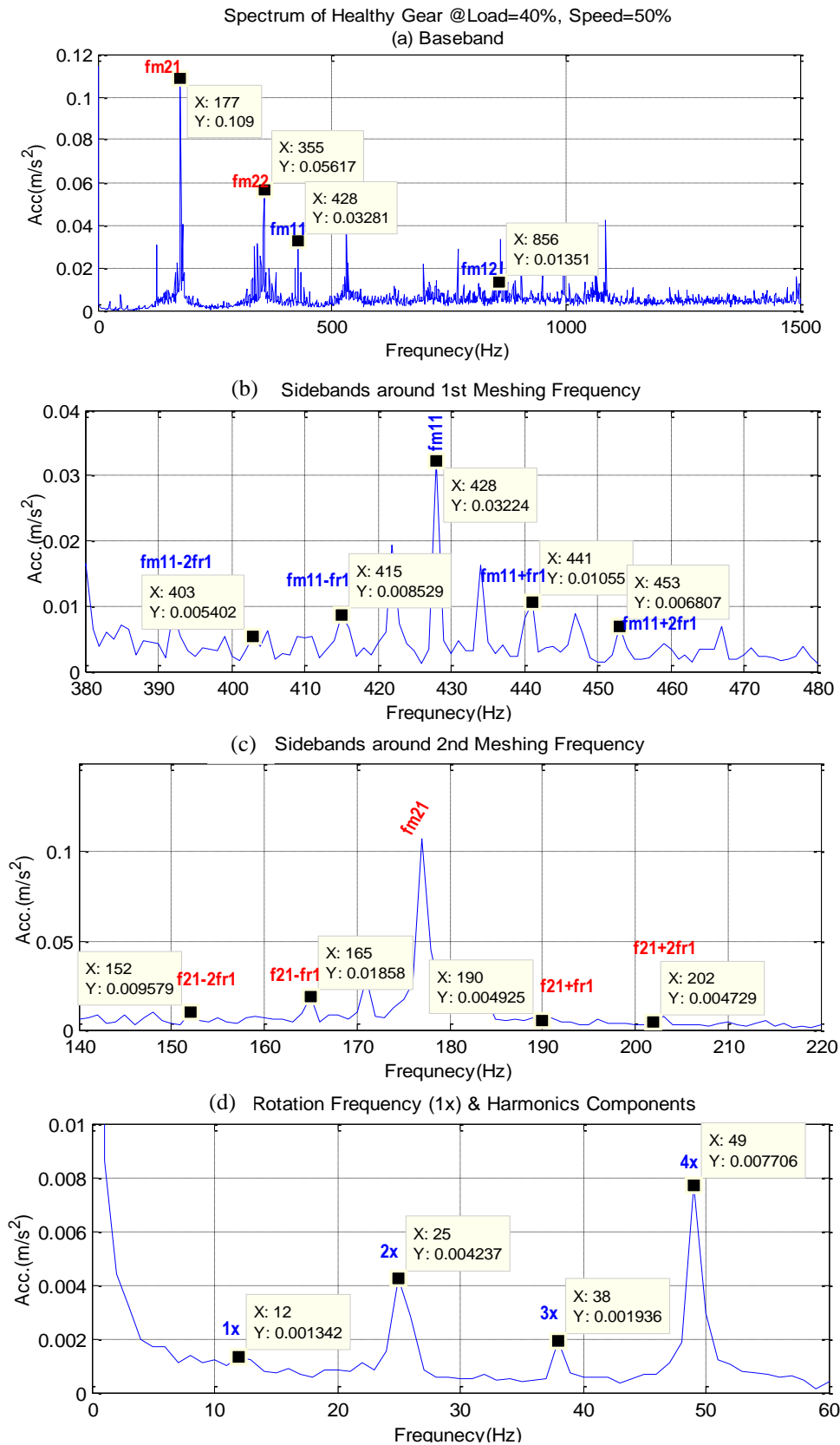


Figure 3.15-Gearbox vibration baseline data (in the frequency domain) at low ($L=40\%$, $S=50\%$) operating conditions

CHAPTER 3

TEST FACILITIES, TEST PROCEDURE AND BASELINE VIBRATION

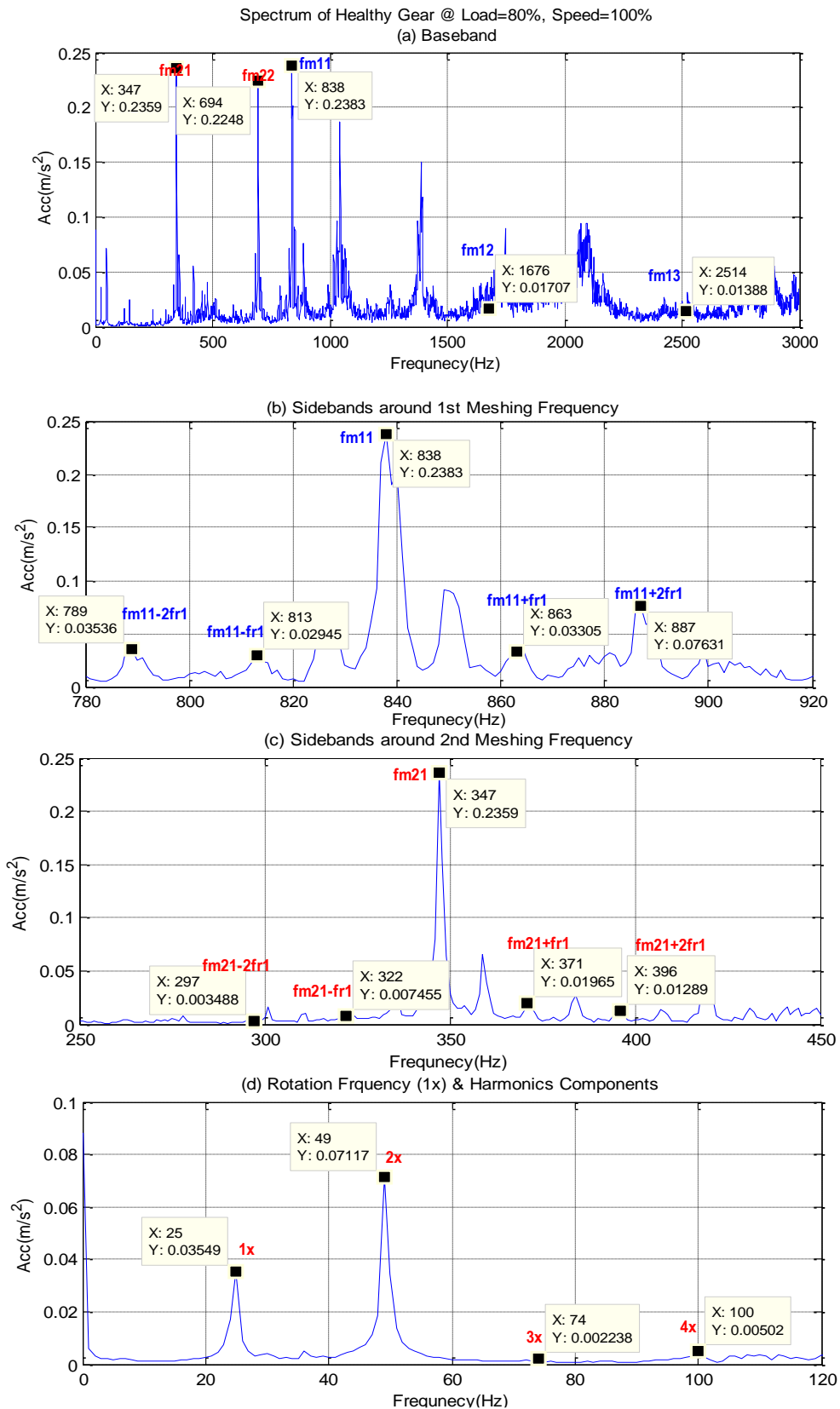


Figure 3.16-Gearbox vibration baseline data (in the frequency domain) at high (L=80%, S=100%) operating conditions.

CHAPTER 3
TEST FACILITIES, TEST PROCEDURE AND BASELINE VIBRATION

Figures 3.17 and 3.18 show how the amplitude of the first (f_{m11}) and second stage (f_{m21}) of meshing frequencies changes with operating conditions (i.e. speed and load).

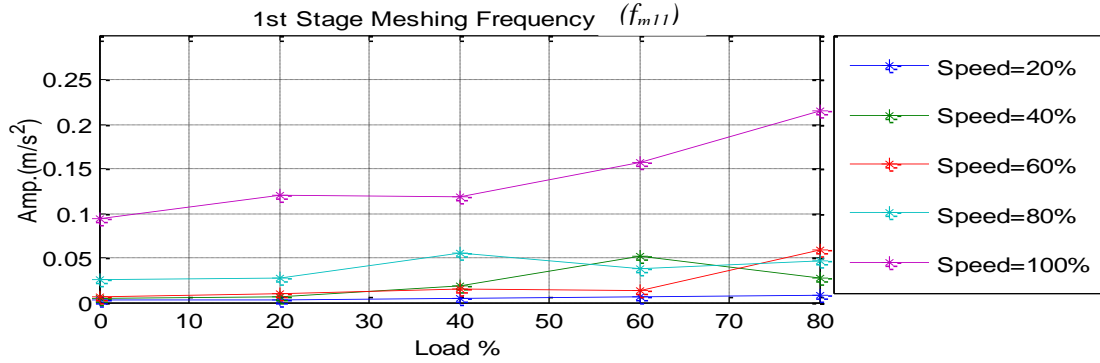


Figure 3.17-Variation in first meshing frequency amplitude for various gear operating conditions.

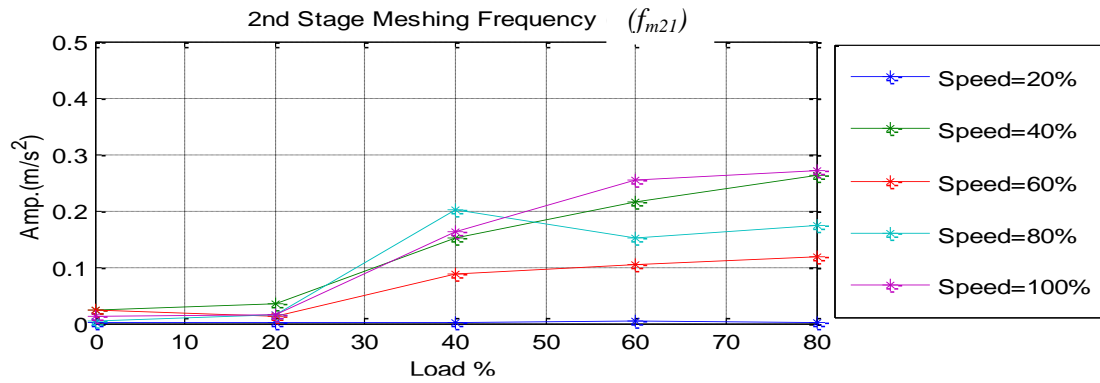


Figure 3.18-Variation in second meshing frequency amplitude for various gear operating conditions.

These figures show that the amplitude of the gear meshing components is highly affected by operating parameters such as load, implying that the gear meshing frequency amplitude alone is not a good indicator of gear health condition.

Figure 3.18 also shows that the overall vibration level increases at high applied loads, since the load was applied on the output side (second stage), the amplitude increase of f_{m21} is more pronounced than that of f_{m11} .

3.6.3 Signature in the time-frequency domain (CWT representations)

As indicated in the time domain signals, vibrations from the gearbox clearly have many local spikes. As well as this, it can be seen that gears with local faults produce short transients. These features of signals can't be characterised by normal frequency analysis, instead a joint time-frequency method is often used for analysing them.

CHAPTER 3

TEST FACILITIES, TEST PROCEDURE AND BASELINE VIBRATION

CWT is demonstrated to be more efficient than many others methods, including short-time Fourier Transform (STFT) which is based on a wavelet that looks very similar to transient signals. This study, therefore, applies CWT to the gear vibration data sets.

To calculate CWT with optimal resolution in the time and frequency domain, the

Morlet wavelet centre frequency ω_0 is set to 7rad/s or $f_0 = \frac{\omega_0}{2\pi} = 1.114\text{Hz}$ for all

the gear operating conditions so that a comparison can be made easily. The FFT size is set to 2^{18} data points, equivalent to 5.2429 seconds to obtain a large enough frequency range and resolution for differentiating the meshing frequencies. In addition, to avoid a high calculation load, the octave band based fast calculation procedure was performed with 12 voices per octave.

Figures 3.19 and 3.20 show the baseline results of the CWT by applying Equation 2.18 to vibration signals in Figures 3.13 and 3.14. To reflect the key features, the CWT results are presented in colour. The baseline images of the CWT describe when a signal component occurs and how its frequency spectrum develops with time, allowing more features of vibration to be recognised.

From Figures 3.19 and 3.20 it can be seen that CWT image patterns are clearly different for different operating conditions. For both operating conditions, the periodic feature can be clearly seen. The fundamental and second tooth meshing frequencies are visible, though the energy of the vibration signal is mainly concentrated around the fundamental meshing frequency. In low operating conditions, the first and second stage meshing frequencies are clearly visible at 177Hz and 428Hz respectively. At high operating conditions these frequencies are instead visible at 347Hz and 838Hz.

The wavelet transformation results in good frequency resolution at low frequencies and gradually deteriorates as it moves to higher frequencies as seen in both figures. This varying resolution on the time-frequency plane is due to the change in the size of the wavelet during the analysis.

In addition, the low frequency characteristics of the vibration signal can be captured and displayed more clearly when compared with higher frequency regions. Because of the normal (healthy) condition, the amplitude plot of the wavelet does not change

CHAPTER 3
TEST FACILITIES, TEST PROCEDURE AND BASELINE VIBRATION

significantly and most of the signal energy remains in the fundamental meshing frequency region.

However, the patterns of the energy distribution and the degree of concentration of the signal energy represented in the figures exhibit distinguishable characteristics. Regardless of gear operating conditions, the interaction between the gear meshing harmonics from different gears in the gearbox generates horizontal bands in the frequency range between 0-0.9 kHz for a low operating condition and between 0-1.8kHz for a high operating condition. This occurs due to first and second stage meshing gears. It can be seen that there are some regions on the time-frequency plane where the density of the vibrational energy has increased.

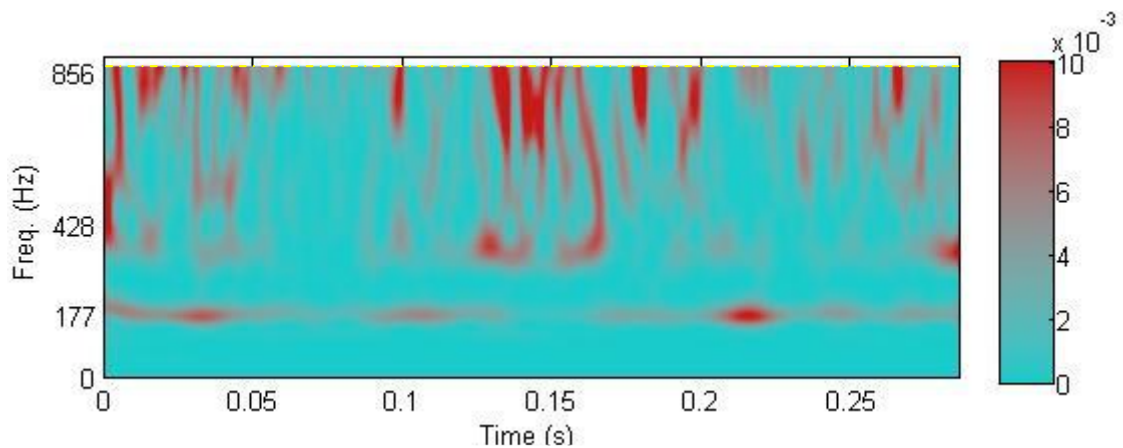


Figure 3.19- Gearbox vibration baseline data (in the time-frequency domain) at low ($L=40\%$, $S=50\%$) operating conditions

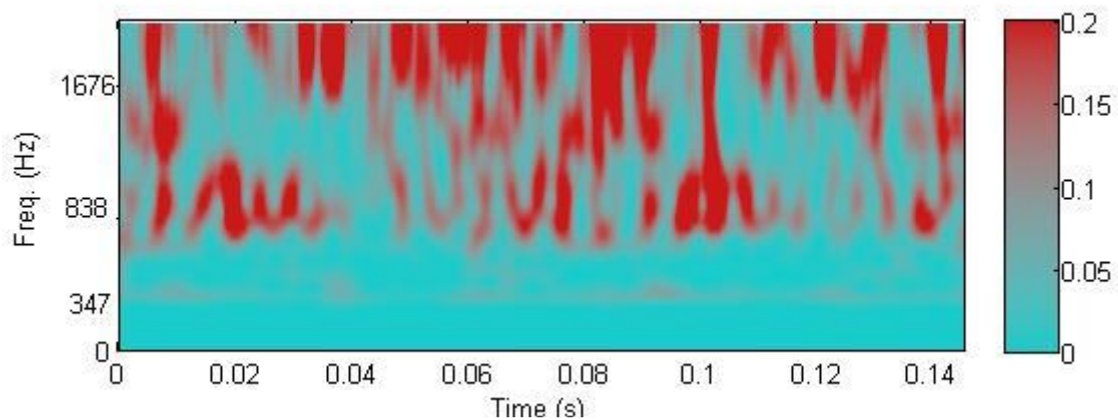


Figure 3.20- Gearbox vibration baseline data (in the time-frequency domain) at high ($L=80\%$, $S=100\%$) operating conditions

CHAPTER 3

TEST FACILITIES, TEST PROCEDURE AND BASELINE VIBRATION

At low operating conditions as shown in Figure 3.19, as long as the gearbox is operating properly, dominant fundamental gear meshing (428 Hz) and second stage meshing (177 Hz) generate two horizontal bands (strips) in the image. It can be seen that a fraction of the signal energy leaks and stretches into the low frequency band (0~0.9 kHz) with increasingly high intensity at specific instants of time. A portion of signal energy leaks into a specific frequency band, especially in high frequency regions beside the first harmonic of the gear meshing frequency. The leakage of energy has a slowly increasing trend to begin with and as high operating conditions are reached the slope tends to be wider. This wide band characteristic is mainly due to the periodic impulse trains generated from the high load. This observation suggests that a relationship exists between the fraction of energy in this region and the operating condition of the gearbox.

However, as the operating condition increases, it causes the spectral pattern to change. The strip at the frequency range around 1 kHz in the case low operating condition and 2kHz in the case high operating condition, show where a resonance in the gear system (most of the structural vibrations) may exist. For example, at low operating conditions the presence of meshing gears is suggested by one section of high amplitude values in between 0 and 0.5 kHz where the gearbox is operating properly.

At a high operating condition a concentration of high energy peaks falls between 0.8 and 2.0 kHz. High operating load and speed conditions cause the distribution of peak amplitude values to stretch towards the higher frequency region and appear at different time units and frequencies in the contour.

3.7 Summary

The test rig facility and data acquisition software were developed as detailed in this chapter. In Section 3.1.1 two stage helical reduction gearbox manufactured by David Brown Radicon Limited was selected for this research project. Consequently the environment in which the practical research work was conducted was similar to an industrial environment and practical gearbox applications.

The baseline vibration data for a healthy gearbox have been established and are discussed in Section 3.6.

CHAPTER 3

TEST FACILITIES, TEST PROCEDURE AND BASELINE VIBRATION

The baseline vibration signals were recorded by the transducer mounted on the gearbox casing and the baseline data (waveform) corresponding to low and high operating conditions was discussed in Section 3.6.1. The vibration signals obtained for both operating conditions are characterized by an excessive noise level and are non-stationary and nonlinear in nature. In addition, the RMS values increase in a nearly linear fashion with loads and speeds - lower operating conditions produce lower vibration and viscera. This confirms that higher operative conditions cause higher dynamic loads on the gears and bearings etc to produce higher vibration levels. Section 3.6.2 showed the typical baseline vibration spectrum at low and high conditions respectively. Both spectra are rich with components due to the pinion/gear mesh of the first and the second stages and their sidebands and the first and second stage meshing frequencies and their harmonics for both operating conditions are clearly illustrated in the baseline spectra.

Section 3.6.3, shows the baseline results of the CWT by applying Equation 2.18 to vibration signals in Section 2.3.4. To reflect the key features, the CWT results are presented in colour. The baseline images of the CWT describe when a signal component occurs and how its frequency spectrum develops with time, allowing more features of vibration to be recognised.

CHAPTER 4

CONVENTIONAL CONDITION MONITORING OF A GEAR SYSTEM

In this chapter, the vibration signals for different gear conditions (healthy and faulty) and different operating conditions were recorded from a sensor mounted on the gearbox casing. These signals were analyzed using conventional methods made in the time, frequency and joint time-frequency (Morlet continuous wavelet transform) domains to obtain a set of effective features for detecting and diagnosing the seeded gear tooth faults. The time domain analysis leads to popular statistical feature parameters such as peak value, RMS, kurtosis and crest factor. The frequency domain analysis (standard Fourier Transform) analysis produces spectral features including amplitudes at meshing frequencies, their harmonics and their associated sidebands. The set of these features is evaluated in the separation of faults under different conditions. In the same way the time-frequency representations of the vibration data are also obtained but feature parameters are not developed due to the fact that they have little consistency with the fault levels induced. This study demonstrates that conventional methods are not able to show the presence and progression of tooth breakage faults in gears and demonstrates the need for further development of analysis methods to overcome the problems identified in the diagnosis of gear faults.

4.1 Introduction

There are many conventional techniques used to monitor the condition of rotating machinery. Most of them are easy to understand and are also simple to implement. Moreover, they are all reported in the literature and systems exist to provide good performance monitoring.

To evaluate these monitoring techniques, faults were induced in the gearbox under investigation. Methods were selected from reviews of several commercial software packages used to analyse vibration data sets. Methods used include common statistical parameters calculated in the time domain with the characteristic frequency features calculated in the frequency domain.

In addition, the CWT representations have also been calculated to establish more effective methods of examining changes due to faults in the joint time frequency domain.

4.2 Time Domain Analysis

When a gearbox is operating under faulty conditions it is expected that the vibration will be large and hence statistical parameters that describe the characteristics of signals will vary accordingly. In this section, the vibration waveforms are examined to confirm this hypothesis and three statistical parameters have been calculated. The peak value and root mean square (RMS) were calculated to reflect the strength of the signal amplitude, with peak value measuring predominantly local changes while RMS measured mostly overall changes in the system. In addition, the kurtosis was calculated to highlight local changes, and the peak factor, to provide a general measure of overall changes. Both kurtosis and peak value were calculated to reflect signal structures with dimensionless parameters to avoid the influence of operating parameters.

4.2.1 Time Domain Signals (Waveform)

Typical vibration waveforms from the transducer, mounted on the gearbox casing are presented in Figure 4.1. Waveforms for one healthy and three faulty gear systems (Fault 1, Fault 2 and Fault 3) are shown. To demonstrate signal sensitivity to operating conditions, results are presented for low and high operating conditions.

CHAPTER 4

CONVENTIONAL CONDITION MONITORING OF A GEAR SYSTEM

Analysis of vibration signals as shown in Figure 4.1 has demonstrated that the signals are very complex and a significant amount of information regarding the waveform of the signals is unknown. All waveforms show a degree of distortion but no obvious fault symptoms were found even under the very severe fault condition such as Fault 3.

As can be seen in Figure 4.1 there are clear differences between the waveforms of different gear conditions for both low and high (i.e., Speed (S) and Load (L)) operating conditions. The amplitude of the signal in the low operating condition is much smaller than that of the high operating condition. This shows that the operating condition has a significant effect on the gear diagnosis.

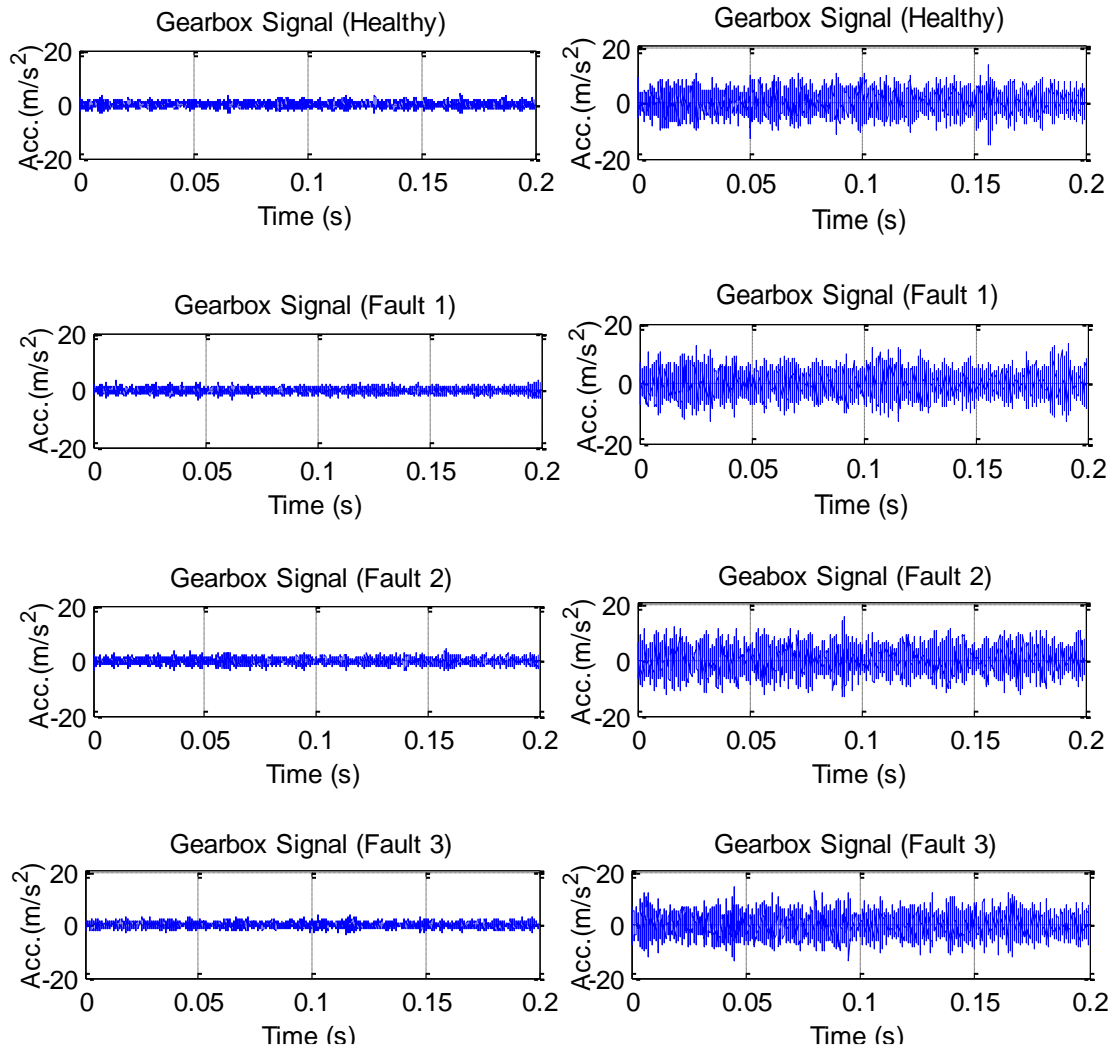


Figure 4.1- Local vibration signals for healthy and faulty gear systems at low operating conditions (L=40%, S=50%) (Left) and at high operating conditions (L=80%, S=100%) (Right)

CHAPTER 4

CONVENTIONAL CONDITION MONITORING OF A GEAR SYSTEM

To identify and understand more accurately the signals from the healthy and faulty gears under different operating conditions, four types of time domain statistical parameters were calculated: peak value, RMS, crest factor and kurtosis, which are given in Equations 2.1-2.4, and were extracted from the time domain vibration signal. The statistical parameters were computed under various rotational speed and load scenarios. Speed ranged from 20% to 100% and load from 20% to 80%. Both parameters were sampled at 20% increments and results for the time domain statistical parameters under these operating conditions are shown in Figures 4.2- 4.5.

These parameters characterize the time-domain vibration signal statistically to produce an overall indication of some aspects of the machine status and due to their simplicity and wide use in engineering applications; they are commonly used for fault or abnormality indication. However, individual statistical parameters are not a reliable indicator of machine condition because of the high complexity of vibration signals. Statistical information from all time-domain parameters should be considered collectively and processed in parallel to provide a more reliable analysis.

4.2.2 Signal Strength based Diagnosis (Peak value and RMS)

The peak value and RMS are simple descriptive quantities used to measure overall vibration levels. The average peak value and RMS of healthy and faulty conditions have been derived from time domain signals. Figures 4.2 and 4.3 show how these parameters vary with advancing tooth breakage under different gear operating conditions.

The results from Figures 4.2 and 4.3 show that peak value and RMS increase fairly linearly with the speed and load. This confirms that the operational conditions of the gears can alter the vibration signal and therefore highly affect the overall peak value and RMS.

The slight change in the peak and RMS values of the vibration signal between healthy and faulty conditions at low and high operating conditions does not provide significant information about the pinion gear condition. It can be concluded that the peak value and RMS data do not exhibit a reliable trend with fault progression even when the severity of the fault is high (Fault 3).

CHAPTER 4

CONVENTIONAL CONDITION MONITORING OF A GEAR SYSTEM

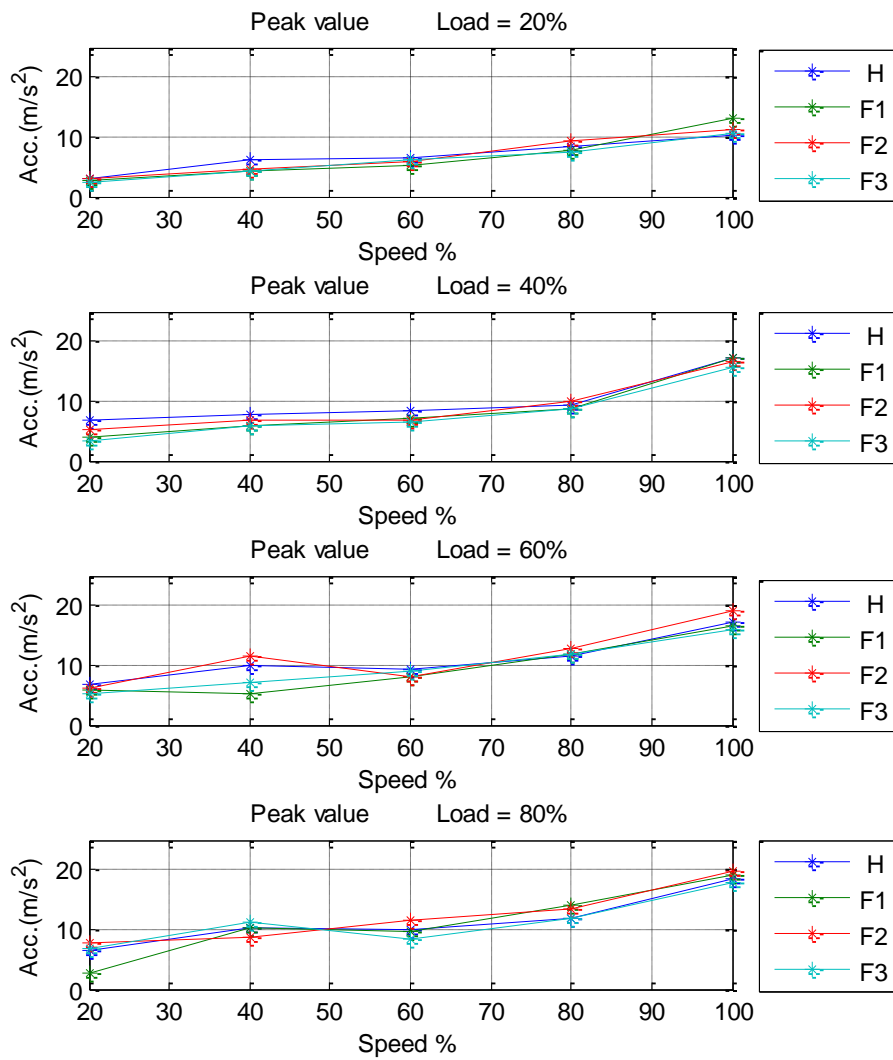


Figure 4.2- Average Peak value of the vibration signal for healthy and faulty gears

CHAPTER 4

CONVENTIONAL CONDITION MONITORING OF A GEAR SYSTEM

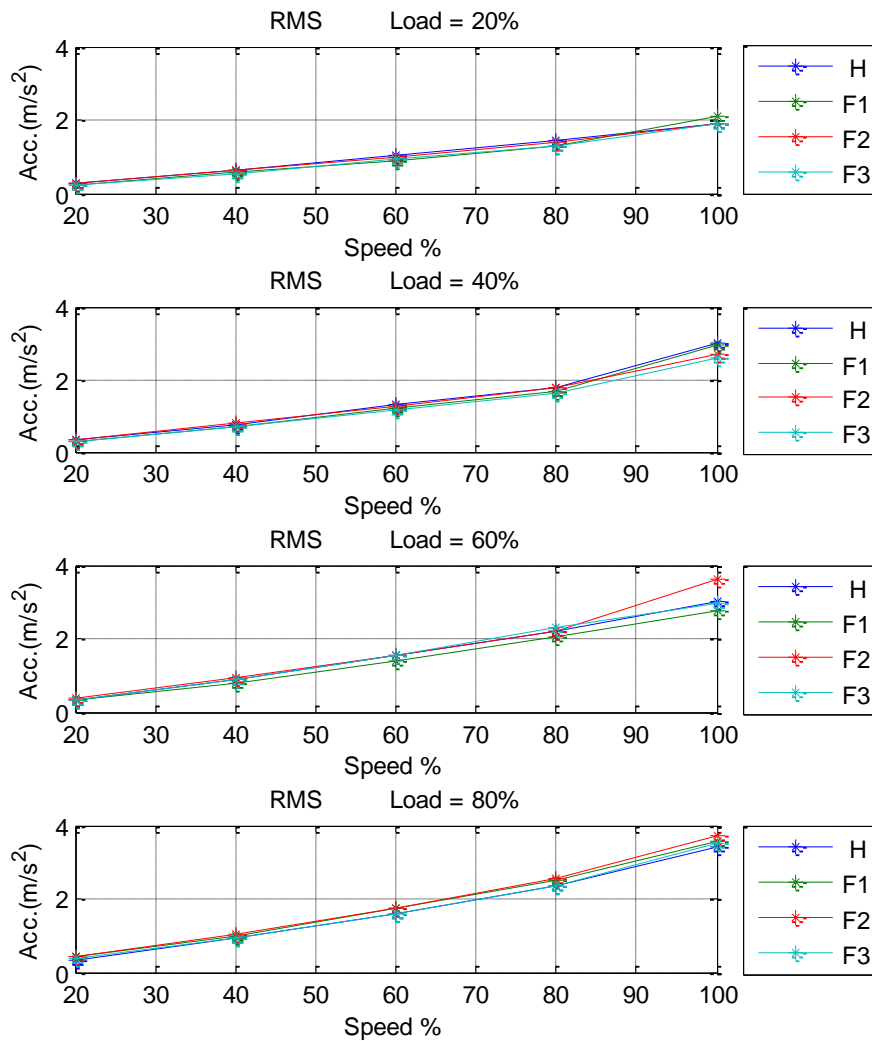


Figure 4.3- Average value of RMS of the vibration signal for healthy and faulty gears

4.2.3 Signal Structure based Diagnosis (Crest Factor and Kurtosis)

The kurtosis value (or fourth statistical moment) and crest factor are also frequently used statistical parameters in CM. Figure 4.4 and 4.5 show the kurtosis and crest factor data for the vibration signals from the gearbox. As previously, results for one healthy and three faulty gear systems under different operation conditions are shown. Operating conditions were measured via a transducer located on the gearbox casing.

It can be seen that, both kurtosis and crest factor do not exhibit a reliable trend with fault progression at all operating conditions. For instance, for the healthy gear status,

CHAPTER 4

CONVENTIONAL CONDITION MONITORING OF A GEAR SYSTEM

kurtosis and crest factor were higher than under faulty conditions. At low speed, kurtosis and crest factor clearly indicate the gear statuses.

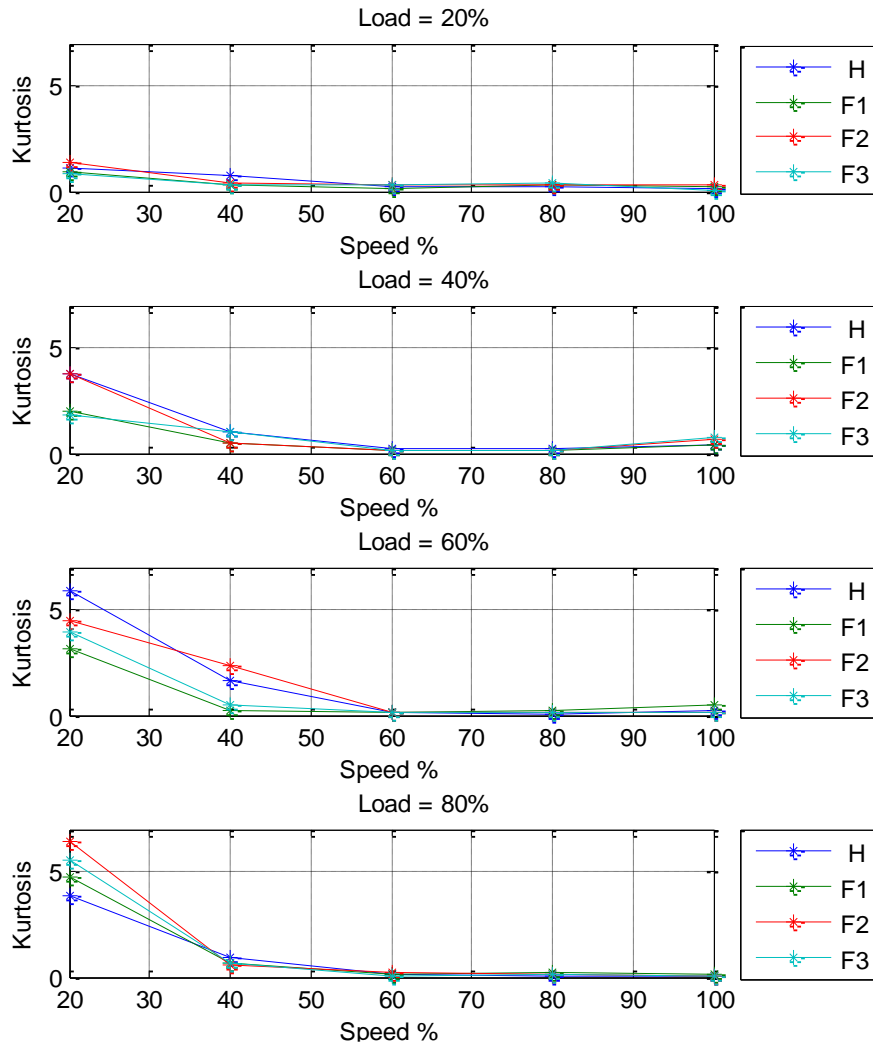


Figure 4.4-Average values of Kurtosis of the vibration signal for healthy and faulty gears

However, as operating conditions increase, the results reveal no significant change between gear statuses. This could lead to an incorrect diagnosis if used on their own for CM. It can be concluded that both parameters are insufficiently sensitive for detection of fault conditions at all operating conditions and are not sensitive enough to this particular type of fault.

CHAPTER 4

CONVENTIONAL CONDITION MONITORING OF A GEAR SYSTEM

It has been found that, unlike other parameters such as peak value and RMS, kurtosis and crest factor are highly dependent on operating conditions and have a non-linear relationship.

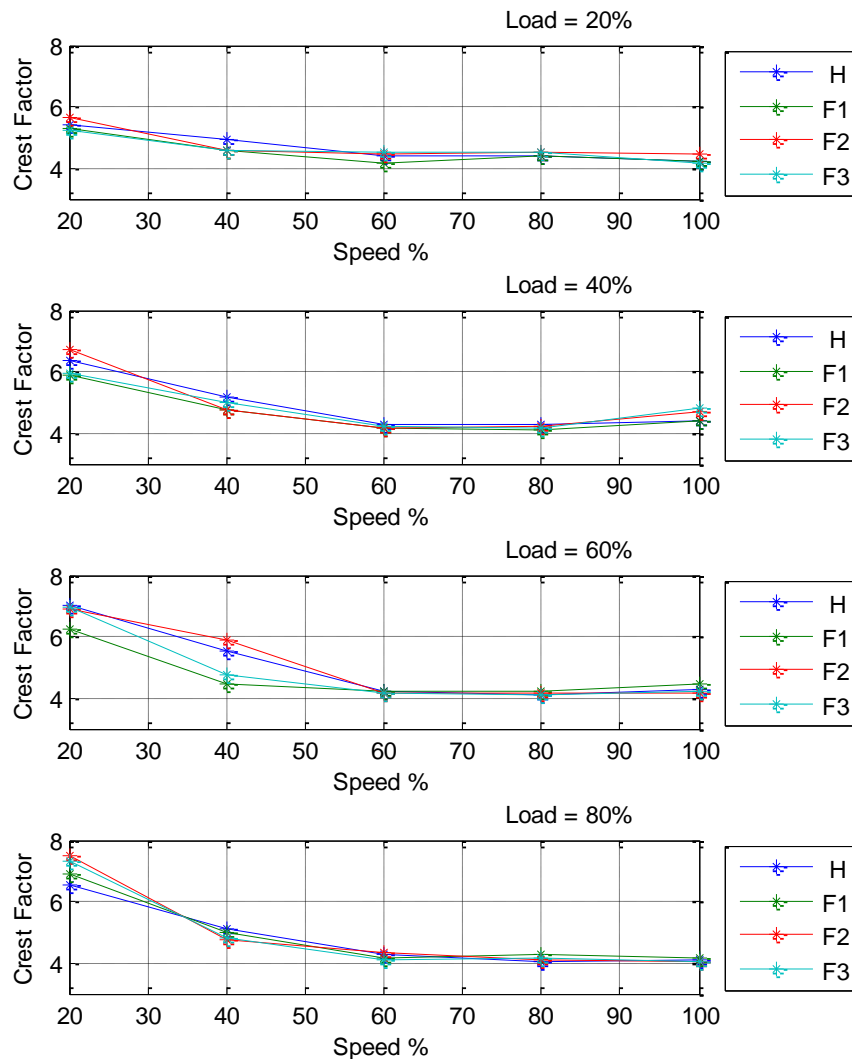


Figure 4.5-Average values of Crest factor for the vibration signal of healthy and faulty gears

It can be argued that the magnitude of kurtosis and the crest factor approaches a linear relationship at rotational speeds above 60%. Both the crest factor and kurtosis are measures of the spikiness of a waveform. As indicated in Figure 4.4 and 4.5, they are at a maximum value at lower speeds and when the load is approximately 60% to 80%. Both parameters decrease in magnitude at speeds 60% and above. Due to the high non-linearity of the spikiness indices, it is difficult to monitor the development of gear faults using these features.

CHAPTER 4

CONVENTIONAL CONDITION MONITORING OF A GEAR SYSTEM

In summary, the statistical parameters which have been considered are not capable of demonstrating the presence and progression of tooth breakage faults in gears.

Different operating conditions, such as load, create different tooth deflections and thus different amounts of gear vibration. Therefore, the time-domain signal from a healthy and faulty gear displays a clear, irregular waveform with small spikes of high frequency components superimposed upon it. Limited information was extracted from the vibration waveforms. The main feature of the signals is large numbers of sinusoidal waveforms occurring at different frequencies, with noise superimposed on each. The complexity does not make it easy to extract useful information regarding the gearbox condition. It is most likely that the difference in amplitudes was due to different operating conditions. There are also similarities in the general pattern of the measured vibration signals.

Figures 4.2-4.5 show how these parameters vary with different operating conditions and the four gearbox conditions. The results reveal the significant effect of different operating conditions on the statistical measures of gearbox vibration. In particular, the peak value and RMS increases linearly with operating conditions whereas Kurtosis and Crest factor are non-linear.

The observed values for a damaged gear tend to slightly change from the values of a normal gear at all operating conditions. However, the presence of a defect and its severity cannot be detected when the peak and RMS values of a given vibration signal are compared with those from a normal gear. On the other hand, kurtosis and crest factor reflect the “spikiness” of the vibration signal and, in the early stages of gear damage, increase as the vibration increases. As the damage increases still further, the vibration becomes more random and the values for crest factor and kurtosis reduce to more normal levels. Thus, statistical analysis based on kurtosis and crest factor lacks the ability to detect gear defects at later stages.

The limitations of these simple measurements are such that, even if used simultaneously, they could lead to an incorrect fault diagnosis. More advanced signal processing such as frequency domain and joint time-frequency techniques should be applied for gear CM purposes.

4.3 Frequency Domain Analysis

4.3.1 Characteristics of Gearbox Spectrum

The vibration spectra recorded from the gearbox casing for healthy and faulty gears under the same and different operating conditions are shown in Figures 4.6 and 4.7. The following analysis focuses on the low frequency range and in particular, the variation characteristics at rotational frequencies and meshing frequencies as calculated in section 3.6.

Figures 4.6 and 4.7 depict peak values corresponding to the two main fundamental meshing frequencies f_{m11} (838 Hz at high operating conditions and 428Hz at low operating conditions) and f_{m21} (347 Hz at high operating conditions and 177Hz at low operating conditions). The harmonics peak values f_{m12} (1676 Hz at high operating conditions and 856Hz at low operating conditions), f_{m22} (694 Hz at high operating conditions and 355Hz at low operating conditions) corresponding to the 1st and 2nd meshing frequencies as well as sidebands for low and high operating conditions are also depicted in Figures 4.6 and 4.7.

It can be seen that the spectral amplitudes of the two main fundamental meshing frequencies and their harmonics change with the gear operating conditions and severity of the faults. In both figures, where the gearbox was operated in the same speed and load, peaks appear to increase in amplitude with the introduction of faults. It can be also seen that the spectral amplitudes at the meshing frequency and its sidebands increase with the severity of the faults.

Figures 4.6 and 4.7 show the amplitude of peaks corresponding to the meshing frequencies of the first stage f_{m11} and, second stage f_{m21} , and their harmonics f_{m12} and f_{m22} are consistently the largest feature of the spectrum, dominating the signals for the different gear statuses. Thus, this feature could be used to detect gear faults reliably. In addition, these figures show clear discrete components; the mesh frequency and sidebands are smeared due to slight speed fluctuations.

CHAPTER 4
CONVENTIONAL CONDITION MONITORING OF A GEAR SYSTEM

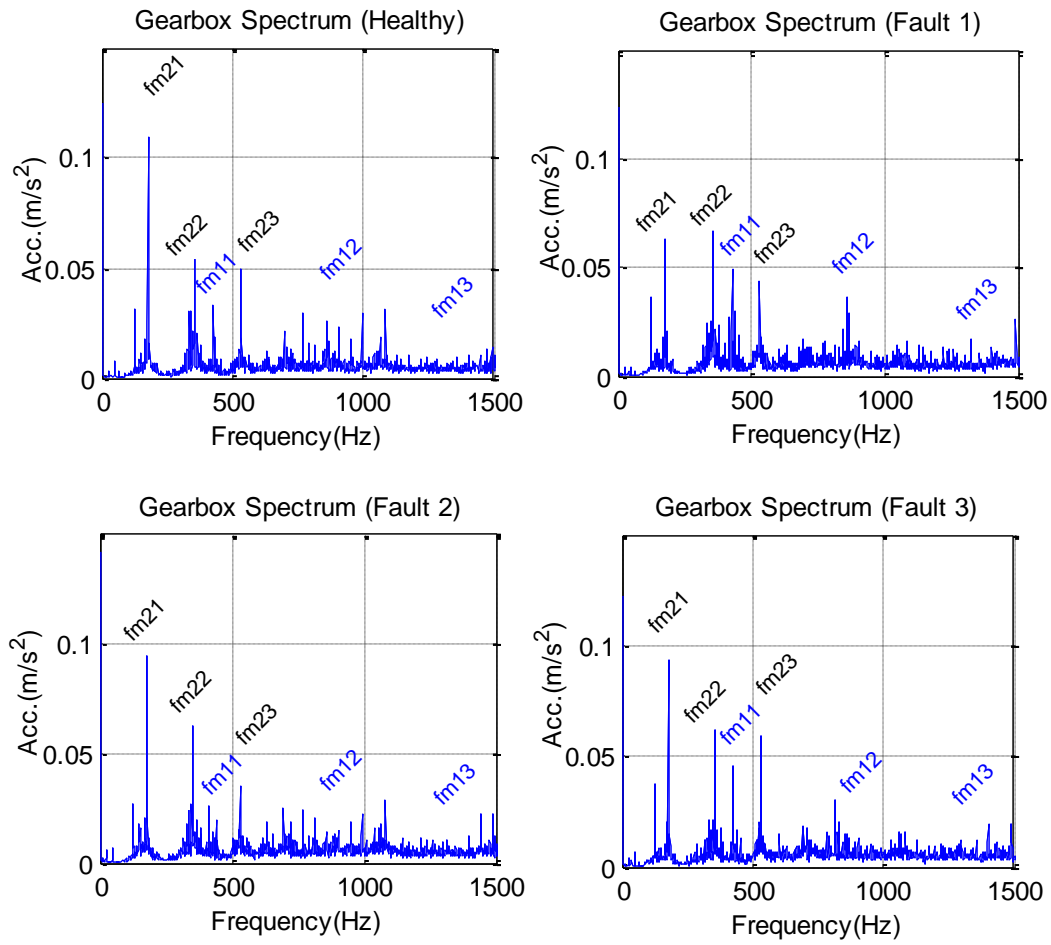


Figure 4.6-Spectrum of local vibration signals for healthy and faulty cases at low ($L=40\%$, $S=50\%$) operating conditions

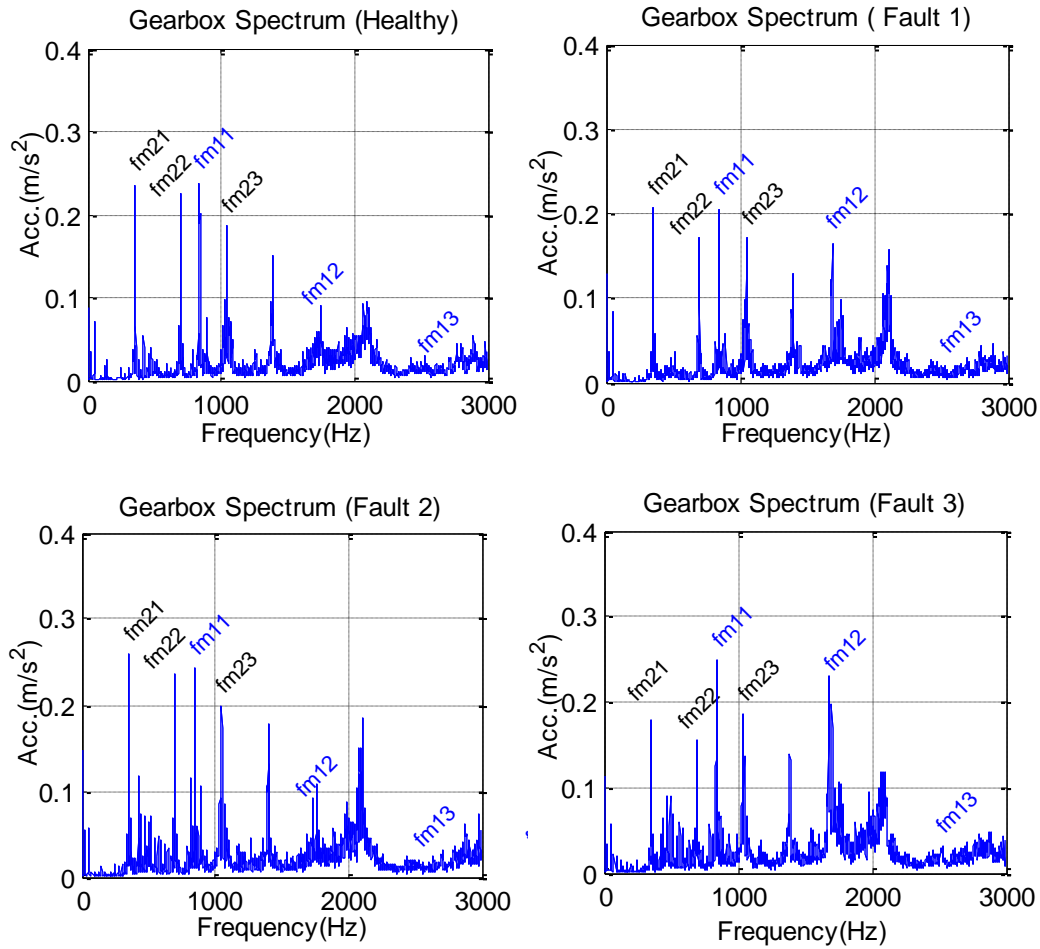


Figure 4.7-Spectrum of local vibration signals for healthy and faulty systems at high ($L=80\%$, $S=100\%$) operating conditions

4.3.2 Meshing Frequency based Diagnosis

Figures 4.8 and 4.9 depict the spectral amplitude values corresponding to the fundamental meshing frequency (f_{m11}) and second stage meshing frequency (f_{m21}), and how these amplitudes change with the gear operating conditions and severity of the faults.

The results presented in Figures 4.8 and 4.9 show that the spectral amplitude values corresponding to the two fundamental meshing frequencies (f_{m11} , f_{m21}) vary with the severity of the gear faults and the operating condition. There is no consistent increase in their amplitudes with the introduction of faults and with an increase in operating conditions. As a consequence, these features cannot be used to indicate faults effectively.

CHAPTER 4

CONVENTIONAL CONDITION MONITORING OF A GEAR SYSTEM

It can be concluded that the spectral amplitude values did not show any significant variation that may indicate fault conditions. It seems, therefore, that these features are not sensitive enough to detect this particular type of fault.

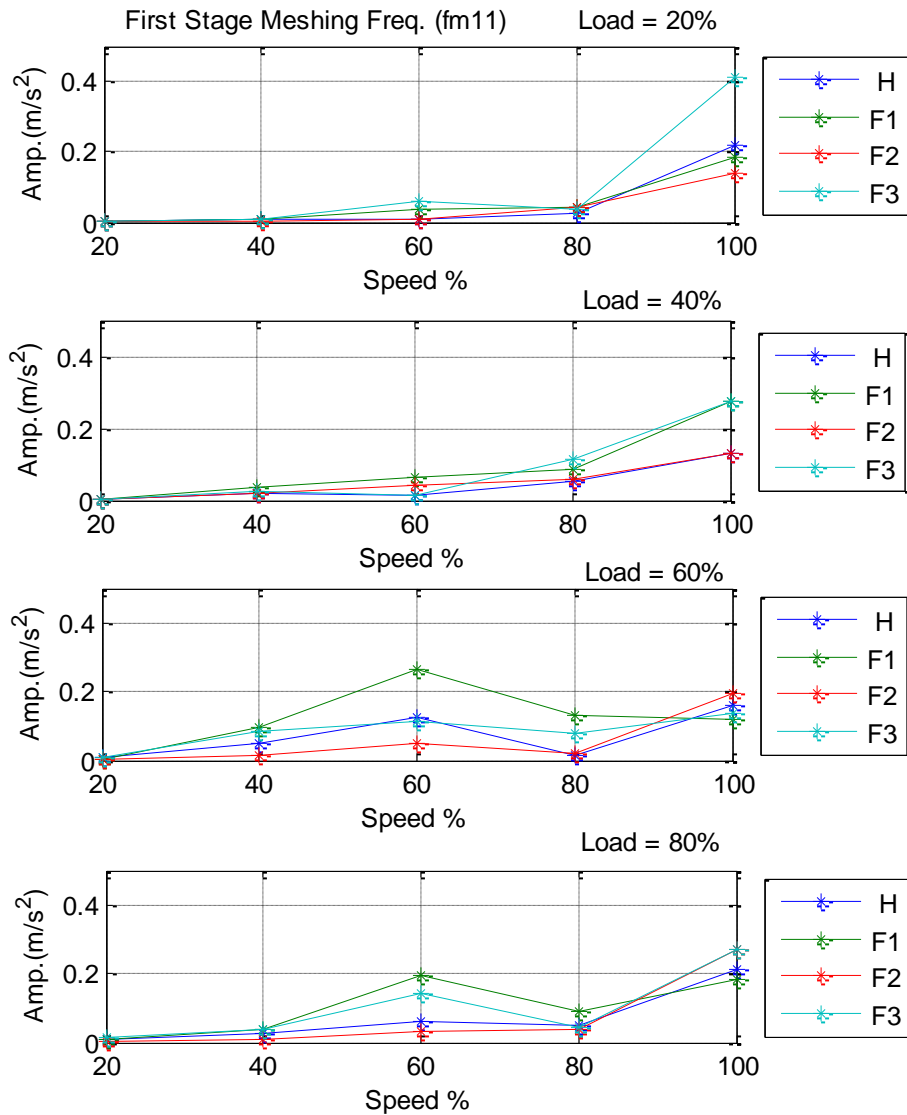


Figure 4.8-First stage meshing frequency (f_{m11}) amplitude measured on the gearbox casing for healthy and faulty gears at different operating conditions.

CHAPTER 4
CONVENTIONAL CONDITION MONITORING OF A GEAR SYSTEM

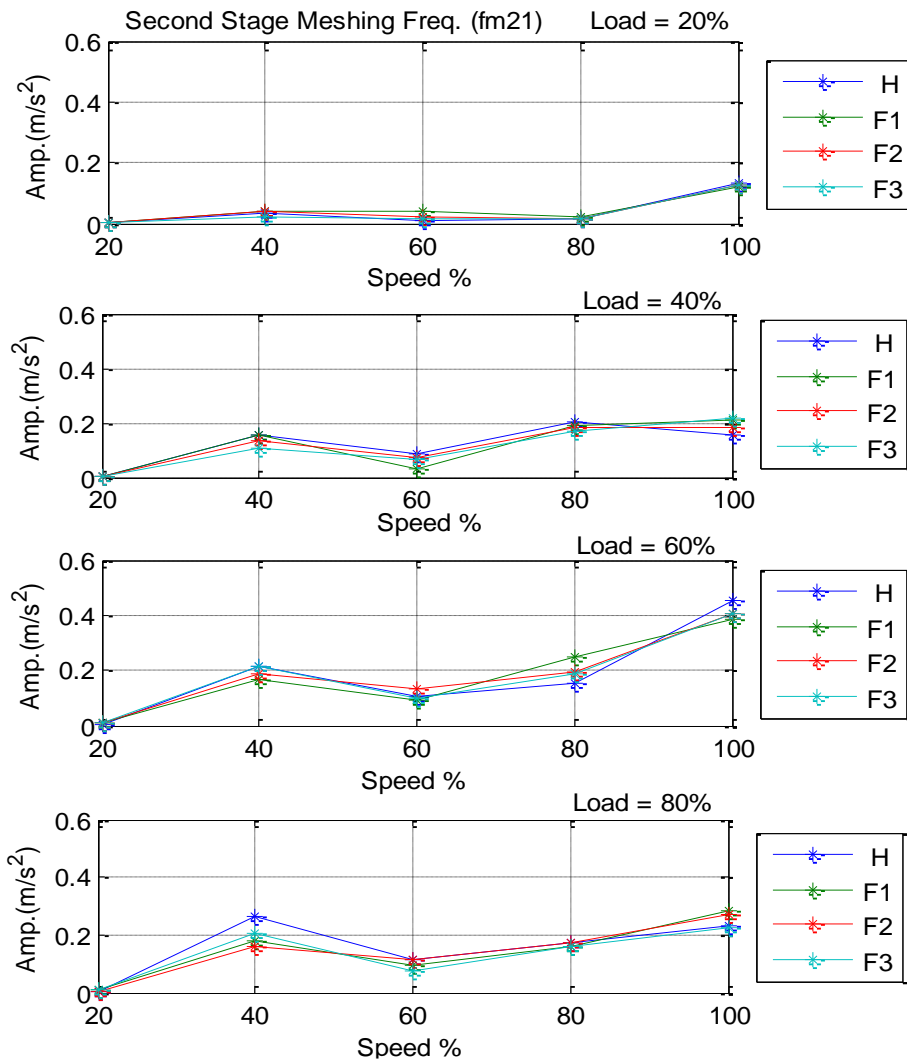


Figure 4.9-Second Stage Meshing Frequency (f_{m21}) amplitude measured on the gearbox casing for healthy and faulty gears at different operating conditions.

4.3.3 Sideband based Diagnosis

As mentioned in section 2.2.2, sidebands of the gear meshing frequency are caused by amplitude modulations and can be very useful for gear damage assessment.

This analysis technique concentrates on the vibration content of the sidebands around the fundamental meshing frequency f_{m11} .

It is anticipated that defects such as a broken gear tooth can be identified by increased amplitudes and the number of sidebands around the meshing frequency in the spectrum.

CHAPTER 4

CONVENTIONAL CONDITION MONITORING OF A GEAR SYSTEM

These sidebands are separated by integer multiples of the gear rotation frequency and originate from fluctuations in shaft rotation which occur because of local gear faults.

The average amplitude of the sidebands around the meshing frequency is extracted from the vibration signal spectrum and used to characterise the change in amplitude of the characteristic frequency. The selected sidebands are $f_{m1l} \pm f_{r1}$ and are harmonics of the shaft frequency (f_{r1}) modulated by the meshing frequency (f_{m1l}).

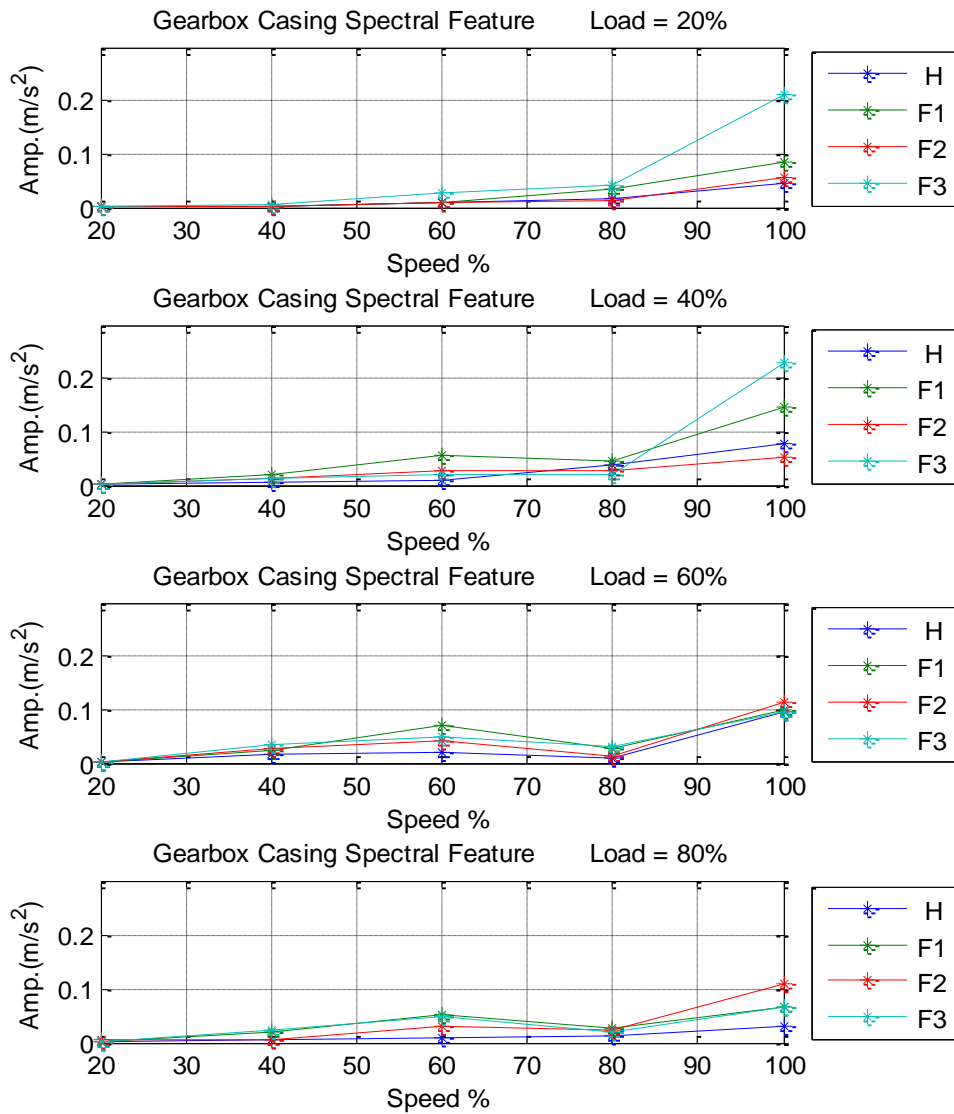


Figure 4.10-Average amplitudes of two sidebands around f_{m1l} on the gearbox casing for healthy and faulty gears under different operating conditions

It can be seen from Figure 4.10 that the average amplitude does not change at low rotational speeds. More importantly, the results appear to show an increase in the average amplitude value for most of the applied loads as faults are introduced, especially Fault 3. Given these results, the average amplitude data cannot be used effectively to indicate gear faults in all operating conditions.

The results show that the performance of the conventional frequency domain degrades due to the fluctuation of the operating conditions. Therefore, the average amplitude signal derived from the vibration signal spectrum may be effective for detection of local faults induced in the gear system at certain specific operating conditions.

4.4 Continuous Wavelet Transform (CWT) Analysis

Figures 4.11 and 4.12 shows the CWT results in colour images for low and high operating conditions respectively. In each figure, the sub-images from the top to the bottom represent the sequence of Healthy, Fault 1, Fault 2 and Fault 3 gear systems under investigation. In addition, these images represent two revolutions of raw signals and show a frequency range up to the second mesh frequency - the first stage of which is labeled in the frequency axis for ease of analysis.

For the healthy gear under low operating conditions, the results show that the amplitude of the CWT is relatively smooth along the time direction, indicating that the gear transmission is relatively stable. However, a set of high amplitude signals are observed around time = 0.15s within the high frequency range data. These patches may be due to noise as they are not repeated within the cycle of the gear meshing period.

In the case of Fault 1, many sets of high amplitude patches occur. Although no clear repeat patterns are observed over the meshing period, they cannot all be treated as noise because some of them appear to repeat around time = 0.1s and time = 0.016s. Nevertheless, the overall amplitude looks higher compared with that of the healthy gear, which may indicate the presence of the fault.

For both Fault 2 and 3, the CWT result shows clear repeatable patterns along the time direction and the amplitude patches spread from low frequency to high frequency.

CHAPTER 4

CONVENTIONAL CONDITION MONITORING OF A GEAR SYSTEM

The data clearly show the impact effects of tooth breakage and give reliable detection results. However, it is difficult to say that the CWT for Fault 3 is larger than that of Fault 2 based on differences in both pattern and amplitude.

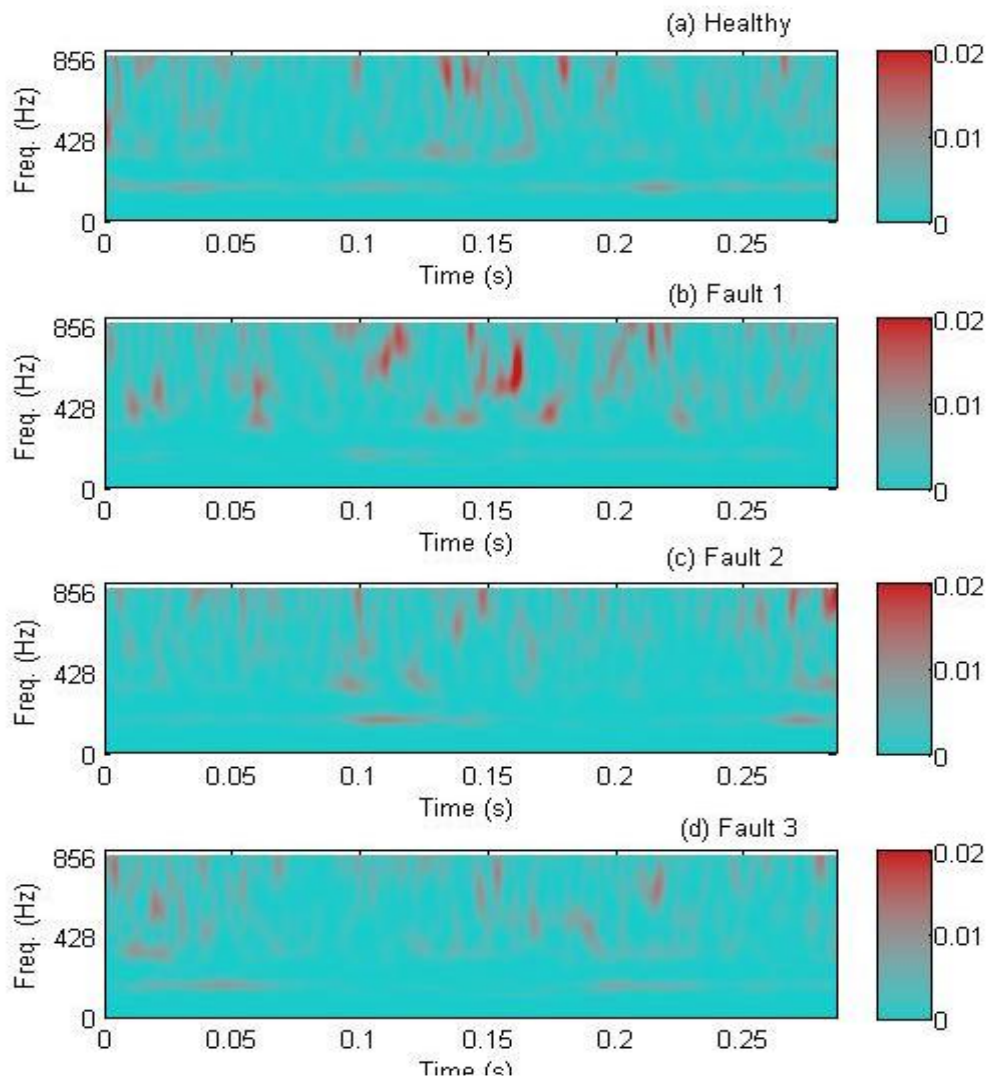


Figure 4.11-CWT vibration measurements for healthy and faulty gears under low ($L=40\%$, $S=50\%$) operating conditions

At high operating conditions as seen in Figure 4.12., the CWT results show an increased number of amplitude patches compared with those at low operating conditions. Moreover, the overall amplitudes increase consistently with fault progression. This means that based on the amplitude changes it is possible to differentiate the different gear fault types.

CHAPTER 4

CONVENTIONAL CONDITION MONITORING OF A GEAR SYSTEM

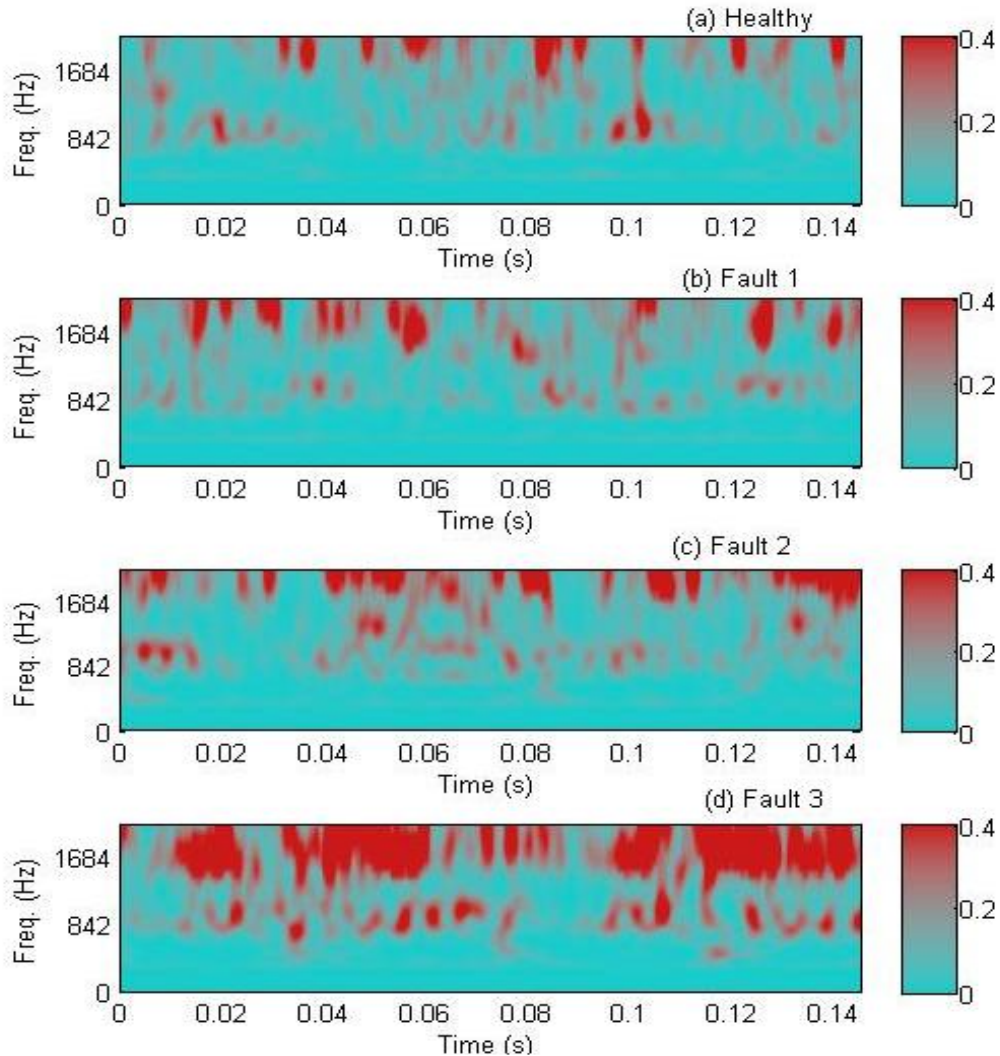


Figure 4.12-CWT vibration measurements for healthy and faulty gears under high ($L=80\%$, $S=100\%$) operating conditions

The repeatable pattern along the time direction, identified for the low operating condition, is also found in the case of the Healthy gear and Faults 1 and 3 but not Fault 2. The CWT for Fault 2 does not show a repeating pattern, which is very difficult to understand as the signal to noise ratio is sufficiently high to resolve any pattern should it be present in the data.

Nevertheless, CWT results allow most of the fault cases to be detected and diagnosed. In particular, the repeatable pattern can be used to diagnose the presence of the fault at the first transmission stage. In addition, analysis also suggests that results could be

improved if a noise suppression method was introduced.

However, the results obtained are not sufficiently consistent to reliably diagnose fault progression under different operating conditions.

4.5 Summary

In this chapter, the vibration signals for different gear conditions (healthy and faulty) and different operating conditions were recorded from a sensor mounted on the gearbox casing. These signals were analyzed using the time, frequency and joint time-frequency (Morlet continuous wavelet transform) domains to obtain a set of effective features for detecting and diagnosing the seeded gear tooth faults.

It was found that the signals were very complex and enormous significant amount of information remained unknown regarding the waveform of the signals. The difference in amplitudes appeared to be due to the different operating conditions. Limited information was extracted from the vibration waveforms and results showed that faults in helical gears were difficult to detect using this approach.

In Sections 4.2.2 and 4.2.3 the peak value, RMS, crest factor and kurtosis were extracted from the time domain vibration signal. These statistical parameters were computed under various rotational speed and load scenarios. The results showed that most statistical parameters were highly affected by operating conditions and gear condition. Comparing the peak and RMS values of a given vibration signal with values determined using vibrations from a normal gear, the presence of a defect and its severity could not be detected. techniques were such that, even if used simultaneously, Statistical analysis based on kurtosis and crest factor lacked the ability to detect gear defects at later stages. The limitations of these simple could lead to an incorrect diagnosis. This suggested that these measurements are not very sensitive to these types of faults (Section 3.4).

CHAPTER 5

MATHEMATICAL MODEL

This chapter presents a mathematical model that simulates vibration signals. The model represents a two stage gear system using a suitable stiffness function to represent the forces acting between each pair of gears. Rotational stiffness and damping are also used to simulate the angular motion of the gears and shafts.

5.1 Introduction

Dynamic modelling of gear vibration allows a deep understanding of the mechanisms which generate vibration in gear transmission systems. Moreover, dynamic modelling helps to characterise the changes of the dynamic properties due to various types of gear faults. This then sets the direction for measurement configuration, data processing selection and diagnosis rule development.

This chapter develops a mathematical model of a two stage gearbox system. The model represents a two stage helical gear system using a suitable stiffness function to represent the forces acting between two pairs of gears. Rotational stiffness and damping are also used to simulate the angular motion of the gears and shafts. Results from the model shows that the frequency spectra of the acceleration outputs take the expected form of the peaks occurring at the meshing frequency and associated harmonics. Furthermore, if the stiffness function between the first pair of gears is simulated with a broken tooth, with varying degrees of damage, the outputs from the model have similar sideband effects to the signals produced in the experimental investigation. It was also shown that the effect of varying loads and speeds in the model produce a corresponding effect to that seen in the experiments. This demonstrates that the model, although fairly simple, can explain the mechanism at work in the real gearbox which has been used in the condition monitoring experiments.

A novel feature of the mathematical model used here is the addition of vertical spring-damper systems used to attach the gears to the casing. To simplify the model, but to demonstrate the basic principles, the casing has simply modelled using two masses. One mass is attached to the pinion and the other to the gear of the first pair of gears. The results show that there are significant differences between the acceleration transmitted through each of the masses. This clearly illustrates, although in a much simplified form, the effects shown in Chapter 8 when accelerometers are placed at different positions e.g.: on the gearbox or on the motor drive casing. The model has similar features to those present in the frequency spectra, but there are variations in amplitude.

This shows that the choice of accelerometer position, and hence the transmission path from the gear source to the sensor, can give rise to significant differences in the vibration signals.

5.2 Modelling Overview

With the growing focus on gears in industrial machinery, a considerable amount of attention has been paid to the study of the dynamic modelling of gears. Many papers have been published concerning the dynamics of gear systems. Some studies have developed sophisticated models which take into consideration the most important dynamic factors in gearboxes such as periodic changes in tooth stiffness, the excitation from gear transmission errors, the coupling effect between the torsional and lateral vibrations of the gears and shafts [114,115,116,117]. In addition, other approaches have focused on modelling of the tooth mesh since the main source of vibration in a geared transmission system is usually the meshing action of the gears [118,119,120]. The purpose of these studies is to deconvolute some of the unknown aspects related to the interaction of non-linear effects including friction forces at the meshing interface and gear backlash with time-varying mesh stiffness.

A computer simulation has been used to study the effects that tooth breakage has on the vibration response of a two-stage gear transmission system with helical gears.

Only the variation in the meshing stiffness has been considered in this work, as it is the fundamental source of vibration in gearbox transmissions.

In summary, the main goal of this modelling has been to study of gear tooth stresses, natural frequencies of the system, vibration characteristics of the gear system such as amplitudes and spectral components, noise radiation etc. Depending on the different applications, mass-spring or mass-spring-damper SDOF/MDOF models of the one/two-stage gear systems have been used. Earlier studies have considered torsional vibrations of systems [121].

More recently, models which consider lateral vibrations or combined torsional and lateral vibrations have been developed [114,122]. In these models, the gear mesh stiffness has been modelled as a constant, a simple sinusoidal function, a Fourier series, a rectangular waveform corresponding to a single-and double-tooth-pair mesh, an approximation function and a derived expression. In the solution of dynamic

equations, analytical, approximately analytical and numerical methods have been employed.

For some very simple SDOF mathematical models, approximate analytical solutions are given. For complicated MDOF system models, especially when both torsional and lateral vibrations are being considered, numerical techniques must be employed. Amongst these numerical methods, Runge-Kutta integration techniques are more popular due to accuracy and the calculation time required.

5.3 Mesh Stiffness for Helical Gears Mating

The mathematical model of the force between a meshing gear pair will depend on a number of factors such as mesh stiffness, tooth error, moment of friction and backlash [114].

A gear pair with no faults can be defined as a mathematical function of the time over one meshing period T / z_1 , where T is the period of rotation of the pinion shaft and z_1 the number of pinion teeth. Alternatively, the gear pair can be defined as functions of the angular displacement of the pinion shaft between 0 and $2\pi / z_1$.

For the simplified model only the most important of these, the mesh stiffness $k(t)$ has been considered. Other factors could have been added but mesh stiffness was considered the main feature for demonstrating the gearbox vibration. Faults due to broken teeth, of varying degrees of severity, could also be easily added to the model.

Mesh stiffness can be defined as the ratio between the force acting along the line of action and the tooth displacement along the same line. To obtain $k(t)$ for numerical simulation, the stiffness for a single pair of meshing teeth was initially studied. The stiffness for a meshing gear pair is given by a number of different factors [123]: the stiffness of the Hertzian contact, the bending stiffness of the two teeth (from the pinion and the driven gear) and the axial stiffness of the two teeth. The combination of these factors leads to an increase in the amplitude of the stiffness in the middle phase of the meshing period.

These approximations are commonly used because of the difficulty in accurately predicting the actual pattern of the stiffness variation in practical situations. This study

CHAPTER 5

MATHEMATICAL MODEL

assumes, therefore, that the tooth mesh stiffness has the combined profile as shown in Figure 5.1.

The profile uses a piecewise-linear function to represent the transient value of the stiffness during mesh-in and mesh-out of a gear pair. The stiffness is assumed to have constant amplitude in the middle section of the tooth pair. The maximum stiffness value of a single gear pair is of the order of 10^7 N/m [9].

For a single tooth pair in contact, the mesh stiffness remains relatively constant due to the fact that the loss of stiffness in one tooth is compensated by the gain in stiffness of the mating tooth. As the gears rotate the point of contact moves up along one tooth and moves down along the mating tooth.

As the gears rotate, the numbers of teeth in contact vary, and as a consequence, the effective length of the line of contact changes causing variations in mesh stiffness. For spur gears, where the contact ratio is low, these variations are largely due to the load transfer occurring over a single tooth and a double tooth pair. In the case of a helical gear pair mesh, the change in total length of line of contact is small due to large contact ratios (between two and three teeth). As a result, mesh stiffness variations are significantly smaller when compared with those of spur gears. As a consequence, many helical Gear Dynamic Models (GDM) treat mesh stiffness as a constant and its time averaged value is used. [124].

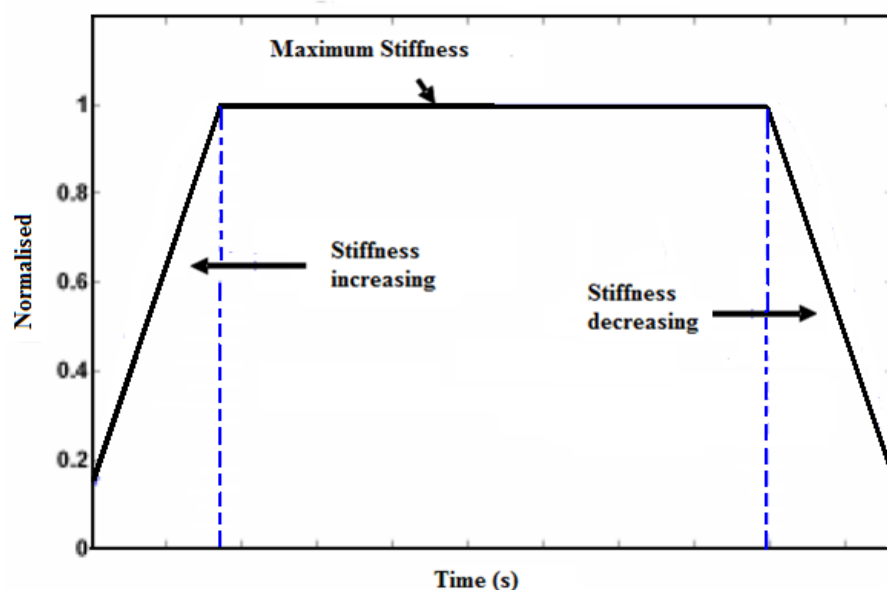


Figure 5.1- Stiffness of a single pair of teeth

CHAPTER 5

MATHEMATICAL MODEL

For the simplified model used in this study, the meshing stiffness, as a function of angular displacement, is estimated from two parameters: contact ratio ε_c and overlap ratio ε_a . The ε_c parameter measures the contact between adjacent teeth in a transverse section and the ε_a parameter measures the overlap of adjacent teeth in the axial or face-width direction.

The profile of single pair stiffness can be considered to be piecewise linear, as shown in Figure 5.1:

In Figure 5.2, the x -axis denotes the number of base pitches and must be multiplied by $2\pi / z_1$ to give the angular variation. The total meshing stiffness can then be obtained by summing the stiffness of a single pair over all teeth, advancing by one tooth at a time for the total of z_1 pinion teeth.

Figure 5.2 (a) shows the resulting meshing stiffness waveform for the underlying gear pair of this study. Since $\varepsilon_c + \varepsilon_a = 4.249$, the maximum number of teeth in contact is five and the minimum number is four. The fluctuation between the maximum and minimum number of teeth in contact is the fundamental source of vibration for the gear. Note that the period of the fluctuation is just $2\pi / z_1$. This shows that even if there are no faults or manufacturing errors, the gear pair still produces vibrations.

When manufacturing errors exist, the fluctuation of the stiffness will not be uniform. Both the maximum and minimum number of contacting teeth pairs will vary with angular position, as will the error amplitude. This usually results in larger variation of the stiffness amplitude and consequently higher amplitude vibrations.

CHAPTER 5

MATHEMATICAL MODEL

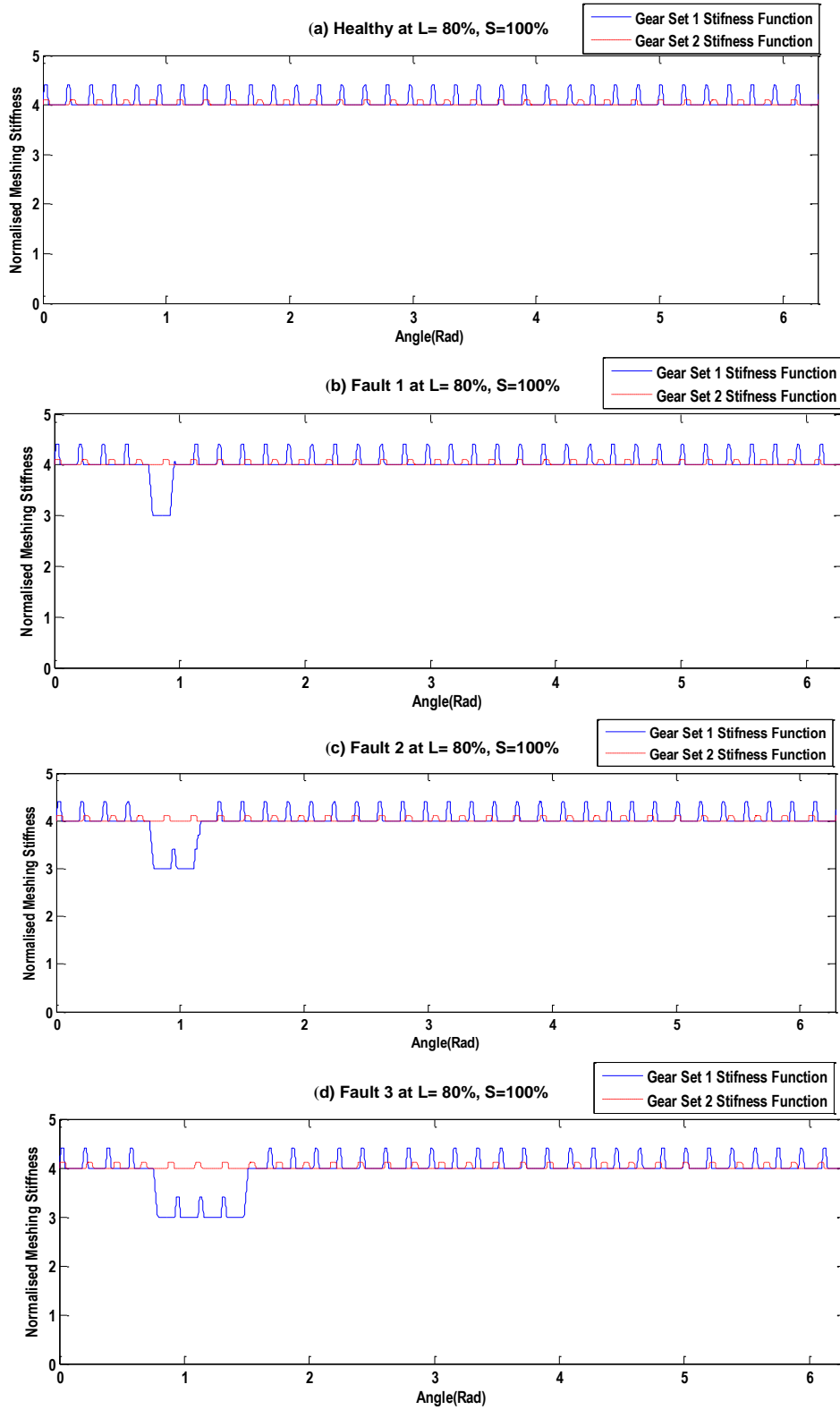


Figure 5.2- The meshing stiffness function k_1 and k_2 for the pinion and the gear of the first pair of gears (within one shaft period) shown in blue and red as a function of angular displacement θ . Here (a) is the healthy case and (b), (c) and (d) show various severity of faults due to a broken tooth.

Broken teeth are a common failure in helical gears. The gear fault starts with a small amount of damage to the tooth profiles, which causes a change in the meshing stiffness. The plots in Figure 5.2 (b), (c) and (d) show the effect of a single damaged tooth on the meshing stiffness where various percentages (25%, 50%, and 100% respectively) of a single tooth are assumed to be missing. The results show that local faults result in a sudden drop in the stiffness amplitude. In addition, at lower stiffness values, the width of the interval increases as the severity of the fault increases, although the value of the low amplitude remains the same. Such sharp drops in the stiffness value are expected to cause corresponding rises in the amplitude of the system vibration.

5.4 Dynamic Model of a Helical Gearbox

As mentioned previously, the primary aim of this mathematical model is to investigate the vibration characteristics of a gearbox, both in the time and the frequency domain. Early studies considered torsional vibrations of a one stage system [121], but in recent years dynamic models of gear transmission systems using torsional or both torsional and lateral vibrations have been developed [114,115,116,117]. These models provide insight into the working of such systems and establish a basis for understanding both local and remote fault diagnosis.

In such models, the gear mesh stiffness can be considered as a constant, a simple sinusoidal function, a Fourier series, or a piecewise linear waveform corresponding to the single-and double-tooth-pair meshes. Either an approximation function or a derived expression can be used. In the solution of dynamic equations, analytical, approximately analytical or numerical methods are employed.

The model used here is a Multiple Degree of Freedom (MDOF) system using standard mass-spring-damper components based on the investigations of Bartelmus [114]. The mesh stiffness functions k_1 and k_2 used between gear pairs are based on the simplified piecewise linear analysis and tooth breakage faults as described earlier and can be easily introduced into the model. Damping that is proportional to the mesh stiffness is also added to represent the forces between the gear pairs.

CHAPTER 5

MATHEMATICAL MODEL

A two stage system has been modelled with shafts that allow torsional vibrations but also, for the first gear pair only, vertical vibrations where the gears are attached to the casing. The casing itself has been considered as two parts, both of which are able to undergo vertical vibrations. A simplified model of a casing having two different mass/stiffness characteristics allows the effect of vertical accelerations at two different points to be measured. Horizontal vibrations (x-coordinate) have been ignored as it has been assumed that these die away with damping. A schematic diagram is shown in the following Figure 5.3.

CHAPTER 5
MATHEMATICAL MODEL

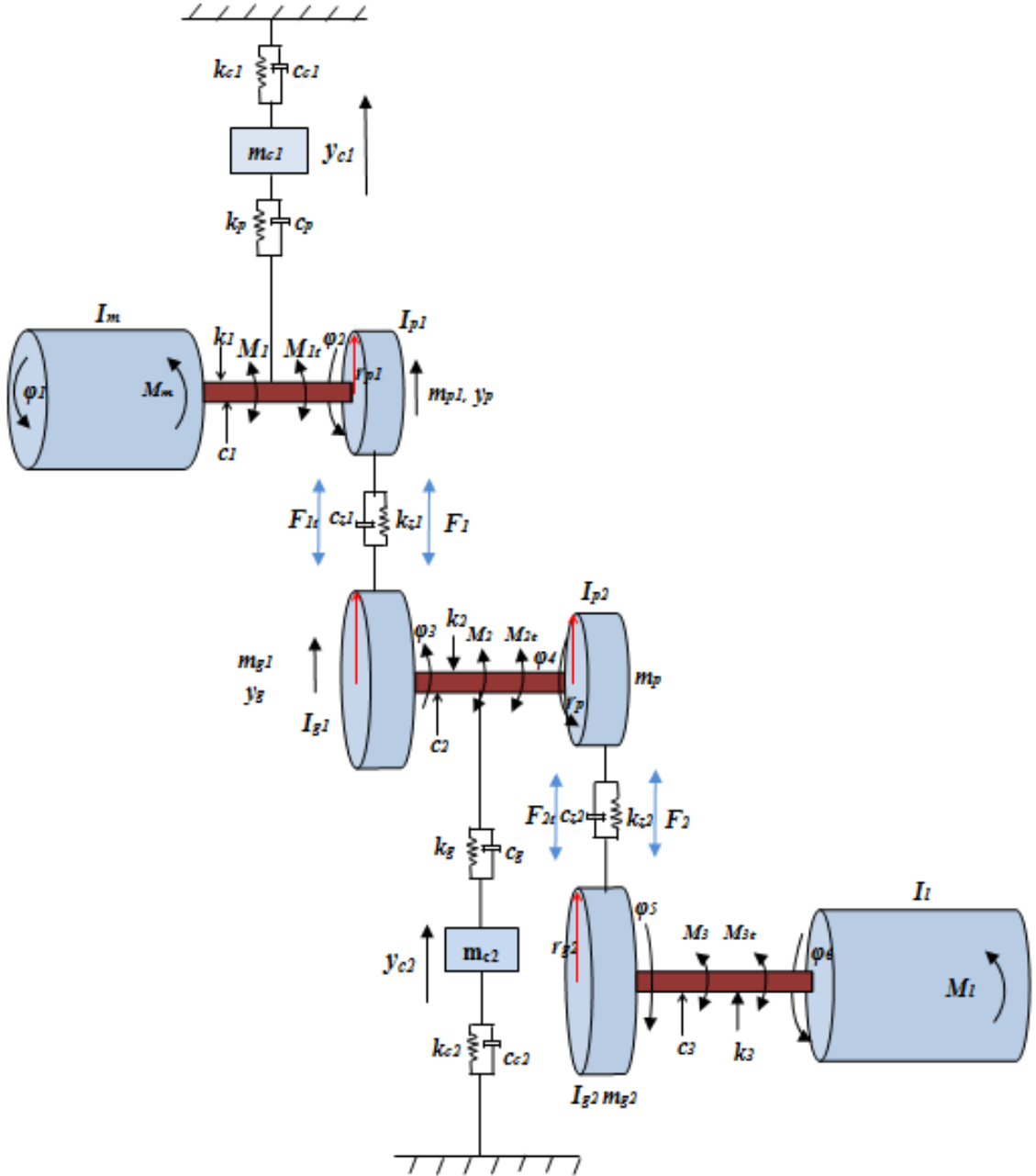


Figure 5.3-Two-Stage gearbox models with torsional and vertical (y-coordinate) vibration of the first gear pair.

For this system the equations of motion may be written as follows:

Equations due to rotational motion;

$$I_m \ddot{\phi}_1 = M_m (M_1 - M_{1t}) \quad (5.1)$$

CHAPTER 5
MATHEMATICAL MODEL

$$I_{p1}\ddot{\phi}_2 = M_1 + M_{1t} - r_{p1}(F_1 + F_{1t}) \quad (5.2)$$

$$I_{g1}\ddot{\phi}_3 = r_{g1}(F_1 + F_{1t}) - (M_2 + M_{2t}) \quad (5.3)$$

$$I_{p2}\ddot{\phi}_4 = M_2 + M_{2t} - r_{p2}(F_2 + F_{2t}) \quad (5.4)$$

$$I_{g2}\ddot{\phi}_5 = r_{g2}(F_2 + F_{2t}) - (M_3 + M_{3t}) \quad (5.5)$$

$$I_l\ddot{\phi}_6 = M_3 + M_{3t} - M_l \quad (5.6)$$

Equation governing the vertical motion of the pinion of the first gear pair;

$$m_{p1}\ddot{y}_p = (F_1 + F_{1t}) - k_p(y_p + y_{c1}) - c_p(\dot{y}_p - \dot{y}_{c1}) \quad (5.7)$$

For the vertical motion of the corresponding gear;

$$m_{g1}\ddot{y}_g = (F_1 + F_{1t}) - k_g(y_g + y_{c2}) - c_g(\dot{y}_g - \dot{y}_{c2}) \quad (5.8)$$

For the vertical motion of casing one;

$$m_{c1}\ddot{y}_{c1} = k_p(y_p + y_{c1}) + c_p(\dot{y}_p - \dot{y}_{c1}) - k_{c1}y_{c1} - c_{c1}\dot{y}_{c1} \quad (5.9)$$

For the vertical motion of casing two;

$$m_{c2}\ddot{y}_{c2} = k_g(y_g + y_{c2}) + c_g(\dot{y}_g - \dot{y}_{c2}) - k_{c2}y_{c2} - c_{c2}\dot{y}_{c2} \quad (5.10)$$

Moments and forces can be written in the following form;

$$M_1 = k_1(\phi_1 - \phi_2) \quad (5.11)$$

$$M_{1t} = c_1(\dot{\phi}_1 - \dot{\phi}_2) \quad (5.12)$$

$$M_2 = k_2(\phi_3 - \phi_4) \quad (5.13)$$

$$M_{2t} = c_2(\dot{\phi}_3 - \dot{\phi}_4) \quad (5.14)$$

$$M_3 = k_3(\phi_5 - \phi_6) \quad (5.15)$$

$$M_{3t} = c_3(\dot{\phi}_5 - \dot{\phi}_6) \quad (5.16)$$

$$F_1 = k_{z1}(r_{p1}\phi_2 - r_{g1}\phi_3) \quad (5.17)$$

$$F_2 = k_{z2}(r_{p2}\phi_4 - r_{g2}\phi_5) \quad (5.18)$$

CHAPTER 5
MATHEMATICAL MODEL

$$F_{1t} = c_{z1}(r_{p1}\dot{\phi}_2 - r_{g1}\dot{\phi}_3) \quad (5.19)$$

$$F_{2t} = c_{z2}(r_{p2}\dot{\phi}_4 - r_{g2}\dot{\phi}_5) \quad (5.20)$$

Where

I_m = Moment of inertia for electric motor

I_l = Moment of inertia for the load system

I_{p1} = Moment of inertia of gear one (pinion one) in the first stage

I_{g1} = Moment of inertia of gear two in the first stage

I_{p2} = Moment of inertia of gear one (pinion two) in the second stage

I_{g2} = Moment of inertia of gear two in the second stage

F_1, F_2 = gearing stiffness forces

F_{1t}, F_{2t} = gearing damping forces

M_m = input motor torque

M_1, M_{1t} = internal moment and coupling damping in first shaft

M_2, M_{2t} = internal moment and coupling damping in second shaft

M_3, M_{3t} = internal moment and coupling damping in third shaft

ϕ_1 = angular displacement of load system;

ϕ_2, ϕ_3 = the angular displacement of gear one (pinion) and gear two in first stage respectively

ϕ_4, ϕ_5 = the angular displacement of gear one (pinion) and gear two in second stage respectively

ϕ_6 = angular displacement of the load system

r_{p1}, r_{g1} = base circle radius of gear one and gear two in the first stage

CHAPTER 5

MATHEMATICAL MODEL

r_{p2}, r_{g2} = base circle radius of gear one and gear two in the second stage

y_p, y_g = vertical displacement of the pinion and the gear in the first stage

y_{c1}, y_{c2} = vertical displacement of the upper and lower casings

m_{p1}, m_{g1} = the mass of the pinion and the gear in the first stage

m_{p2}, m_{g2} = the mass of the pinion and the gear in the second stage

m_{c1}, m_{c2} = mass of the upper and lower casing

c_p = first stage pinion shaft damping

c_g = first stage gear shaft damping

c_1 = shaft one damping

c_2 = shaft two damping

c_3 = shaft three damping

c_{z1} = first stage gearing damping

c_{z2} = second stage gearing damping;

c_{c1} = upper casing support damping

c_{c2} = lower casing support damping

k_p = first stage pinion shaft stiffness

k_g = first stage gear shaft stiffness

k_1 = shaft one stiffness (rotational stiffness)

k_2 = shaft two stiffness

k_3 = shaft three stiffness

k_{z1} = first stage gearing stiffness (meshing stiffness)

k_{z2} = second stage gearing stiffness

CHAPTER 5

MATHEMATICAL MODEL

k_{c1} = upper casing support stiffness

k_{c2} = lower gearing support stiffness

The meshing stiffnesses are given by $k_{z1}=k_{t1}k_1(\theta)$ and $k_{z2}=k_{t2}k_2(\theta)$ where k_1 and k_2 are the piecewise linear functions of the angle of shaft rotation θ , as explained in the previous section and k_{t1} and k_{t2} are suitably chosen constant parameters (see Table 5.1).

It is assumed that the corresponding damping coefficients are proportional to the stiffnesses, i.e. $c_{z1} = \mu_1 k_{z1}$ and $c_{z2} = \mu_2 k_{z2}$, where μ_1 and μ_2 are given in Table 5.1

The values of mass, moments of inertia, pitch radii, and gear characteristics (number of teeth, contact ratio, overlap ratio) were based, as far as possible, on the real values of the gearbox under investigation. The parameter values are given in Table 5.1. The various stiffness values used in the model were estimated only and for the shafts and bearings were seen to be similar to those used in previous investigations [125]. Damping coefficients were calculated from the corresponding mass/moment of inertia and stiffness and relatively high values of the damping ratio ζ were assumed in each case to minimise the time needed for transients to die away in the numerical solution of the model.

The analysis procedure of gearbox dynamic performance is depicted in Figure 5.4. The model was used three major procedures, such as calculating the gearbox physical parameters, solving the space state equations and comparing the predicted and measured dynamic performance of gearbox on time and frequency domain.

CHAPTER 5
MATHEMATICAL MODEL

Table 5.1: Main parameters of the gear transmission system

Parameter	Value
First shaft mass (m_{s1})	1.42kg
Second shaft mass (m_{s2})	0.95kg
Third shaft mass (m_{s3})	3.34kg
First stage gear 1 (pinion) mass (m_{p1})	0.23 kg
First stage gear 2 mass (m_{g1})	1.546kg
Second stage gear 3 (pinion) mass (m_{p2})	0.663kg
Second stage gear 4 mass (m_{g2})	1.493kg
Contact ratio (ϵ_c)	1.359
Overlap ratio (ϵ_a)	2.890
Base radius of shaft 1 (r_{s1})	0.015m
Base radius of shaft 2 (r_{s2})	0.0117m
Base radius of shaft 3 (r_{s3})	0.0153m
Base radius of gear 1 (r_{p1})	0.0217m
Base radius of gear 2 (r_{g1})	0.0117m
Base radius of gear 3 (r_{p2})	0.01525m
Base radius of gear 4 (r_{g2})	0.0222m
Moment of inertia of shaft one (M_1)	0.0032 kg.m ²
Moment of inertia of shaft two (M_2)	0.00013 kg.m ²
Moment of inertia of shaft three (M_3)	0.00078 kg.m ²
Moment of inertia of gear one (I_{p1}) (stage one)	0.000042 kg.m ²
Moment of inertia of gear two (I_{g1}) (stage one)	0.00073 kg.m ²
Moment of inertia of gear three (I_{p2}) (stage two)	0.000154 kg.m ²
Moment of inertia of gear four (I_{g2}) (stage two)	0.00074 kg.m ²
Scaling factor for damping in the calculation of c_p, c_g, c_{c1} (ζ)	4
1 st stage gearing damping (c_{z1})	435.7295
2 nd stage gearing damping (c_{z2})	831.1938
1 st stage gearing damping coefficient (μ_1)	4.357*10 ⁻⁵
2 nd stage gearing damping coefficient (μ_2)	8.3119x10 ⁻⁵
Moment of motor (I_m)	8.4759x10 ⁻⁴
Moment of load system (I_l)	33.88x10 ⁻⁴
Pinion shaft stiffness (k_p)	1.0x10 ⁶
Gear shaft stiffness (k_g)	2.0x10 ⁶

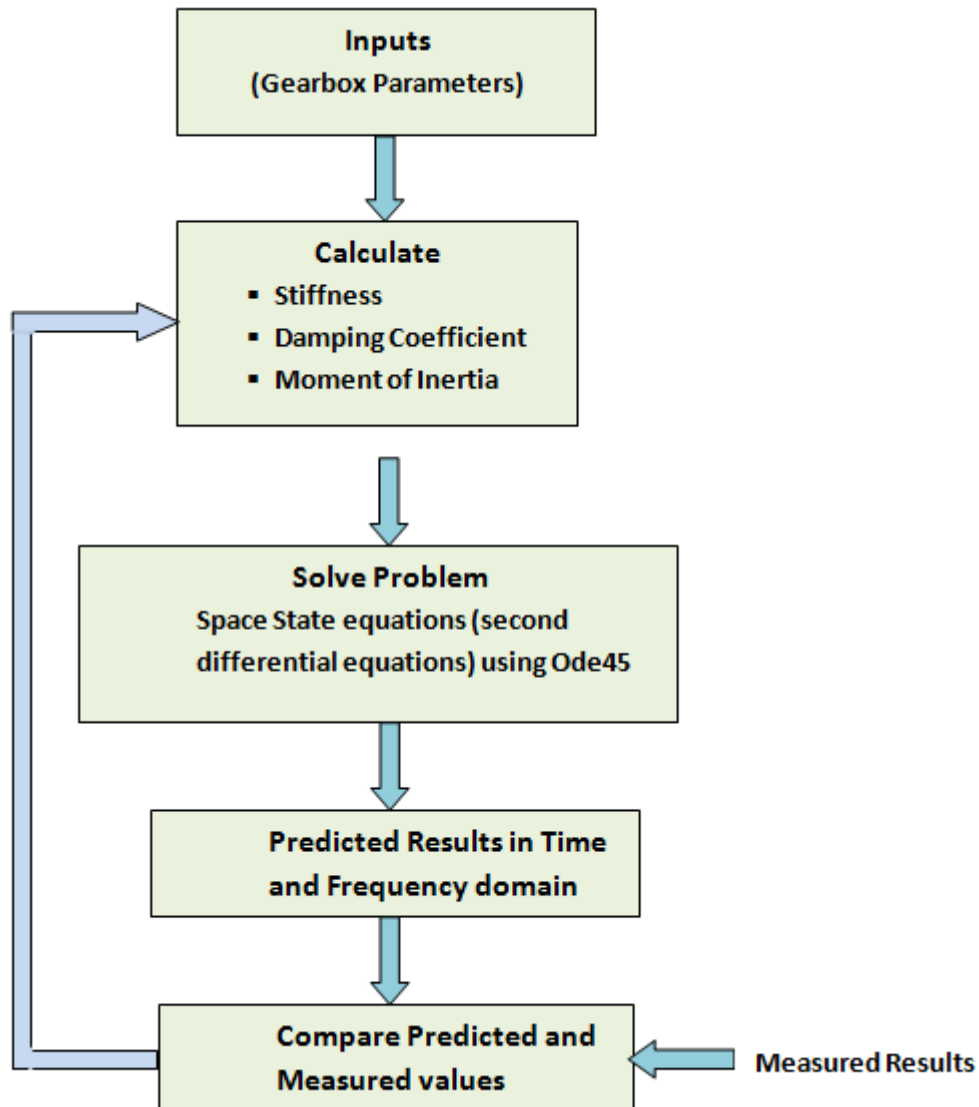


Figure 5.4- Analysis procedure of gearbox dynamic performance

5.5 Numerical Implementation of the Model

The second order differential equations in the model were converted to first order equations to solve them using standard numerical algorithms. The Runge-Kutta formula is the most popular algorithm and was used for modelling in the first instance [126]. It was found that by applying standard Runge-Kutta methods in Matlab, the ode45 function took more than 1 hour for completion of a single run.

CHAPTER 5

MATHEMATICAL MODEL

This demonstrated that the Runge-Kutta method is inefficient for the solution of these equations. Further analysis of the equations showed that the model is a stiff system. The equations describing angular motions have a much slower variation rate with time than those describing lateral motions. According to recommendations in the Matlab instruction manual and in reference [127], the stiff solver ode115s function should be selected to solve the equations. This reduced the run time to less than 10 minutes and it was decided, therefore, that the ode115s function would be used throughout this simulation study.

To perform spectral analysis, each simulation run lasted as long as 15 turn of the input shaft or more than 4 turns of the output shaft. This data size is sufficiently long to obtain a spectrum with high frequency resolution and to differentiate between different sideband components once any transient data due to inaccuracies in the conditions initially assigned have been removed.

Figure 5.5 shows a typical solution for the angular speed of the input shaft. It can be seen that there is a clear transient response at the beginning of the simulation process, which needs to be removed for spectral calculation and waveform extraction. In contrast, the solution in the steady state is relatively stable and shows the speed fluctuation features on both the input and output shafts. This demonstrates that the ode115s solver can produce reliable solutions for the model.

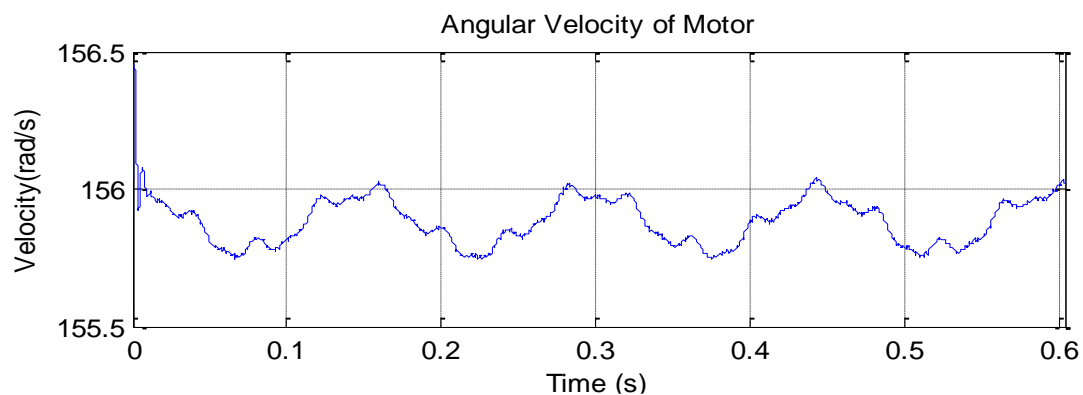


Figure 5.5-Angular speed for the input shaft

5.6 Model Parameter Tuning and Calibration

Most of the model parameters including masses and shaft stiffness are measured or calculated based on the gearbox design information. However, mesh stiffness is difficult to be obtaining directly because of the complexity of the tooth profile. Based on Finite Element Analysis of the gear tooth stiffness given in [128], the average stiffness amplitude is estimated to be the order of 10^7 N/m [9] and its accurate values are then estimated by matching the simulated result with that of measurements in the frequency domain.

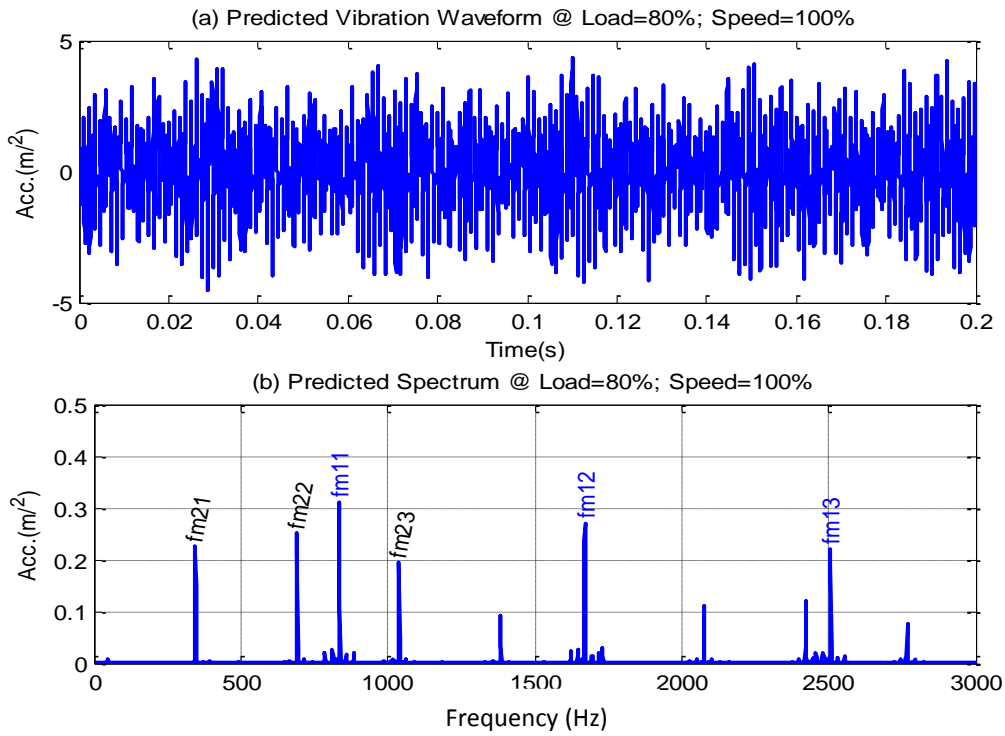


Figure 5.6-Predicted Vibration Waveform (a) and Spectrum (b)

In addition, the parameters of the gearbox case system were also estimated based on a comparison between the predicted waveform and spectrum and the measured waveform and spectrum as shown in Figure 5.6 and 5.7 respectively, both at high operating conditions (80% load and 100% speed). The outputs presented in Figure 5.6(a) and 5.7(a) show the time domain vibration waveform of the predicted and measured results. The time period is from 0 to 0.2s and, since one shaft revolution is 0.0402s, the vibration signal contains approximately 5.0 revolutions in total.

CHAPTER 5

MATHEMATICAL MODEL

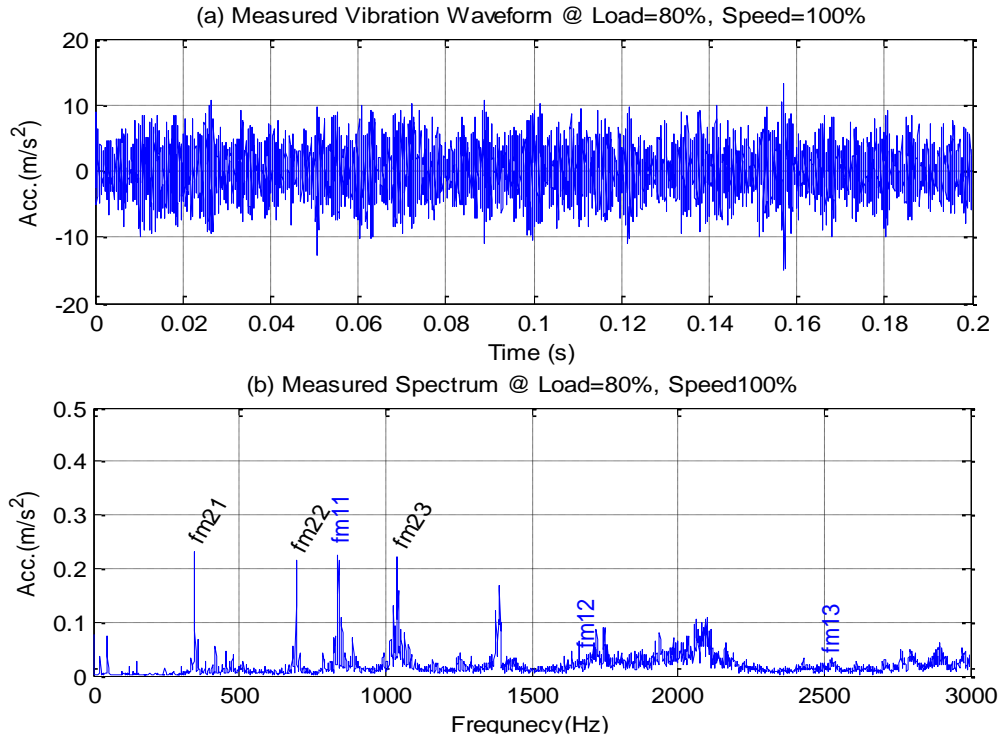


Figure 5.7-Measured Vibration Waveform (a) and Spectrum (b)

As seen in Figures 5.6a and 5.7a there is a similarity between the amplitudes of predicted and measured data for the same operating conditions. The amplitude of the measured signal is higher than that of the predicted signal because of the background noise interference which was detected when actual (measured) data was collected from the test rig.

For comparison with the measured gear vibration signal, a Fourier Transform was applied to the predicted signal in order to observe more detail, and some examples of the power spectrum density plots of healthy (no tooth breakage) pinion simulation are presented in Figures 5.6b-5.7b. In these figures, distinct fundamental frequencies and harmonics (f_{m11} , f_{m12} , f_{m21} , f_{m22} and f_{m13} , f_{m23}) are the most dominant spectral components in the signal and can be visually observed. Their amplitudes are the largest in the signal.

The predicted and measured vibration spectra were obtained from a single position. The actual (measured) vibration spectrum is richer in frequency content and exhibits a large number of sidebands around f_{m11} and f_{m12} as compared with the simulated

spectrum. As mentioned previously, this is largely due to the background noise interference picked up when actual data was collected from the test rig. It can be seen that there is considerable similarity between the spectrum signatures obtained from the model and from real measured data. For this reason, the time domain and frequency domain signal of the healthy gear tooth has been considered as a reference signal, and has been used for comparison with faulty gear tooth vibration signals for the simulation study in section 5.8.

5.7 Simulation Study of Faulty Gears

The simulation results of the gear transmission system model outlined in Section 5.4 were compared with data from an experimental study on the real test rig to determine whether the model is reliable for understanding vibration characteristics for remote gear fault prediction with acceptable accuracy. This section compares the results obtained from both the model simulation and from the real test rig based on frequency domain analysis.

Figures 5.8-5.9 show the vibration spectra of healthy and faulty gears obtained from the model (predicted) for position one and position two. Results from the actual test rig (measured) for the gearbox casing and motor casing are shown in Figures 5.10-5.11. Both simulated and measured results from the two locations in Figures 5.8-5.11 exhibit the fundamental frequency component and its third harmonic.

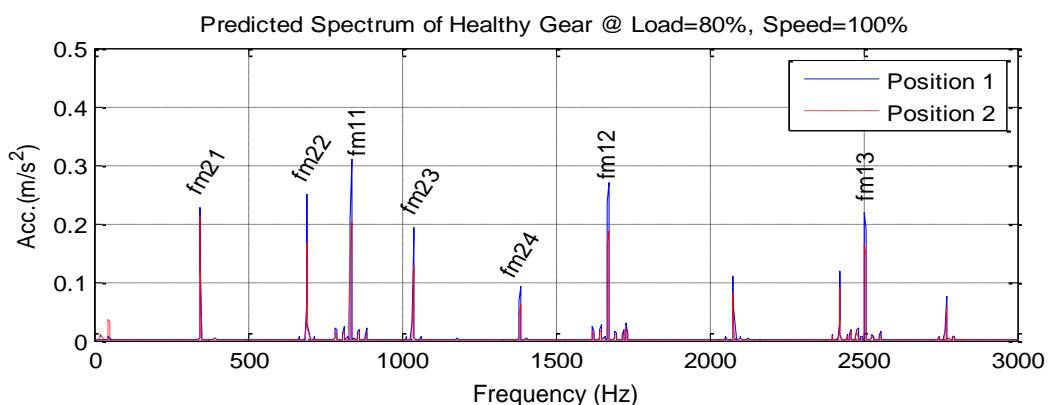


Figure 5.8-Predicted spectrum of the vertical acceleration of position one and two of a healthy gear

CHAPTER 5

MATHEMATICAL MODEL

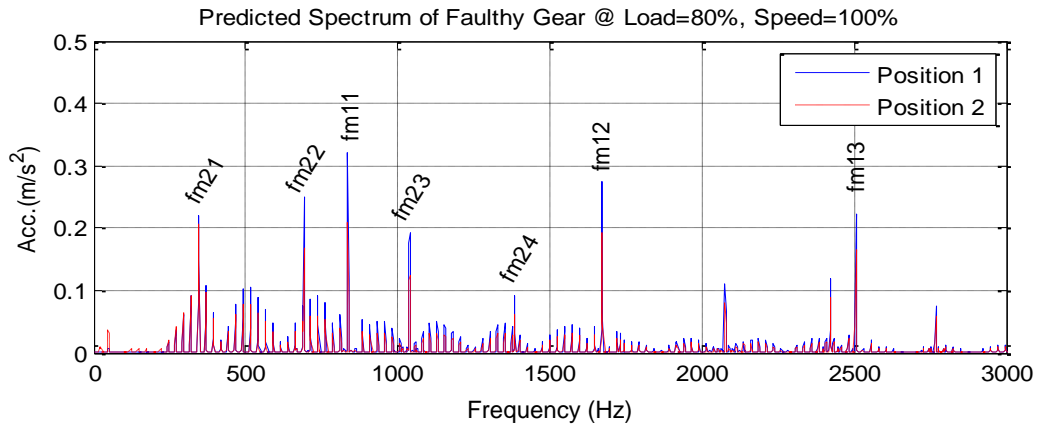


Figure 5.9- Predicted spectrum of the vertical acceleration of position one and two of a faulty gear

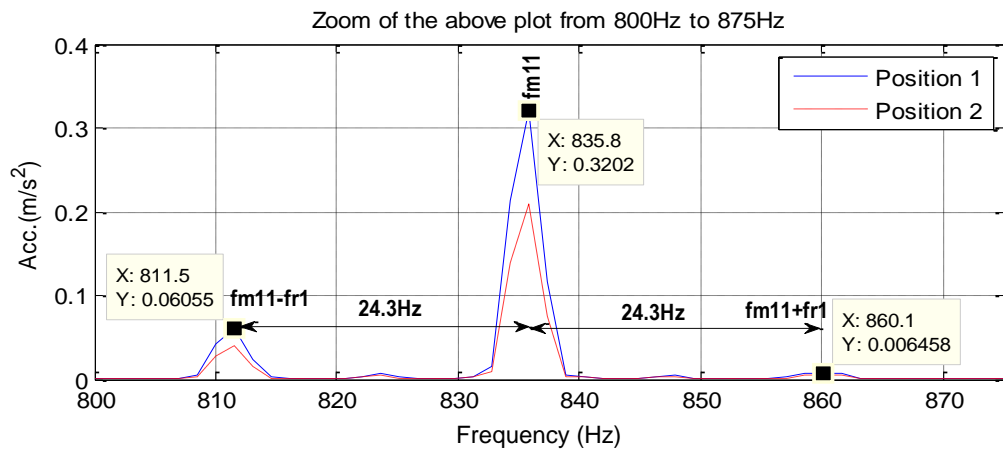


Figure 5.9(a)-Sidebands around the first meshing frequency (f_{m11})

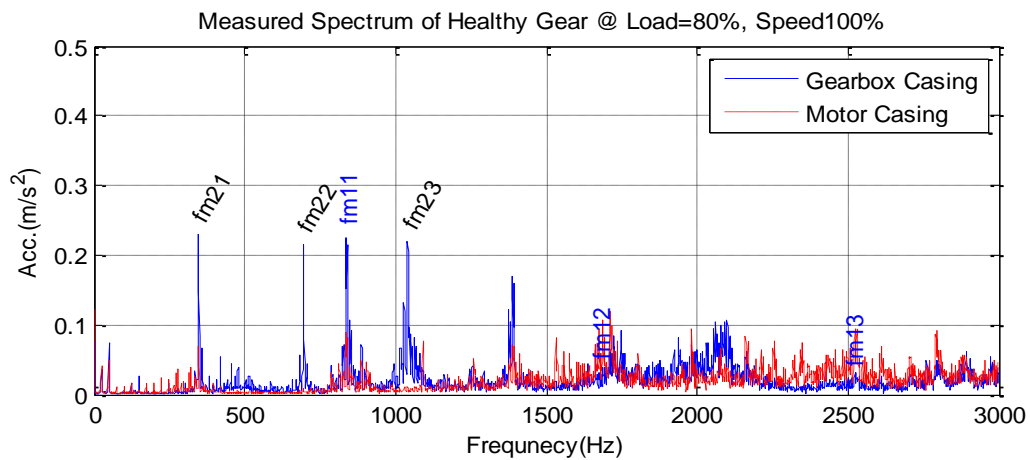


Figure 5.10-Measured spectrum of the gearbox casing and motor casing for a healthy gear

CHAPTER 5

MATHEMATICAL MODEL

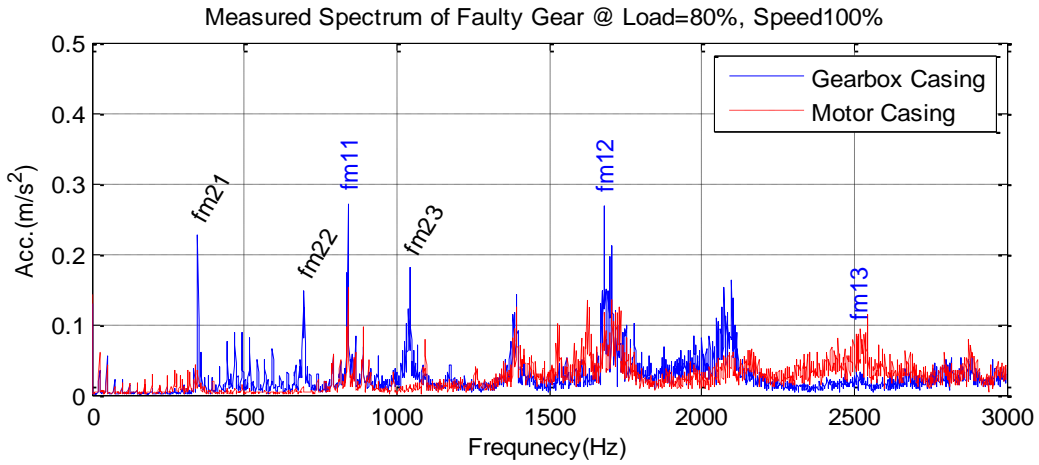


Figure 5.11-Measured spectrum of the gearbox casing and motor casing for a faulty gear

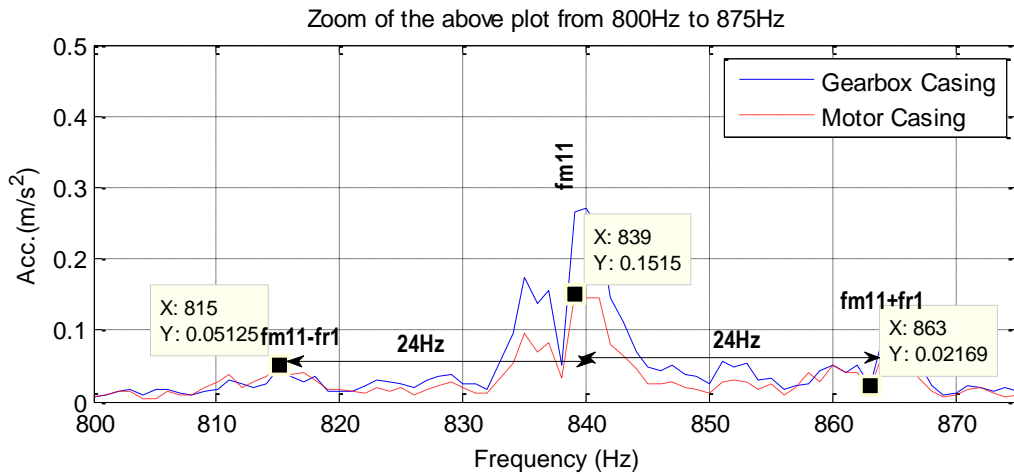


Figure 5.11(a)-Sidebands around the first meshing frequency (f_{m11})

These figures show that the amplitude peaks corresponding to the first stage and second stage meshing frequencies and their harmonics are consistently the largest feature of the spectrum, and are common to the two measurement positions.

Theoretically, the sidebands around the fundamental frequency (f_{m1}) are due to the modulations caused by the shaft frequency (f_{r1}). As seen in the previous figures, the modulation sidebands become very significant and are located on both sides of the gear tooth meshing frequencies and their harmonics (f_{m11} , f_{m12} , f_{m21} , f_{m22} and f_{m13} , f_{m23}). As shown in figures 5.8a and 5.10a, these sidebands are spaced by the rotational frequency (f_{r1}) of the pinion.

CHAPTER 5

MATHEMATICAL MODEL

Compared with the predicted and measured spectra of the healthy gear, shown in Figures 5.8 and 5.10, the faulty gear spectra in Figures 5.9 and 5.11 indicate an additional set of sidebands corresponding to modulation of the rotational speed with fundamental frequencies. It can be seen that the fault causes the following changes to the vibration spectrum signature:

- a) A large number of sidebands are generated around the fundamental meshing frequencies (f_{m11} , f_{m21}) and their harmonics ($2*f_{m11}$, $3*f_{m11}$, $2*f_{m21}$, $3*f_{m21}$,) at both positions in the two figures.
- b) Higher amplitudes are observed for the sidebands due to the super-positional effect of the faulty gear.
- c) Amplitudes of the sidebands around the fundamental meshing frequency and first order harmonic of the motor casing are lower amplitudes of the gearbox casing due to the transmission path effect.

Comparing the simulation spectra displayed in Figures 5.8 and 5.9 with actual data recorded in Figures 5.10 and 5.11, it can be seen that the measured spectra in both locations (the gearbox casing and motor casing) are richer in rotation components (sidebands) than the simulated spectra in both locations (position one and two). This is because of the background noise interference which was detected when the actual data were recorded. However, the simulated results agree closely with the experimental measurements recorded on the test rig.

If the first meshing frequency (f_{m11}) in Figures 5.9 and 5.11 are inspected at much higher resolution, then the sidebands can be clearly seen. It can then be determined that the distance between every two adjacent sidebands is equal to the input shaft frequency.

Figures 5.9a and 5.11a show the zoomed FFT-spectra of Figures 5.9 and 5.11 respectively from 800Hz to 875Hz. Two strong sidebands are presented around the first stage meshing frequency. The frequency interval is 24 Hz which is exactly the same as the rotating speed of the input shaft.

Figures 5.12 and 5.13, show the predicted and measured amplitude values of the first stage meshing frequency for different sensor locations at different gear operating conditions. Figure 5.12, shows the predicted and measured amplitude values of the

CHAPTER 5

MATHEMATICAL MODEL

first stage meshing frequency for position one and the gearbox casing. Figure 5.13 shows the predicted and measured amplitude values of the first stage meshing frequency for position two and the motor casing.

From these figures it can be seen that the values of the predicted and measured amplitudes in both locations gradually change with gear operating condition and severity of the fault. However, there is again considerable similarity between the amplitude values obtained from the model and those obtained from real measured data. In addition, it can also be seen that the higher the rotational speed, the better the resolution of the frequency spectrum and therefore it is easier to identify the meshing frequencies.

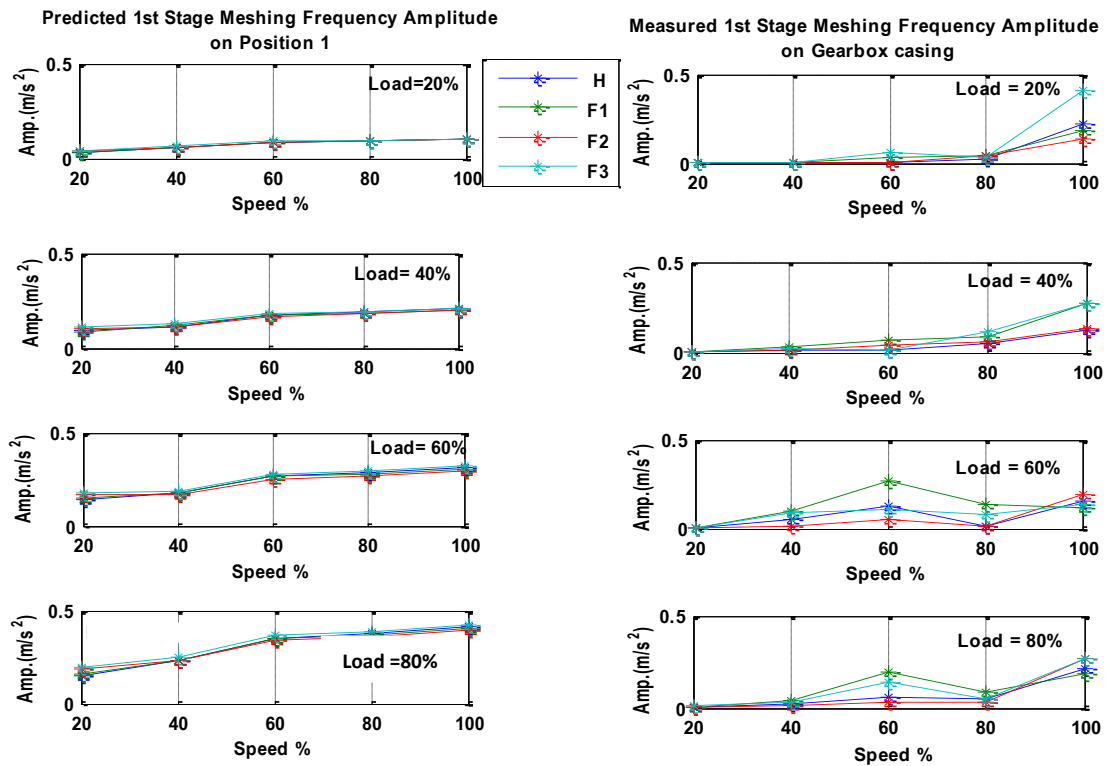


Figure 5.12- Predicted (left) and measured (right) amplitudes of the 1st stage meshing frequency at position one and on the gearbox casing for different gear operating conditions

CHAPTER 5

MATHEMATICAL MODEL

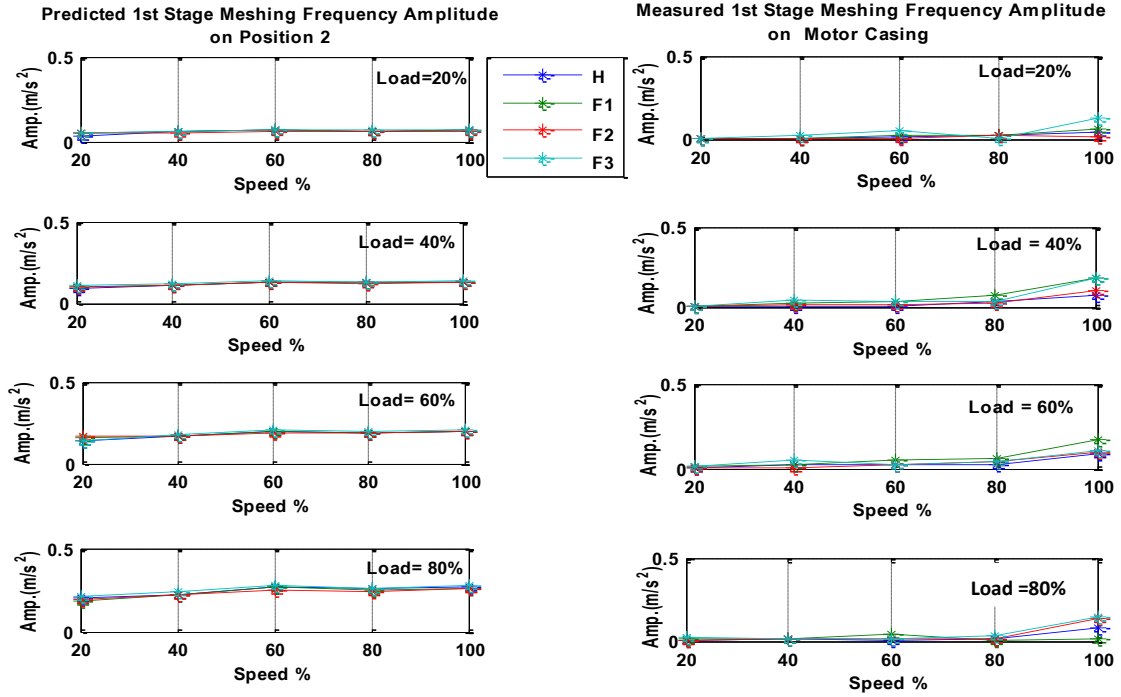


Figure 5.13 - Predicted (left) and measured (right) amplitudes of the first stage meshing frequency at position two and on the motor casing for different gear operating conditions

It is also possible to compare the predicted spectral features from the model at various shaft speeds and applied loads (see Figure 5.14 and 5.15) with the actual measured values. The features can be defined as the average amplitude of the sidebands $[(f_{m11} \pm f_{r1})/2]$ around the first meshing frequency (f_{m11}) in the signal spectrum, which enables the condition of the gears to be characterised.

There is again considerable similarity between the feature amplitudes obtained from the model and those obtained from the measured data actually recorded.

CHAPTER 5

MATHEMATICAL MODEL

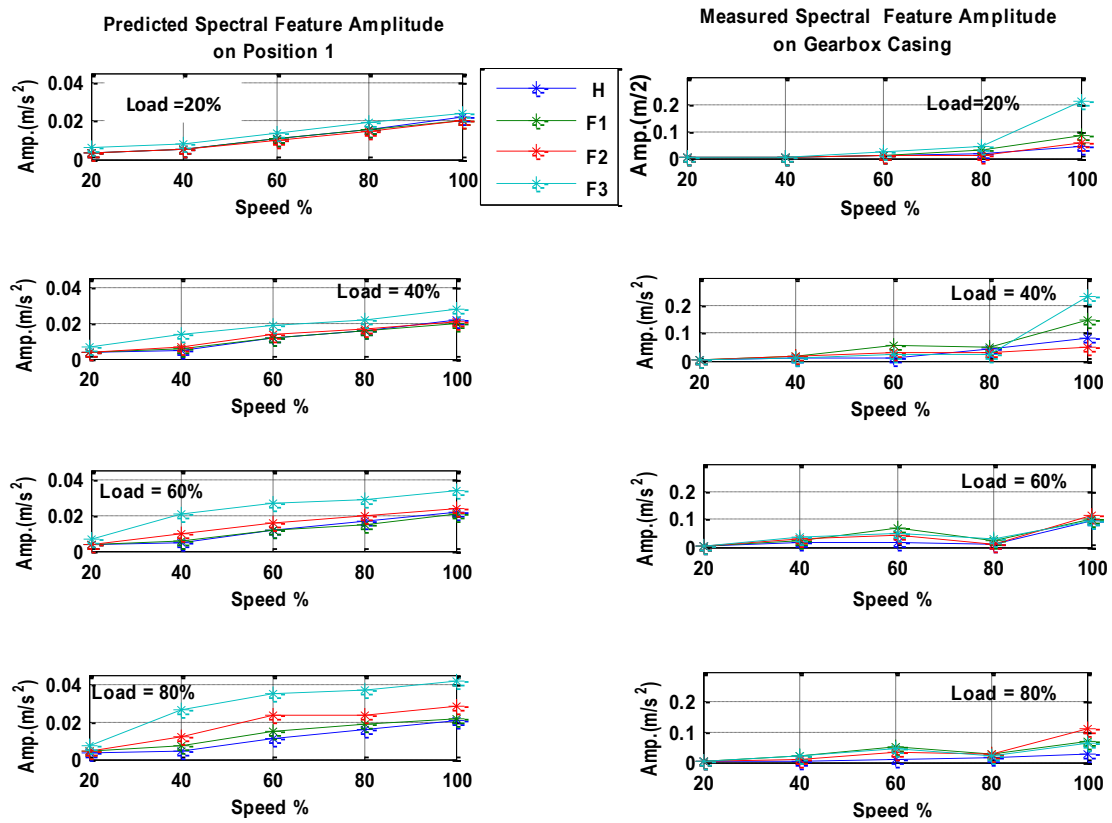


Figure 5.14 - Predicted (left) and measured (right) spectral features at position one and on the gearbox casing for different gear operating conditions

CHAPTER 5

MATHEMATICAL MODEL

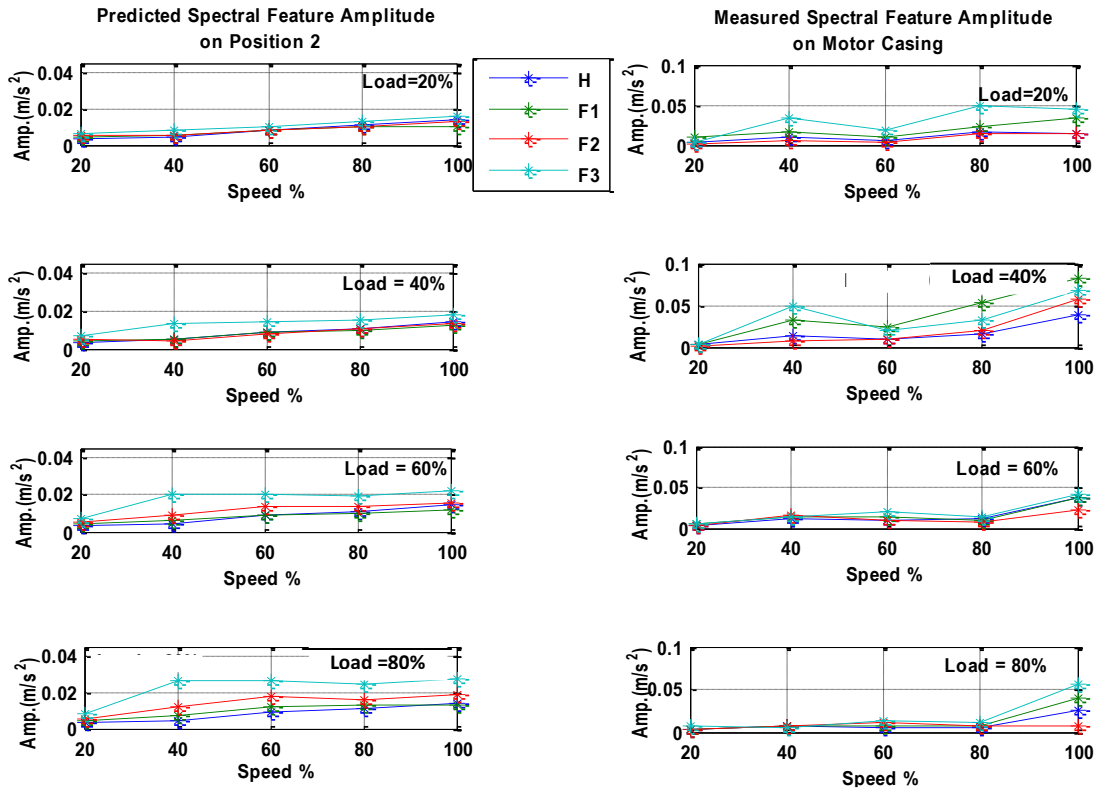


Figure 5.15 - Predicted (left) and measured (right) spectral features at position two and on the motor casing for different gear operating conditions

5.8 Summary

In this chapter the numerical simulations and measured results (spectra) exhibit the same signature for the fundamental frequency component and its harmonics. This demonstrates a good correlation between actual and simulated results.

From comparisons of results in Section 5.7 the results of gear transmission system model and the simulation study was significantly correlated with those produced from the actual data collected from the gear test rig. It can be concluded, therefore, that the model developed does highlight key features in the test rig when measurements are taken from either the gearbox casing or the motor casing. For example, the attachment of the gears and associated shafts to different vibration masses resulting in different amplitudes at the main meshing frequencies.

CHAPTER 6

EFFECTIVENESS OF TIME SYNCHRONOUS AVERAGING

Time synchronous averaging (TSA) has been reported widely as an effective method in processing vibration signals for the monitoring of rotating machinery. In this chapter, this method is applied to the vibration signals from the gearbox to obtain the angular domain signals, the order spectra and to determine the order-frequencies to further characterise the gearbox vibration in these new domains. By comparing these new results with the results in Chapter Four, it has found that TSA is a better method for resolving different faults under variable operating conditions.

6.1 Introduction

The traditional signal processing techniques which were used for the signal evaluation presented in Chapter Four assumes that the motor speed remains constant. The gearboxes are subjected to varying tooth mesh stiffnesses which results in load oscillation and hence speed variations. These speed variations result in frequency content variations in the time record, showing non-stationary effects in the signals. As conventional Fourier Transform analysis is based on stationary signals, direct FFT of the vibration signals will produce inaccurate results and this is especially true when a multistage gearbox is considered. Multistage gearboxes produce not only many mesh frequency components but also multiple modulations between mesh frequencies and shaft frequencies. This means that the frequency density is very high and direct FFT of the raw signals often fails to resolve the frequency content properly, which in turn results in poor performance of overall fault detection [129].

In addition, gearbox vibration is also highly contaminated by various random noises associated with the measurement process e.g. lubrication fluid turbulence etc. Conventional FFT based analysis ignores signal phase information and therefore has limited effect on reducing noise of this type.

As reviewed in Chapter Two, TSA aligns signals according to angular positions of a particular rotating shaft, which allows phase information to be taken into account and to elimination the influences of speed variation. As a result, TSA has been found to be very efficient in processing signals due to time varying processes and in the suppression of noise from uncorrelated sources such as random noise and vibrations from nearby components.

To study the effectiveness of TSA, the results obtained in Chapter Four are compared with those obtained when TSA is applied to waveform characteristics, spectral patterns and their corresponding feature parameters under different operating loads and fault conditions. In addition, CWT of TSA is also compared with conventional CWT results of raw signals as a further method of examining and characterising vibrations.

CHAPTER 6

EFFECTIVENESS OF TIME SYNCHRONOUS AVERAGING

These studies are based on previous research by *Andrew et al* [130] and *Jing* [131] to understand gearbox vibrations and present a full demonstration of TSA based approaches in detecting and diagnosing the presence of gear faults under different operating conditions.

6.2 Implementation of TSA

To accurately characterise and correctly isolate gear fault from vibration signal measurements through time based acquisition, it is essential to track the running speed of the gear and to determine accurately the angular positions of the shaft at different instants in time. The vibration data in the time domain can then be resampled according to the positions in the angular domain of the shaft of interest. This process, called the synchronous sampling technique [132], allows accurate angular alignment of the vibration signal. The component of the signal arising from mechanical faults at fixed angular positions can be greatly enhanced whilst noise with random angular positions is suppressed through averaging across different revolutions of data sets.

The synchronous sampling technique combines the shaft speed signal generated by a tachometer with the vibration signal generated by an accelerometer and interpolates the vibration signals into a data point per fraction of angular rotation [101,133], with the result that the vibration signals are then presented in the angular domain instead of time domain. An FFT is then performed on the angular domain vibration signal to produce an order spectrum. Carrying out an order analysis enables the isolation of repetitive vibrations from mechanical components even when the speed of the machine is changing. With order analysis, it is possible to separate, detect and quantify fault signatures.

There are many TSA methods. For computational efficiency and reliable implementation, a shaft encoder based method has been adopted in this research. The shaft encoder, mounted on the input shaft, produces 360 pulses per turn as the angular position reference signal. The vibration and reference signals were measured simultaneously and sampled at a rate of 50 kHz for 20 seconds at each of the operating settings.

CHAPTER 6

EFFECTIVENESS OF TIME SYNCHRONOUS AVERAGING

For each measurement, 10^6 data points were recorded with $(10^6/50000)$ 20 second time duration. From the pulse signal, the speed of the input shaft was estimated, as 24.6543 Hz. Therefore, for a 20 second data collection period, this corresponds to 493 revolutions of the pinion. The mesh frequency, f_{m11} , corresponding to this measurement is (24.6543×34) , which equals 838.2Hz. Due to the shaft speed variation, the signal is divided into $10^6/493 \approx 2028$ lengths. By eliminating the transient data of the first and the last revolution, only 491 revolutions of data were used and lengths varied around 2028 depending on the variations in shaft speed. An interpolation technique which is evaluated in [101,131,133] was applied to each of the 491 signals to a length of 2048 ($= 2^{11}$) - the closest power of 2 for 2028 and forms a data matrix of 2048 x 491. It has been shown that this 491 time average allows a sufficient reduction of random noise and other shaft related components to clearly pinpoint the localised fault positions.

To obtain an order spectrum with sufficient resolution, the data matrix of 2048 x 491 is reshaped into a matrix of $[(2048 \times 4) \times (491/4)] = 48192 \times 122$ as an average. The reduction of average times has little effect on the averaged results when compared with that of average in 491 times. Moreover, the new data length of 48192 results in an order spectrum that represents two shaft-related peaks with four data point intervals different spectral peaks can be clearly distinguished. Nevertheless, the order spectrum produces clear features for the faulty gears which are in agreement with previous understanding.

6.3 TSA Signal in the Angular Domain

TSA of the time domain signal results in a new data sequence whose amplitudes vary with angular positions rather than time instants. Obviously, the TSA signal can be explored using conventional statistical approaches to find signal strength and structure characterisation.

6.3.1 Waveform Characteristics

A fault such as a broken tooth on a gear will cause an impact each time it goes into mesh and this sudden impact results in changes in the amplitude of the vibration

CHAPTER 6

EFFECTIVENESS OF TIME SYNCHRONOUS AVERAGING

signal during the mesh period. The duration period and amplitude level of a local variation can provide essential information about the gear condition. Obviously, higher amplitudes of load oscillation will produce higher vibrational signal amplitudes. This feature can therefore be used for fault detection and severity estimation.

The amplitude of the vibration signal is also sensitive to the tooth loading. Thus, if load fluctuates during gearbox operation, it is expected that the amplitude of vibration would vary. The source of this type of modulation can either be due to external load fluctuation or manufacturing errors. For example, tooth errors or eccentricity of one gear in the gearbox can cause amplitude modulation. As shown in Figures 6.1 and 6.2, even a healthy gear can have this type of modulation.

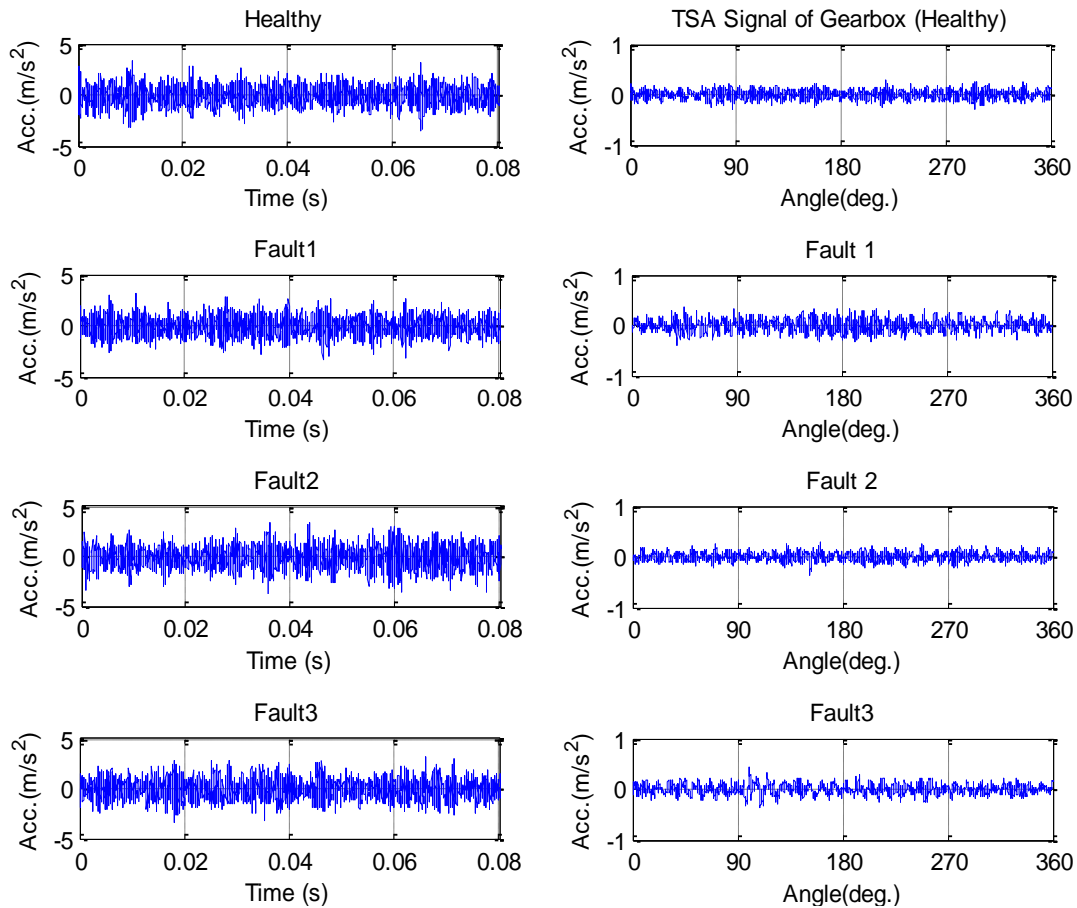


Figure 6.1- Time domain (left) and angular (right) waveforms for a healthy and three faulty gear types at low operating ($L=40\%$, $S=50\%$) conditions

CHAPTER 6

EFFECTIVENESS OF TIME SYNCHRONOUS AVERAGING

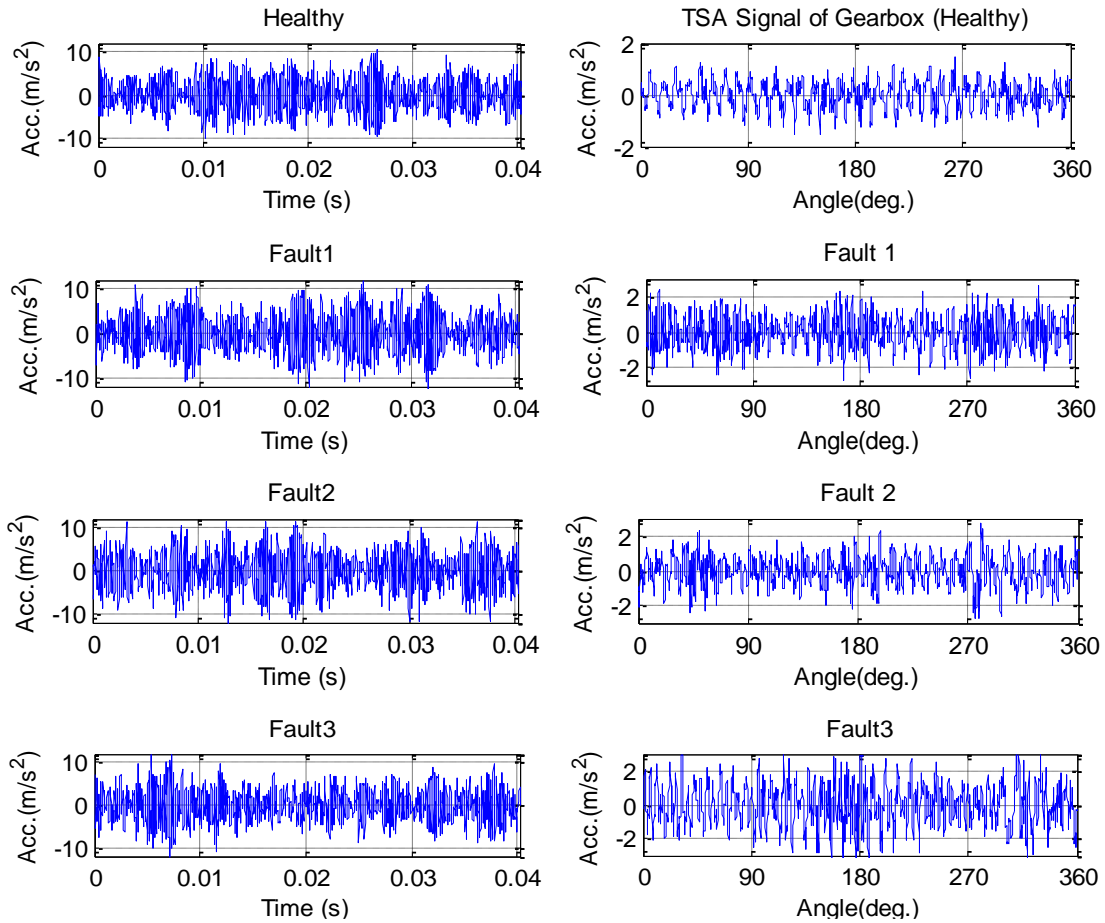


Figure 6.2- Time domain (left) and angular (right) waveform for a healthy and three faulty gear systems at high operating ($L=80\%$, $S=100\%$) conditions

A more localised fault, however, would tend to give further modulation by a short impulse repeated in every revolution. Although these short impulses could be smeared by the noise and the error appearing in the time domain waveform, they would be more clearly visible in the angular waveform.

The time domain waveforms (left) and angular (TSA) waveforms (right) of healthy and three faulty gear cases (Fault 1, Fault 2 and Fault 3) under low and high operating conditions are shown in Figures 6.1 and 6.2 respectively.

Time domain waveforms in the left hand side of Figures 6.1 and 6.2 show how the vibration changes over the time. Every time the gear teeth mesh together, the extent of damage can be assessed through the changes in the time waveform as presented.

CHAPTER 6

EFFECTIVENESS OF TIME SYNCHRONOUS AVERAGING

As previously discussed in section 4.2.1, the time domain waveforms shown to the left in Figures 6.1 and 6.2 do not reveal any significant information about the condition of the gearbox. Both figures show a significantly different pattern between healthy and faulty gear conditions. Interestingly, the faulty conditions at both low and high operating conditions appear to produce a smaller variation of the waveform over the entire cycle. Such a difference does not reveal sufficiently detailed information about the gearbox condition to enable a reliable diagnosis to be made.

The right hand plots in Figures 6.1 and 6.2 show the angular domain signals resulting from the TSA of the time domain waveform averaged over 491 shaft rotations. TSA suppresses all vibrations from the gearbox which are asynchronous with the rotation of the gear, leaving only the vibration produced during one rotation of the gear on the input shaft. Therefore, local variations in the vibration signal become more visible.

At low operating conditions, as shown in Figure 6.1, the amplitudes of the time domain waveform (raw signals) vary from -5 to 5 m/s² while the angular waveform amplitudes vary from -1.0 to 1.0 m/s². At high operating conditions, shown in Figure 6.2, the amplitudes of the time domain waveform vary from -10 to 10 m/s² while the angular waveform amplitudes vary from -2 to 2 m/s². This considerable reduction in TSA signal amplitude shows the effectiveness of the TSA process in reducing the noise and other asynchronous signals. In general, the waveform comparison between the two types of signals reveals the following main observations:

- ✚ Vibration signal amplitudes increase with high operating conditions.
- ✚ The angular domain signals for both low and high operating conditions are primarily the culmination of the meshing frequency and harmonics.
- ✚ The local variations in the vibration signal become more visible in the angular waveforms because the TSA technique tends to reduce the noise and cancel out the vibration components that are not synchronised with the rotation of gear.
- ✚ The angular domain signal at high operation conditions shows the effect of higher speed and load becoming more pronounced on the TSA signal. Remarkably, the TSA vibration signal amplitudes increase with the severity of seeded faults.

It can be seen that the smaller fault (Fault 1) has little noticeable effect on the angular waveform. The periodic feature can only be observed under high load and speed operating conditions illustrated by the third and fourth rows in the right hand side of Figure 6.2. For example, under high operating conditions, the amplitudes of the waveforms recognizably increase with the introduction of faults and the amplitudes for Healthy, Fault 1, Fault 2 and Fault 3 conditions are approximately 1.7, 2.1, 2.3 and 2.7 m/s² respectively. However, the small local fault (Fault 1 with 25% tooth removal) creates small impulses in the vibration signal and thus the average vibration signal, to which there is little noticeable effect, does not highlight any small variations in the signal.

It is obvious that an advanced tooth breakage such as Fault 3 can be detected immediately by a visual inspection of the signal average. The large amplitude of vibration signal around that tooth indicates reduced meshing stiffness.

For the same gear status, different patterns are seen between the angular waveforms in the low and high operating conditions shown in Figures 6.1 and 6.2. However, at low operating conditions, the TSA signals produce ambiguous information for distinguishing between gear fault cases.

It can be concluded that after TSA, the angular waveform patterns associated with the meshing teeth can often be compared with conventional time domain waveforms. In some cases, it is possible to identify damage from inspection. However, in the case of a small fault such as Fault1, it may be difficult to identify it from physical inspection because of the high contact ratio (the average number of teeth in contact during a mesh cycle). Many techniques have been proposed to increase the detectability of damage from the TSA signal to enable easier detection of the early onset of gear failure.

6.3.2 Signal Strength based Diagnosis (Peak value and RMS) after TSA

To conduct a quantitative comparison between the two types of signals and different types of fault, common waveform parameters including RMS and peak value are calculated to examine the characteristics of signal strength over different conditions.

Figures 6.3 and 6.4 show the average of peak values and RMS of the vibration signal

CHAPTER 6

EFFECTIVENESS OF TIME SYNCHRONOUS AVERAGING

for healthy and faulty gears (Fault1, Fault 2 and Fault 3) at different operating conditions with (right) and without (left) TSA.

The results reveal significant changes between the peak values and RMS values with and without TSA confirming that the attenuation and interference of vibration signals may significantly alter the overall peak and RMS values.

The results in Figures 6.3 and 6.4 shows that the peak value and RMS of the signal increase fairly linearly from low to high operating conditions. This confirms that the operation condition of the gears may alter the vibration signal but does not exhibit a reliable trend with fault progression even at high fault severity (Fault 3).

Figures 6.3 and 6.4 also show that the TSA of the peak value and RMS vibration signal increase monotonically with respect to the operating condition and exhibit a reliable trend with gear fault progression especially at high load operating conditions.

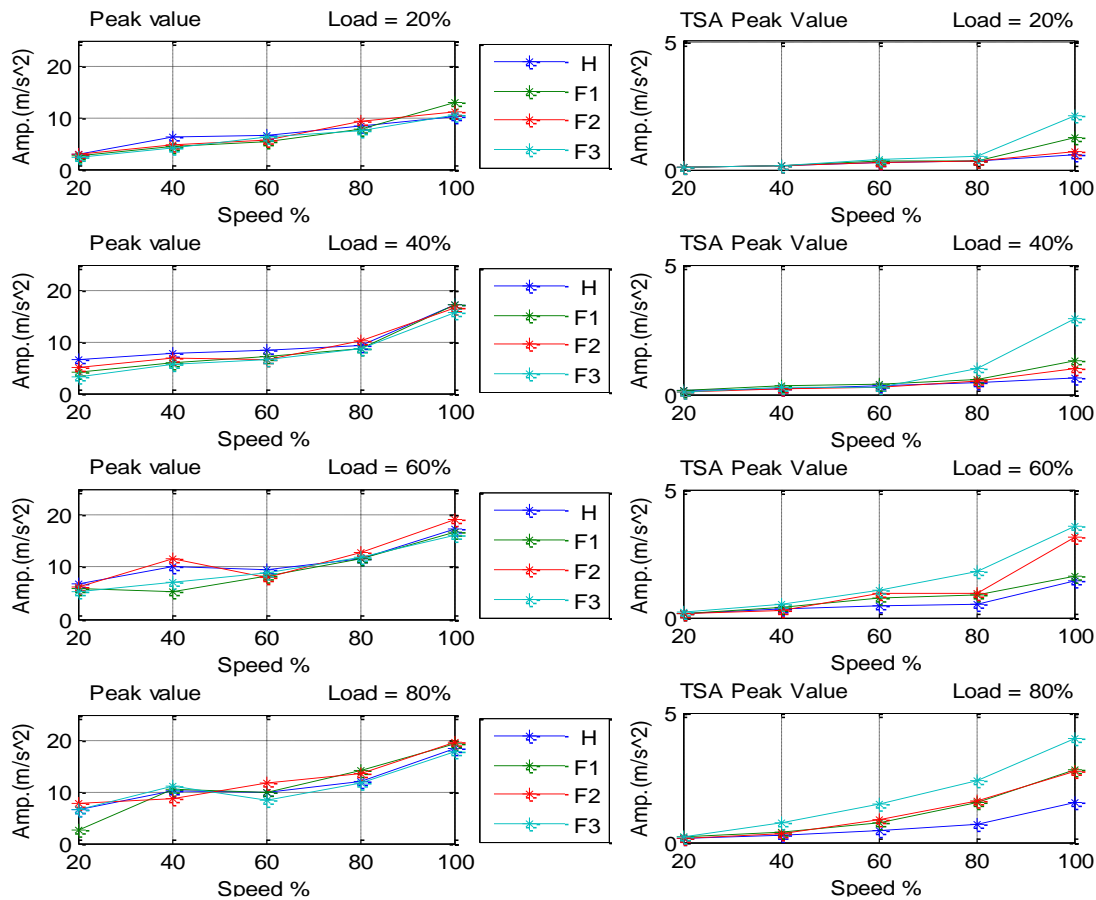


Figure 6.3- Average peak values without (left) and with (right) TSA for healthy and faulty gears under different operating conditions.

CHAPTER 6

EFFECTIVENESS OF TIME SYNCHRONOUS AVERAGING

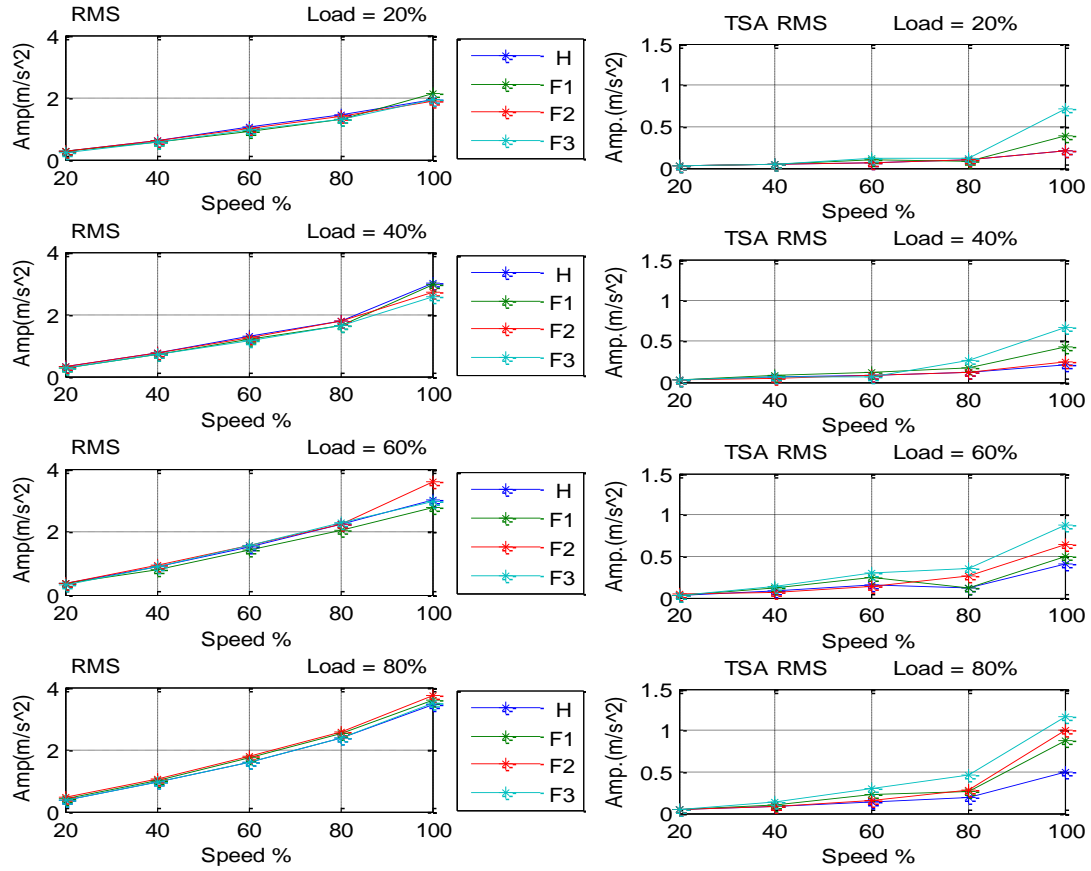


Figure 6.4-Average RMS without (left) and with (right) TSA for healthy and faulty gears under different operating conditions

The significant change in the peak and RMS values of the TSA vibration signal between healthy and faulty conditions at high operating conditions reflect significant information about the pinion gear condition. However, at high load (80%) and high speed, the presence of defects is detected by the increase in vibration levels confirming the possibility of distinguishing between fault severities at high operating conditions.

As shown in Figures 6.3 and 6.4, the peak value and RMS vibration signals with and without TSA are highly dependent on load and speed and non-linear with respect to operating condition.

The peak value and RMS can be measured for different vibration levels and increase monotonically with respect to operating condition. It can be argued that both parameters approach a linear relationship with respect to operating condition.

By comparing the peak values with (right) without (left) TSA in Figure 6.3 and comparing the RMS with (right) and without (left) TSA in Figure 6.4, it can be concluded that the TSA provides better detection performance because of its capabilities of noise reduction and nonlinear effect detection.

6.3.3 Signal Structure based Diagnosis (Kurtosis and Crest Factor) after TSA

Figures 6.5 and 6.6 show the average of kurtosis and crest factor of the vibration signal for healthy and faulty gears (Fault 1, Fault 2 and Fault 3) at different operating conditions with (right) and without (left) application of TSA. These two parameters are dimensionless and give more indication of the difference in signal patterns.

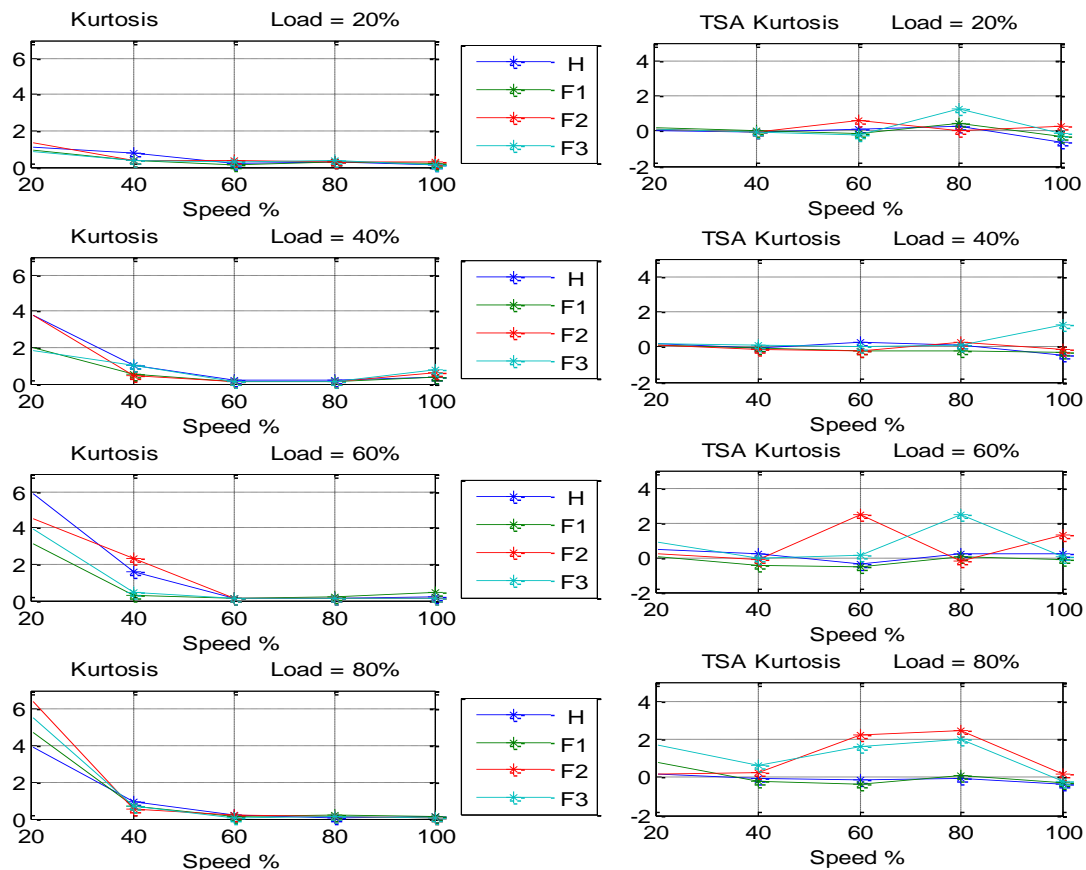


Figure 6.5-Average values of kurtosis before (left) and after (right) TSA for healthy and faulty gears under different operating conditions

Both parameters are measures of spikiness in the vibration waveform. The values for kurtosis and crest factor before and after TSA analysis showed a significant change in magnitude when comparing data for both healthy and faulty gear types at all operating

CHAPTER 6

EFFECTIVENESS OF TIME SYNCHRONOUS AVERAGING

conditions. However, the kurtosis and crest factor of the vibration signal before and after TSA do not exhibit reliable trends with fault progression at all operating conditions.

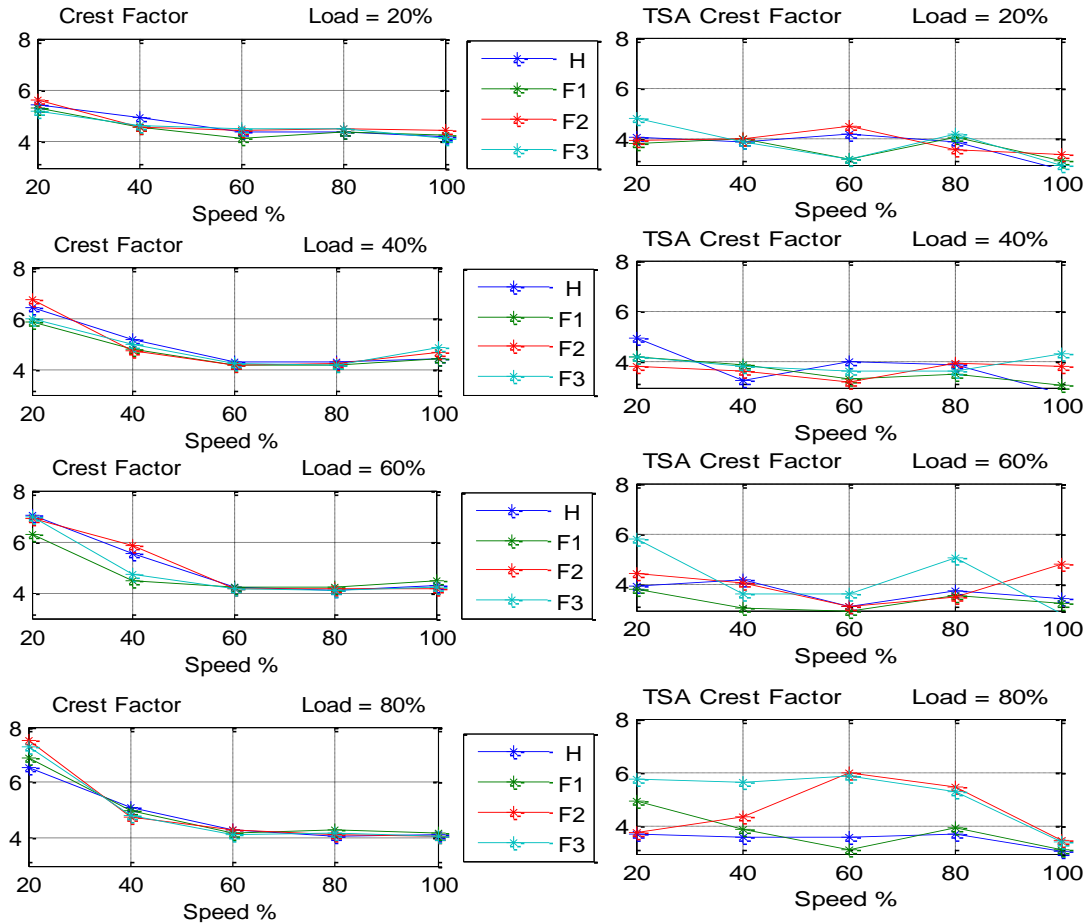


Figure 6.6-Average values of crest factor before (left) and after (right) TSA for healthy and faulty gears under different operating conditions

It can be concluded that even when TSA is applied both parameters are unlikely, on their own, to be effective parameters for determining gear status. As the data show, there is little variation in the magnitudes of either parameter for the four gear cases examined even under different operating conditions. Simultaneous observation of these statistical quantities may provide no reliable decision-making for gear fault diagnosis. Therefore, more advanced signal processing techniques such as /or order spectrum domain or CWT have to be used for future analysis.

6.4 Order Spectrum of TSA Signal

As mentioned in section 4.3, the FFT process transforms time domain data in Figures 6.1 and 6.2 to the frequency domain, creating a conventional spectrum. Signals that are periodic in the time domain appear as peaks in the frequency domain. In order analysis, the FFT transforms the angular domain data into an order spectrum. Signals that are periodic in the revolution appear as peaks in the order domain. The main difference between order analysis and conventional domain analysis is that the resulting spectrum is a function of order (harmonics of rotation speed) as opposed to a function of frequency (i.e. Hz).

Figures 6.7 and 6.9 shows the conventional FFT spectrum of a healthy and three different severities of faulty gears (Fault 1, Fault 2, Fault 3) under low and high operating conditions respectively. Figures 6.8 and 6.10 show the order spectra of the same measurement. The y-axis in the figures is amplitude; the x-axis is frequency for the conventional spectra and orders of rotation for the order spectra.

6.4.1 Characteristics of the Order Spectrum

An obvious difference between the conventional and order spectra as shown in figures 6.7 to 6.10 is the alignment of the peaks. Each line of peaks in the order spectrum clearly indicates a relationship between vibration and shaft position. The peaks in the conventional spectrum are difficult to relate to shaft speed.

The first order (1st order) corresponds to the rotational speed of the input shaft (24.66 Hz). The tooth number of the first pinion gear pair (driving gear) is 34; therefore the 34th order component represents the fundamental gear meshing frequency in the order spectrum. The other significant orders (33rd and 35th) are the sidebands around the fundamental gear meshing frequency.

The following analysis is focuses on the low frequency range. In order to investigate the influence of TSA on the vibration signal, the variation of the gear characteristic frequency (f_{m11}) and its sidebands in the conventional spectrum is compared with corresponding orders (34th, 33rd and 35th) in the order spectrum.

Under low and high operating conditions, conventional spectra in Figures 6.7 and 6.9

CHAPTER 6

EFFECTIVENESS OF TIME SYNCHRONOUS AVERAGING

and order spectra in Figures 6.8 and 6.10, show clear discrete components in the low frequency range.

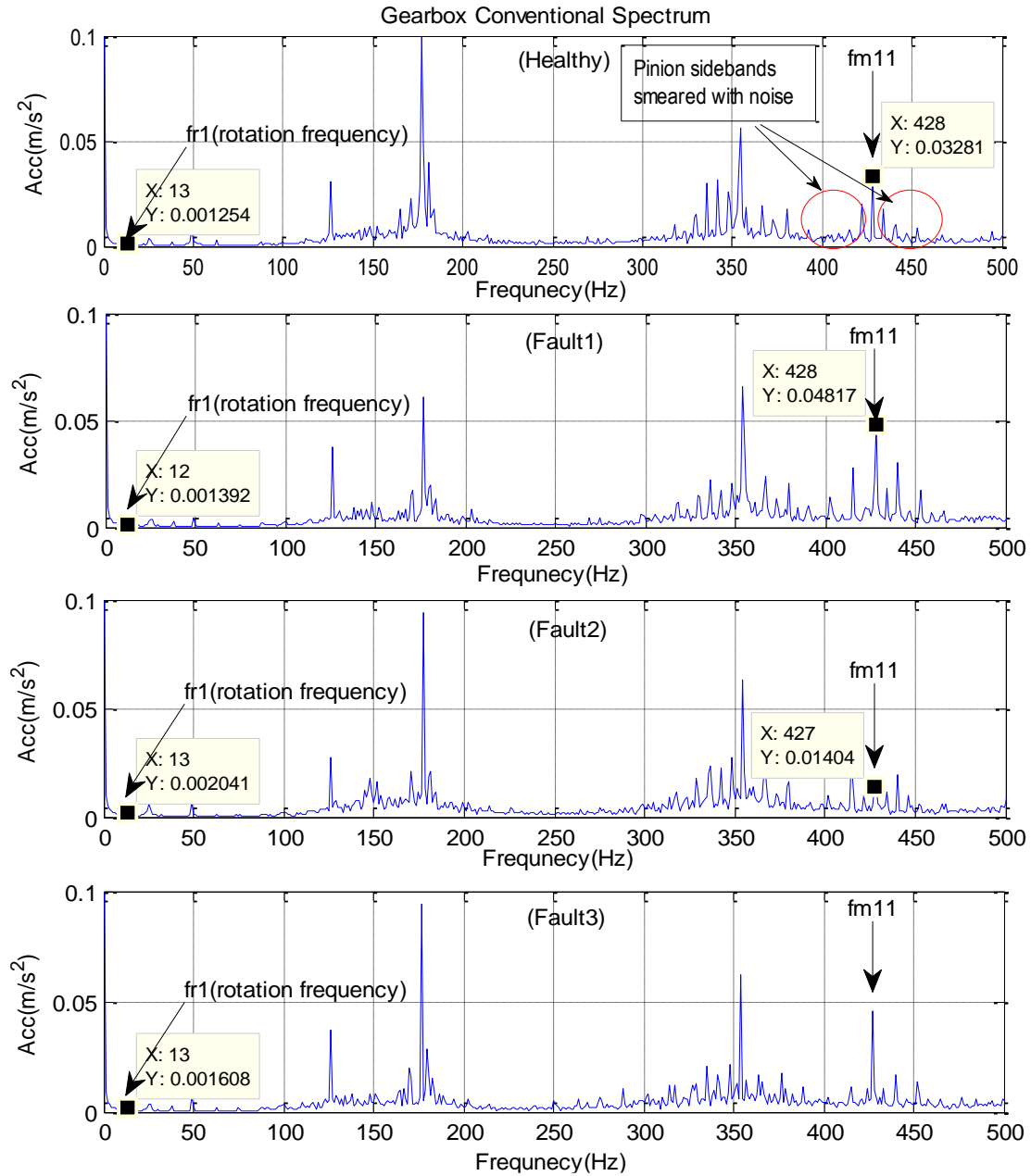


Figure 6.7-Conventional spectra for healthy and faulty gears under low ($L=40\%$, $S=50\%$) operating conditions

These components represent the synchronous components (fundamental meshing frequency and sidebands) of the first stage. It can be seen that the amplitudes of the

CHAPTER 6

EFFECTIVENESS OF TIME SYNCHRONOUS AVERAGING

meshing frequency and sidebands change with gear operating condition and severity of the faults. As shown in figures 6.7 and 6.9, the value of the meshing frequency (f_{m11}) in the conventional spectra of healthy and faulty gears at both the low and high operating conditions has changed slightly due to speed variations.

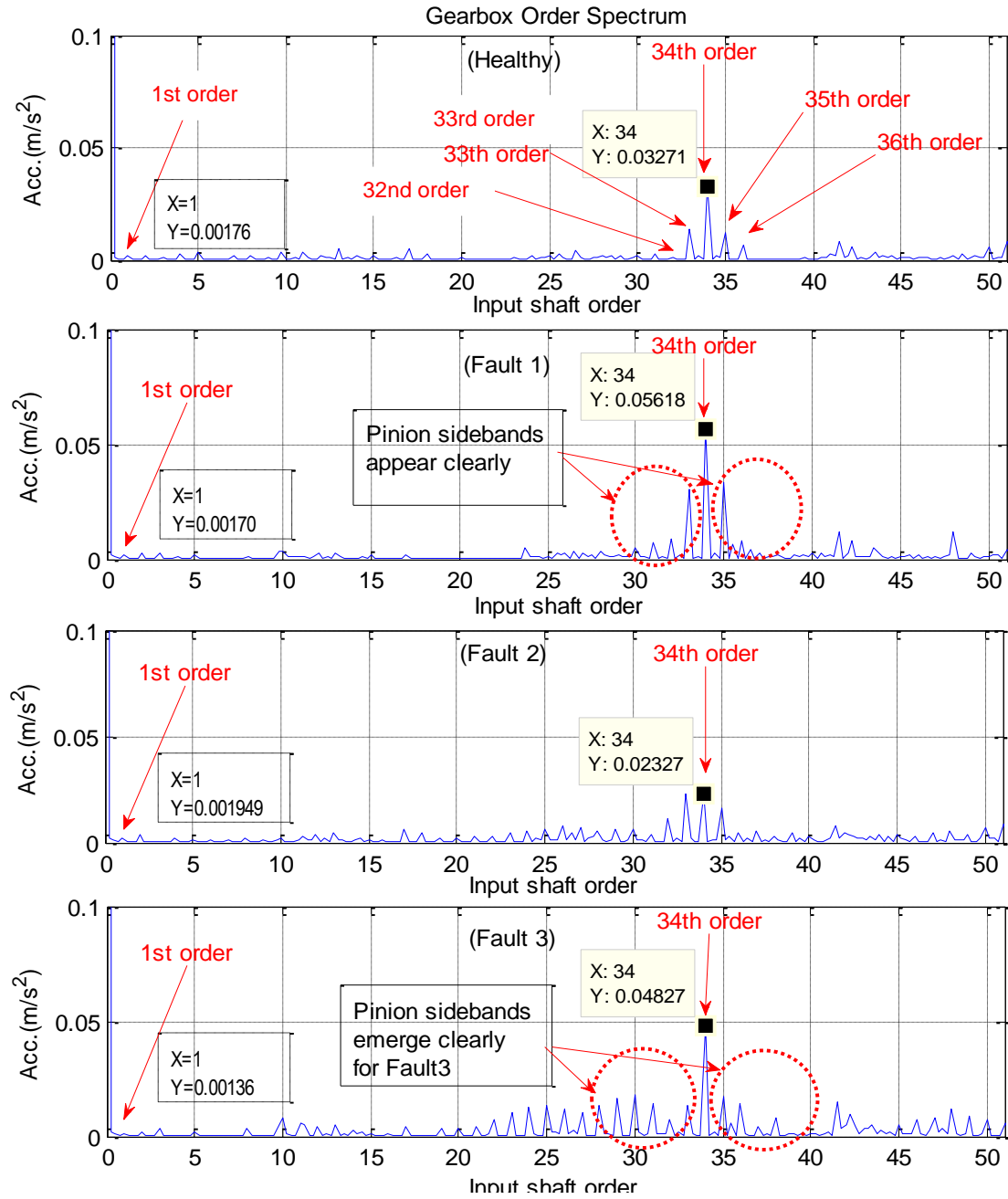


Figure 6.8-Order spectra for healthy and faulty gears under low ($L=40\%$, $S=50\%$) operating conditions

CHAPTER 6

EFFECTIVENESS OF TIME SYNCHRONOUS AVERAGING

However, in the order spectra shown in Figures 6.8 and 6.10 the 34th order value does not appear to change. This confirms that TSA analysis removes interference from the speed of rotation and additive random noise.

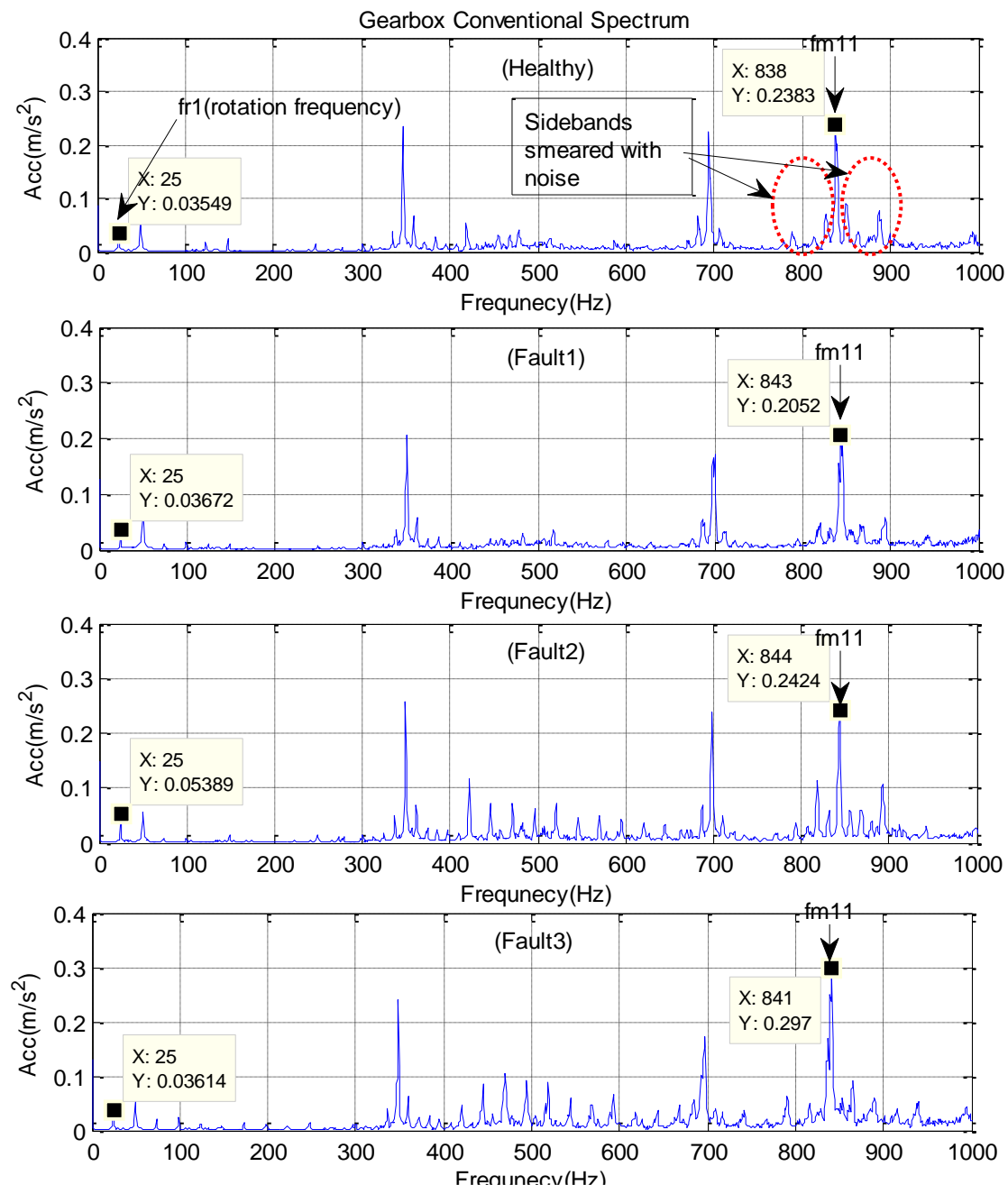
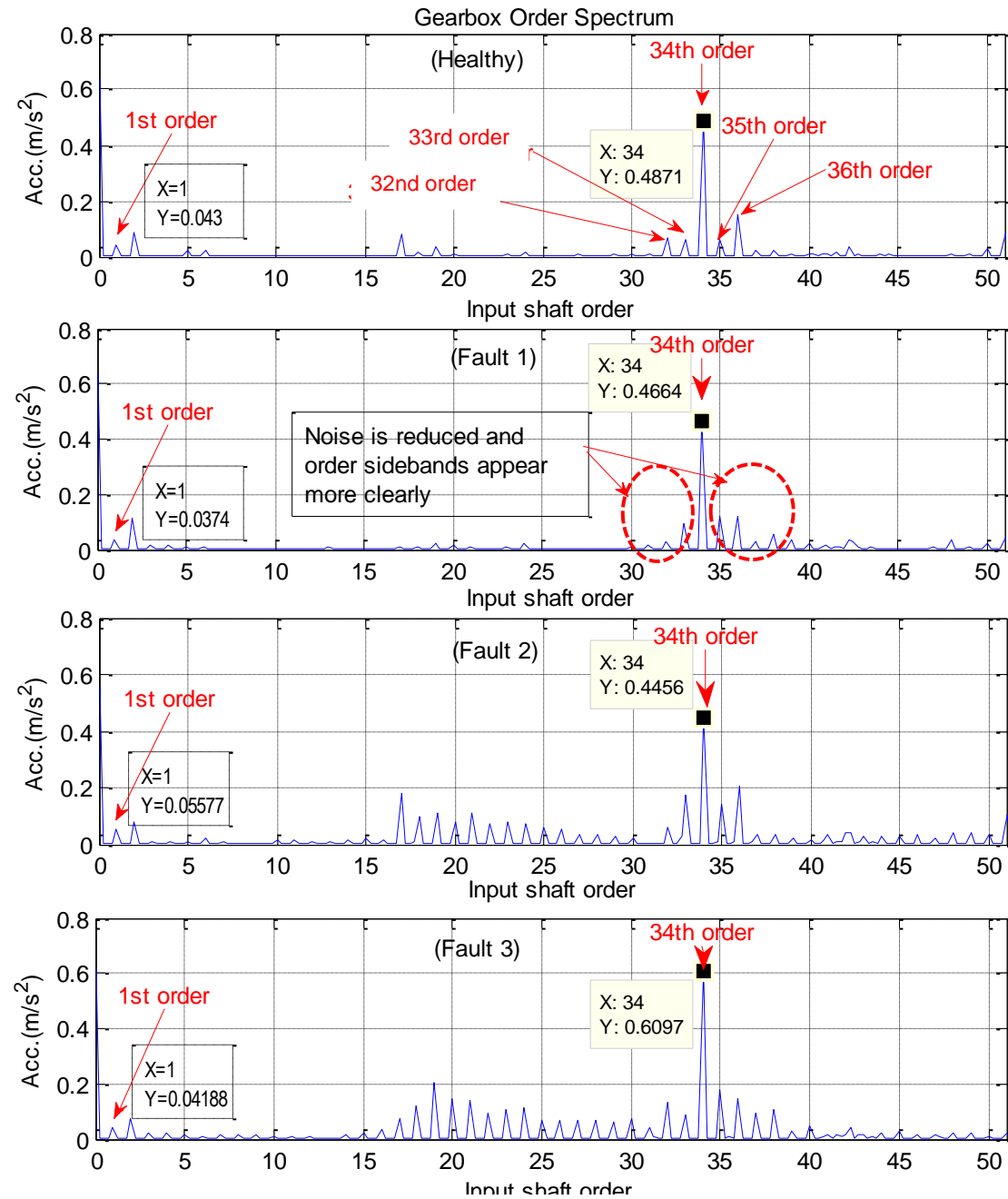


Figure 6.9-Conventional spectra for healthy and faulty gears under high (L=80%, S=100%) operating conditions

CHAPTER 6

EFFECTIVENESS OF TIME SYNCHRONOUS AVERAGING

In the conventional spectra, at low operating conditions (Figure 6.7) and high operating conditions (Figure 6.9) the synchronous component (f_{m11}) for healthy and faulty gears has a higher amplitude and the sidebands do not appear clearly because they are smeared with non-synchronous background noise.



*Figure 6.10-Order spectra for healthy and faulty gears under high
(L=80%, S=100%) operating conditions*

CHAPTER 6

EFFECTIVENESS OF TIME SYNCHRONOUS AVERAGING

The order spectra, at low and high operating conditions (Figures 6.8 and 6.10), the synchronous component (34th order) for healthy and faulty gears has the highest amplitude and is seen most clearly. The non-synchronous background noise components are greatly reduced. In addition, the 34th order is slightly changed in amplitude and the more severe the fault (Fault 3) the higher the amplitude.

At high operating conditions, as seen in Fig 6.10, the number of sidebands around the 34th order increases with the severity of the faults and amplitudes are significantly larger.

For Fault 3 under low operating conditions, the meshing frequency (f_{11}) in the conventional spectrum (Figure 6.7) and the 34th order in the order spectrum (Figure 6.8) are clearly seen. However, the sidebands around f_{11} in the conventional spectrum are not seen as clearly as in the order spectrum around the 34th order.

For Fault 3 at high operating conditions, as seen in Figures 6.9 and 6.10, the meshing frequency (f_{11}) in the conventional spectrum and 34th order in the order spectrum have the highest amplitudes and the sidebands around the 34th order in the order spectrum are seen more clearly.

However, the amplitudes of the tooth meshing frequency (34th order) in the order spectra shown in figures 6.8 and 6.10 do not provide a trend consistent with the severity of the gear damage.

It can be concluded that the gear faults can be distinguished more easily according to spectral peak values at the special frequencies following TSA. The results have shown that conventional spectral analysis techniques are not sensitive to fault diagnosis and analysis based on TSA signals is a more appropriate solution for fault diagnosis.

6.4.2 Performance of Mesh Order Based Diagnosis

Figure 6.11 shows the magnitude of meshing frequency amplitudes of conventional and order spectra (left and right respectively) and how these change with gear status (Healthy, Fault 1, Fault 2, Fault 3) under low and high operating conditions.

As can be seen in Figure 6.11, at low operating conditions the meshing frequency (f_{m11}) amplitudes in the conventional spectrum and the 34th order in the order spectrum

CHAPTER 6

EFFECTIVENESS OF TIME SYNCHRONOUS AVERAGING

show a significant change in magnitude, and both spectra cannot differentiate between gear statuses. At high operating conditions the effects of the faulty gears can be seen more clearly for both methods, but the order spectra demonstrate more consistently the difference in the range of faults. This also confirms that the TSA technique removes the interference from rotational speed and additive random noise.

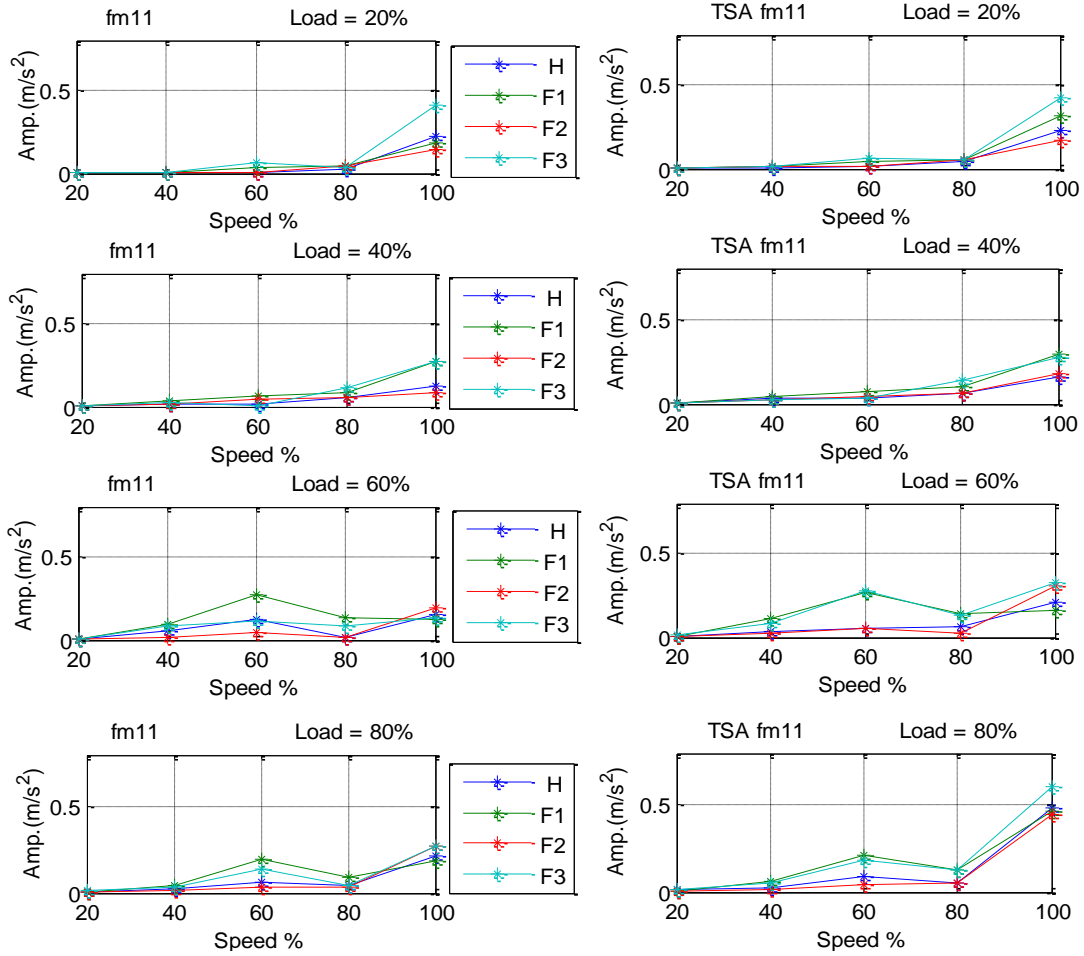


Figure 6.11-TSA mesh frequency (f_{m11}) amplitude of the gearbox casing for healthy and faulty gears and different operating conditions

6.4.3 Performance of Sideband Order based Diagnosis

In this section the spectral feature described in section 4.3.3 is compared with spectral features (average amplitude of the 33rd order \pm 35th order) extracted from the order spectrum.

Figure 6.12 shows conventional and order spectral features (left and right sides of the diagram respectively).

CHAPTER 6

EFFECTIVENESS OF TIME SYNCHRONOUS AVERAGING

As seen in conventional spectra (left), the spectral feature does not show any significant change between the gear statuses at all operating conditions. Whilst the order spectral feature (right) does not perform well under low operating conditions, it is effective in detecting local faults induced in the gear system under high speed and load conditions.

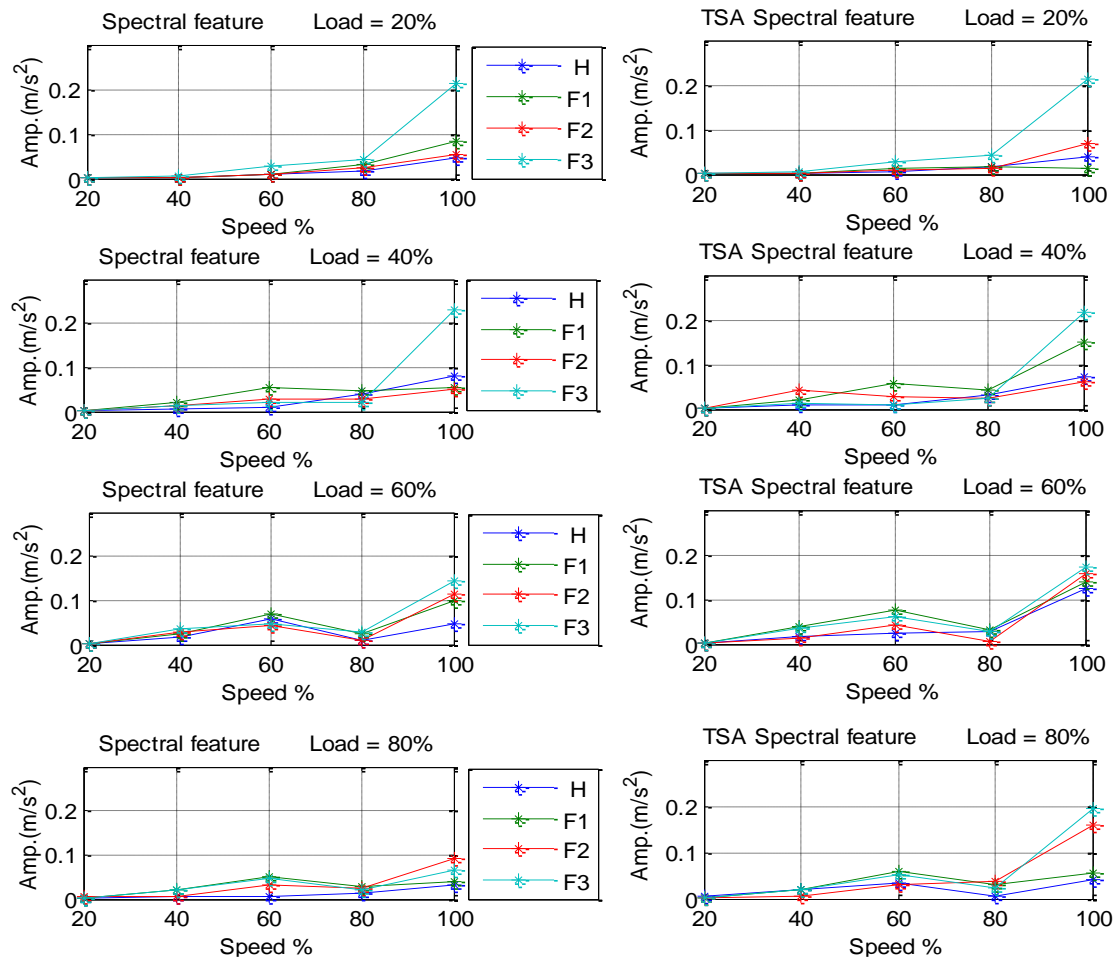


Figure 6.12-TSA Spectral feature of the gearbox casing for healthy and faulty gear at different operating conditions

From Figures 6.11 and 6.12, the amplitudes of the tooth meshing frequency and spectral features do not provide a trend consistent with the severity of the gear damage. Although the figures show some increase in amplitudes, it is hard to differentiate the severity of the underlying faults. More advanced signal processing such as frequency domain and joint order-frequency techniques could be applied for gear CM purposes.

6.5 Continuous Wavelet Transform Analysis of TSA Signals

In this section, the TSA signal is further processed using CWT analysis to find more accurate and reliable diagnosis methods. To highlight the effectiveness of this TSA-CWT combined approach, the CWT of TSA signal is compared directly with the conventional CWT results previously discussed in Chapter 4. The features obtained using this method are examined against vibration models and simulation results to identify the capabilities of the TSA-CWT combined method in detecting the presence and the severity of the above mentioned gear faults under different operating conditions.

Figures 6.13 and 6.14 present the results from both the TSA-CWT and raw signal CWT under low and high operating conditions. Both sets of data are calculated using the same FFT window and Morlet wavelet, which have been shown to be optimal in highlighting fault characteristics.

For more accurate visualization of the time (angle) and frequency characteristics, the results are presented as colour images. In each figure, the sub-images from top to bottom represent the Healthy, Fault 1, Fault 2 and Fault 3 cases in sequence. In addition, these images represent two revolutions of raw signals and show a frequency range up to the second mesh frequency for the first stage for ease of analysis.

The effects of the TSA-CWT combination on two distinctive CWT components were examined. *Firstly*, the fundamental and second tooth meshing frequencies, which show the pattern of vibration strength of the meshing process in both the time (angle) and frequency directions. A homogeneous amplitude vibration along the time direction indicates a healthy gear transmission. In contrast, *the second* CWT component is the oscillatory pattern in the time-frequency plane where the more oscillatory the pattern, the less smooth the gear transmission is or is indicative of a fault condition. In particular, if the pattern oscillates in the time direction following the period of a gear rotation, the fault can be identified as being associated with the rotating shaft. In addition, the height and the spread of the pattern can be used to quantify the severity of the fault. In general, the larger the pattern, the more severe the fault due to high vibration caused by high tooth impact due to a local fault.

CHAPTER 6
EFFECTIVENESS OF TIME SYNCHRONOUS AVERAGING

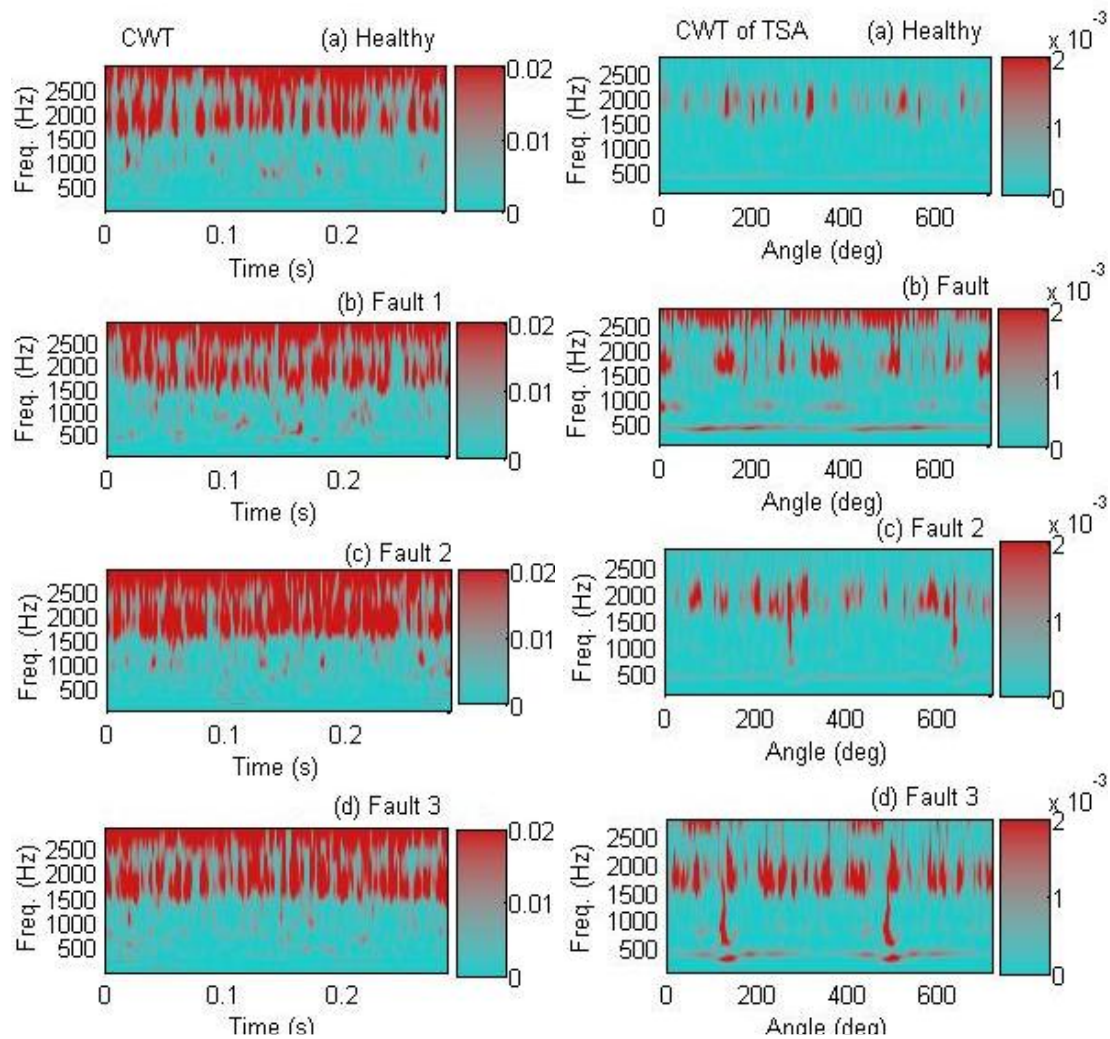


Figure 6.13- CWT (left) and CWT of TSA (right) of vibration measurements for healthy and faulty gear cases at low operating conditions

From both figures, a periodically oscillatory pattern can be clearly seen using a combination of TSA with CWT at low and high operating conditions. Moreover, the patterns localized in angular position and frequency response show the typical characteristics of the transient responses for faulty gears due to short time impacts of tooth breakage, showing that combined TSA-CWT enhances the fault features significantly. This is clearly seen at high operation conditions where the localized patterns appear at the same angular positions.

In addition, the CWT amplitudes for a healthy gear show a more homogeneous distribution in the time (angle) direction.

CHAPTER 6
EFFECTIVENESS OF TIME SYNCHRONOUS AVERAGING

In the frequency direction, vibration amplitudes are distributed mainly in the frequency range around 2 kHz, where an excessive energy for the vibration signal exists. However, Fault 2 shows more distinctive amplitudes around 3 kHz, showing a slightly different pattern from the other gear sets, indicating the diversity of the dynamic characteristics.

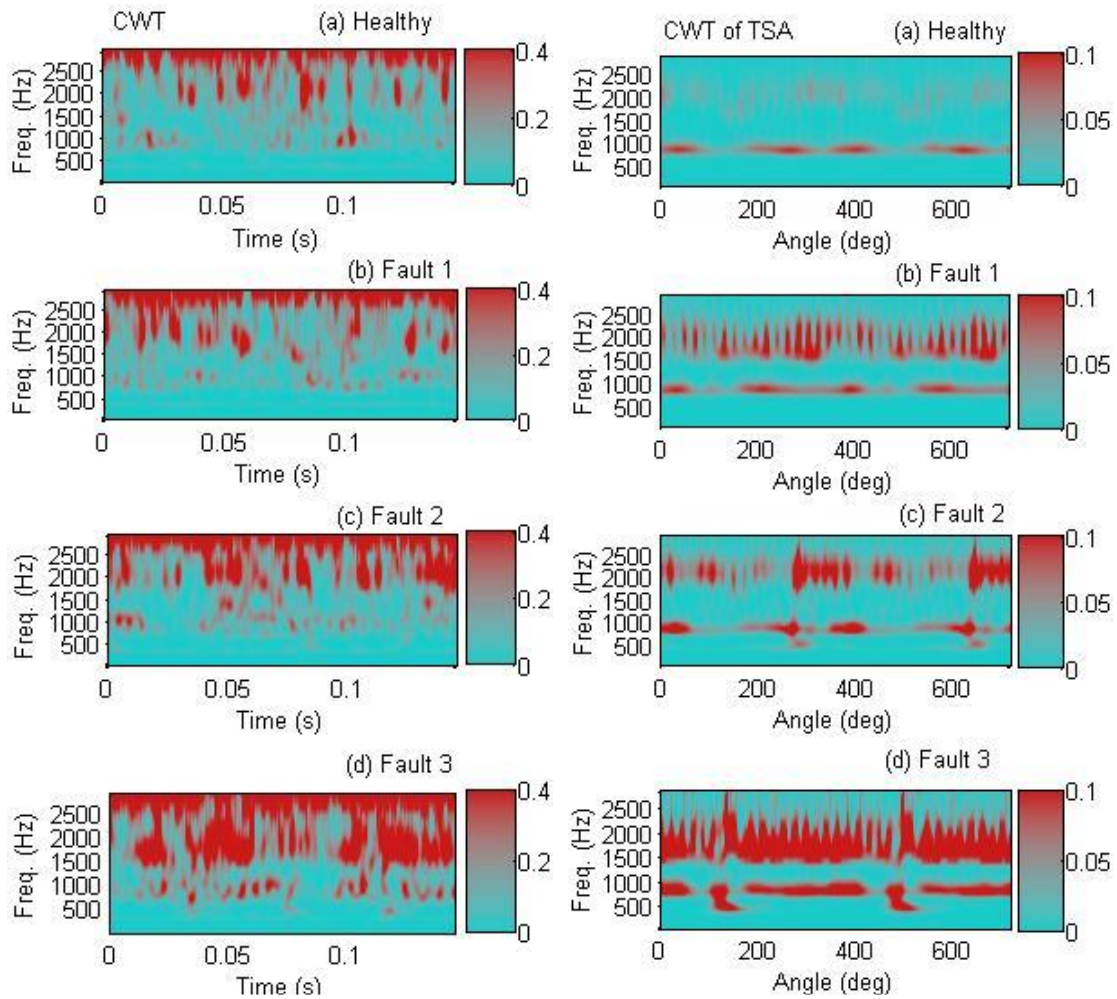


Figure 6.14 CWT (left) and CWT of TSA (right) of vibration measurements for healthy and faulty gear cases at high operating conditions

Vibration amplitudes at the meshing frequency ($\approx 428\text{Hz}$) can be seen to be more significant in the case of Fault 2 at low operating conditions whereas at high operating conditions, vibration amplitudes at $\approx 838\text{Hz}$ are more significant in the case of Fault3. This is consistent with the severity of the faults and proves that the low frequency components may be also useful for fault diagnosis.

CHAPTER 6

EFFECTIVENESS OF TIME SYNCHRONOUS AVERAGING

Under high speed and load operating conditions, TSA-CWT representation exhibits similar patterns to those of low speed and load operating conditions, showing that the result is less sensitive to speed variation.

It can be seen in Figure 6.14 that vibration amplitudes become much higher for both the homogeneous amplitudes at the meshing frequency of 838Hz and its higher order harmonics as do the localized peaks due to fault induced impacts. Faults 2 and 3 can be easily distinguished from the healthy case and Fault 1 by the distinctive localized peaks.

Although CWT patterns share the above general characteristics, it has been found that there are significant differences between gear cases. For example, the gearbox vibration in Figure 6.13 shows more homogeneous amplitudes for the Healthy, Fault 1 and Fault 3 cases than for Fault 2. Therefore it is difficult to develop an independent feature parameter to represent the fault severity advancement based on these results for all operating conditions.

These inconsistent results obtained from different gear sets demonstrate that manufacturing errors and diversities have a high influence on diagnostic accuracy. More advanced methods such as model based analysis may be required to avoid these influences and is an important issue to be investigated in the future.

The application of CWT to detect tooth breakage produced locally yields interesting results at different operating conditions. The increase in tooth breakage under both low and high operating conditions was expected to create significant changes in the gear vibration signals. At low gear operating conditions, conventional techniques could not be used to indicate fault severity precisely but the CWT analysis was able to distinguish between different fault severities even under low gear operating conditions.

For example, vibration amplitudes at the meshing frequency ($\approx 428\text{Hz}$) were seen to be more significant in the case of Fault 2 at low operating conditions. At high operating conditions vibration amplitudes at $\approx 838\text{Hz}$ were more significant in the case Fault 3. This is consistent with the severity of the faults. It shows that the low frequency components may also be useful for local fault diagnosis.

Based on the time-frequency patterns obtained by the wavelet analysis of the TSA signal, an effective feature has been found to detect a fault and indicate its severity. The experimental results show that this feature performs reliably when the vibration signal was measured locally (from the gearbox casing). However, it is still difficult to distinguish gear health conditions accurately when the signal to noise ratio of the vibration signal is low at very low operating conditions.

The results have proved that combining the CWT and TSA signals is very promising in the analysis of the vibration signal and the fault diagnosis of the gearbox.

6.6 Summary

In this chapter the conventional time domain waveforms under different operating conditions were compared with the angular waveforms obtained by TSA under the same operating conditions. The results confirmed that the TSA technique improved the signal to noise ratio (SNR) making local variations in the vibration signal much more visible.

In Section 6.3.2, a quantitative comparison between the two types of signals and different types of fault was conducted; the characteristics of signal strength over different operating conditions were examined using peak and RMS values. These results showed the peak value and RMS of the vibration signal provided a better detection performance because of the TSA's nonlinear effect detection and its capability for noise reduction.

In Section 6.3.3, kurtosis and crest factor (dimensionless parameters) were extracted to give more of an indication of the difference in the signal patterns. The results showed that the kurtosis and crest factor of the of the vibration signal with and without TSA do not exhibit a reliable trend with fault progression under all operating conditions.

TSA was applied to the vibration signal from the gearbox so that the order spectrum could be obtained in order to further characterise gearbox vibration in this new domain (Section 6.4). TSA results in Section 6.4.1 which shows that at special frequencies the faults of the gears can be more easily distinguished.

At some operating condition more consistent difference for the range of faults can be

CHAPTER 6

EFFECTIVENESS OF TIME SYNCHRONOUS AVERAGING

seen in order spectrums. This also confirms that the TSA technique removes the interference of rotation speed and additive random noise (Section 6.4.2).

The order of spectral features under different operating condition was extracted from the order spectrum of the TSA signal and compared with conventional spectral features in order to investigate the influences of TSA on the vibration signal (Section 6.4.3). The results showed that the spectral feature (the average amplitude of the $f_{m11} \pm f_{r11}$) of the conventional spectrum did not show any significant change between gear statuses under all operating conditions. While the order spectral feature (average amplitude of the 33th order \pm 35th order) does not perform well at low operating conditions, it is effective in detection of local faults induced in the gear system under high speed and load conditions.

In Section 6.5, the TSA signal was processed using CWT in order to find more accurate and reliable diagnosis results. The results of the CWT of the TSA signal were compared directly with the conventional CWT results discussed in Chapter 4.

Section 6.5 has shown that the conventional CWT and the CWT of the TSA results were both able to detect various faults at early stages, but the CWT of TSA signals was more sensitive with regards to the detection of early fault symptoms (Section 4.4).

The results proved that the method of combining CWT with the TSA signal is very promising in the analysis of the vibration signal and the fault diagnosis of gearboxes. This means it can therefore be applied in order to detect and diagnose gear fault remotely (Section 8.4).

CHAPTER 7

FREQUENCY RESPONSE FUNCTION (FRF) MEASUREMENTS

In this chapter, the frequency response function (FRF) is used to study the dynamic characteristics of the experimental test rig. The FRFs of the system were determined using specialised frequency analysis equipment with an electromagnetic shaker. FRFs are used to study the transmission path effect on the vibration signal generated in the gear transmission system. There are however, problems relating to the identification of the dynamic properties of the gearbox components.

7.1 Introduction

The transmission path consists of the structures which provide a mechanical path from the vibration source (the meshing gears) to the measurement point (the transducer). Typically, it will contain both the static structure of the gear transmission system casing and the rotating elements between the vibration source and the transducer including the shaft, bearings, and gears. The transmission path acts as a filter between the vibration source and the measurement point and changes both the amplitude and the phase of the vibration signal, depending on its frequency.

Vibration signals at a frequency which correspond to the resonance of one or more elements within the transmission path may be amplified, whereas vibration at a frequency corresponding to a node will be attenuated. In addition impulses, due to their wide frequency content, will invariably excite one or more of the resonant nodes in the transmission path. These will normally decay exponentially due to mechanical damping in the system. Changes in the transmission path can be caused by several factors, the most obvious being the changing of the transducer's location in relation to the vibration signal source. It is essential to consider these effects when modelling the vibration of the relevant components. Other factors which may change the transmission path include variations due to the motion of rolling elements in a bearing and non-periodic variation due to structural damage in the gearbox casing. These, however, are not considered in this work.

By using signal processing analysis techniques, measurements performed on the operating gearbox can be used to analyze potential faults [68]. The frequency spectra measured are actually a combination of the unknown excitation force (caused by distributed faults such as the wear of gear teeth etc.) and the structural response of the gearbox casing. Information about the characteristics of the structure itself is generally ignored even though, as shown in this chapter, the vibration signal can be significantly affected by the transmission path effects.

The approach considered here takes into account the structure of the gearbox. By using an FFT analyzer to measure the ratio of the response at different positions on the gearbox casing with a given measured input force, the frequency response

function (FRF) can be calculated. From a set of FRF measurements made at defined points on the structure (the gearbox casing) we may begin to see how the excitation force caused by gear faults is modified by the transmission path.

7.2 Frequency Response Function (FRF) Overview

The Frequency Response Function is a fundamental measurement that isolates the inherent dynamic properties of a mechanical structure [134].

Several experimental modal parameters such as natural frequencies, mode shapes and associated damping ratios can be extracted from a set of FRF measurements.

The FRF describes the input-output relationship between two points on a structure as a function of frequency.

An FRF is a measure of how much acceleration response a structure has at an output Degree Of Freedom (DOF), per unit of excitation force at an input DOF. As can be seen in Figure 6.1 the FRF can be defined as the ratio of the Fourier transform (FT) of an output response $X(\omega)$ divided by the Fourier transform of the input force $F(\omega)$. In the input/output measurements, the gearbox casing is excited at only one point, the shaft, and the response is measured at different points using transducers distributed at different positions on the gearbox casing. These measurements are usually performed using a specialist multi-channel digital analyzer. By moving the response point while the excitation point remains fixed an entire row or column of the n-DOF system FRF matrix can be measured.

The relationship between the input (force excitation) and output (vibration response) of a linear system is shown in Figure 6.1 and given by:

$$Y_i = \sum_j H_{ij} X_j \quad (7.1)$$

where Y_i is the output spectrum at DOF i , X_j is the input spectrum at DOF j , and H_{ij} is the FRF between DOF j and i . The output is the sum of the individual outputs caused by each of the inputs. Equation 6.1 gives the output at any DOF i , with the input at DOF j , as:

$$Y_i = \sum_j H_{ij} X_j \quad \text{or} \quad H_{ij} = Y_i / X_j \quad (7.2)$$

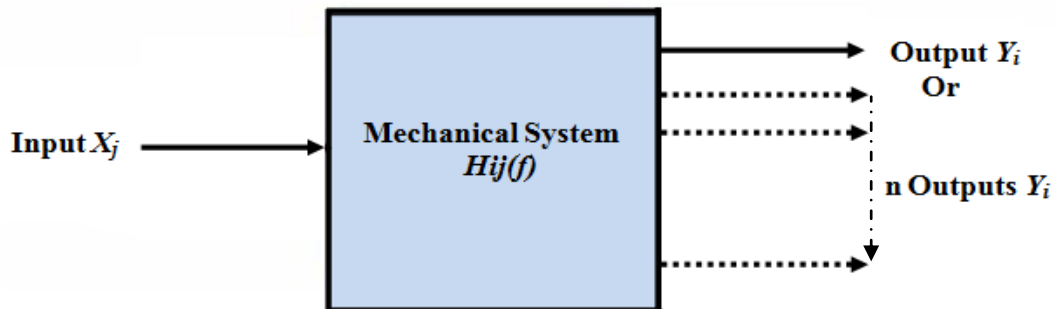


Figure 7.1-Single input multiple output system analysis

In order to explore the effect of transmission paths on vibration signals due to path attenuation and interference noise, an investigation was carried out on the gear test rig. The FRF measurement system is shown in Figure 7.2 and the schematic diagram in Figure 7.3.

Figure 7.2 consists of the structure (the gearbox) to be tested, a force impulse shaker and five acceleration sensors located in different locations fixed to the gearbox casing.

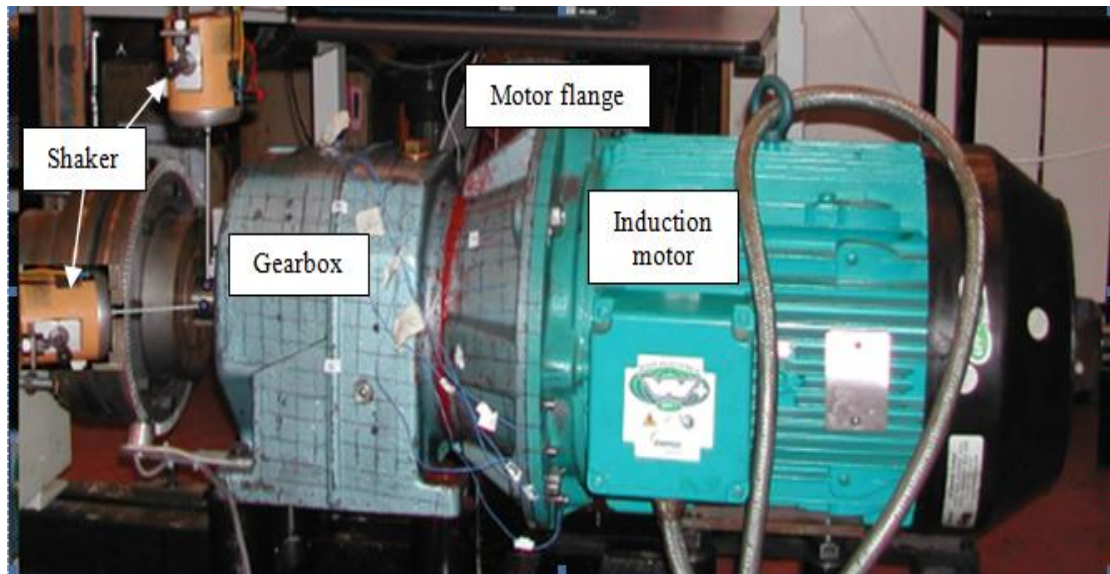


Figure 7.2-Test rig and shaker position

7.3 Frequency Response Function (FRF) Measurement

7.3.1 Shaker Test Setup

The equipment used for the shaker test is shown in the schematic diagram, Figure 7.3. An LDSTM shaker (type 201) is used to excite the structure (the gearbox casing) to which the shaker is attached by a suitable thin metal rod (the stinger). This enables the shaker to impart force on the structure along the axis of the stinger, the axis of the

CHAPTER 7
FREQUENCY RESPONSE FUNCTION (FRF) MEASUREMENTS

force measurement. The FRFs were measured with the shaker in both horizontal and vertical positions (see Fig 7.2).

This transducer was connected between the shaker and the stinger to measure the input force. The shaker was suspended using a rigid supporting fixture and the suspension frequency was assumed to be much lower than that of the fundamental frequency of the gearbox casing and so was neglected.

Due to the limitation of the equipment, five (IC) type accelerometers (S_1 , S_2 , S_3 , S_4 and S_5) were attached at different locations on the gearbox casing using a thin film of adhesive. This enabled five FRFs to be obtained simultaneously. By moving the accelerometers around the gearbox casing it was possible to determine the FRFs at over 200 different nodes.

Signals from the force transducer and the accelerometers were fed into to an LMSTM Scadas multichannel signal processing unit, from which an output signal was used to drive the shaker through a power amplifier.

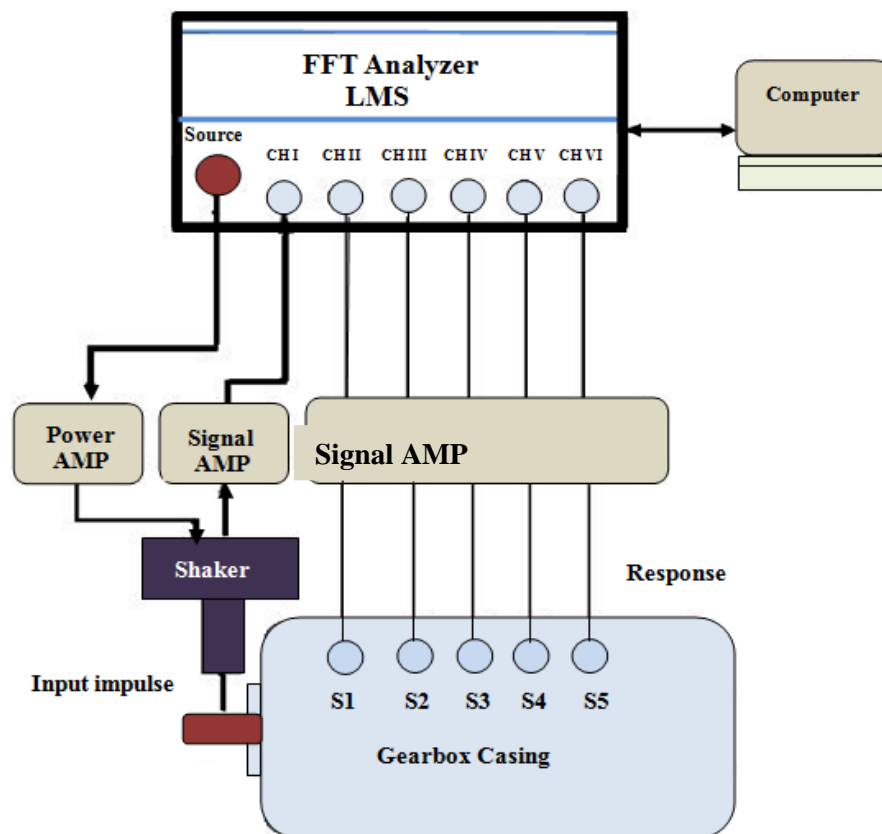


Figure 7.3 - A schematic diagram of the shaker test setup

CHAPTER 7

FREQUENCY RESPONSE FUNCTION (FRF) MEASUREMENTS

A random signal input to the shaker, band-limited to a frequency range of 2.5 kHz (easily covering the frequency range of interest for a gearbox) was used and in order to minimise the leakage effect, a Hanning window was also used.

The frequency ranges used in the tests were different, reflecting the range of resonant frequencies and mode shapes that were important for each specific element. For this study, a frequency range of 0 to 2.5 kHz was sufficient to include the first and second stage meshing frequencies and several harmonics. The FRFs were obtained by exciting the gearbox with an impact shaker.

The signal processor was connected to a PC running suitable data acquisition and FRF analysis software. This enabled averages to be taken which could virtually eliminate random (non-coherent) noise and effectively cancel out nonlinear distortion.

The excitation signal of the shaker and the response signal of the test sensor location were acquired in the time domain using the multi-channel analyzer and the averages taken at five inputs. The Fast Fourier Transform (FFT) provides the corresponding power spectral densities. By dividing the power spectrum response by the power spectrum excitation, the Frequency Response Function (FRF) can be found.

Two frequencies, the first stage meshing frequency (= 802.5Hz) and the second stage meshing frequency (= 325Hz) were selected to study the effect of the transmission path on the vibration signal. The FRF amplitudes at these frequencies from different locations on the gearbox casing and motor casing are shown in Figures 7.4 and 7.5.

7.4 Result and Discussion

7.4.1 Characteristics of the FRFs

The most direct way to evaluate the effect of the transmission path on the vibration signal is to compare the FRF measured at different locations on the test rig using the shaker test. The meshing frequencies can be extracted from a set of FRF measurements between one reference position (on the shaft) and a number of measurement positions taken from the model.

CHAPTER 7
FREQUENCY RESPONSE FUNCTION (FRF) MEASUREMENTS

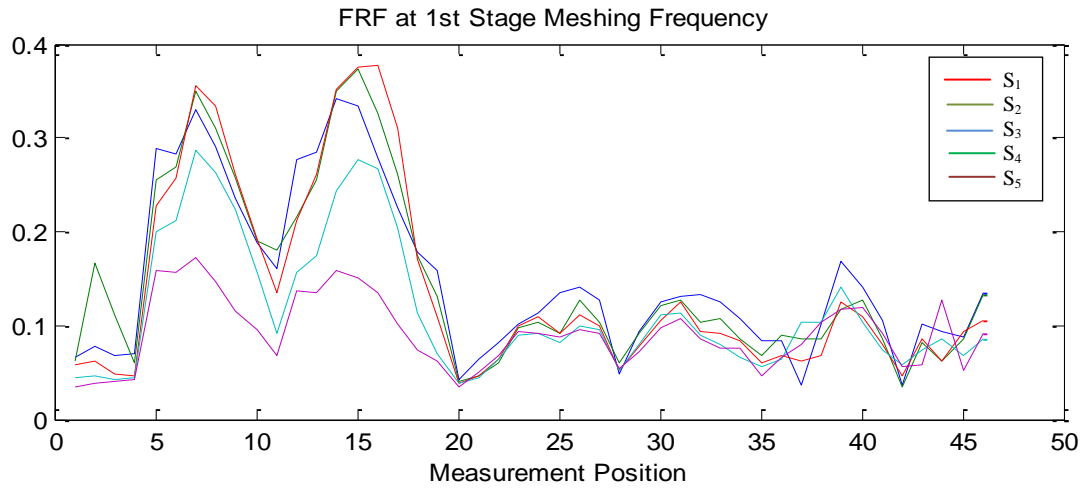


Figure 7.4-FRF amplitudes at 802.5 Hz

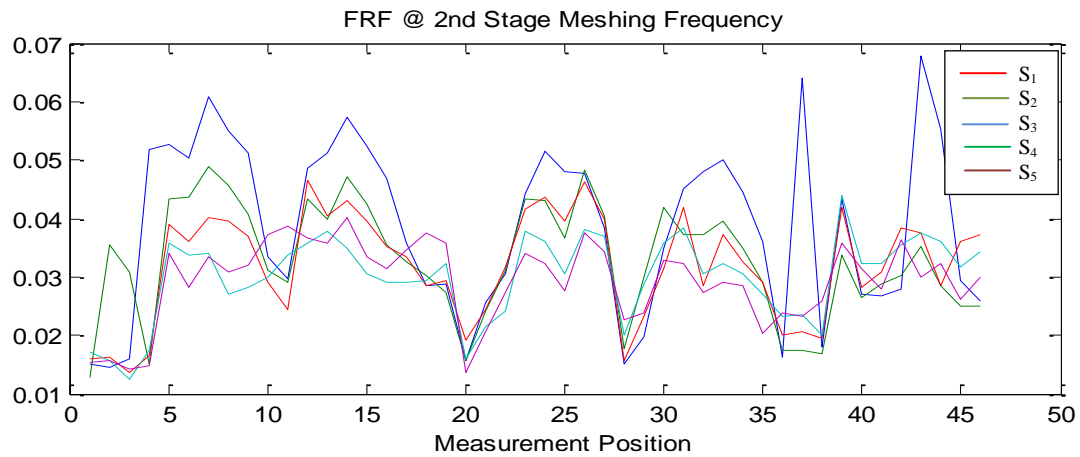


Figure 7.5-FRF amplitudes at 325 Hz

These figures show how the FRF, and hence the vibration signal, changes with the path transmission on the gearbox casing and the motor flange. The sensors at node number 16 give the highest frequency response for both meshing frequencies, whilst node position 20 gives the lowest frequency response.

Figures 7.6 and 7.7 show the location of the sensors on the gearbox casing (represented by grey nodes) and the motor flange (represented by pink nodes). The size of the nodes provides information as to how the FRF amplitude at 802.5 Hz and 325 Hz changes with the location of the sensor as a result of the transmission path effect.

CHAPTER 7

FREQUENCY RESPONSE FUNCTION (FRF) MEASUREMENTS

The enlarged nodes were chosen to record the FRF amplitudes on the gearbox casing and the motor flange shown below in figure 7.8 as well as recording the signals from the fault detection on both the gearbox casing and the motor flange discussed in the next section.

In both spectra, there are several peaks at the frequency bands 500Hz-1500Hz and 1900Hz-2200Hz. These peaks may occur as a result of several test rig component resonances. There are clear differences between the FRFs the attenuation or amplification of the vibration signals is a result of the transmission path effect, i.e. the amplitudes of the FRF at the motor flange are generally lower than those on the gearbox casing. Furthermore, the FRF for the motor flange is relatively flat over the entire frequency range when compared to the FRF for the casing.

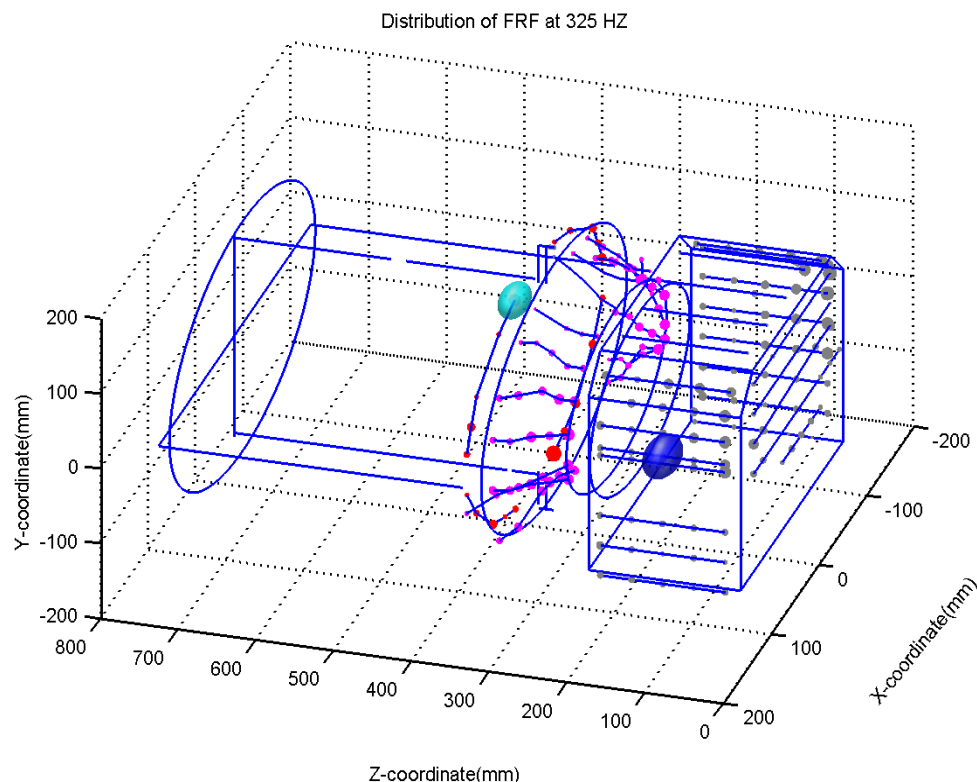


Figure 7.6-Typical distribution of FRF amplitudes at a low frequency range

CHAPTER 7

FREQUENCY RESPONSE FUNCTION (FRF) MEASUREMENTS

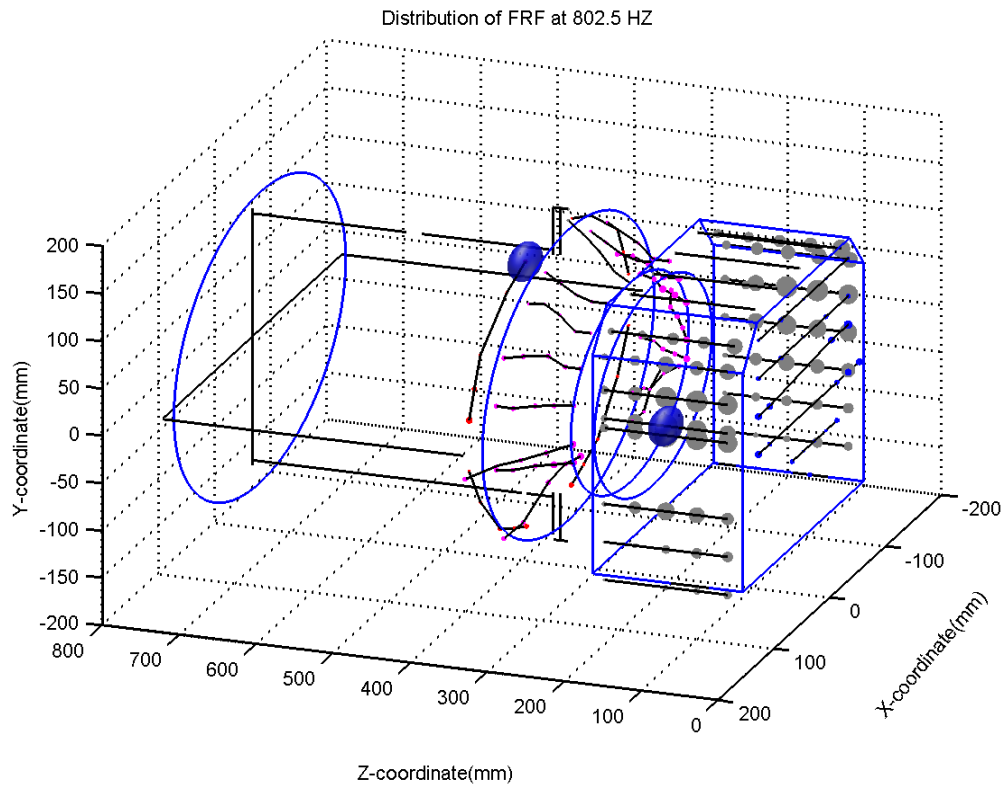


Figure 7.7-Typical distribution of FRF amplitudes at a high frequency range

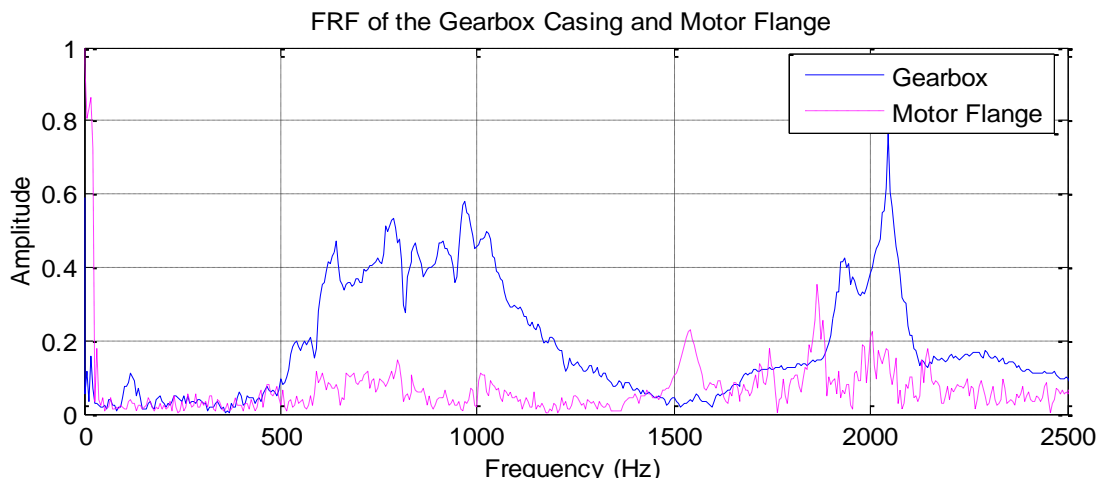


Figure 7.8-Comparison of the FRF measured from the gearbox casing and motor flange

7.4.2 Performance of Gear Fault Detection

The frequency spectra measured at the same nodes on the gearbox casing and motor flange for 50% motor speed and 80% load are shown in Figure 7.9, and for 100% motor speed and 80% load in Figure 8.10.

CHAPTER 7

FREQUENCY RESPONSE FUNCTION (FRF) MEASUREMENTS

In both cases the spectra are given for a “healthy” gearbox as well as for a gearbox with faults. As mentioned above, the peak at 325Hz corresponds to the second stage meshing frequency and the peak at 802.5Hz corresponds to the first stage meshing frequency. It can be seen that the higher amplitude for signals from sensors mounted on the gearbox casing compared to the motor flange -- especially in the range 1900Hz to 2200Hz but also in the lower range 500Hz-1500Hz -- is consistent with the FRF measurements taken at the same points.

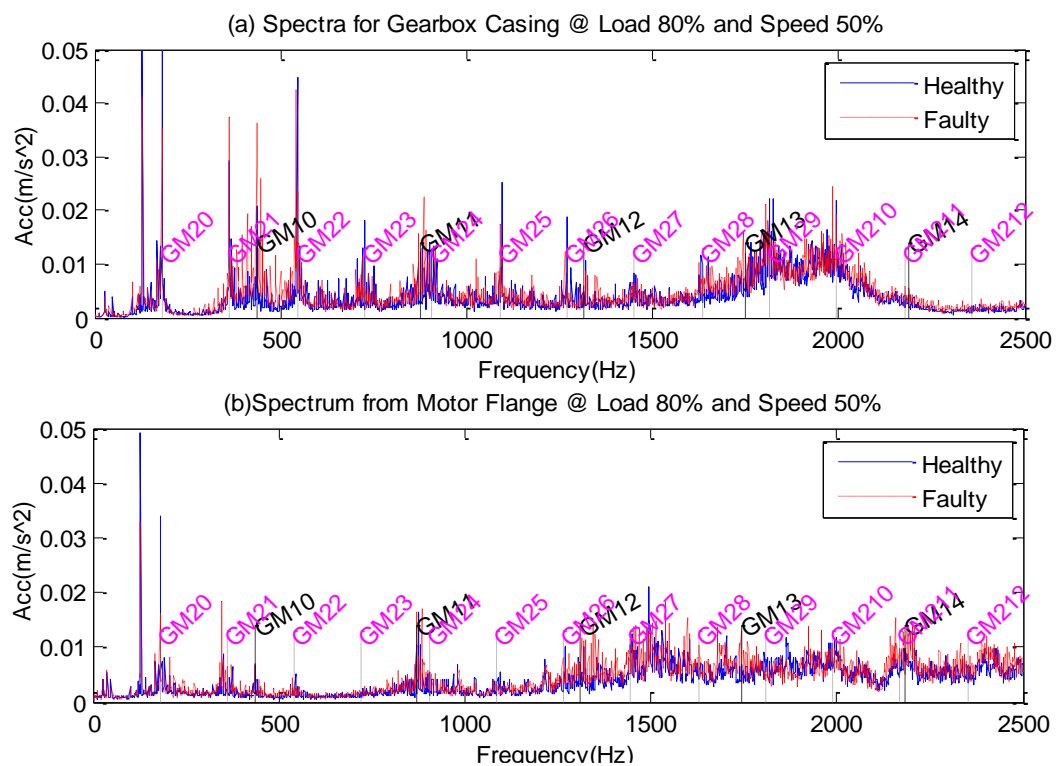


Figure 7.9 –Frequency spectra at 50% speed obtained (a) from the signal obtained from the gearbox casing and (b) obtained from the motor flange.

Whilst it would seem that more accurate FRF measurements are needed to give a closer correspondence, theoretically the ratio between the complex frequency spectra of the two signals should be the same as the ratio of the complex FRFs. The results obtained so far indicate the influence of the transmission path on the signals used to monitor faulty gears.

CHAPTER 7

FREQUENCY RESPONSE FUNCTION (FRF) MEASUREMENTS

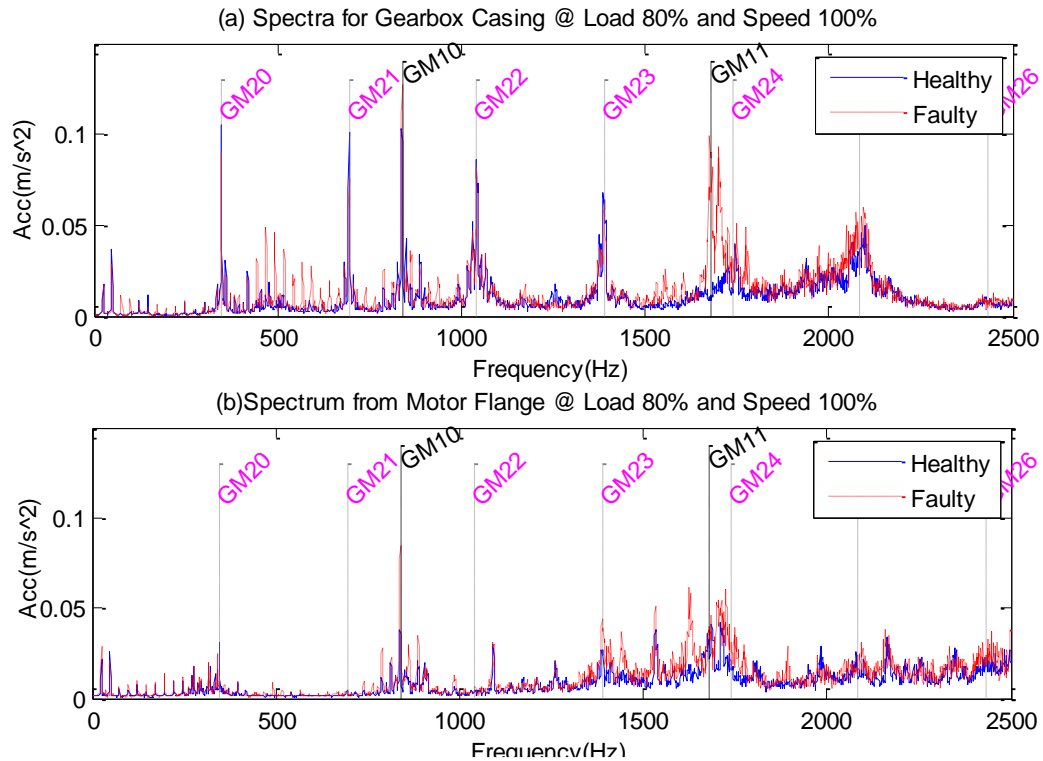


Figure 7.10 –Frequency spectra at 100% speed obtained (a) from the signal obtained from the gearbox casing and (b) obtained from the motor flange.

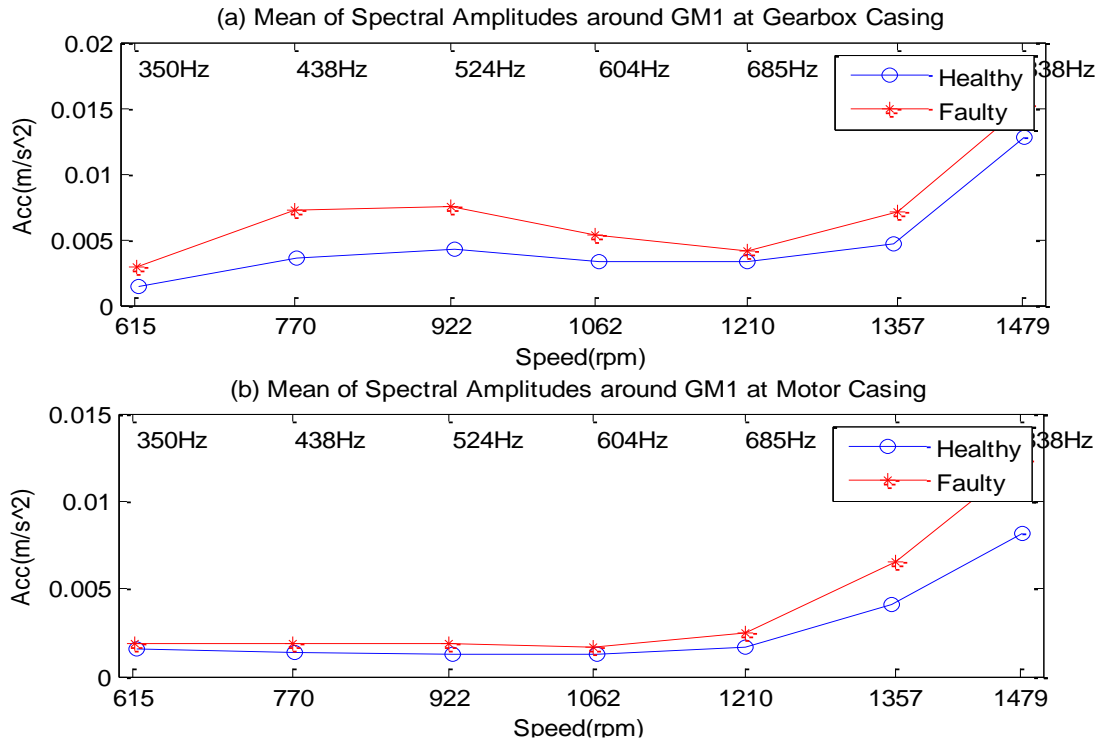


Figure 7.11-Comparison of the vibration amplitudes around meshing frequency.

CHAPTER 7

FREQUENCY RESPONSE FUNCTION (FRF) MEASUREMENTS

In addition, in the frequency range from 500Hz to 600Hz, there are distinctively high amplitudes from the gearbox casing for the faulty condition, showing efficient performance in separating the healthy and faulty conditions. The effects of amplification by the transmission path in this range can be seen clearly.

Figure 7.11 shows the results obtained by averaging the spectral amplitudes in a frequency band of three times the rotating frequency around the meshing frequency. The trend over speed, or frequency for the gearbox casing, shows a minimum of approximately 685 Hz. Once more this shows the effects of the transmission path. In contrast, the trend for the motor flange increases steadily. This trend is not unexpected as the excitation sources usually have an increasing profile as the speed increases and is not distorted by the transmission path. It may, therefore, be claimed that the latter trend can give better results in the discrimination of fault severity.

7.5 Summary

As shown in Section 7.4, the most direct way to evaluate the effect of the transmission path on the vibration signal is to compare the FRF measured at different locations on the test rig using the shaker test.

In Section 7.4.1, the measured FRFs from the input signal of a shaker on the gearbox shaft to the outputs from sensors mounted over the gearbox housing and motor flange provides some understanding of how the position chosen for mounting an accelerometer affects the outcome for the condition monitoring of a gearbox. Although the FRFs measured in this way can only give an approximate analysis of the transmission path effects in practice – given that the vibration source is not just the vibrations of one end of the shaft – the results obtained were consistent with the differences between the vibration signals obtained from condition monitoring bearings with known faults. Furthermore, it was found that higher FRF amplitudes help in improving detection sensitivity but may also result in inappropriate severity classification.

CHAPTER 8

PERFORMANCE EVALUATION OF REMOTELY MEASURED VIBRATION

In this chapter, vibration data recorded from two accelerometers located on the gearbox casing and the motor flange was analyzed using different signal processing methods to investigate the effect of path transmission (transducer location) on the detection and diagnosis of the seeded gear tooth faults. Results from the angular domain, the order spectrum and the order-frequency analysis are presented to show that these techniques may be used for fault detection in gearboxes and that the effect of the path transmissions can be observed on the vibration signals.

8.1 Introduction

As the gearbox and motor are in a compact construction, with the shaft and housing connected, some of the impacts and vibration responses will also transfer to the motor housing. It is possible, therefore, to detect the impacts from the remote accelerometer located on the motor flange. As discussed in Chapter 6, the TSA reduces the noise and cancel out the vibration components which are not synchronised with the rotation of the gear of interest. This improves the signal to noise ratio (SNR) of the vibration signal for accurate diagnostic feature calculation.

In this chapter, the TSA vibration signals recorded from the two accelerometers located on the gearbox casing and motor flange were analyzed by applying various signal processing methods to the TSA signals to investigate the effect of path transmission (transducer location) on the detection and diagnosis of the seeded gear tooth faults under different operating conditions.

8.2 TSA Signal in the Angular Domain

8.2.1 Waveform Characteristics

Angular waveforms (time synchronous averaged for one revolution) of vibration signals from accelerometers located on the gearbox casing (local) and motor flange (remote) for a healthy gear and three faulty cases (Fault 1, Fault 2 and Fault 3), at different operating conditions are shown in Figures. 8.1. Signals from both sensors show only slight differences in the waveforms for the different gear statuses at different operating conditions. The sensor amplitudes of the signals at the motor flange are lower than those on the gearbox casing sensor due to the attenuation of the transmission paths on the vibration signal.

The periodic feature can only be observed under high load and high speed operating conditions as is illustrated by the data shown third and fourth rows of Figure 8.1. The transient responses can be clearly seen in the case of Fault 2 from both local and remotely measured vibrations.

There are clear differences between the waveforms of the different gear conditions. In both figures, the pattern of the angular waveforms changes with the severity of the fault.

CHAPTER 8

PERFORMANCE EVALUATION OF REMOTELY MEASURED VIBRATION

For identical faults, different patterns can be seen, especially in the case of Fault 3. This illustrates that when the gear vibrations are measured remotely, more interference of the signal is observed through the path transmission and other interference noise sources, such as the supporting bearings and the instruments used to drive the motor.

However, comparison of the vibration signals in Figure 8.1 confirms that there is a significant amount of unknown information regarding the waveform of the signals.

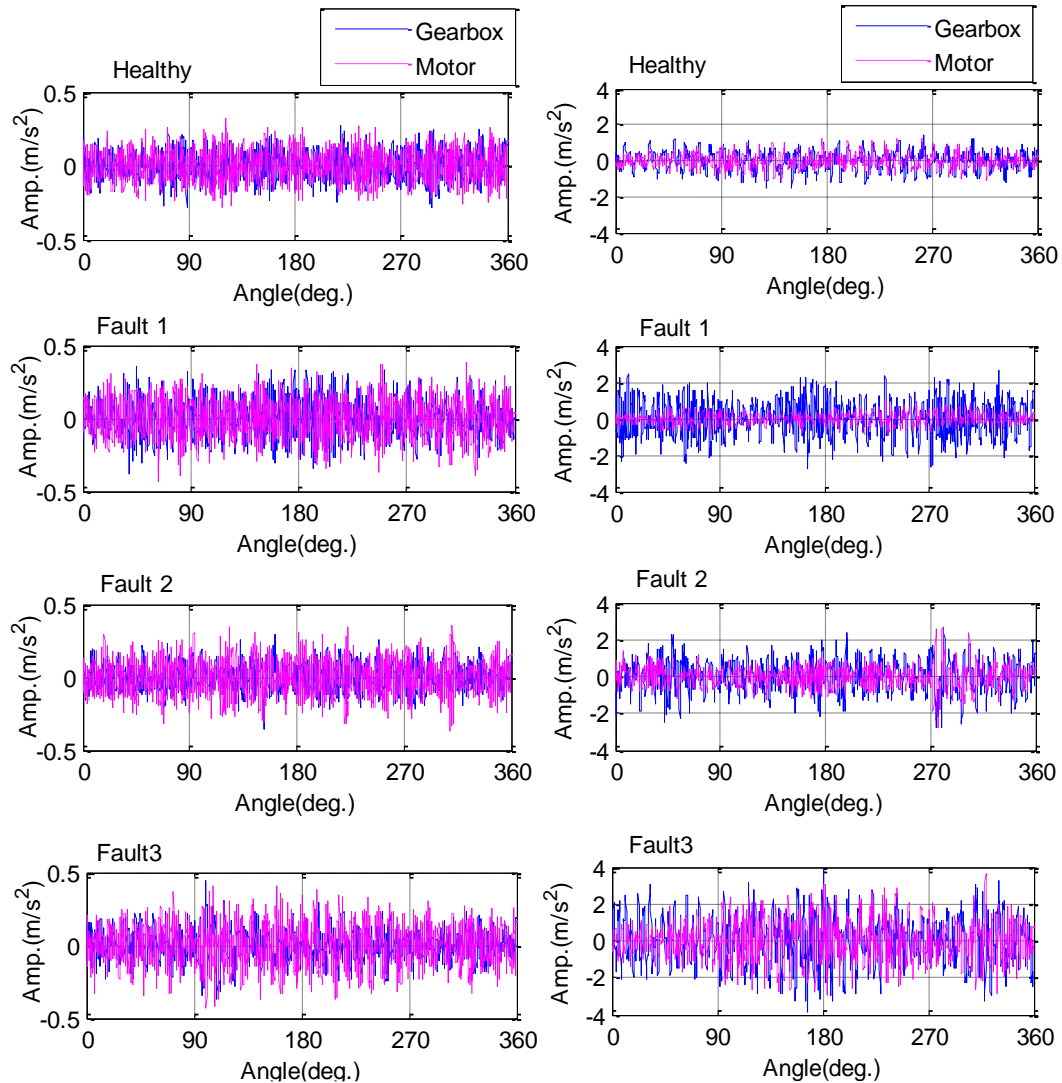


Figure 8.1 –Angular vibration waveform for healthy and faulty gear systems under low (L=40%, S=50%) (left) and high (L=80%, S=100%) (right) operating conditions

All the waveforms from both locations show a degree of distortion and no obvious fault symptoms were observed even under severe fault conditions. The presence of a

transmission path may not significantly alter the overall vibration level but may cause a statistically significant change in the shape of the signal.

To identify and better understand the effects of path transmission on the signal from the healthy and faulty gears, four statistical parameters: peak values, RMS values, Kurtosis, and Crest factor were calculated for the waveforms under different operating conditions.

8.2.2 Signal Strength based Diagnosis using Peak and RMS Values of TSA Signals

Figures 8.2 and 8.3 shows the average values of signal peak and RMS values of the local and remote TSA vibration signals for healthy and faulty gears under different operating conditions. Comparison of signals from the two different transducer positions, showed some following similarities, namely that the values from the motor flange increase with load, which are the same as that of the gearbox casing. It shows that the measured vibration is well correlated to vibration and hence can be used as a basis for fault diagnosis.

The values from the motor flange also show similar trends with speed to the values from the gearbox, confirming that it is also likely to produce good diagnosis results.

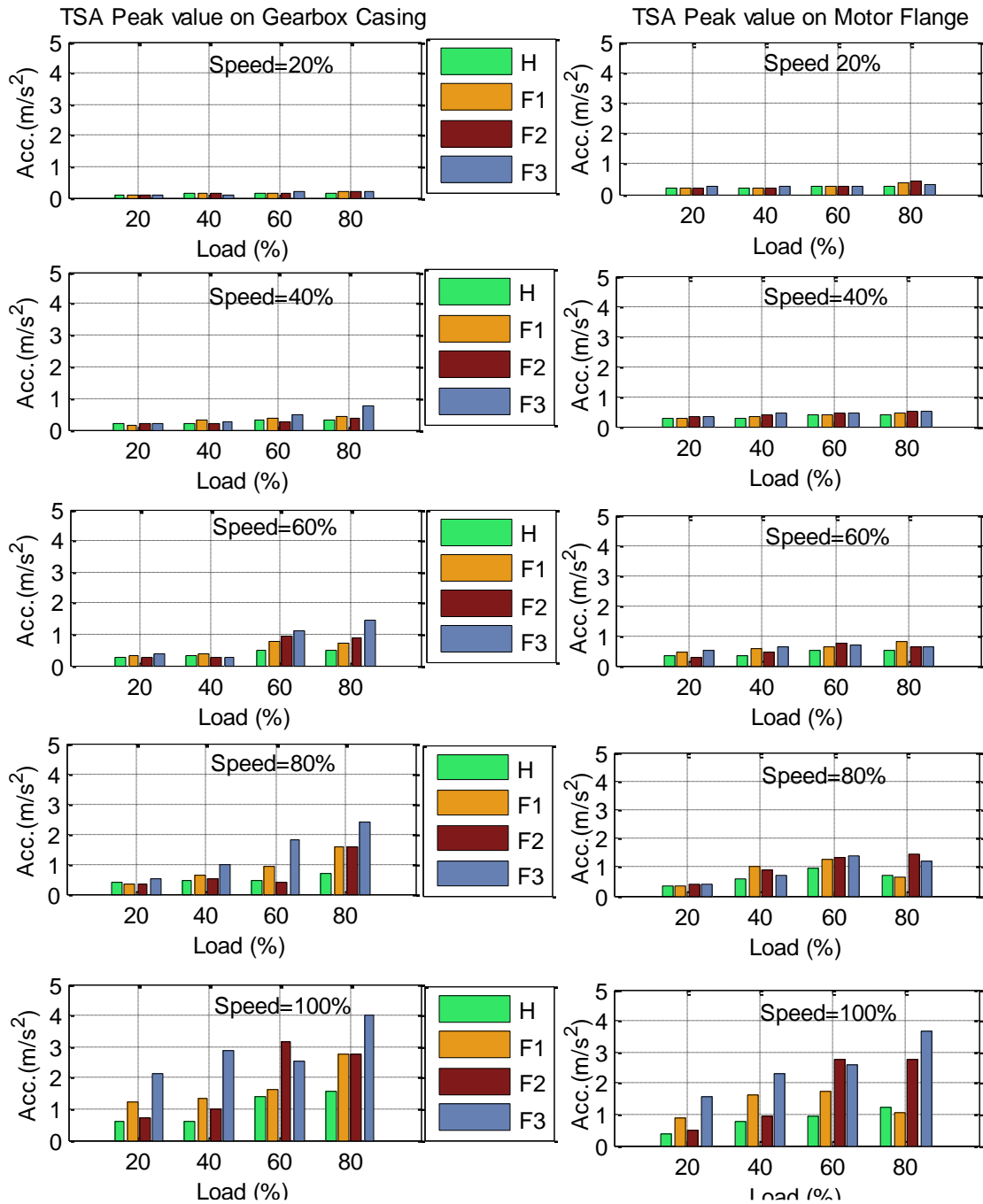
There are, however, the following significant differences:

1. The values are significantly lower, showing the high effect of path attenuation. This degrades detection sensitivity. In particular, the fault case F3 could not be separated from case F2. In general, the faulty case could be separated from healthy case.
2. The variation trend over load and speed has clear inconsistency under a number of operating conditions, showing considerable distortion of the path. Especially at the speed of 60% and 80% case F2 and case F3 cannot be quantified correctly because the amplitude is not proportional to that from the gearbox casing.

In general, the detection and diagnosis results are similar to those of the gearbox and it can be used for remote monitoring.

CHAPTER 8

PERFORMANCE EVALUATION OF REMOTELY MEASURED VIBRATION



The results in Figures 8.2 and 8.3 show that both parameters are affected by the gear operation conditions; this confirms that operation condition of the gears may alter the vibration signal highly affecting the overall peak value and RMS.

CHAPTER 8

PERFORMANCE EVALUATION OF REMOTELY MEASURED VIBRATION

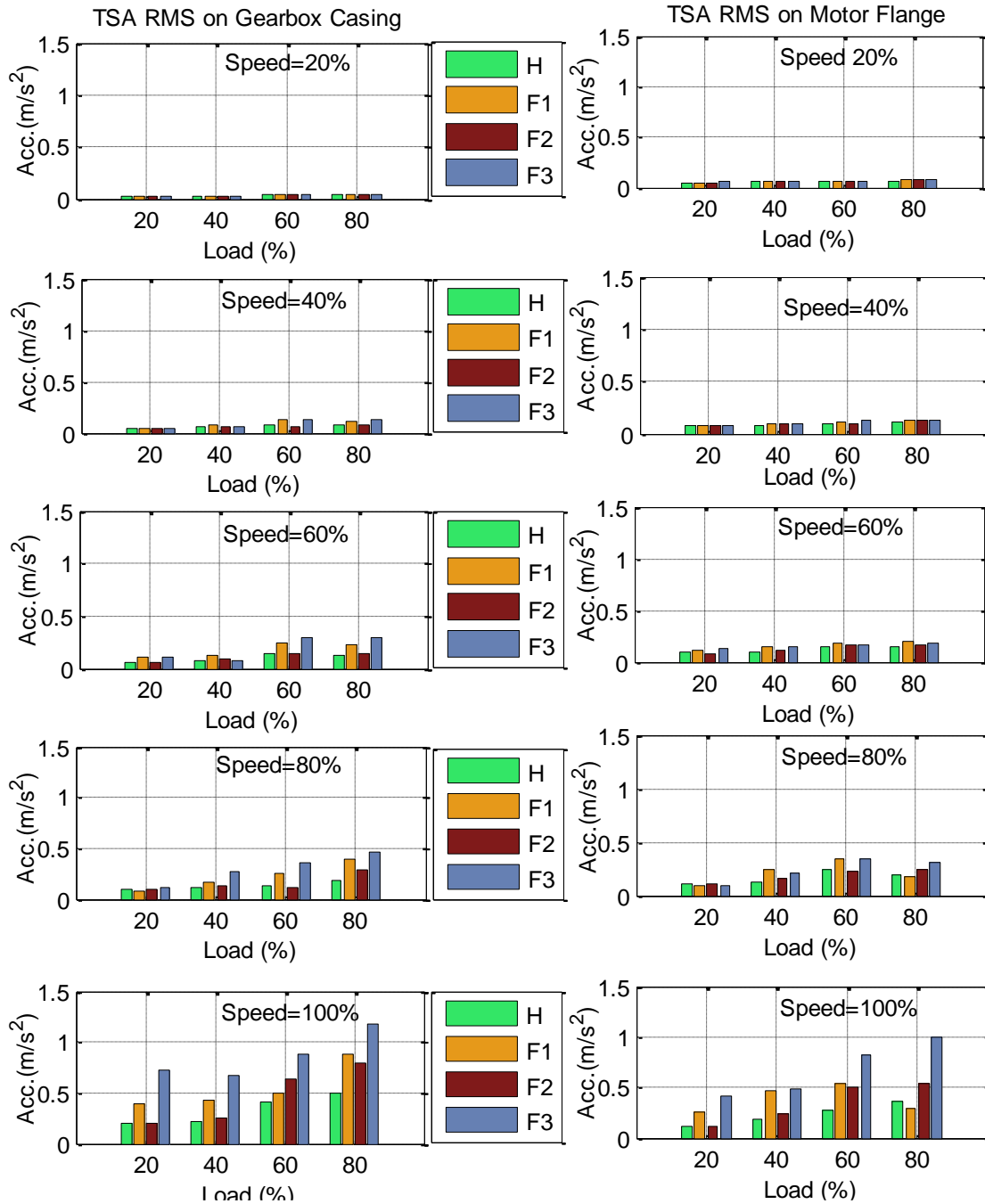


Figure 8.3 Average values of RMS of TSA vibration signal for healthy and faulty gears

8.2.3 Signal Structure based Diagnosis using Kurtosis and Crest Factor of TSA Signals

As discussed in section 8.2.2, vibration amplitudes vary significantly with load and speed. In order to develop a monitoring feature which is less independent of operating

CHAPTER 8

PERFORMANCE EVALUATION OF REMOTELY MEASURED VIBRATION

conditions, two common parameters, kurtosis and crest factor, are explored in this section.

Figures 8.4 and 8.5 show the average values of kurtosis and crest factor for the local and remote TSA vibration signals of healthy and faulty gears under different operating conditions. Comparing the values between two different transducer positions, the following similarities can be observed:

1. Under different loads

The values from motor flange show clear inconsistency under all operating conditions, similar to those of the gearbox casing. This shows that the measured vibration is not correlated to vibration used for fault diagnosis.

2. Under different speeds

The values from the motor flange show a dissimilar trend those from the gearbox, confirming that it is unlikely to produce good diagnosis results.

However, we can see the following significant differences of comparing the values between two different transducer positions:

The variation trend over load and speed has clear inconsistency under all operating conditions, potentially showing considerable distortion of the transmission path.

In general, the detection and diagnosis results are not similar to that from the gearbox and it cannot be used for remote monitoring.

It can be concluded that at both sensor locations kurtosis and crest factor are not sensitive enough to detect fault conditions at all operating conditions and are not sensitive enough to identify this particular type of fault.

CHAPTER 8

PERFORMANCE EVALUATION OF REMOTELY MEASURED VIBRATION

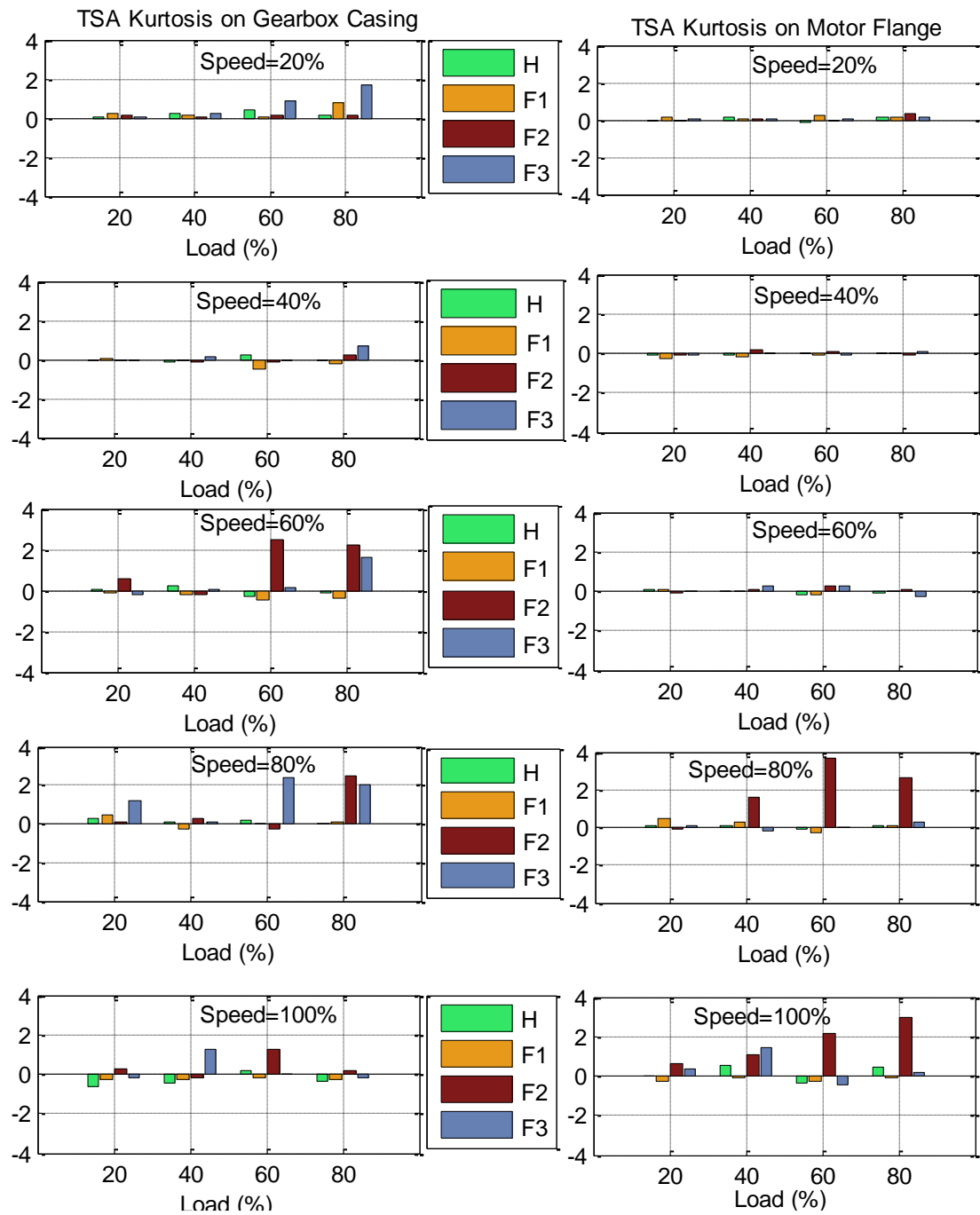


Figure 8.4 Average values of kurtosis of the TSA vibration signal for healthy and faulty gears

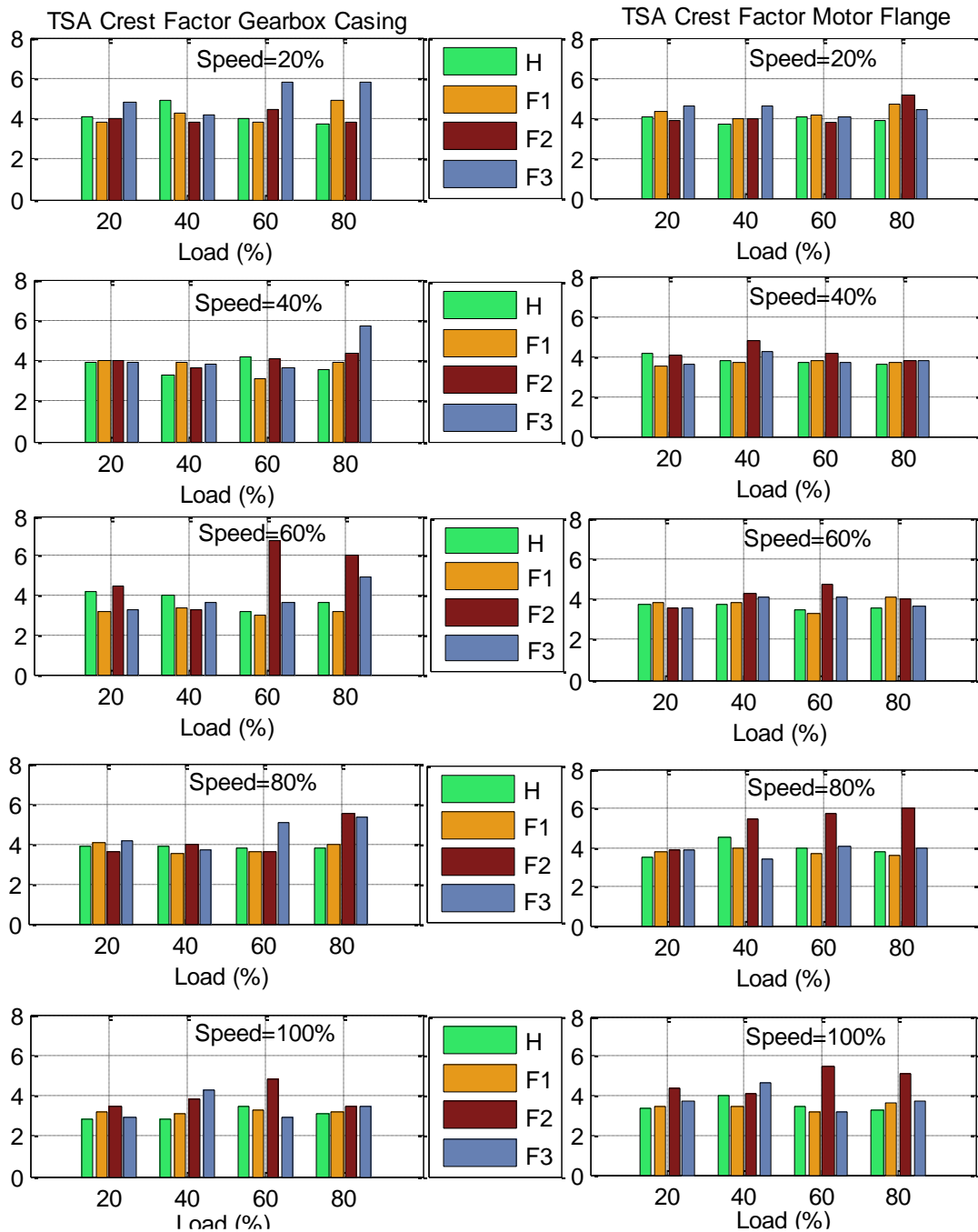


Figure 8.5 Average values of crest factor of the TSA vibration signal for healthy and faulty gears

8.3 Order Spectrum of TSA Signal

8.3.1 Characteristics of Order Spectrum

The order spectrums of the healthy and faulty gears under low and high operation conditions recorded locally and remotely are shown in Figures. 8.6 and 8.7. These

CHAPTER 8

PERFORMANCE EVALUATION OF REMOTELY MEASURED VIBRATION

figures depict the peak values corresponding to the first stage meshing frequency (34^{th} order) and sidebands at the 31^{th} , 32^{th} , 33^{th} , 35^{th} , 36^{th} and 37^{th} order for the two locations and under different operation conditions.

From Figures 8.6 and 8.7 it can be seen there are clear discrete components showing the amplitude peak value corresponding to the 34^{th} order and this peak is consistently the largest value of the spectrum.

As seen in Figures 8.6 and 8.7, due to local fault, the amplitudes of the order component peaks in all three fault plots have changed compared to the healthy condition. This is to be expected because the stiffness between the teeth changes and consequently causes changes in the vibration amplitude. This is especially the case for the 34^{th} order, which corresponds to the fundamental meshing frequency.

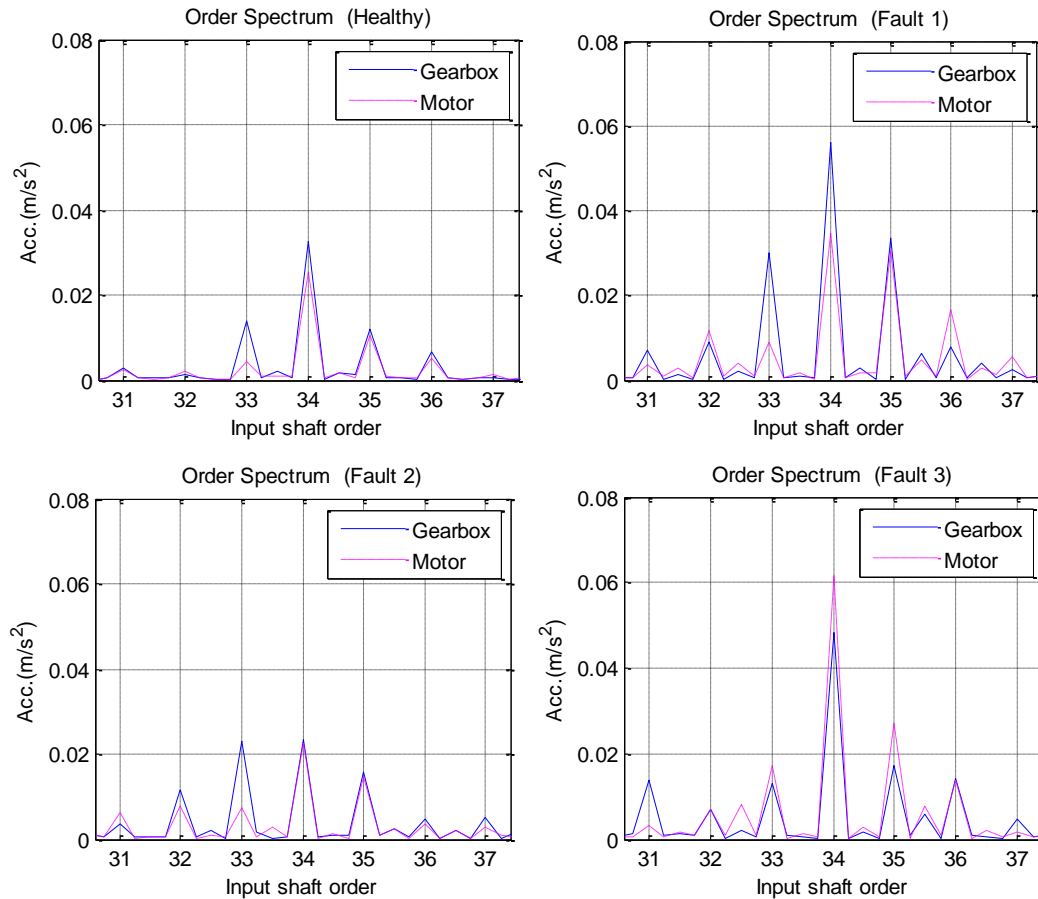
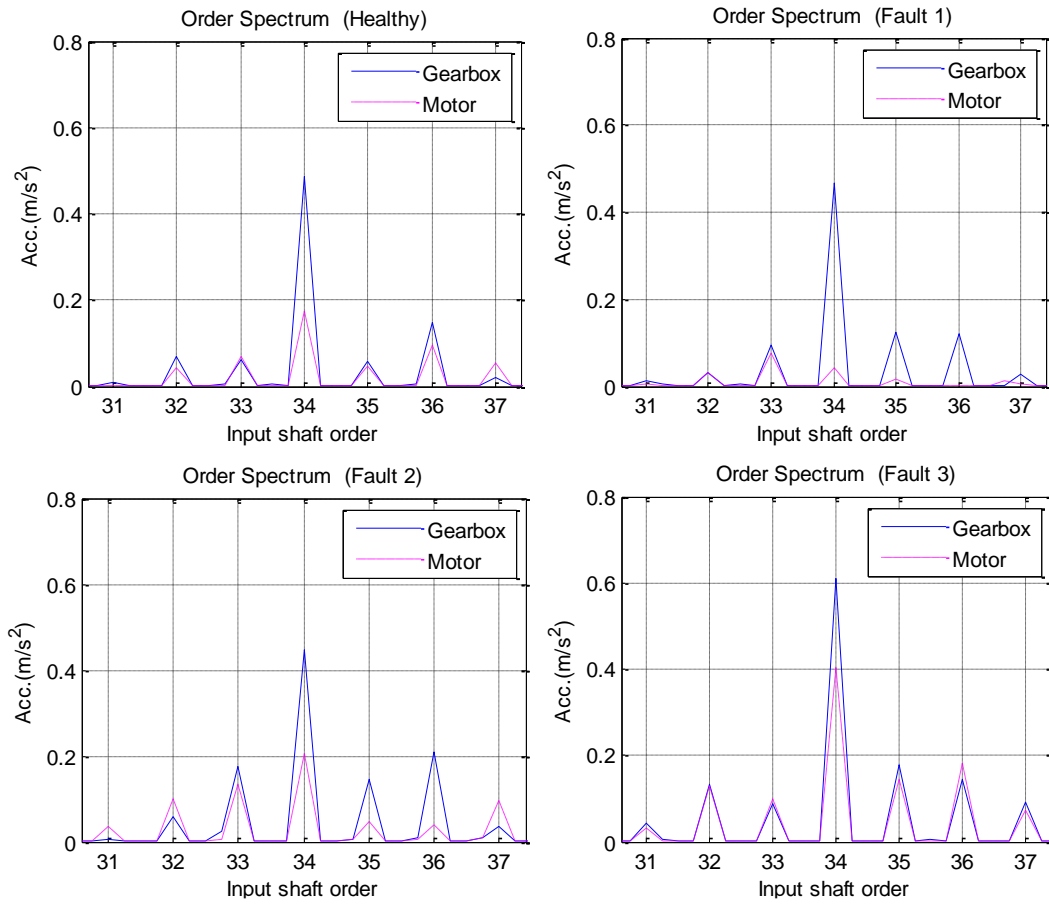


Figure 8.6. TSA spectrum of signals for healthy and faulty cases at low ($L=40\%$, $S=50\%$) operation conditions

CHAPTER 8

PERFORMANCE EVALUATION OF REMOTELY MEASURED VIBRATION



*Figure 8.7. TSA spectrum of signals for healthy and faulty cases at high
($L=80\%$, $S=100\%$) operation conditions*

With different gear operation conditions but the same location, as seen in Figures 8.6 and 8.7, the spectrum of the vibration signals shows that the spectral amplitudes at the 34th order and its sidebands (31th, 32th, 33th, 35th, 36th and 37th) increase by approximately ten times with increasing load at the same location, This confirms that different loads create different tooth deflections and therefore different amounts of gear vibration.

In Figure 8.6, in which the gearbox was operated under low ($L=40\%$, $S=50\%$) gear operation conditions the amplitudes of order 34 and its sidebands in both locations cannot provide a trend which is consistent with the severity of the damage. Although the figure shows some increased amplitude features, it is difficult to identify the severity of the faults based on them.

In comparison with low operating condition, the order spectrum in Figure 8.6, the order spectrum of the high operating condition seen in Figure 8.7 shows that the amplitude of the sidebands around tooth meshing frequencies increase with the severity of the faults in both locations, providing more consistent results with regards to fault severity. The order spectrum of Fault 3 can be seen to have a much higher amplitude when compared with Fault 1, and Fault 2.

In addition, Figure 8.7 shows that the amplitudes of the order 34 and its sidebands (31^{th} , 32^{th} , 33^{th} , 35^{th} , 36^{th} and 37^{th}) appear to increase in amplitude with the introduction of faults at two locations. These amplitudes change with the severity of the faults. More importantly, the results from the motor casing show the difference between faults as clearly as the results gained from the gearbox casing. Amplitudes of the signals at the motor casing are lower than those on the gearbox casing as a result of the effect of transmission paths on the vibration signal.

As shown in Figure 8.6 and Figure 8.7, the amplitudes of the order 34 and its sidebands (31^{th} , 32^{th} , 33^{th} , 35^{th} , 36^{th} and 37^{th}) are consistently the largest feature of the spectrum, dominating the signals for the different gear statuses. Thus the amplitudes and features of the order 34 can be defined as the average amplitude of the sidebands around the meshing frequency in order spectrum and can be used to detect gear faults remotely.

8.3.2 Performance of Mesh (34^{th}) Order Based Diagnosis

Figure 8.8 shows the spectral amplitude values corresponding to the order 34 (the first stage meshing frequency) for the gearbox casing and motor flange as well as how this amplitude changes with the gear operating conditions and the severity of the faults.

Comparing the mesh (34^{th}) order amplitude values between two different transducer positions, the following similarities may be identified:

1. Under different load

The mesh (34^{th}) order amplitude values from the motor flange change with loads which are the same as that of the gearbox casing. At a high load ($L=80\%$) the spectral amplitude shows the highest values, the same as those seen on the gearbox casing.

In addition, under a high load, the gear faults can be more easily distinguished, particularly the high sever fault (Fault 3).

This shows that under a high load the mesh (34th) order amplitude values are correlated to the vibration and hence can be used for fault diagnosis.

2. Under different speeds

The mesh (34th) order amplitude values from the motor flange show a similar trend with speed to that of the gearbox, confirming that good diagnosis results are likely to be obtained.

However, it does have the following significant differences:

1. The spectral amplitudes values are significantly lower, showing the effect of path attenuation. This degrades the detection sensitivity. In particular, a high severity fault such as F3 could not be separated from F2.
2. The variation trend over load and speed shows clear inconsistency under a number of different operating conditions, displaying considerable distortion of the path. At the speed of 60% case F1 and F3 cannot be quantified correctly because the amplitude is not proportional to that of the gearbox casing.

In general, the detection and diagnosis results are similar to those obtained from the gearbox and can be used for remote monitoring.

CHAPTER 8

PERFORMANCE EVALUATION OF REMOTELY MEASURED VIBRATION

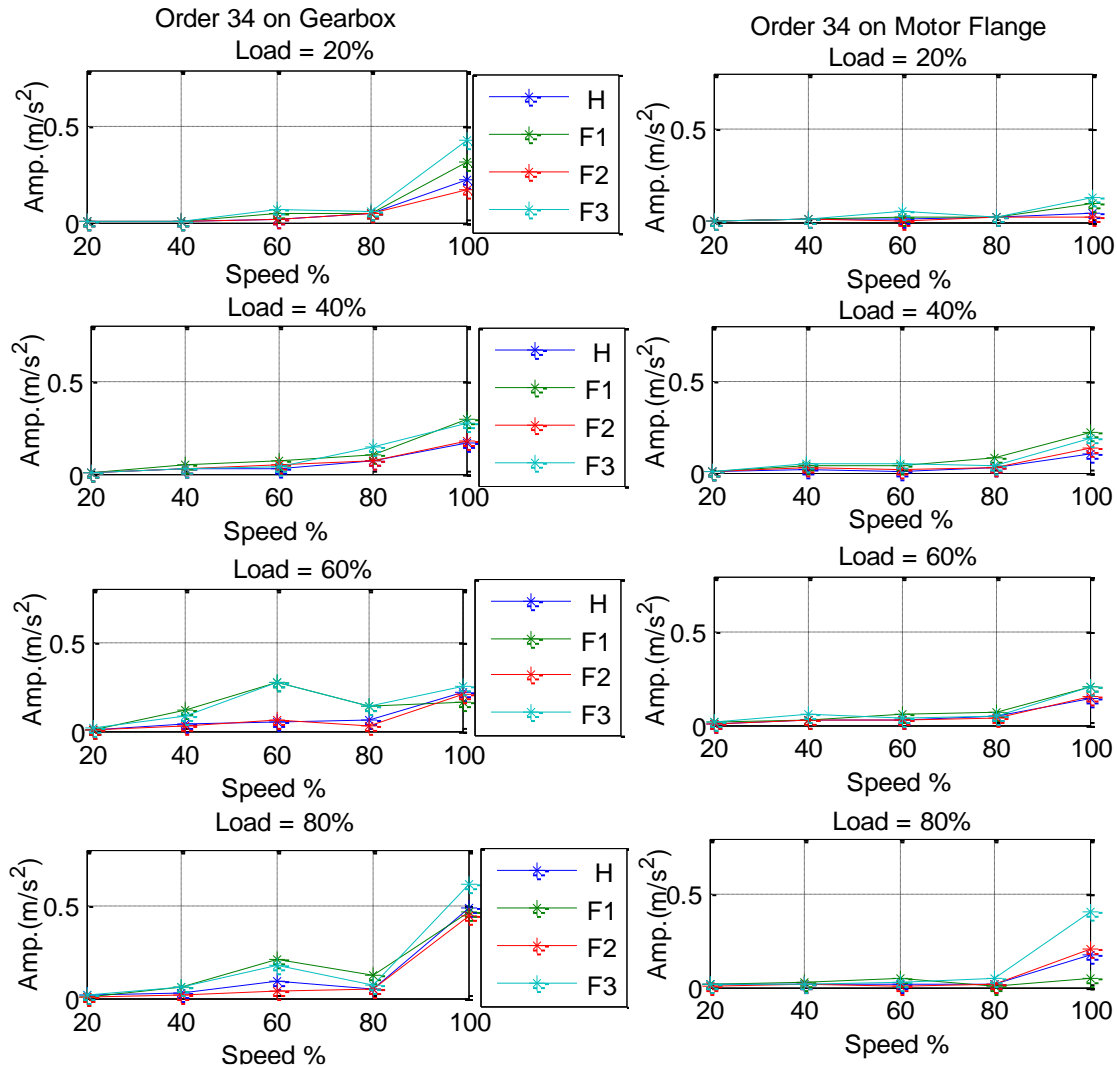


Figure 8.8-Order 34 amplitudes on the gearbox casing (left) and the motor flange (right) for healthy and faulty gear conditions at different operating conditions

It can be concluded that the special analysis results described above illustrate that spectral analysis based on order analysis can achieve the same results at a remote position, though the amplitude of the spectrum is attenuated. Therefore, fault diagnosis from a remote position is achievable with some special spectral analysis techniques.

8.3.3 Performance of Sideband based Diagnosis

It is obvious from Figures 8.6 and 8.7 that there is significant change in the amplitude of the sidebands (31^{th} , 32^{th} , 33^{th} , 35^{th} , 36^{th} and 37^{th} orders) of the faulty spectrum

when compared to those of the healthy spectrum. This change in these amplitudes clearly suggests that an abnormality has occurred in the gear driving system. Hence, the change in the amplitude of the sidebands can be used as an indicator for the presence of fault at both locations.

Figures 8.9 and 8.10 show the order of the sidebands (around the main 34th order) at the two locations (the gearbox casing and motor flange) under different operating conditions. These conditions are used in order to investigate the effect of the path transmission (the transducer location) on the detection and diagnosis of the seeded gear tooth faults.

As can be seen in Figures 8.6 and 8.7, both order spectrums are rich with discrete order sidebands components. To further identify and understand the effects of the path transmission on the signal from the healthy and faulty gears, an examination of the spectrum is carried out according to the amplitudes of two spectral features contents: A) Sideband feature one which is the average amplitudes of the two [(order 33+ order 35)/2] sidebands around first stage meshing frequency (34th order); B) Sideband feature two which is the average amplitudes of the four [(order 32+order 33+order 35+order 36)/4] sidebands around first stage meshing frequency (34th order).

A. Sideband Feature one

Figure 8.9 shows the values of feature one with the four gear statuses at two locations with different gear operating condition. Comparing values of Sideband feature one between two different transducer positions, it has found following *similarities*.

1. Under different loads

The feature one values from the motor flange change with operating loads which are the same as that of the gearbox casing.

At a low operating load there is no consistent increase in feature one when faults are introduced, unlike the findings from the gearbox casing, we may therefore infer that this feature cannot effectively indicate faults or distinguish between gear statuses.

The values of feature one for all gear statuses at a high operating load are higher than those at a low operating load, the same as the values at the gearbox casing.

In addition, especially under high load ($L=80\%$), the faults of the gears can be easily

CHAPTER 8

PERFORMANCE EVALUATION OF REMOTELY MEASURED VIBRATION

distinguished, especially the high sever fault (Fault 3). These results are as clear as those from the gearbox casing. Similarly, the values of feature one appear to increase with the introduction of faults.

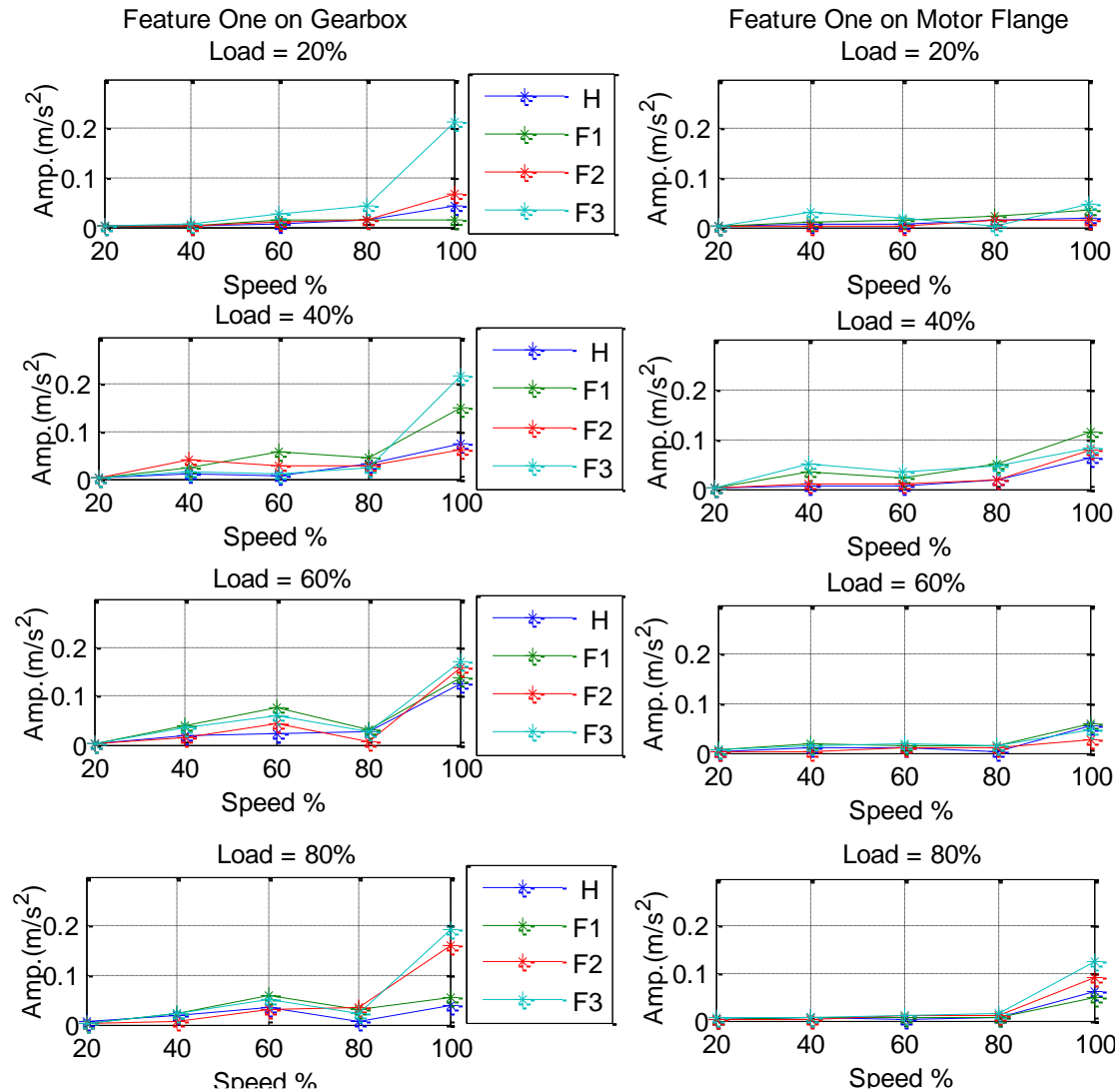


Figure 8.9-Feature one amplitudes on the gearbox casing (left) and motor casing (right) for healthy and faulty cases under different operating conditions

1. Under different speed

The feature one values from the motor flange shows a similar trend with regards to speed to that of the gearbox. This confirms that feature one is likely to produce good diagnosis results. It does, however, have the following significant differences:

CHAPTER 8

PERFORMANCE EVALUATION OF REMOTELY MEASURED VIBRATION

- I. The feature one value is significantly lower, showing the high effect of path attenuation, lowering the detection sensitivity particularly under a speed between 20 and 80%. At this speed range, a low severity fault such as F1 could not be separated from F2.
- II. The variation trend over load and speed shows clear inconsistency under a number of operating conditions, resulting in considerable distortion of the path. This is especially true at a speed of 60%. F1 and F3 cannot be quantified correctly because the feature value is not proportional to that of the gearbox casing.

In general, the detection and diagnosis results are similar to that of the gearbox casing and can be used as a basis for remote monitoring.

B. Sideband Feature two

Figure 8.10 shows the values of the feature two with the four gears at different locations under different operating conditions.

Through the comparison of the feature two values between two different transducer positions, the following similarities can be identified:

1. Under different loads

Under a different operating load, as is seen in Figure 8.10, the feature two values increase consistently alongside the load, also these values appear an increase in the amplitude with the introduction of faults which are the same as that of the gearbox casing. More importantly, the results from the motor flange show the difference between faults as clearly as the results from the gearbox casing.

The slight change in feature two between healthy and faulty conditions at a low operating load reflect significant information about the pinion gear's status as clearly as the results from the gearbox casing.

At a high operating load ($L=80\%$), the values of feature two change consistently with the severity of the faults and can be easily distinguished between pinion gear status.

CHAPTER 8

PERFORMANCE EVALUATION OF REMOTELY MEASURED VIBRATION

More importantly, the results from the motor casing show the difference between faults as clearly as those from the gearbox casing.

It can be concluded that feature two exhibits a reliable trend with fault progression especially with the most severe fault condition (as seen in Fault 3).

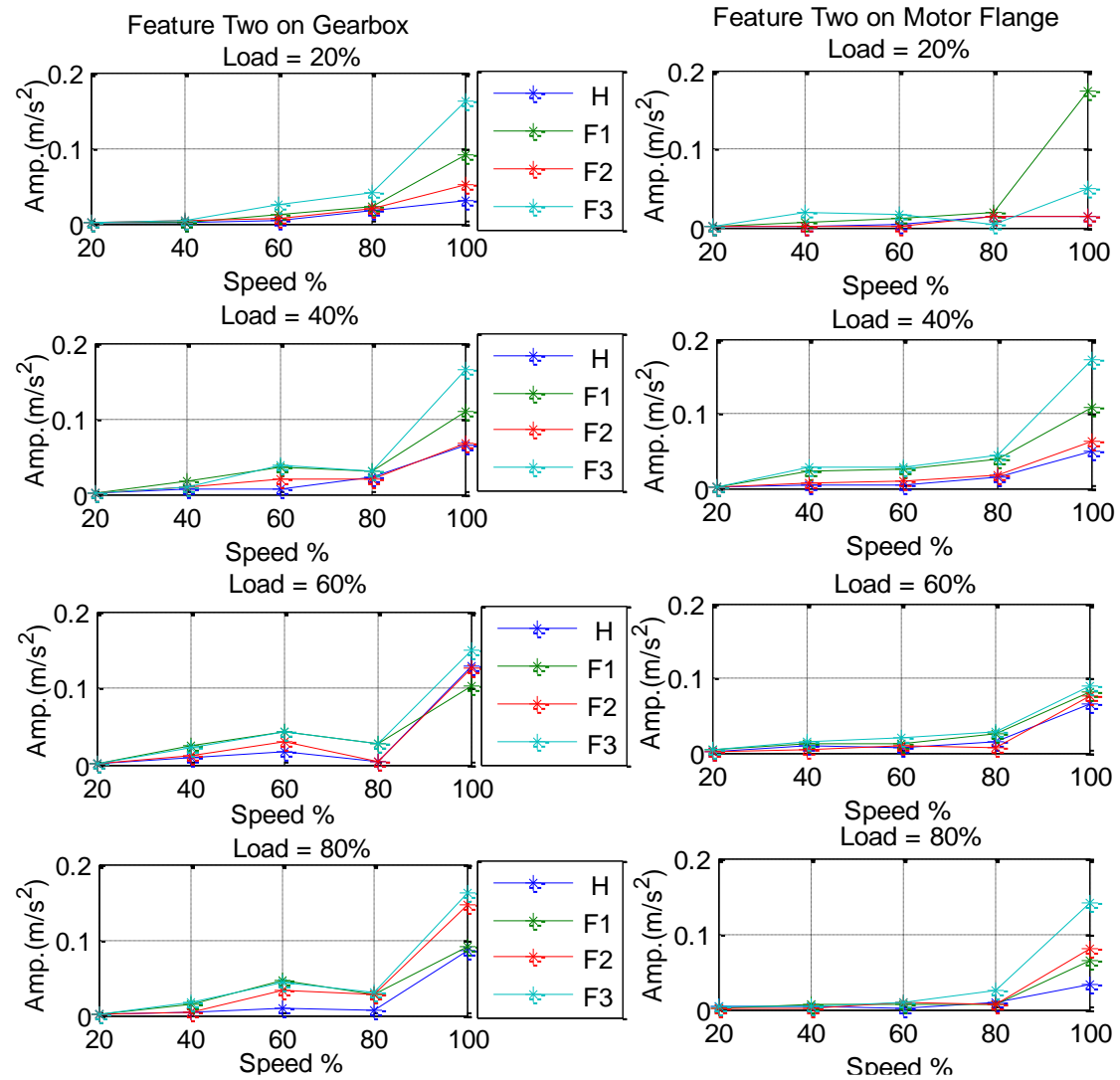


Figure 8.10-Feature two amplitudes on the gearbox casing (left) and motor casing (right) for healthy and faulty gear cases under different operating conditions

1. Under different speeds

The feature two values from the motor flange show a similar trend regarding speed to those of the gearbox, confirming that they are likely to produce good diagnosis results.

However, it does have the following significant differences:

- I. The feature two values are significantly lower, showing the high effect of path attenuation.
- II. The variation trend over speed shows clear inconsistency under a number of operating conditions, showing considerable distortion of the path. At the speed between 20%-60%, gear statuses cannot be quantified correctly because the feature value is disproportional to that of the gearbox casing.

In general, the detection and diagnosis results are similar to those from the gearbox and it can be used as a base for remote monitoring.

8.4 Continuous Wavelet Transform (CWT) Analysis of the TSA Signal

8.11 shows the CWT results by applying Equation 2.21 to the TSA signal in Figure 8.1. In order to visualise the time and frequency characteristics more accurately, the results are presented in the form of colour images. As the vibration is presented jointly in both the angular and the frequency domains, the difference between the TSA signal-CWT patterns for different fault cases and the accelerometer positions under the low operating condition can be clearly identified.

The CWT of the vibrations for both accelerometer positions shows two distinctive patterns: a uniform one and a localised one along the angular direction. A periodic feature of the localised pattern can be identified clearly in the angular direction indicating the oscillation of the input gear. As the severity of the gear fault becomes higher, the patterns become more localized in the angular position. This shows the typical characteristics of the transient responses due to the periodic impulses of a faulty tooth, showing that TSA signal-CWT significantly enhances the fault features.

In the frequency direction, the patterns are distributed mainly in the frequency range around 2kHz, where a resonance in the gear system may exist. However, Fault 2 shows more distinctive amplitudes around 3kHz, showing a different resonance from other gear sets. This may indicate the effect of nonlinear stiffness and manufacturing errors on the frequency responses.

CHAPTER 8

PERFORMANCE EVALUATION OF REMOTELY MEASURED VIBRATION

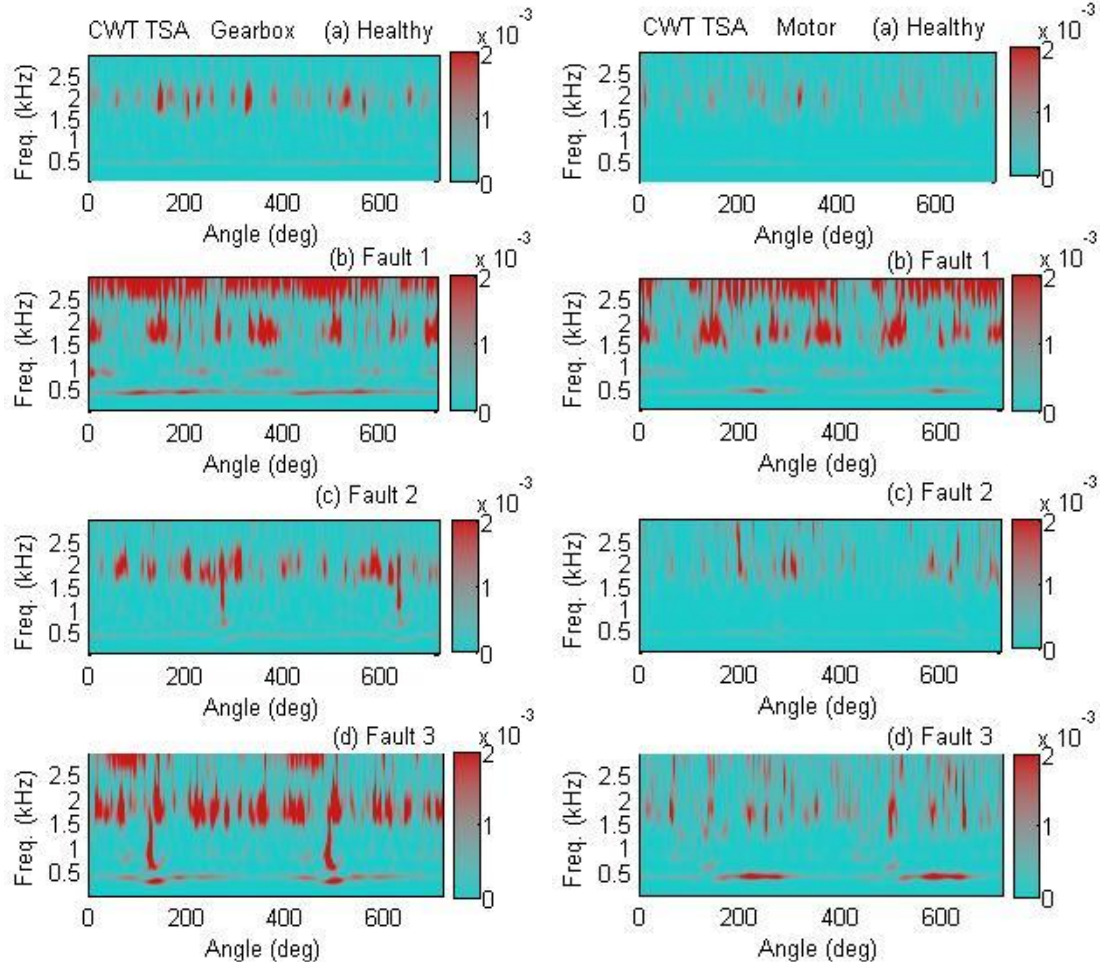


Figure 8.11 - CWT of TSA vibration signal from the gearbox casing and motor flange for healthy and faulty gears under low operating conditions (40% load and 50% speed)

Interestingly, the vibration amplitudes at meshing frequency ($\approx 428\text{Hz}$) can be seen to be more significant in the motor flange when compared to those at the gearbox casing, with the exception of Fault 2. This is consistent with the vibration attenuation mechanism. High frequency amplitude at 3kHz are reduced more with transmission distance whilst the amplitude at meshing ($\approx 428\text{Hz}$) can transfer relatively faraway. This shows that low frequency components may be more useful for remote measurement based fault diagnosis.

Moreover, the localized patterns appear at a similar angular position and frequency range for the transducers at both the gearbox and motor flange. This indicates that the

CHAPTER 8

PERFORMANCE EVALUATION OF REMOTELY MEASURED VIBRATION

transmission path has little distortion to the vibration responses and proves that the remote accelerometer can capture the fault patterns and can be used for monitoring faults.

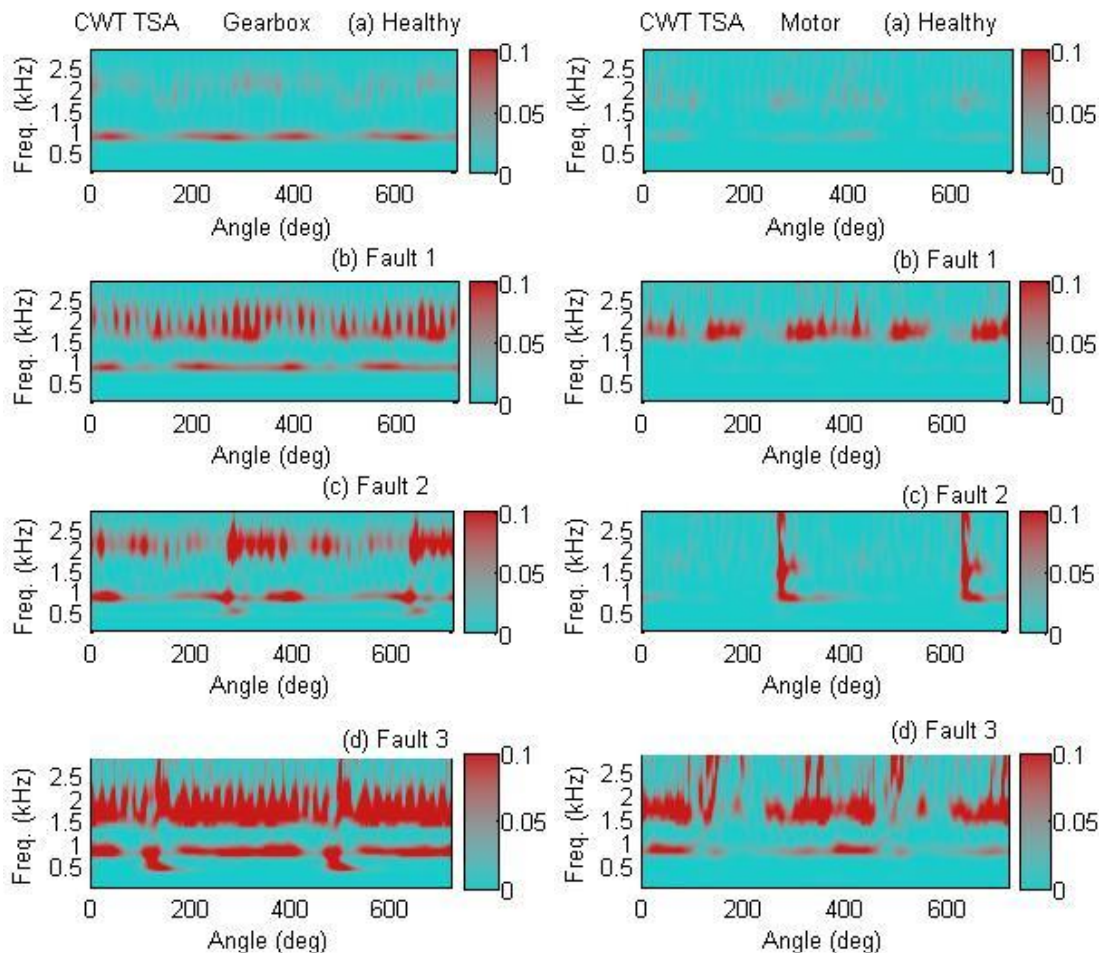


Figure 8.12 - CWT of TSA vibration signals from the gearbox casing and motor flange for healthy and faulty gears under high operating conditions (80% load and 100% speed)

However, the amplitudes of the vibration on the motor flange are clearly smaller than those of the gearbox casing. This indicates that a large attenuation from the transmission path. Particularly, the high frequency vibrations are more attenuation than that of low frequency, which is consistent with the general characteristics of vibration transmission and needs to be take into account for remote sensor based monitoring.

CHAPTER 8

PERFORMANCE EVALUATION OF REMOTELY MEASURED VIBRATION

Nevertheless the CWT representations show that vibration from the remote accelerometer is consistent with that of the gearbox casing and that it is possible to use the remote measurements for fault detection and diagnosis.

Under the high operating condition, the CWT results in Figure 8.12 have very similar characteristics to those at low operating conditions. However, as shown in Figure 8.12, the vibration amplitudes become much higher for the uniform amplitudes due to the meshing frequency ($\approx 838\text{Hz}$), its higher order harmonics and the localized patterns due to fault induced impacts. Faults 2 and 3 can still be easily identified by the distinctive localized peaks from the healthy case and Fault 1.

Although the CWT patterns share the above general characteristics, the dissimilarity between each class of gear cases is quite significant. For example, the gearbox vibration shown in Figure 8.13 shows more homogeneous amplitudes for cases: Health, Fault 1 and Fault 3 than that of Fault 2. It is therefore difficult to develop a simple feature parameter to represent the comprehensive characteristics of CWT patterns for fault severity advancement directly.

From the above study, it can be concluded that TSA signal -CWT representations allows an in-depth understanding of the gear vibrations even when the vibration signal is measured remotely from the motor flange. It confirms that the transmission path has a nearly linear attenuation to the vibration and that remote measurements can give a good indication of gearbox vibrations for condition monitoring.

It is, however, still difficult to distinguish gear health conditions accurately when the SNR of the vibration signal is low. In future work, higher dimensional features will be considered containing more information to achieve a more robust performance under different operating conditions of a gearbox.

8.5 Summary

In this chapter the angular domain, the order spectrum and the order-frequency analysis were used in order to investigate the effect of path transmission (transducer location) on the detection and diagnosis of the seeded gear tooth faults.

In Section 8.1, the local and remote angular waveforms of the vibration signals for all gear statutes under different operating conditions shows a degree of distortion and no

CHAPTER 8

PERFORMANCE EVALUATION OF REMOTELY MEASURED VIBRATION

obvious fault symptoms were exited, even under Fault 3. The presence of a transmission path may cause a statistically significant change in the shape of the signal.

Sections 8.2.2 and 8.2.3 show the peak value, RMS, crest factor and kurtosis of the TSA vibration signal for two different locations. These statistical parameters were computed under various rotational speed and load scenarios.

The results in Section 8.2.2 shows that the peak value and RMS results from the motor flange were similar to those from the gearbox therefore showing that it could be used for remote monitoring. Both parameters were affected by gear operating conditions; this confirms that the operational condition of the gears may alter the vibration signal and therefore highly affect the overall peak value and RMS.

Kurtosis and crest factor based on the TSA signals were explored in Section 8.2.3. In general, the detection and diagnosis results from the motor flange were similar to those from the gearbox showing that it could potentially be useful for remote monitoring.

The order spectrums of the healthy and faulty gears under low and high operation conditions recorded both locally and remotely were shown in Section 8.3. This section showed that the amplitudes of the order 34 and its sidebands were consistently the largest features of the spectrum, dominating the signals for the different gear statuses. In general, the detection and diagnosis results from the motor flange were similar to those from the gearbox, showing that it could potentially be used for remote monitoring.

In Section 8.4, the CWT of the TSA signal from motor flange (remote) was compared directly with the CWT of the TSA signal from gearbox casing discussed in Chapter 6. The results showed that the TSA signal -CWT patterns are obviously different for different fault cases and accelerometer positions under different operating conditions. It confirms that the transmission path has a nearly linear attenuation to the vibration and that a remote measurement can still give an acceptable indication of the gearbox vibrations for condition monitoring. It is, however, still difficult to distinguish gear health conditions accurately when the SNR of the vibration signal is low. In future

CHAPTER 8

PERFORMANCE EVALUATION OF REMOTELY MEASURED VIBRATION

work, higher dimensional features will be considered containing more information in order to achieve a more robust performance under different operating conditions.

CHAPTER 9

CONCLUSIONS AND FUTURE WORK

This chapter summarises the achievements of the research work and explains how the objectives stated in Chapter One were achieved. A summary of the author's contributions to knowledge and the novel aspects of the research work are also included. Finally, recommendations for future work for the remote condition monitoring of gear transmission systems are provided and conclusions made.

9.1 Review of the Objectives and Achievements

This chapter describes the achievements and contributions carried out during this research work. This research has focused on the remote CM of a two stage helical gear transmission system. Theoretical analysis and experimental studies were carried out on gearbox vibration signal characteristics, and a selection of signal processing methods and techniques were implemented to investigate the effect of the transmission path on the vibration signal. The key achievements of the research work recognized in this thesis are detailed below.

Objective 1: To develop experimental procedures for remote CM of a two stage helical gear transmission system, primarily focusing on a faulty gear (pinion) in the first stage gear transmission system.

Achievement 1: The test rig facility and data acquisition software were developed as detailed in Chapter 3. A two stage helical reduction gearbox manufactured by David Brown Radicon Limited, shown in Figure 3.1, was selected for this research project. Consequently the environment in which the practical research work was conducted was similar to an industrial environment and practical gearbox applications. A number of measurement transducers were used on the test rig to monitor the function of the gearbox CM. Both local and remote transducers were used in this experiment. The rig was used to investigate the effect of path transmission on a vibration signal collected from two different locations as described in Chapter 8. Furthermore, the test rig was used to provide experimental data for validating the mathematical model of the two-stage helical gearbox (Chapter 5). Finally, designs for the gearbox test rig were provided for use in other research projects.

Objective 2: To establish a series of quantified faults within the helical gearbox (the inclusion of gear teeth with different severities of tooth breakage: 25%, 50% and the complete removal of a tooth at the first stage pinion). The impact of fault severity on the transmission path of the vibration signal was then studied.

Achievement 2: The most common fault in industrial gearboxes is broken teeth such

CHAPTER 9

CONCLUSIONS AND FUTURE WORK

as those which have been seeded into the test rig. These faults frequently occur in many industrial applications such as in vessel thrusters and helicopters. The simulation of this fault was achieved by removing 25%, 50% and one complete tooth from the 1st stage pinion in the tooth width (Section 3.4). Repeating the experiment with different fault severities (25%, 50% and complete tooth removal) and different gear operating conditions (speeds 20% to full 100% and loads 20% to 80%) were studied and data collected both locally and remotely. The reproducibility of the results obtained was tested by repeating the experiment with the same faults many times under the same operating conditions.

Objective 3: To carry out a review of the literature for commonly used vibration techniques including simple / early gearbox fault detection methods such as time, frequency and order domains to advanced signal processing techniques such as continuous wavelet transform (CWT).

Achievement 3: Relevant techniques are briefly discussed in Chapter 2 to assist in the understanding of results presented in the following chapters. Signals originating from the gearbox were expected to be non-stationary and non-linear. They have been processed using traditional signal processing methods and advanced wavelet transforms before and after time synchronised averaging (TSA). The effects of the transmission paths on the raw vibration signals were also investigated.

Objective 4: To collect and analyse vibration data for healthy gears under different operating conditions using conventional methods in the time, frequency and joint time-frequency domains respectively. Baseline results for the healthy gear (see Chapter 3), were then referenced for comparison with more advanced methods.

Achievement 4: The baseline vibration data for a healthy gearbox have been established and are discussed in Section 3.6. Successful experiments have been carried out to monitor the frequencies of the vibration spectra of a healthy gearbox. Sources of vibration were identified theoretically, and frequencies at which they occur were predicted precisely (see Figures 3.17 and 3.18). This method is believed to be one of the first successful attempts to establish a detailed baseline spectrum for the

CHAPTER 9

CONCLUSIONS AND FUTURE WORK

detection and diagnosis of faults within gearboxes using vibration analysis (Section 3.6.2).

Objective 5: To record the vibration signals for different gear conditions at different operating conditions from a sensor mounted on the gearbox casing and to analyse signals using conventional methods in the time, frequency and the joint time-frequency domains (using a Morlet continuous wavelet transform). To then obtain an effective set of features for detecting and diagnosing seeded gear tooth faults.

Achievement 5: The vibration signals were examined under different operating conditions (Section. 4.2.1). It was found that the signals were very complex and enormous significant amount of information remained unknown regarding the waveform of the signals. The difference in amplitudes appeared to be due to the different operating conditions. Limited information was extracted from the vibration waveforms and results showed that faults in helical gears were difficult to detect using this approach.

In Sections 4.2.2 and 4.2.3 the peak value, RMS, crest factor and kurtosis were extracted from the time domain vibration signal. These statistical parameters were computed under various rotational speed and load scenarios. The results showed that most statistical parameters were highly affected by operating conditions and gear condition. Comparing the peak and RMS values of a given vibration signal with values determined using vibrations from a normal gear, the presence of a defect and its severity could not be detected. Statistical analysis based on kurtosis and crest factor lacked the ability to detect gear defects at later stages. The limitations of these simple techniques were such that, even if used simultaneously, could lead to an incorrect diagnosis. This suggested that these measurements are not very sensitive to these types of faults (Section 3.4).

Nevertheless, the spectrum is more reliable than the time domain regarding fault sensitivity. The results in Section 4.3, however, showed that the use of such analyses may enhance the ability to differentiate between healthy and faulty gear patterns in different frequency domains. Due to the joint ability of illustrating both time and

CHAPTER 9

CONCLUSIONS AND FUTURE WORK

frequency information simultaneously with time-frequency localisation capability, the sensitivity of these techniques to the early detection of faults was enhanced (section 4.4). The features observed are not consistent with fault progression under different operating conditions and so it is not necessary to perform feature calculation. In addition, the analysis also suggests that the results may become better quality if a noise suppression method such as time synchronised averaging (TSA) is used.

Objective 6: To build and develop a mathematical model representing a two stage gear system in order to gain a better understanding of the vibration generation mechanisms in gear transmission systems. This helps to characterise the changes of the dynamic properties due to various types of gear faults, which then allows for measurement setup, data processing selection and diagnosis rule development.

Achievement 6: The use of vibration for detecting gear faults has been studied using a numerical simulation based on the construction of the two stage helical gearbox. The model consists of two gears equations including the gearbox casing (Section 5.4). The model also represents a two stage helical gear system using a suitable stiffness function to represent the forces acting between two pair of gears. Rotational stiffness and damping were also used to simulate the angular motion of the gears and shafts. A novel feature of the mathematical model is the addition of the vertical spring-damper systems attaching the gears to the casing. To simplify the model, but still demonstrate the basic principles, the casing was simply modelled by two masses. One mass was attached to the pinion and the other to the gear of the first pair of gears. Significant differences between the acceleration transmitted through each of the masses were shown.

The major problem with this model is the dynamics of the gears during the meshing. Numerical solutions of the equations which form the model (Section 5.4) show that the spectrum of a faulty gear is dominated by the fundamental meshing frequency but also by a number of pronounced sidebands that spread around it. These sidebands are largely determined by the primary shaft speed and the gear meshing frequencies. When a local fault is introduced to the gear, the model predicts that the amplitude of these sidebands will increase, and more sideband components and additive impulsive

CHAPTER 9

CONCLUSIONS AND FUTURE WORK

components will appear around the fundamental meshing frequency and higher order harmonics. These features, which form the basis of a possible detection mechanism, have been confirmed through tests (Section 5.7).

This demonstrated that the model, although fairly simple, can be used to explain the mechanism at work in the real gearbox used in condition monitoring.

When compared, the model predictions and experimental results were in agreement with one another (Chapter 5).

Objective 7: To investigate the influence of Time Synchronous Averaging (TSA) on the vibration signal. The results of applying traditional signal processing techniques, as seen in Chapter 4, were compared to the results obtained by applying TSA.

Achievement 7: The conventional time domain waveforms under different operating conditions were compared with the angular waveforms obtained by TSA under the same operating conditions (Section 6.3.1). The results confirmed that the TSA technique improved the signal to noise ratio (SNR) making local variations in the vibration signal much more visible.

In Section 6.3.2, a quantitative comparison between the two types of signals and different types of fault was conducted; the characteristics of signal strength over different operating conditions were examined using peak and RMS values. These results showed the peak value and RMS of the vibration signal provided a better detection performance because of the TSA's nonlinear effect detection and its capability for noise reduction.

In Section 6.3.3, kurtosis and crest factor (dimensionless parameters) were extracted to give more of an indication of the difference in the signal patterns. The results showed that the kurtosis and crest factor of the of the vibration signal with and without TSA do not exhibit a reliable trend with fault progression under all operating conditions.

TSA was applied to the vibration signal from the gearbox so that the order spectrum could be obtained in order to further characterise gearbox vibration in this new domain (Section 6.4). TSA results in Section 6.4.1 which shows that at special frequencies the faults of the gears can be more easily distinguished. At some operating condition more consistent difference for the range of faults can be seen in

CHAPTER 9

CONCLUSIONS AND FUTURE WORK

order spectrums. This also confirms that the TSA technique removes the interference of rotation speed and additive random noise (Section 6.4.2).

The order of spectral features under different operating condition was extracted from the order spectrum of the TSA signal and compared with conventional spectral features in order to investigate the influences of TSA on the vibration signal (Section 6.4.3). The results showed that the spectral feature (the average amplitude of the $f_{m11} \pm f_{r11}$) of the conventional spectrum did not show any significant change between gear statuses under all operating conditions. While the order spectral feature (average amplitude of the 33th order \pm 35th order) does not perform well at low operating conditions, it is effective in detection of local faults induced in the gear system under high speed and load conditions.

In Section 6.5, the TSA signal was processed using CWT in order to find more accurate and reliable diagnosis results. The results of the CWT of the TSA signal were compared directly with the conventional CWT results discussed in Chapter 4.

Section 6.5 has shown that the conventional CWT and the CWT of the TSA results were both able to detect various faults at early stages, but the CWT of TSA signals was more sensitive with regards to the detection of early fault symptoms (Section 4.4).

The results proved that the method of combining CWT with the TSA signal is very promising in the analysis of the vibration signal and the fault diagnosis of gearboxes. This means it can therefore be applied in order to detect and diagnose gear fault remotely (Section 8.4).

Objective 8: To perform frequency response function (FRF) using a vibration shaker in order to study the transmission path effect on the vibration signal generated in the gear transmission system.

Achievement 8: Frequency analysis equipment with an electromagnetic shaker was used to measure the FRF at different locations on the test rig (Section 7.3.1). The FRFs were determined using five IC type accelerometers attached at 200 different locations over the gearbox casing and motor flange. A signal including the 1st stage and the 2nd stage meshing frequencies was selected to study the effect of the

CHAPTER 9

CONCLUSIONS AND FUTURE WORK

transmission path on the vibration signal. These meshing frequencies were extracted from a set of FRF measurements between one reference position on the shaft and a number of measurement positions within the model. It can be seen that sensors located at certain nodes produced higher frequency responses and results in Section 7.4.1 confirmed that the vibration signals were highly affected by the path from the gearbox casing to the motor flange.

Objective 9: To investigate the effect of path transmission (transducer location) on the detection and diagnosis of seeded gear tooth faults.

Achievement 9: In Chapter 8 the angular domain, the order spectrum and the order-frequency analysis were used in order to investigate the effect of path transmission (transducer location) on the detection and diagnosis of the seeded gear tooth faults.

Section 8.1 showed the local and remote angular waveforms of the vibration signals for a healthy gear and three faulty gears under different operating conditions. All the waveforms from both locations show a degree of distortion and no obvious fault symptoms were exited, even under severe fault conditions. The presence of a transmission path may not significantly alter the overall vibration level but may cause a statistically significant change in the shape of the signal.

In Sections 8.2.2 and 8.2.3, the peak value, RMS, crest factor and kurtosis were extracted from the TSA vibration signal of two different locations. These statistical parameters were computed under various rotational speed and load scenarios.

Sections 8.2.2 showed that the detection and diagnosis results from the motor flange were similar to those from the gearbox therefore showing that it could be used for remote monitoring. The results in Sections 8.2.2 also showed that both parameters were affected by gear operating conditions; this confirms that the operational condition of the gears may alter the vibration signal and therefore highly affect the overall peak value and RMS.

Kurtosis and crest factor based on the TSA signals were explored in Section 8.2.3. In general, the detection and diagnosis results from the motor flange were similar to those from the gearbox showing that it could potentially be useful for remote monitoring. The order spectrums of the healthy and faulty gears under low and high operation conditions recorded both locally and remotely were shown in Section 8.3. The results

CHAPTER 9

CONCLUSIONS AND FUTURE WORK

showed that the amplitudes of the order 34 and its sidebands (31st, 32nd, 33th, 35th, 36th and 37th) were consistently the largest features of the spectrum, dominating the signals for the different gear statuses. The amplitudes of the order 34 and two features defined as the average amplitude of the sidebands around the meshing frequency in the order spectrum were selected to detect gear faults remotely. In general, the detection and diagnosis results from the motor flange were similar to those from the gearbox, showing that it could potentially be used for remote monitoring (Section 8.3).

In order to gain better understanding of the gear vibrations when the vibration signal is measured remotely from the motor flange, the remote (motor flange) CWT of the TSA signal was compared directly with the CWT of the TSA signal discussed in Chapter 6 (Section 8.4).

The results showed that as the vibration is presented jointly in both the angular and frequency domains. It can be seen more clearly that TSA signal -CWT patterns are obviously different for different fault cases and accelerometer positions under low operating conditions. It confirms that the transmission path has a nearly linear attenuation to the vibration and that a remote measurement can still give an acceptable indication of the gearbox vibrations for condition monitoring. It is, however, still difficult to distinguish gear health conditions accurately when the SNR of the vibration signal is low. In future work, higher dimensional features will be considered containing more information in order to achieve a more robust performance under different operating conditions.

Objective 10: To provide guidelines for future research in this field.

Achievement 10:

A number of possible directions are given for future work (Section 9.5, below) on the remote CM monitoring of a gearbox using different simulated faults whilst utilizing the same techniques developed in this research. Furthermore, the model developed for a two stage helical gearbox is now ready to be extended for use with multi-stage gearboxes.

9.2 Conclusions on the Gear Transmission System CM Using Vibration Analysis

From the research work and results reported in this thesis it is possible to conclude the following:

9.2.1 Experimental Study

Investigation and analysis of vibration data from the gear system has confirmed the following:

1. Examination of vibration signals under different operating conditions has showed the signals to be very complexes and there is an enormous amount of unknown information associated with the waveform of the signals. The difference in amplitudes of the signals was due to different operating conditions and limited information could be extracted from the vibration waveform. Results from the vibration waveform showed that faults in helical gears are difficult to detect using this approach.
2. Most statistical parameters were highly affected by both the operating and gearbox conditions. Comparison of the peak and RMS values of a given vibration signal with values determined using vibrations from a normal gear could not detect the presence or severity of a gear defect. In the early stages of gear damage, kurtosis and crest factor values increase as the vibration increases. However, as the damage further increases, the vibration becomes more random and the values for crest factor and kurtosis reduced to normal levels. Therefore, statistical analysis based on kurtosis and crest factor lacks the ability to detect gear defects at later stages. The limitations of these measurement techniques are such that even if used simultaneously they may lead to an incorrect fault diagnosis. This suggests that they are not very sensitive to gear tooth breakage faults.
3. The results obtained demonstrate the capacity of the vibration analysis for the detection of gear faults. It is concluded that vibration analysis can be used as a reliable technique to identify the health status of the gearbox driven by the motor.
4. Spectra can be used more reliably in fault detections than time domain analysis and are more sensitive to fault detection. The results in Figures. 4.6 and 4.7 showed that the use of such analyses can enhance the ability to differentiate between

CHAPTER 9

CONCLUSIONS AND FUTURE WORK

healthy and faulty gear patterns in frequency domains under certain gear operating conditions.

5. The performance of the conventional frequency domain analysis degrades due to the fluctuation of the operating conditions. However, vibration signal spectral features may be effective in detection of local faults induced in the gear system under certain gear operating conditions.
6. Time-frequency methods were more sensitive and reliable for identifying and characterising fault symptoms. The presentation of time and frequency information together with time-frequency localisation capability enhanced the sensitivity of these techniques with regards to the early detection of faults. For instance, the features observed were not entirely consistent with fault progression under different conditions and it was not necessary to perform feature calculations. In addition, analysis also suggested that the results could improve if a noise suppression method such as time synchronised averaging feature calculations. In addition, analysis also suggested that the results could improve if a noise suppression method such as time synchronised averaging (TSA) had been used.
7. TSA suppressed all vibrations from the gearbox which were asynchronous with gear rotation, leaving only the vibration produced during one rotation of the gear on the input shaft. Therefore, local variations in the vibration signal became much more visible.
8. The conventional time domain waveform and angular waveform (after TSA) consisted of a large number of sinusoidal waveforms at different frequencies, with less noise superimposed on the angular waveform. Patterns associated with the meshing teeth of the angular waveform often emerged more clearly and it was possible to identify gear damage more easily. This confirms that the TSA technique tends to reduce the noise and cancel out the vibration components which are not synchronised with the rotation of the gear.
9. The significant change between the peak and RMS values with and without TSA confirms that TSA provides better detection performance because of its capabilities for noise reduction and the detection of nonlinear effects.
10. Kurtosis and crest factor analysis of the vibration signal without and with TSA do not exhibit reliable trends for the diagnosis of fault progression at all operating

CHAPTER 9

CONCLUSIONS AND FUTURE WORK

- conditions. Therefore, more advanced signal processing techniques such as spectrum/or order domain or TSA-CWT have to be used for future analysis.
11. Order spectra showed more consistent differences for the range of faults being investigated. It was also confirmed that the TSA technique removed interference associated with rotational speed and additive random noise.
 12. The effect of the transmission path on the vibration signal was also evaluated by comparing the Frequency Response Function (FRF) measured different locations on the test rig using the shaker test (Section 7.3.1). The results confirmed that the vibration signals were highly affected by the path transmission on the gearbox casing and the motor flange.
 13. Based on the time-frequency patterns obtained from the wavelet analysis of the TSA signal, an effective feature was found fault detection and indication of fault severity. The results have proved that the combination of CWT with the TSA signal is a very promising method for the analysis of the vibration signal and fault diagnosis of the gearbox.
 14. A degree of distortion can be seen in all the angular vibration waveforms from both locations and no obvious fault symptoms were diagnosed even for severe fault conditions. Although the presence of a transmission path may not significantly alter the overall vibration level, it may cause a statistically significant change in the shape of the signal.
 15. The peak value and RMS values from the motor flange showed a similar trend with speed to those from the gearbox, confirming that it is a possible method for producing good diagnosis results.
 16. At both sensor locations the kurtosis and crest factor lacked the sensitivity to detect fault conditions at all operating conditions.
 17. The amplitudes of the 34th order and its sidebands (31th, 32th, 33th, 35th, 36th and 37th) appeared to increase in amplitude with the introduction of faults at two locations. The amplitudes of the signals at the motor casing were lower than those on the gearbox casing due to the effect of transmission paths on the vibration signal.
 18. The special analysis results described in Sections 8.3.1 and 8.3.2 illustrated that spectral analysis based on order analysis can achieve similar results at a remote

position, though the amplitude of the spectrum was attenuated. Therefore, fault diagnosis from vibration signals recorded at a remote position is possible with the use of some special spectral analysis techniques.

19. The TSA-CWT representations allow an in-depth understanding of the gear vibrations even when the vibration signals are measured remotely from the motor flange. It confirms that the transmission path has a nearly linear attenuation to that of the vibration and that remote measurement can still provide a good indication of the gearbox vibrations for condition monitoring.

It is still difficult to distinguish gear health conditions accurately when SNR of the vibration signal is low.

9.2.2 Conclusions on the Gear Transmission System Model

1. The two-stage gearbox mathematical model developed as part of this research has been examined under a number of different operating conditions.
2. A simple model of a two-stage gear system has been developed to simulate gearbox imperfections. The model represents a two stage helical gear system with a suitable stiffness function to represent the forces acting between two pair of gears. Rotational stiffness and damping are also used to simulate the angular motion of the gears and shafts. The model was validated against a set of results obtained from the experimental measurements with the aid of a numerical simulation (see Sections 5.5). The achieved results allow the conclusion that the predicted results, based on the model, are very similar to the experimental results and so vibration can play a significant role in the remote detection of faults such as broken teeth under different operation conditions.
3. The mathematical simulation showed that the meshing stiffness function k_1 and k_2 for the pinion and the gear were affected by the increased fault severity.
4. Both the model results and the actual results obtained from the laboratory experiment were validated against one other, and it was concluded that the results were suitably related enough for the model to be accepted as a practical basis for remote fault detection.

9.3 Novel Feature Summary and Contribution to Knowledge

The research project presented in this thesis incorporated a number of important issues that were novel and not previously implemented by other researchers or practitioners. These aspects of novelty are summarized below.

- **Novelty One:**

The author of this thesis believes that the way in which vibration signal has been examined remotely using traditional and advanced analysis techniques with the assistance of a mathematical model (a two-stage gearbox) and mathematical simulations to predict results that successfully correlate with the investigational findings is novel (see Chapter 5). The author is aware of the use of vibration signal analysis to identify and diagnose faults remotely in other machines and apparatus such as pumps, induction motors, etc.

- **Novelty Two:**

FRFs are used to study the transmission path effect on the vibration signal generated in the gear transmission system. This problem is related to the identification of the dynamic properties of gearbox components.

- **Novelty Three:**

It is assured that the application of the use of vibration signals for remote detection and diagnosis of local gear faults is entirely novel. In addition, no work has been found describing in any detail the traditional and advanced analysis of vibration under different gear operation conditions.

9.4 The contributions to knowledge of this project:

- **The First Contribution**

The application of vibration analysis for remote detection and diagnosis of helical gear faults has not been previously investigated.

- **The Second Contribution**

The author could not find any reports of using traditional and advanced techniques for remote fault detection and diagnosis for a 2-stage helical gearbox and believes that the use of these techniques to examine vibration signal for the remote CM of the gear transmission system is unique.


- **The Third Contribution**


Modelling a two stage helical gear system in association of the use of a no stationary stiffness function to represent the forces acting between two pair of gears and the use of a lumped system to represent the gear casing has not previously approached in this way.


- **The Fourth Contribution**

As no reports have been found of using the TSA signal -CWT representations for remote fault detection and fault diagnosis for helical gears, the author believes that the use of the TSA signal -CWT representations technique to analyse the remote CM of a helical gearbox is unique.

9.5 Recommendations for Future Work on Remote CM of Gearboxes:

 **Recommendation 1:** More experimental work is needed to further evaluate the sensitivity and reliability of the proposed detection method on a simpler gearbox, (e.g. a single stage gearbox) to gain a better understanding of the effect of path transmission on the vibration signal.

 **Recommendation 2:** Since gear characteristics differ for the same type and size of gear, from one gear to another; gear faults should be simulated on the same gear for both healthy and faulty conditions. The spectrum characteristics of identical gears should be investigated in more detail because results from this research have shown that apparently identical gears can still produce different components in the vibration spectrum.

 **Recommendation 3:** Since gear characteristics differ for the same type and size of gear, gear faults should be simulated on the same gear for both healthy and faulty conditions. The spectrum characteristics of identical gears should be investigated in more detail because results from this research have shown that apparently identical gears can still produce different components in the motor current spectrum.

 **Recommendation 4:** It is still difficult to distinguish gear health conditions

CHAPTER 9

CONCLUSIONS AND FUTURE WORK

accurately when the SNR of the vibration signal is low. In future work, higher dimensional features should be considered containing more information to achieve a more robust performance under different operating conditions.

REFERENCES

- [1]. Dalpiaz, G.; Rivola, A.; Rubini, R.: Effectiveness and sensitivity of vibration processing techniques for local fault detection in gears. *Mechanical System and Signal Processing*, 14, 3, pp. 387-412, 2000.
- [2]. Meltzer, G. and Nguyen Phong Dien: Some new advances in gear diagnostics by application of the wavelet transform. *Strojnícky Časopis*, 54, 3, pp. 129-148, 2003
- [3]. Lin J., M.J. Zuo, Gearbox fault diagnosis using adaptive wavelet filter, *Journal of Mechanical Systems and Signal Processing* 17 (6) pp. 1259–1269, 2003.
- [4]. Zheng H. Z., Li, X. Chen, Gear fault diagnosis based on continuous wavelet transform, *Journal of Mechanical System and Signal Processing* 16 pp. 447–457. 2002.
- [5]. Morris, R. and Pardue, F. - *The Reliability Based Maintenance Strategy: A Vision for Improving Industrial Productivity*, Computational Systems Incorporated (CSI), Knoxville, Tennessee, USA, 1994.
- [6]. Thompson, S. *Tribology Solutions: Section 1-* Computational Systems Incorporated (CSI), Knoxville, Tennessee, USA. 2000.
- [7]. Reintjes, J., Mahon, R., Duncan, M., Tankersley, L., Schultz, A., Chen, V., Kover, D., and Howard, P.- *Optical Debris Monitor*, NDT and E International, Vol. 30, No. 5, pp. 326. 1997.
- [8]. Wang, L. and Gao, R. - *Condition Monitoring and Control for Intelligent Manufacturing*, first ed. Springer, London 2006.
- [9]. Regeai M. N. - *Helical Gearbox Fault Detection Using Motor Current Signature Analysis*, PhD Thesis, The University of Manchester 2007.
- [10]. Ma, J. & Li, J. - On localized gear defect detection by demodulation of vibrations - a comparison study. *American Society of Mechanical Engineers, Manufacturing Engineering Division, MED*, 2(1), 565-576. 1995.
- [11]. Fakhfakh, T., Chaari, F., and Haddar, M.- Numerical and experimental analysis of a gear system with teeth defects. *Int. J Adv Manuf. Technol.*, 25:542-550. 2005.

REFERENCES

- [12]. Serridge, M.- Ten Crucial Concepts Behind Trustworthy Fault Detection in Machine Condition Monitoring, Proc. first Int. Machinery Monitoring and Diagnostics Conference and Exhibit, Las Vegas, NV, Sept., pp. 722-723, 1989.
- [13]. Xu, M. -The State-of-the Art of Machinery Condition Monitoring/Fault Diagnosis Techniques in China and some Development Trends, Proc. first Int. Machinery Monitoring and Diagnostics Conference and Exhibit, Las Vegas, NV, Sept., pp. 466-471, 1989.
- [14]. Work, Victor, Machinery Vibration: Measurement and Analysis, McGraw-Hill Inc., 1991
- [15]. Martin, H., and Ismail, F. - *Review of Gear Damage Monitoring Techniques*, first IMMDC Conference, Las Vegas, pp. 183-189, 1989.
- [16]. Wang, W., and McFadden, P. - *Application of Orthogonal Wavelets to Early Detection of Wavelets*, Mechanical Systems and Signal Processing, Vol.9, No. 5, pp. 497-507, 1995.
- [17]. Stander, C. J., Heyns, P. S. and Schoombie, W. - *Using Vibration Monitoring for Local Fault Detection on Gears Operating Under Fluctuating Load Conditions*, Mechanical Systems and Signal Processing, Vol. 16, No. 6, pp. 1005-1024, 2002.
- [18]. Stevens, P., Hall, D., Smith, E. - *A Multidisciplinary Research Approach To Rotorcraft Health And Usage Monitoring*, American Helicopter Society 5second Annual Forum, Washington, D. C., pp. 1732-1751, 1996.
- [19]. Randall, R. B.- *A New Method of Modelling Gear Faults*, ASME Journal of Mechanical Design, Vol. 104, No. 2, pp. 259-267, 1982.
- [20]. White, G. - *Amplitude Demodulation- A New Tool for Predictive Maintenance*, Sound and Vibration, 25(9), pp.14-19, 1991.
- [21]. Wang, W., and McFadden, P- *Early Detection of Gear Failure by Vibration Analysis .I. Calculation of the time-frequency distribution*, Mechanical System and Signal Processing, 7(3), 193-203, 1993.
- [22]. Baydar, N., Ball, A., and Gu, F. - *Detection of Gear Failures via Vibration and Acoustic Signals Using Wavelet Transform*, Mechanical Systems and Signal Processing, 17(4).pp. 787-804 ,2003.
- [23]. Lee J. H., Kim J. and Kim H. J. - *Development of Enhanced Wigner-Ville Distribution Function*, Mechanical Systems and signal Processing 15(2) 367-398, 2001.

REFERENCES

- [24]. Staszewski, W.J., and Tomlinson, G.R. - *Application Of The Wavelet Transform To Fault Detection In A Spur Gear*, Mechanical Systems And Signal Processing, Vol. 8, No. 3, pp. 289-307, 1994.
- [25]. Sung, K.C., Tai, H.M., and Chen, C.W.- *Locating Defects of a Gear System by the Technique of Wavelet Transform*, Mechanism And Machine Theory, Vol. 35, No. 8, pp. 1169-1182, 2000.
- [26]. Peng, Z.K., And Chu, F.L. - *Application of Wavelet Transform in Machine Condition Monitoring and Fault Diagnostics: A Review With Bibliography*, Mechanical Systems And Signal Processing, Vol. 18, No.2, pp. 199-221, 2004.
- [27]. Shigley, J., and Mischke C.- *Mechanical Engineering Design*, NY McGraw Hill Book Co., Inc., ISBN: 0072921935, 1989.
- [28]. Dudley, D.W. - *Gear Handbook*. NY, McGraw-Hill Book Co. Inc., ISBN: 0070179034, 1962.
- [29]. Huangshan wannan machinery Co., Ltd. , 2011, Tuesday 22 November 2011 at 08:56, <http://www.allproducts.com/machine/wannan/Product2010818203148.html>
- [30]. David Brown Radicon Gearbox Catalogue, DATE Series M, (cat.M08).
- [31]. Wright, D. - *Notes on Design and Analysis of Machine Elements*, T.U. of, Editor. Department of Mechanical and Materials Engineering: Western Australia, 35 Stirling Highway CRAWLEY WA 6009, 2005.
- [32]. Wang, W., and Mc Fadden, P. - *Decomposition of Gear Motion Signals and its Application to Gearbox Diagnostics*. Journal of Vibration and Acoustics, 117: p. 363, 1995.
- [33]. Frost, L., and Sullivan, R.- *Increasing Competition and the need for Planetary Solutions Spur Changes in the European Gearboxes and Geared Motors Market.*, in Newswire Europe Ltd, 2005.
- [34]. Xi'an AMCO Machine Tools Co., Ltd Co., Ltd. , 2011, Tuesday 22 November 2011 at 09:41, <http://www.allproducts.com/machine/amco/Product-201134141515.html>.
- [35]. Merritt, H. E. - *Gears*, third edition, Pitman Press, ISBN 0-333-35045-6, 1954.
- [36]. Alban E. - *Systematic Analysis of Gear Failures*, American Society of Metals. Metals Park, Ohio, 1985.

REFERENCES

- [37]. Smith, J.D. - *Gears and their Vibration: A Basic Approach to Understanding Gear Noise*, NY: Marcel Dekker, Inc., ISBN: 082471797X, 1983.
- [38]. Geartech- *Gear Failure Atlas*. Townsend, MT: Geartech, (1999).
- [39]. Choy, F., Zakrajsek, J., Handschuh, R., and Townsend, D.- *Vibration Signature Analysis of a Faulted Gear Transmission System*, Journal of Propulsion and Power. 12, pp. 289-295, 1996.
- [40]. Barbar, A. - *Handbook of Noise and Vibration Control*, sixth Edition), Elsevier Science Publisher Ltd., UK, 1992.
- [41]. Smith, J. D. - *Gear Noise and Vibration*, Marcel Dekker, NY, 1999.
- [42]. Li, C.J and Yoo, J.- *Prognosis of Gear Tooth Crack Growth*. Proc. 52th Meeting of the Society of mechanical failures Prevention Technology, Virginia Beach, VA, p 419-428, 1998.
- [43]. Welbourn D. B. - *Fundamental Knowledge of Gear Noise*, A Survey. Proc. Noise & Vib. of Eng. and Trans., I Mech E., Cranfield, UK, July pp. 9–14, 1979.
- [44]. Chad E. F. - *Synchronous Sampling Sideband Orders from Helical Planetary Gear Sets*’’ Master Thesis, Aug., Blacksburg, Virginia, USA, 1998.
- [45]. White, C.J. - *Detection of gear failure*, Workshop in On-condition Maintenance, ISVR, Southampton Jan 5-6, 1972.
- [46]. Forrester, B. D., *Advanced Vibration analysis Techniques for Fault Detection and Diagnosis in Geared Transmission Systems*. PhD Thesis, Swinburne University of Technology, Melbourne, 1996.
- [47]. Hedlund, J and Lehtovaara, A., *Modelling of helical gear contact with tooth deflection*, Tribology International, Volume 40, Issue 4, Pages 613-619, 2007.
- [48]. Andersson, A., Vedmar L., *A Dynamic Model to Determine Vibrations in Involute Helical Gears*, Journal Sound and Vibration, 260 (2), pp195, 212, 2003.
- [49]. Runkel, J., Sudmersen, V., Reimche, U., and Stegemann, D. - *Condition Monitoring of Industrial Machines*, Institute of Nuclear Engineering and Non-destructive Testing, University of Hannover, Germany 1996.

REFERENCES

- [50]. Wang, W.- *Early Detection of Gear Tooth Cracking Using the Resonance Demodulation Technique*, Mechanical Systems and Signal Processing 15 887-903, 2001.
- [51]. Randall, R.B. – *Separating Excitation and Structural Response Effects in Gearboxes*, Institution of Mechanical Engineers, Conference on Vibration and Rotating Machines, C305/84, 1984.
- [52]. Yesilyurt, I. *Gear fault detection and severity assessment using vibration analysis*, PHD. Thesis. Manchester: The University of Manchester, 1997.
- [53]. Martin, H. R.. *Detection of gear damage by statistical vibration analysis*, Proceeding of the Institute of Mechanical Engineers, Part-C, 395-401, 1992.
- [54]. Mitchell L. et al., *Review of Vibration Analysis Methods for Gearbox Diagnostics and Prognostics*, Proc. 54th Meeting of the Society for Machinery Failure Prevention Technology, May 1-4, pp. 623-634, 2000.
- [55]. Li, C., and Limmer, J.. *Model-based condition index for tracking gear wear and fatigue damage*. Wear, 241:26-32, 2000.
- [56]. De Almeida, Rui Gomes Teixeira; da Silva Vicente, Silmara Alexandra; Padovese, Linilson Rodrigues. *New Technique for Evaluation of Global Vibration Levels in Rolling Bearings*. Shock and Vibration Vol. 9, pp 225–234, 2002.
- [57]. Decker H.J. and Lewicki D. G.. *Spiral Bevel Pinion Crack Detection in a Helicopter Gearbox*, Proc. American Helicopter Society 59th Annual Forum, Phoenix, AZ, pp. 1222-1232, 2003.
- [58]. Večeř, P., Kreidl, M., and Šmíd, R. . *Condition Indicators for Gearbox Condition Monitoring Systems*, Acta Polytechnica 45(6) Czech Technical University in Prague, 2005.
- [59]. Hasan Ozturk, „Nov.,’Gearbox Health Monitoring and Fault Detection Using Vibration Analysis. PhD Thesis, Dokuz Eylul University, Izmir, Turkish, 2006.
- [60]. Swansson, N.S., *Application of Vibration Signal Analysis Techniques to Signal Monitoring*, Conference on Friction and Wear in Engineering, Institution of Engineers, Australia, Barton, Australia, pp. 262–267, 1980.
- [61]. Hahn, G., Shapiro, S. S. 1967. *Statistical Models in Engineering*, John Wiley& Sons.

REFERENCES

- [62]. Jaehong Suh'. On-Line Machinery Health Diagnosis and Prognosis for Predictive Maintenance and Quality Assurance of Equipment Functioning A PhD Thesis, Pennsylvania State University May 2001.
- [63]. Stewart, R.M. 1982, Application of Signal Processing Techniques to Machinery Health Monitoring, Chap 23 of Noise and Vibration, John Wiley& Sons.
- [64]. Randall, R. B.- *A New Method of Modelling Gear Faults*, ASME Journal of Mechanical Design, Vol. 104, No. 2, pp. 259-267,1982.
- [65]. Stevens, P., W., Hall, D., L. and Smith, E., C. 1996. *A Multidisciplinary Research Approach To Rotocraft Health and Usage Monitoring*, American Helicopter Society 5second Annual Forum, Washington, D.C., pp. 1732-1751.
- [66]. Kwok F. T., "Survey of Diagnostic Techniques for Dynamic Components," ARL-TR-5082, January 2010.
- [67]. Blankenship G. W. and Singh R., "Analytical Solution for Modulation Sidebands Associated with a Class of Mechanical Oscillaotrs," Journal of Sound and Vibration, vol. 179, no. 1, pp. 13-36, 1995.
- [68]. McFadden P. D. and Smith J. D., *An explanation for the asymmetry of the modulation sidebands about the tooth meshing frequency in epicyclic gearbox vibration*, in Proceedings of the Institution of Mechanical Engineers 199, , pp. 65-70, 1985.
- [69]. Nooli P. K., *A versatile and Computationally Efficient condition Indicator for AH-64 Rotorcraft Gearboxes*, Degree of Master of Science University of South Carolina, 2011.
- [70]. Wang W.J., McFadden P., *Application of wavelets to gearbox vibration signals for fault detection*, Journal of Sound and Vibration 192 (5) 927–939, 1996.
- [71]. McFadden P.D., *Window functions for the calculation of the time domain averages of the vibration of the individual planet gears and sun gear in an epicyclic gearbox*, Journal of Vibrations and Acoustics 116, 179–187,1994.
- [72]. Suh, I.S., *Application of Time-Frequency Representation Techniques to the Impact-Induced Noise and Vibration from Engines*, Diamler Chrysler. SAE Technical Paper # -01-0453, 2002.
- [73]. Yen, G., Lin, Kuo-Chung,. *Fault Classification on Vibration Data with Wavelet Based Feature Selection Scheme*, IEEE pp. 1644-1649, 2005.

REFERENCES

- [74]. Atles L. E., Gray D. B., Siva B. N., *Application of Time Frequency Analysis to signal from Manufacturing and Machine Health Monitoring*, Processing of the IEEE, Vol. 84, No. 9, pp. 1319-1329, September 1996.
- [75]. Strang G., Nguyen T., *Wavelets and filter banks*, Wellesley-Cambridge Press, 1996.
- [76]. Ruqiang Y., *Base Wavelet Selection Criteria for Non-Stationary Vibration Analysis in Bearing Health Diagnosis*. A PhD Thesis, 2007.
- [77]. Bollahbal D., Golnaraghi F., Ismail F., Amplitude and phase wavelet maps for the detection of cracks in geared system, *Mechanical Systems and Signal Processing*, 13(3), pp. 423-436. 1999.
- [78]. Forrester, B.D. – *Analysis of Gear Vibration in the Time-frequency Domain*, Proceeding of the 44th Meeting of the Mechanical Failures Prevention Group of the Vibration Institute, Virginia Beach, Virginia, p.225-234, 3-5 April, 1989.
- [79]. Forrester, B.D. - *Time-frequency Analysis in Machine Fault Detection*, Time-frequency Signal Analysis, Melbourne, Longman Cheshire-1992.
- [80]. Ville, J., *Theorie et Applications de la Notion de Signal Analytique*, Cables et Transmission, Vol. 2A(1), pp. 61-74, Paris. (English translation by I. Selin: Theory and Application of the Notion of Complex Signals, Report T-92, RAND Corporation, Santa Monica, California, 1948.
- [81]. Preeti R., Fred T., and Gregory H., *Real-time monitoring of vibration using the Wigner Distribution*, Sound and vibration, pages 22-25, May 1990.
- [82]. Cohen L., *Time-frequency distributions- a review*, In Proceedings of the IEEE. Vol. 77/7. Page 941-981, 1989.
- [83]. Vladimir V. P., *Detection and Quantification of the Gear Tooth Damage from the Vibration and Acoustic Signatures*, PhD thesis, University of Akron, May 1999.
- [84]. Forrester, B.D., *Use of the Wigner-Ville Distribution in Helicopter Transmission Fault Detection*, Proceeding of the Australian Symposium on Signal Processing and Applications – ASSPA-89, Adelaide, Australia, p.77-82, 17-19 April, 1989.

REFERENCES

- [85]. McFadden, P.D., Wang, W.J., *Time-frequency Domain Analysis of Vibration Signals for Machinery Diagnostics(1)- Introduction to the Wigner-Ville Distribution*, Department of Engineering Science, University of Oxford, Report No. OUEL1859/90, 1990.
- [86]. Baydar, N., Gu, F., Ball, A. and Li, J. - *Helical Gear Fault Detection and Diagnosis using a Varying-time Frequency Distribution*, Proceedings of the First International Conference on the Integration of Dynamics, Monitoring and Control (DYMAC '99), Manchester, UK, p.109-115, 1999.
- [87]. Baydar, N. and Ball, A. - *A Comparative Study of Acoustic and Vibration Signals in Detection of Gear Failures Using Wigner-Ville Distribution*, accepted for publication in Mechanical Systems and Signal Processing, 2000.
- [88]. Staszewski, W. and Tomlinson, G., *Time-frequency Analysis in Gearbox Fault Detection Using the Wigner-Ville Distribution and Pattern Reorganization*, Mechanical Systems and Signal Processing, 11(5), pp.673-692, 1997.
- [89]. Cohen, L., *Generalized Phase-space Distribution Functions*. Journal of Mathematical Physics, Vol. 7, pp. 781-786, 1996.
- [90]. Claasen, T.A.C.M., and Mecklenbrauker, W.F.G., *The Wigner Distribution- A tool for Time-Frequency Signal Analysis*, Part I: Continuous Time Signals", Philips Journal of Research, Vol. 35, No. 3, pp.217-250, 1980.
- [91]. Joel D. L., *Improved Methods of Vibration Measurement, Gear Fault Detection and Bearing Fault Detection for Gearbox Diagnostics*, PhD Thesis, Rensselaer Polytechnic Institute, Troy, NewYork, 2001.
- [92]. Gregorio A., Mario S., and Amerigo T., *Application of Wigner-Ville Distribution to measurements on transirnt signals*, IEEE Transactions of Instrumentation and Measurement, 43(2): 187-193, April 1994.
- [93]. Olivier Rioul and Martin Duhamel "Fast Algorithms for Discrete and continuous Wavelet Transform. IEEE Transaction on Information Theory", 38(2): 569-586. March 1992.
- [94]. Mallat, S., *A Wavelet Tour of Signal Processing*, Academic Press, second Edition, 87, 1999
- [95]. Vetterli, M., *Wavelets and Filter Banks: Theory and Design*, IEEE Transactions on Signal Processing, vol. 40, no. 9, pp 2207-2232, 1992.

REFERENCES

- [96]. Jianyou Zhou. Vibration Signature Analysis for Fault Detection in Gear and Bearing Components, A PhD Thesis, Faculty of the University of Akron, 2003.
- [97]. Li, X., Tso, S.K., and Wang, J., Real-Time Tool Condition Monitoring Using Wavelet Transforms and Fuzzy Techniques, *IEEE Transactions on Systems, Man, and Cybernetics – Part C: Application and Reviews*, Vol. 30, No. 3, pp. 352-357, 2000.
- [98]. Abu-Mahfouz, I., Drill Flank Wear Estimation Using Supervised Vector Quantization Neural Networks, *Neural Computing and Applications*, 14(3), pp. 167-175, 2005.
- [99]. Yang, W. X. and Ren, X. M., Detecting Impulses in Mechanical Signals by Wavelets, *EURASIP Journal on Applied Signal Processing*, Vol. 8, pp. 115~1162, 2004.
- [100]. Liu, H., Zuo, H., Jiang, C., and Qu, L.. An improved algorithm for direct time-domain averaging, *Mechanical Systems and Signal Processing*, 14(2), pp. 279-285, 2000.
- [101]. Eric B., Michael K., *A Review of Time Synchronous Averaging Algorithms*, Annual Conference of the Prognostics and Health Management Society, 2009.
- [102]. McFadden, P.D., A revised model for the extraction of periodic waveforms by time domain averaging, *Mechanical Systems and Signal processing*, vol. 1(1), pp. 83-95, 1987.
- [103]. McFadden P.D., *Interpolation techniques for time domain averaging of gear vibration*, *Mechanical Systems and Signal processing*, 3(1), pp. 87-97, 1989.
- [104]. Fyfe K. R., Munck E. D. S., *Analysis of computed order tracking*. *Mechanical Systems and Signal Processing*, 11, (2):187-205, 1997.
- [105]. Tian H., Luan J., *Application of order tracking analysis in gear wearing fault diagnosis*, *Journal of Ordnance Engineering College*, 10, 17(5):57-60, 2005.
- [106]. Jason R. B., *Improving the Analysis of Operating Data on Rotating Automotive Components*, PhD Thesis, University of Cincinnati Dec.1990.
- [107]. Mark L. - *Using Ac Motor as a Transducer for Detecting Electrical and Electromechanical Faults*, Master Degree Thesis , University of Huddersfield, 2011.
- [108]. Slemon, G. R. and Straughen, A., *Electrical Machines*. Addison Wesley, 1980.

REFERENCES

- [109]. European Electric Motors; Written by Dr David G Searle; A Drives and Controls Publication, published on behalf of Eurotherm Drives Ltd. New Courtwick Way, Littlehampton, West Sussex, BN17 7PD; ISBN 0 907485 10.
- [110]. Licht, T. R., Serridge, M., *Piezo-electric Accelerometers and Vibration Pre-amplifier Handbook*, Bruel & Kjaer Publications, pp. 12-37, 1987.
- [111]. Khadapkar S. S., *Failure Identification of Gear Systems using Hilbert-Huang Transform and Artificial Neural Networks*, Master Degree dissertation, Binghamton University New York, 2006.
- [112]. Riley C. M., *Current-based sensorless vibration monitoring of small AC machines*, Georgia Institute of Technology, Atlanta, GA, Ph.D. Thesis 1998.
- [113]. Roux W. L., *On-line detection of rotor faults in permanent magnet machines using only terminal quantities*, Georgia Institute of Technology, Atlanta, GA, Ph.D. Thesis, 2007.
- [114]. Bartelmus, W., *Mathematical modelling and computer simulations as an aid to gearbox diagnostics*, Mechanical System and Signal Processing, 15, 5, pp. 855-871, 2001.
- [115]. Howard, I. et. al., *The dynamic modelling of a spur gear in mesh including friction and a crack*, Mechanical System and Signal Processing, 15, 5, pp. 831-853, 2001.
- [116]. Vinayak, H. and Singh, R., *Multi-body dynamics and modal analysis of compliant gear bodies*, Journal of Sound and Vibration, 210, 2, pp.171-214, 1998.
- [117]. Huang, K. J. and Liu, T.S., *Dynamic analysis of a spur gear by the dynamic stiffness method*, Journal of Sound and Vibration, 234, 2, pp. 311-329, 2000.
- [118]. Parker, G. R. et. al., *Non-linear dynamic response of a spur gear pair: Modelling and experimental comparisons*, Journal of Sound and Vibration, 237, 3, pp. 435-455, 2000.
- [119]. Theodossiades, S. and Natsiavas, S., *Non-linear dynamics of gear-pair systems with periodic stiffness and back-lash*, Journal of Sound and Vibration, 229, 2, pp. 287-310, 2000.

REFERENCES

- [120]. Velez, P. and Maatar, M., *A mathematical model for analyzing the influence of shape deviations and mounting errors on gear dynamic behaviour*, Journal of Sound and Vibration, 191, 5, pp.629-660, 1996.
- [121]. Sato K., Yamamoto S., and Kawakami T., *Bifurcation Sets and Chaotic States of a Gear System Subjected to Harmonic Excitation*, Computational Mechanics, 7:173-182, 1991.
- [122]. Kahraman A., Effect of axial vibrations on the dynamics of a helical gear pair, Journal of Vibration and Acoustics, 115 (1993) 33-39.
- [123]. Amabili, M. and Rivola, A., *Dynamic Analysis of Spur Gear Pairs: Steady-state Response and Stability of the SDOF Model with Time-Varying Meshing Damping*, Mechanical Systems and Signal Processing, Vol. 11 No. 3, pp 375-390, 1997.
- [124]. Sinisa D. – *Finite Element Model of a Double-Stage Helical Gear Reduction* , A Mater Degree Dissertation, University of Windsor , 2006.
- [125]. Siyan W., Gearbox Dynamic Simulation and Estimation of Fault Growth, M.Sc Degree, Edmonton, Alberta, Spring 2007.
- [126]. Dormand, J. R. and Prince P. J., *A family of embedded Runge-Kutta formulae*, J. Comp. Appl. Math., Vol. 6, , pp. 19-26,1980.
- [127]. Shampine, L. F., Reichelt M. W., and Kierzenka J.A., *Solving Index-1 DAEs in MATLAB and Simulink*, SIAM Review, Vol. 41, , pp 538-552,1999.
- [128]. Du S., Randall R B and Kelly DW., *Modelling of spur gear mesh stiffness and static transmission error*”. Proc Instn Mech Engrs Vol 212 Part C, pp 287-297, 1998.
- [129]. Zhang N., *Advanced Signal Processing Algorithms and Architectures for Sound and Vibration*, National Instruments NI-Week Conference; Presentation TS 1577; Austin, Texas, USA; Aug, 2008.
- [130]. Andrew K.S. J., Daming L. and Dragan B. - *A review on Machinery Diagnostics and Prognostics Implementing Condition-Based Maintenance*, Mechanical Systems and Signal Processing, Vol. 20, Issue 7, pp 1483-1510, October 2006.
- [131]. Jing Y. - *Wavelet Analysis with Time-Synchronous Averaging of Planetary Gearbox Vibration Data for Fault Detection, Diagnostics, and Condition Based Maintenance*, Mechanical and Electronics Engineering (ICMEE), 2nd International Conference on vol-132, Print ISBN: 978-1-4244-7479-0. 2010.

REFERENCES

- [132]. Preston J., *Emerging Challenges and Technologies in Signal Processing for Prognostics and Health Management in Wind Energy*, Annual Conference of the Prognostics and Health Management Society, 2010.
- [133]. Decker, H., Zakrajsek, J. - *Comparison of Interpolation Methods as Applied to Time Synchronous Averaging*, ARL-TR-1960, MFPT, April 19-22, 1999.
- [134]. Herlufsen, H., *Model Analysis using Multi-reference and Multiple-Input Multiple-Output Techniques*, Brüel & Kjær, Application Note 2004.

APPENDICES

APPENDIX A: THE ANALYTICAL BASIS OF FREQUENCY ANALYSIS

FFT signal analysis technique is commonly used in industry for data analysis. It is based on the conception that the spectral content, rather than the vibration amplitude is the key to determining the machine condition. Therefore, instead of analysing the vibration signal directly in the time domain, the FFT of the vibration signal is analysed.

The Fourier Transform (FT) is the analytic basis of frequency analysis:

$$X(f) = \int_{-\infty}^{\infty} x(t) \exp(-j2\pi ft) dt \quad (A1)$$

And the inverse of the transform is:

$$x(t) = \int_{-\infty}^{\infty} X(f) \exp(-j2\pi ft) df \quad (A2)$$

Where: $x(t)$ is the continuous time-domain signal, and $X(f)$ is the frequency spectrum of $x(t)$.

This analysis is based on the idea that any regular periodic function and certain non-periodic functions with finite integral can be expressed as a sum of trigonometric functions in an infinite time framework.

In equation (A2), the continuous time-domain signal $x(t)$ is multiplied with sine and cosine term ($e^{-2\pi jft}$) of the frequency f and then integrating overall times from $-\infty$ to $+\infty$. The value of $X(f)$ depends on whether or not $x(t)$ has a dominant frequency component at frequency f . If $x(t)$ contains a dominant frequency f , then $X(f)$ will be large and if it does not contain frequency f , then $X(f)$ will zero. Since the integration is from $-\infty$ to $+\infty$, it does not matter where in time the component with frequency f appeared and hence it does not impact the result of the integration.

The Fourier transform gives a distinctive representation of the signal in the frequency domain and provides information about which frequencies appear in the signal but not about the time instants in which these frequencies are encountered.

The transform become more useful when used with real, digitally sampled data, i.e.

APPENDIX

Discrete Fourier Transform (DFT). And the DFT is defined by:

$$X(k) = \sum_{n=0}^{N-1} x(n) \exp(-j \frac{2\pi kn}{N}), 0 \leq k \leq N-1 \quad (A3)$$

Where: $x(n)$ is a sampled time-domain signal that is quantized in time as

$$x(n) = x(n)|_{t=nTs} \quad (A4)$$

Where: n is an integer and T is some specified time interval.

The calculation of DFT involves computation of a large number of complex multiplications in order to generate a useful frequency spectrum. This is a computationally exhaustive process and allows not practical when performing real time analysis. For this reason, an algorithm has been developed, known as the Fast Fourier Transform (FFT), which that performs fast implementation of the DFT by greatly reducing the number of computations. FFT is commonly used in signal processing to analyse the frequencies.

FFT of the vibration signal provide us the spectrum in the frequency domain. This spectrum gives information indicating the level of the vibration at particular frequencies. Thus all major frequency components and their amplitudes can be identified and be used for fault detection purposes. The frequency identifies the source of the fault and the amplitude identifies the fault severity. As the fault start to develop in machine components, the vibration spectrum peaks at the defect frequency and its harmonics that is associated with the faulty element. As the severity of the damage increase, the corresponding amplitudes of the peaks in the power spectrum increase.

In practice the Fast Fourier Transform (FFT) algorithm is invariably applied. For a given time-domain signal, the power spectrum estimation shows the signal's power at frequency bins in the frequency-domain. The following equation shows power spectrum, $S_{xx}(f)$ of a time-domain signal, $x(t)$ using Fourier transform (FT);

$$S_{xx}(f) = |FT[x(t)]|^2 \quad (A5)$$

APPENDIX B: SPECIFICATIONS OF THE TEST RIG COMPONENTS

B.1: AC Motor

Manufacturer: Electro-drives Company.

Motor model: V-DA160MJ, 0298659

Rating plate data:

Power = 11 kW

Voltage = 380 – 415 V

Current= 21.5A at full load

Speed = 1470 rpm

Phase: 3

Winding: Y start

Number of Stator Slots: 48

Number of Rotor Slots: 40

The supply voltage at the University of Huddersfield is 415VAC 3-phase measured line-to-line. Reading from the motor nameplate data, the motor power will be 11kW with a no-load motor base speed of 1492RPM.

B.2: Two Stage Helical Gearbox

Manufacturer: David Brown, series M Radicon ^m.

Unit TYPE: M07202-5BMG1A, 11.4 AD

INPUT KW: 11KW

RATE: 2.5 A

ORDER No: 5032382

OIL GRADE: 320

ASSEMBLY: 1A

The gearbox is consisting of two stage helical gear. The first – or primary – stage has two gears and the second stage consists of two gears as well. The specification of the two sets is shown in the Table 3.1.

B.3: DC Motor (Generator)

The information from the DC motor rating plate is given below:

Size: SD 200XLC

No: G63801N

Rated speed: 1750 rpm

Duty type: S1

Ins Class: F

Rated power: 85kW

Armature V: 460, A: 200

Enclosure: IP22

Voltage (excitation): 360V,

Current: 4.7A

DE. 6314 N.D.E.6309

Mass: 48.2Kg

APPENDIX C: ICP-TYPE ACCELEROMETER SPECIFICATIONS

The Specifications for ICP-type Accelerometer are given in Table C.1: PCB Model no. 338C04 Accelerometer:

Table C.1 ICP-type Accelerometer Specifications

Model & Serial Number	PCB Model no. 338C04 Accelerometer
Frequency range	0.5Hz to 10 kHz ($\pm 5\%$) 0.3Hz to 12kHz ($\pm 10\%$) 0.2Hz to 20kHz ($\pm 3\text{dB}$)
Sensitivity	100mV/g ($\pm 10\%$)
Temperature Range	-53 to 93°C
Excitation Voltage	18-30 VDC
Resonant Frequency	$\geq 35\text{kHz}$
Output Bias voltage Level	8 to 12 VDC
Broadband Resolution (1 to 10kHz)	0.0018m/s ² RMS
Discharge Time Constant	0.8-2.4 sec
Measurement Range	$\pm 50\text{g}$ pk

APPENDIX

APPENDIX D: NATIONAL INSTRUMENTATION DATA ACQUISITION CARD SPECIFICATIONS

The Specifications for National Instrumentation data acquisition card are given in Table D.1:
PCI Model no. 6221 DAQ:

Table D.1 National Instrumentation data acquisition card, type PCI 6221 Parameters

Parameter	Performance
No. of Channels	8 differential , 16 single ended
ADC resolution	16 bits
Sampling rate (maximum)	250 kS/sec
Timing accuracy	50 ppm of sample rate
Timing resolution	50 ns
Input voltage range	+/- 10V
Max working voltage	11 V